Université Fédérale
Toulouse Midi-Pyrénées

THÈSE

En vue de l'obtention du
DOCTORAT DE L'UNIVERSITÉ DE TOULOUSE

Délivré par l'Université Toulouse 3 - Paul Sabatier

Présentée et soutenue par

YIYUE JIA

Le 27 octobre 2023

Production d'hormones stéroïdes sexuelles dans le tissu adipeux périprostatique et son rôle dans la progression du cancer de la prostate

---

Ecole doctorale : **BSB - Biologie, Santé, Biotechnologies**

Spécialité : **CANCEROLOGIE**

Unité de recherche :
IPBS - Institut de Pharmacologie et Biologie Structurale

Thèse dirigée par
Catherine MULLER et Delphine MILHAS

Jury

Mme Sophie GIORGETTI-PERALDI, Rapporteure
M. Cyrille DE JOUSSINEAU, Rapporteur
M. Thierry CAPIOD, Rapporteur
M. Frederic BOST, Examinateur
M. Mathieu ROUMIGUIE, Examinateur
Mme Catherine MULLER, Directrice de thèse
Mme Delphine MILHAS, Co-directrice de thèse
Mme Anne BOULOUMIE, Présidente

ACKNOWLEDGEMENTS

Firstly, I would like to extend my deepest gratitude to my dedicated and insightful supervisors, Catherine Muller and Delphine Milhas. Thanks for accepting me as a PhD student even in light of my limited background in biology. Thanks for their continuous guidance and generous support during my entire doctoral period and providing me an excellent experimental platform, which supported my PhD study. I would also like to express my profound thanks to the members of my thesis jury, Cyrille De Joussineau, Thierry Capiod, Sophie Giorgetti-Peraldi for their invaluable input, thoughtful critiques, and the time they dedicated to evaluating my research. Their feedback not only elevated the quality of this thesis but also broadened my perspective. Meanwhile, I would like to thank Fredric Bost for his breakthrough suggestions in my whole thesis journey as my thesis committee member.

Secondly, I would also like to thank all of my colleagues in the MICA team in IPBS-CNRS, Toulouse. David Estève, he always inspired me when I was faced with difficulties and guided me on how to think critically in science. Cynthia Houël, she taught me many experimental skills and instilled in me good experimental habits. Special thanks to Camille Attané and Frédérique Fallone for their contributions to my project and their generous sharing of knowledge and experience. Thanks for Sauyeun Shin, she always gives me timely and important help without hesitation when I was in trouble. I quite enjoyed the chatting time with Charlotte Vaysse every Tuesday. I am indebted to Marie Rebeaud and Marine Hernandez for generously sharing their experiences and for the insightful discussions that shaped my work. I express gratitude to Mathilde Lacombe for her significant contributions to the project as a new Ph.D. student, and the collaboration with her was truly pleasant. I will never forget Mohammed Moutahir who offered me lots of urgent solutions in my lab life. Special appreciation goes to Stéphanie Dauvillier for microscope training and Landry Blanc for his advice regarding my thesis defense.

Finally, I extend my gratitude to my family for their unconditional love, encouragement, and constant companionship. To my friends-Jianjia Ma, Jinyue Zhang, Xue Han, Yushun Tian, Mingmin Zhang, Jiuwen Sun, Yarong Shi, Zicun Cai, Xintong Chen, Kangkang Ge, I am thankful for your continuous presence and the many unforgettable memories we shared in Toulouse. Last but not least, I wish to acknowledge the various individuals I encountered at IPBS over these three years: Eve Pitot, Catherine Tardin, Laurence Salome, Jelena Kolosnjaj Tabi, Sébastien Britton, Jeanne Chauvat, Rousset Stella, and Caroline Ladurantie. Your support has been instrumental in the success of my thesis work.

Life is too short but I appreciated every season I spent in Toulouse because of all of you.

THESIS ABSTRACT

Prostate cancer (PCa) is the most common cancer in men in Western countries. PCa is a hormone dependent cancer, androgens being essential to its development and progression. PCa cells could convert testis-produced testosterone into active form 5α-dihydrotestosterone (5α-DHT) to activate the androgen receptor (AR) signaling for growth. Thus, hormonal therapy such as androgen deprivation therapy is used as a treatment of locally advanced PCa and consists in inhibiting the production of testosterone by the testis. However, the disease will progress into castration resistant PCa (CRPC) after a few years. One emerging mechanism of resistance involves the ability of PCa cells to find alternative sources of sex steroids from tumour environment to produce the active forms of androgens as recently shown for the gut microbiota and cancer associated fibroblasts.

The aim of my project is to determine if periprostatic adipose tissue (PPAT), an adipose depot surrounding the prostate has a specific steroid metabolism that could modify PCa progression which to our knowledge has never been tested. We have demonstrated, here for the first time that PPAT contains higher steroid metabolites such as 5α androstanedione and epiandrosterone compared to the controlled abdominal pelvic adipose tissue (APAT), involved in the alternate routes for 5α-DHT synthesis in CRPC. Within PPAT, mature adipocytes appear to be the main source of androgen metabolites. The regulation of the expression of enzymes involved in steroidogenesis may explain the increased content of 5α-androstanedione and epiandrosterone in PPAT compared to APAT. Furthermore, we demonstrated that PPAT- conditioned medium (CM) can support cell growth and proliferation of an androgen-dependent cell line LNCaP cultivated in androgens-deprived medium but not in androgens containing medium. This effect is inhibited by an AR antagonist bicalutamide and PPAT-CM upregulates the expression of AR targeted genes such as KLK3 and FKBP5. The acute regulation of steroidogenic enzymes in the absence of androgens is reversed by PPAT-CM. Although we did not directly demonstrate the secretion of sex steroid by PPAT, these results bring arguments in favor of a functional effect of the steroids metabolites contained in PPAT on PCa cells.

In conclusion, our studies demonstrated that PPAT is a new source of androgens for CRPC development and paved the way to explain why changes in PPAT (as seen in obesity or during PPAT accumulation independently of obesity) lead to more aggressive PCa that exhibit resistance to androgen deprivation therapy. This work could allow to propose new risk stratifications and/or identify new therapeutic targets.

RESUME DE LA THESE

Le cancer de la prostate (CaP) est le cancer le plus fréquent chez les hommes des pays occidentaux. Le CaP dépend des hormones, les androgènes étant essentiels à son développement et à sa progression. Les cellules du CaP peuvent convertir la testostérone produite par les testicules en une forme active appelée 5α-dihydrotestostérone (5α-DHT) pour activer le récepteur des androgènes (RA) et favoriser la croissance. Ainsi, la thérapie de privation androgénique représente un traitement de choix pour les CaP localement avancés et consiste à inhiber la production de testostérone par les testicules. Cependant, la maladie évoluera vers une forme de CaP résistante à la castration (CPRC) après quelques années. Un mécanisme émergent de résistance implique la capacité des cellules du CaP à trouver d'autres sources d'androgènes dans l'environnement tumoral afin de produire les formes actives d'androgènes, comme cela a récemment été démontré pour le microbiote intestinal et les fibroblastes associés au cancer.

L'objectif de mon projet est de déterminer si le tissu adipeux périprostatique (TAPP), un dépôt adipeux entourant la prostate, possède un métabolisme stéroïdien spécifique qui pourrait modifier la progression du CaP, ce qui, à notre connaissance, n'a jamais été testé. Nous avons démontré ici, pour la première fois, que le TAPP contient des métabolites stéroïdiens plus élevés, tels que la 5α-androstanedione et l'épiandrostérone, par rapport au tissu adipeux pelvien abdominal contrôle (APAT), impliqué dans les voies alternatives de synthèse de 5α-DHT dans le CPRC. Au sein du TAPP, les adipocytes matures semblent être la principale source de métabolites d'androgènes. La régulation de l'expression des enzymes impliquées dans la stéroïdogénèse pourrait expliquer le contenu élevé en 5α-androstanedione et épiandrostérone dans le TAPP par rapport à l'APAT. De plus, nous avons démontré que le milieu conditionné de TAPP peut favoriser la croissance cellulaire et la prolifération d'une lignée cellulaire dépendante des androgènes appelée LNCaP, cultivée dans un milieu privé d'androgènes mais pas dans un milieu contenant des androgènes. Cet effet est inhibé par un antagoniste du RA, le bicalutamide, et le milieu conditionné de TAPP régule positivement l'expression de gènes cibles du RA tels que KLK3 et FKBP5. La régulation des enzymes stéroïdiennes en l'absence d'androgènes est réversée par le milieu conditionné de TAPP. Bien que nous n'ayons pas directement démontré la sécrétion d'androgènes par le TAPP, ces résultats apportent des arguments en faveur d'un effet fonctionnel des métabolites stéroïdiens contenus dans le TAPP sur les cellules du CaP.

En conclusion, nos travaux ont démontré que le TAPP représente une nouvelle source d'androgènes pour le développement du CPRC ce qui permettrait d'expliquer pourquoi les changements dans le TAPP (comme observé dans l'obésité ou lors de l'accumulation de TAPP indépendamment de l'obésité) conduisent à un CaP plus agressif associé à une résistance à la thérapie de privation androgénique. Ce travail pourrait permettre de proposer de nouvelles stratifications des risques et/ou d'identifier de nouvelles cibles thérapeutiques.

Table of Contents

Abbreviations list 5

INTRODUCTION 8

Part 1 Prostate cancer 9

1. Anatomical and physiological description of the prostate 9

1.1 Anatomical description 9

1.2 Localisation and function 10

1.3 Histological description 11

2. Epidemiology of Prostate Cancer 12

3. Diagnosis of Prostate cancer 13

4. Prostate cancer classifications 15

5. Prostate cancer models 18

5.1 In vitro models 18

5.2 In vivo models 24

6. Prostate cancer treatments 26

7. Hormonal treatment and mechanisms of its resistance in PCa 28

7.1 Androgen synthesis by the hypothalamic-pituitary-testicular (HPT) axis 28

7.2 Androgen Receptor (AR) function and activity 29

7.3 First generation hormonal treatment: androgen deprivation therapy (ADT) 32

7.4 Mechanisms of resistance to first generation hormonal treatments 33

7.5 Second generation hormonal treatments 39

7.6 Mechanisms of resistance to second-line treatment and part of first-line treatment 42

7.7 Newest treatment for PCa 49

Part 2 Adipose tissue 52

1. The white adipose tissue 52

2. Composition of white adipose tissue 53

2.1 White adipocytes 53

2.2 SVF 53

3. Extra-cellular matrix (ECM) 56

3.1 Main components of the ECM 57

3.2 Organization of ECM around adipocytes 57

3.3 Degradation or remodelling of ECM 58

3.4 Role of the ECM in AT 59

4. Vascular organization of AT 60

5. AT functions 60

5.1 Lipogenesis 61

5.2 Lipolysis 62
5.3 Secretions 62
5.4 AT modification in obesity 63
Part 3 Periprostatic adipose tissue (PPAT) 68
1. Anatomical description of PPAT 68
2. Characterization of PPAT 69
3. The interplay between PPAT and PCa 69
3.1 The influence of PPAT on PCa development 70
3.2 The influence of PCa cells on PPAT behavior 74
3.3 Beyond obesity 75
Part 4 Steroid hormones and AT 77
1. Steroids quantification and synthesis capacity in AT 77
1.1 Production of sex steroids by different AT in humans and other species 77
1.2 Sex steroid storage in AT 81
1.3 Mechanisms of sex steroids biosynthesis in AT 83
2. General influence of androgens on AT 90
2.1 Body fat distribution regulation by androgens in women and men 90
2.2 Hormone therapy influence on male AT 92
3. Functional effect of androgens on AT 92
3.1 AR expression 92
3.2 Effect of androgens on WAT 93
3.3. Effects of androgens on BAT 99
RESULTS 102
GENERAL DISCUSSION/PERSPECTIVES 129
MATERIALS AND METHODS 135
REFERENCES 141

Abbreviations list

AR Androgen Receptor

AR-KO Androgen Receptor Knock-Out

AR-FL Full-Length Androgen Receptor

ADSC Adipose-Derived Stem Cell

ADT Androgen Deprivation Therapy

ARI AR Inhibitors

AR-Vs AR Splice Variants

Akt Protein Kinase B

AT Adipose Tissue

ATGL Adipose Triglyceride Lipase

AKR1C3 Type 5 17β-hydroxysteroid dehydrogenase

AKR1C2 3α-hydroxysteroid dehydrogenase

AT macrophages (ATM)

BAT Brown Adipose Tissue

BMI Body Mass Index

BPH Benign Prostatic Hypertrophy

CYP11A1 Cytochrome P450 side-chain cleavage

CYP17A1 Cytochrome P450 17α-hydroxylase/17,20-lyase

CRPC Castration-Resistant Prostate Cancer

C/EBP CCAAT/enhancer Binding Proteins

CAF Cancer-Associated Fibroblasts

DHEA Dihydroepiandrosterone

5α- DHT 5α- Dihydrotestosterone

11β-hydroxy dihydrotestosterone (11-keto-DHT)

DHEA-S Dihydroepiandrosterone-Sulphate

DBD DNA-Binding Domain

EMT Epithelial-Mesenchymal Transition

ECM Extracellular Matrix

FFA/FA Fatty Acids

FDA Food and Drug Administration

GR Glucocorticoid Receptor

GnRH Gonadotropin-Releasing Hormone

HPT Hypothalamic-Pituitary-Testicular

HSL Hormone-Sensitive Lipase

HFD High-Fat Diet

HSD17B 17β-hydroxysteroid dehydrogenase

HSD3B1 3 beta- and steroid delta-isomerase 1

11β HSD2 Type 2 11β-hydroxysteroid dehydrogenase

IL Interleukin

ISUP International Society of Urological Pathology

LOD Limit of Detection

LPL Lipoprotein Lipase

LH Luteinizing Hormone

LHRH Luteinizing Hormone-Releasing Hormone

LAM lipid associated macrophages

MRI Magnetic Resonance Imaging

MAGL Monoacylglycerol Lipase

MAT Mamary Adipose Tissue

MMPs Matrix Metalloproteinases

MAPK Mitogen-activated protein kinases

NF-κB the Nuclear Factor-kappa B

OM AT Omental Adipose Tissue

PSA Prostate Specific Antigen

PCa Prostate Cancer

PPARγ Peroxisome Proliferator-activated Receptor gamma

PPAT Periprostatic Adipose tissue

PI3K Phosphoinositide 3-Kinase

PCOS Polycystic Ovary Syndrome

PTEN Phosphatase and Tensin Homolog

SAT Subcutaneous Adipose Tissue

SVF Stroma-Vascular Fraction

SHBG Sex Hormone-Binding Globulin

TG Triglycerides

TNF-α Tumor Necrosis Factor-Alpha

UCP1 Uncoupling Protein 1

VAT Visceral Adipose Tissue

INTRODUCTION

Part 1 Prostate cancer

1. Anatomical and physiological description of the prostate

1.1 Anatomical description

The prostate is a gland annexed to the genital tract, surrounding the urogenital. It is shaped like a flattened cone with an upper base. After a long (estimated 22 years at Stanford University) and tedious (reading and rereading over 1,000 prostatectomy specimens) work, anatomical pathologist John McNeal described 4 distinct prostatic anatomical zones (**Figure 1**):
- **The central zone** which is posteromedial and superior, encompassing the ejaculatory ducts.
- **The peripheral zone** which is posterolateral and inferior and the site of development of 75% of cancers.

- **The transition zone** which is lateral to the urethra. -
- **The fibro-muscular zone** which is anterior to the prostate.

The prostate undergoes several phases of growth over the course of a lifetime, at the expense of the transition zone. Although the organ is virtually non-existent at birth, a first phase of growth is observed at puberty, under the influence of androgens. After the age of 40, a second phase of growth begins, resulting in prostatic hypertrophy in over 50% of men between the ages of 50 and 60, and 90% of men over 80[1] [2]. When this hypertrophy is not associated with cancer, it is called benign prostatic hypertrophy (BPH). It can lead to urinary symptoms due, among other things, to compression of the urethra by an enlarged prostate.

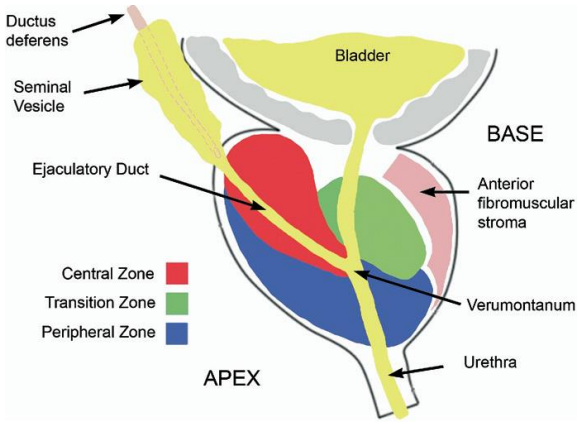


Figure 1. Sagittal view of prostate gland as described by McNeal. (from Ronald J Cohen et al., J Urol, 2008)

1.2 Localisation and function

The prostate is an exocrine gland belonging to the male genital tract. Located below the bladder, behind the pubis and in front of the rectum, it surrounds the urethra from its base (upper part) to its apex (lower end) (**Figure 2**). At its base, the prostate is bounded ventrally by the bladder and dorsally by the vas deferens and seminal vesicles[3].The main function of the prostate is to produce prostatic fluid[4] which accounts for around 20% of seminal fluid, the remaining 80% being secreted by the seminal vesicles. It is this seminal fluid, mixing with sperm from the testicles that forms the sperm. Prostatic fluid contains numerous ions, polyamines and proteins, as well as enzymes that keep sperm in liquid form by preventing coagulation[4]. One of the major enzymes secreted by the prostate and specific to this organ is PSA (Prostate Specific Antigen), a serine protease of the kallikrein family whose main role is to cleave the majority protein in seminal secretions and enable sperm liquefaction[5]. Its production is regulated by androgens and it is secreted in seminal fluid. Physiologically, PSA levels released into the bloodstream are minimal, but in the event of prostatic pathology (inflammation, benign or malignant proliferation) the amount increases[6].

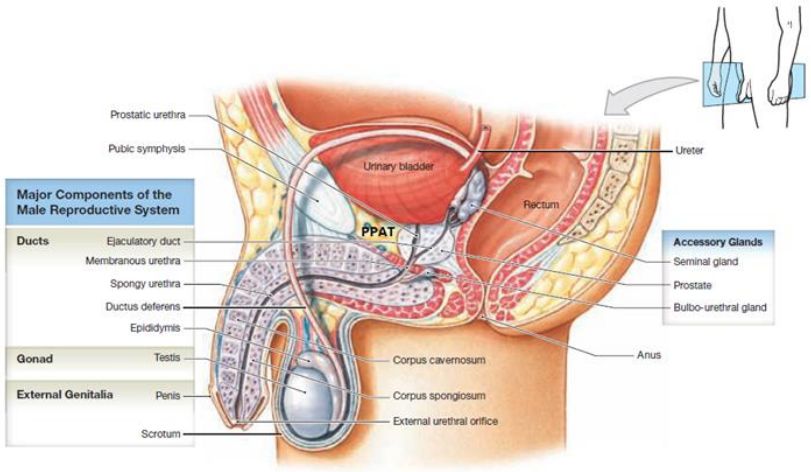


Figure 2. Anatomy of the male urogenital system. PPAT: Periprostatic AT. (adapted from Martini F., Tallitsch R. and Nath J, Human Anatomy, 2017.)

1.3 Histological description

The prostate is a compound gland, made up of 30 to 50 tubule-alveolar glands forming functional units we might call lobules[3]. A distinction is made between the acini, where prostatic fluid is produced, and the ducts where it is excreted. The glandular zones of the prostate are made up of three cell types (**Figure 3**): luminal cells, which are well-differentiated, represent the main population, secrete prostatic fluid and PSA, and are at the origin of cancers; undifferentiated basal cells are located deep down, between the luminal cells and the underlying basement membrane, and part of them are stem cells; and finally, neuro-endocrine cells, a very small population located in contact with the basement membrane and whose action is necessary for the viability and growth of luminal cells[7]. Luminal cells are androgen-dependent, and castration leads to their death by apoptosis. Conversely, basal cells are androgen-sensitive but not totally androgen-dependent, as they survive castration and are then able to reform a complete prostatic epithelium[8].

The glandular cells are separated from the fibromuscular stroma by a basement membrane. This stroma, composed of fibroblasts, myofibroblasts, smooth muscle cells, immune cells and vessels, secretes a large number of growth factors, cytokines and extracellular matrix proteins[9]. The composition of this stroma is androgen-dependent and varies with age. Stroma-epithelium interactions are essential for the physiological development of the prostate[10], but have also been shown to play a major role in the development of prostate pathologies such as BPH and cancer[9,11,12].

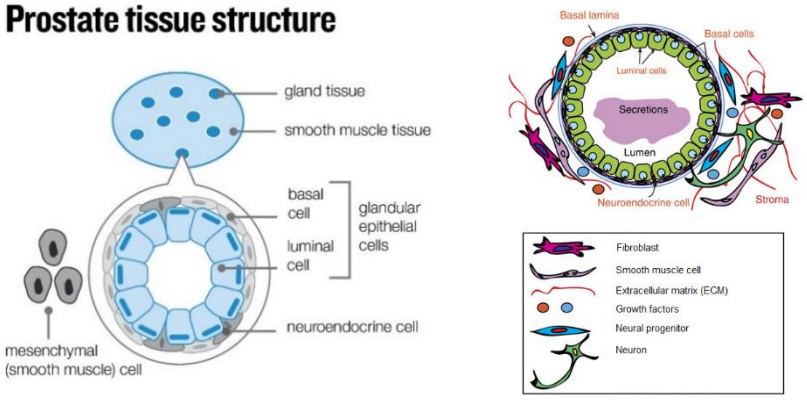


Figure 3. Cellular organization of the prostate. Left, schematic representation of the general organization of the prostate. Adapted from Prostate Cancer UK: https://prostatecanceruk.org/prostate-information/further-help/rare-prostate-cancer. Right, schematic representation of a prostate epithelium and its stroma. (from Zhang et al., Nature Communications, 2016.)

2. Epidemiology of Prostate Cancer

According to the latest epidemiological data available from World Health Organization, prostate cancer (PCa) emerged as the fourth commonly diagnosed cancer worldwide and the second most common cancer in the men from the world behind lung cancer[13]. In terms of mortality, following lung cancer, PCa is in the second place among cancer-related deaths with an estimated age-standardized incidence of 23.6/100,000 men[13]. Great disparities exist throughout the world concerning overall incidence rate which is generally higher in transitioned countries than transiting countries (**Figure 4**). and in some regions, such as Northern and Western Europe, the Caribbean, Australia/New Zealand, South America/North America, Southern Africa and Japan. Specifically, Guadeloupe of France ranked first in 2020 with estimated age-standardized incidence rates (ASR) 183.6. Bhutan ranked last with only 0.9 ASR. However, mortality rates are less variable across the world. In addition, Zimbabwe ranked the first of estimated age-standardized mortality rates in 2020 considering all the age groups.

PCa mortality has been falling steadily since the 1990s. This decline can be attributed to a number of developments: firstly, the use of PSA has made it possible to diagnose tumours at a localized stage, and therefore accessible to curative treatment[14]. Furthermore, the emergence of new therapeutic classes has expanded treatment options and extended the lives of metastatic patients. However, this also leaves significant room for non-specific mortality in these patients, given their notably high competitive morbid-mortality, especially in relation to cardiovascular issues[15,16].

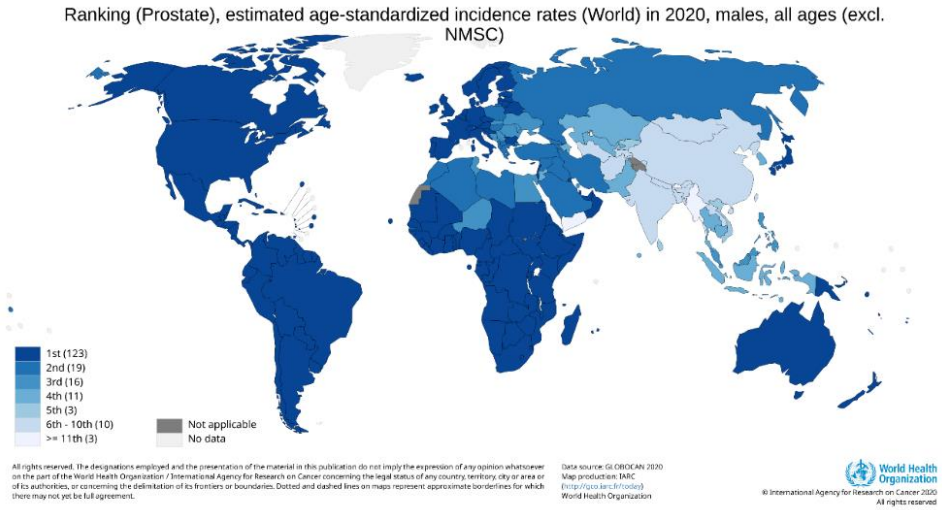


Figure 4. **Estimated age-standardized global incidence of Prostate Cancer in 2020.** (from Globocan https://gco.iarc.fr)

3. Diagnosis of Prostate cancer

Symptoms: The vast majority of PCa are asymptomatic. Urinary disorders in elderly men are most often due to BPH, which is very common in these patients and may coexist with cancer. When the tumour develops, the most common symptoms are haematuria (blood in the urine) or urinary tract obstruction. Long-distance dissemination of the tumour can cause edema of the lower limbs due to obstruction of regional lymph nodes, or bone pain due to metastases. These symptoms appear very late in the history of the disease[17].

Screening: Screening enables the PCa to be detected at an early stage. As PCa remains asymptomatic for a very long time, it is important to detect it before symptoms appear. The screening strategy mainly relies on three tests that are described in the following paragraphs[18].

PSA Measurement: The PSA level has been widely used by practitioners to screen men at risk of PCa and direct them towards histological diagnostic confirmation by prostate biopsies. The PSA threshold usually used is 4 ng/ml[19]. In the PCPT study (Prostate Cancer Prevention Trial) [20], this threshold value provides a sensitivity of 93% and specificity of 24% which is rather low[21]. In fact, there are many false positives especially in patients with prostatic infection and with BPH, which lead to an elevated PSA level[22] [23]. Moreover, certain factors can lower circulating PSA levels, making diagnosis more challenging, such as the use of medications for BPH (5α-reductase inhibitors used to decrease the synthesis of the active androgen 5α-dihydrotestosterone (DHT)), obesity, and certain drugs (aspirin, statins, thiazide diuretics)[24]. Thus, the use of the different forms of PSA such as the kinetics of PSA by analysing the rate of PSA levels rising and the age-related PSA taking the age into account would make it possible to estimate the risk of PCa more precisely. The latest studies on PSA density, calculated by the total PSA/prostatic volume ratio, show a more discriminating value of this marker compared to PSA[25,26].

Rectal Examination**:** This is a procedure conducted by a physician, where they palpate the prostate by inserting a gloved finger into the patient's rectum. This examination helps assess the volume, consistency, and texture of the prostate's surface. It is a relatively insensitive test (the tumour must already be well-developed to be palpable), but it can detect certain cancers even in the presence of a normal PSA level[27].

Complete diagnosis of PCa: The fact that PSA and rectal examination lack precision indicates the need for biopsies[17]. In this case, prostate magnetic resonance imaging (pmMRI), which has

long been used in pre-therapeutic assessments is recommended before conducting prostate biopsies with the primary objective to identify the probable location of the PCa and to conduct targeted biopsies[28]. Prostate biopsy involves the sampling of at least 12 "cores" of prostate tissue, which are then examined under a microscope to detect the presence of cancerous cells[28].The procedure is done through the rectum, where the physician inserts an ultrasound probe to visualize the prostate. The biopsy is performed using a needle guided by ultrasound. Some biopsies are performed blindly, meaning cores are taken randomly from different areas of the prostate, but an increasing number of biopsies are targeted based on predefined areas identified through MRI analysis (known as targeted biopsies)[28].

4. Prostate cancer classifications

Histological classification: PCa is an adenocarcinoma in over 90% of cases. Prof. Donald Gleason (1920-2008) described a histological score used to characterize the aggressiveness of PCa on biopsies or on the prostatectomy specimen for the first time[29]. This Gleason grade represented the degree of differentiation of cancer cells on a scale of 1 to 5. A grade of 1 corresponds to highly differentiated cells, close to healthy prostate cells and generally not very aggressive, whereas a score of 5 corresponds to undifferentiated cells with disorganized architecture and high aggressiveness. Since prostate tumours are heterogeneous, Prof. Gleason combined the most common or aggressive cell grades according to the type of histological sample to create the score: the Gleason score (initially ranging from 2 to 10). This classification was revised for the first time in 2005, in response to a number of shortcomings and the need to keep pace with advances in PCa knowledge. In 2014, the International Society of Urological Pathology (ISUP) proposed a new classification into 5 prognostic groups[30] (**Figure 5**). In particular, the ISUP score makes it possible to differentiate between tumours with a Gleason score of 7 according to majority grade. Epstein et al. confirmed the prognostic value of this new classification in a cohort of over 20,000 patients treated with total prostatectomy and 5,000 patients treated with radiotherapy. The risk of biological recurrence at 5 years after initial treatment varied with ISUP score, from 4% for ISUP 1 scores to 74% for ISUP 5 scores[31]. For over 60 years, the Gleason score has remained the most relevant prognostic criterion in the management of PCa. Several tests (Oncotype, Prolaris and Decipher) based on different molecular signatures could help predict the aggressiveness of PCa and thus aid therapeutic decision-making. However, the data in the literature are based on studies with a low level of evidence, so these tissue biomarkers are still under evaluation[32].

ISUP Score	Gleason Score
Group 1	6 (3+3)
Group 2	7 (3 majority)
Group 3	7 (4 majority)
Group 4	8 (4+4, 3+5, or 5+3)
Group 5	9 or 10

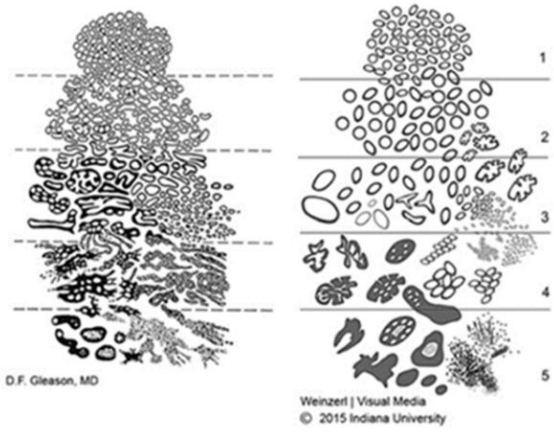


Figure 5. Table of ISUP 2016 prognostic groups and figure of histological aspects of prostatic adenocarcinoma. Original scheme by Dr. Gleason (left) and scheme modified at the 2015 ISUP conference (right). (adapted from Epstein et al., American Journal of Surgical Pathology, 2016.)

Prognosis classification: Estimating the prognosis of a disease is a fundamental step before considering its treatment. In particular, it enables the relationship between the benefits and risks of treatment to be assessed. This step is all the more important in the management of PCa because the prognosis can vary from an indolent disease requiring no first-line treatment to an aggressive disease that is not life-threatening. The Gleason score and PSA level are relevant parameters for estimating the prognosis of PCa that is presumed to be non-metastatic. Similarly, the digital rectal examination provides information on the tumour stage of the PCa according to the TNM (Tumour Node Metastasis) classification (**Figure 6**). These 3 clinic-biological elements were combined in a prognostic classification of the risk of biological recurrence by D'Amico et al in 1998[33]. This classification made it possible to create 3 prognostic groups:

a) Low-risk cancer:
- T1 - T2a And PSA ≤ 10 ng/ml And Gleason ≤ 6
- Biological recurrence-free survival greater than 75% at 5 years after treatment.

b) Intermediate-risk cancer:
- T2b Or PSA 10 - 20 ng/ml Or Gleason = 7
- Biological recurrence-free survival between 50 and 75% at 5 years after treatment

c) High-risk cancer :
- T2c - T3 Or PSA > 20 ng/ml Or Gleason ≥ 8
- Biological recurrence-free survival of less than 50% 5 years after treatment

This classification is still widely used today, despite its limitations such as the lack of distinction between ISUP 2 and 3 tumours and also lack of integration of MRI data and targeted biopsies,

despite their recognized added value in risk stratification[34]. In recent years, other classifications have been proposed to compensate for the shortcomings of D'Amico's classification. The most well-known classification is the one introduced by Zumsteg et al, which established the concept of favorable and unfavorable intermediate risk[35]. This classification, developed based on patients treated with radiotherapy, was subsequently validated in surgical cohorts[36]. More recently, a classification of the risk of progression taking into account information from biopsies targeted on MRI lesions has been reported[34].

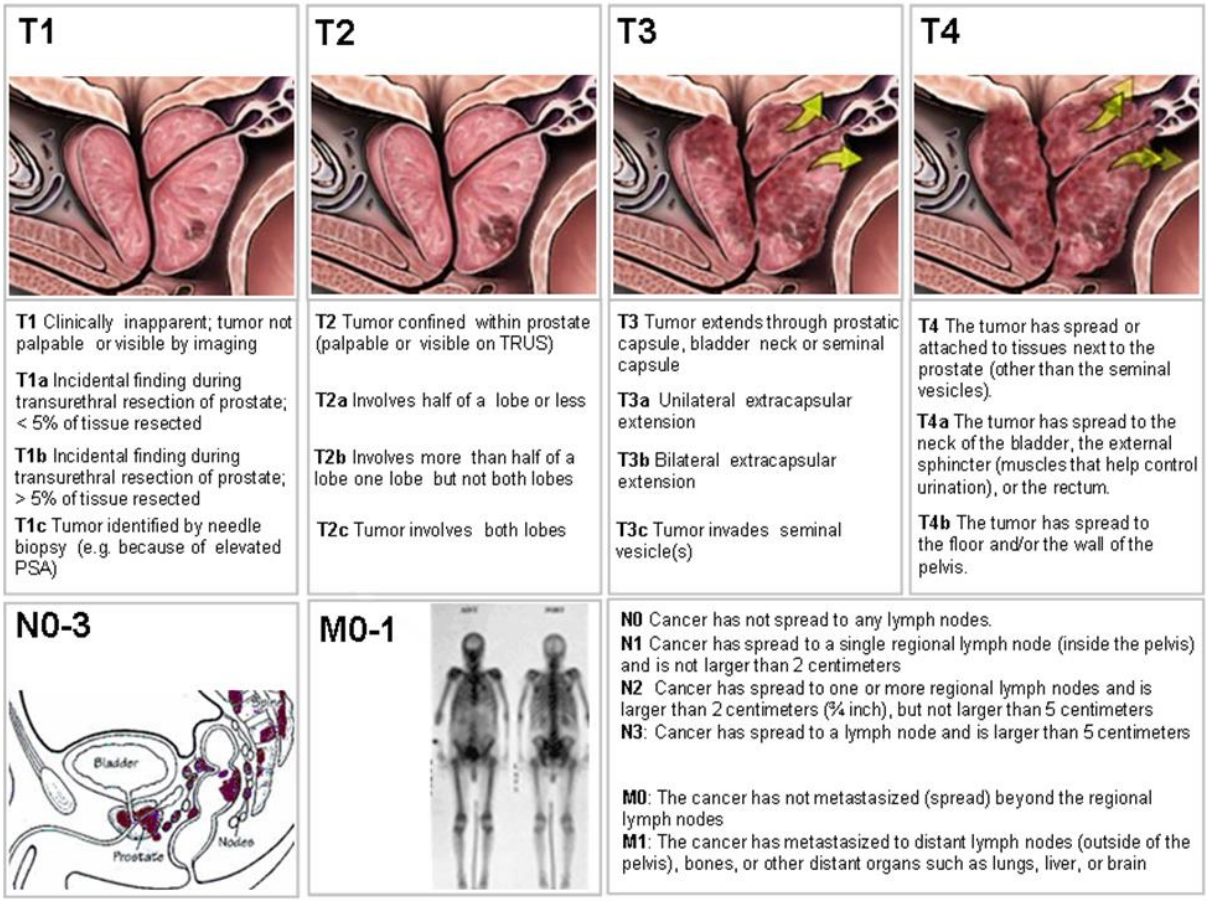


Figure 6. **TNM classification of prostate cancer**. The original and primary source for this information is the AJCC Cancer Staging Manual, Eighth Edition (2017), published by Springer International Publishing.

5. Prostate cancer models

5.1 In vitro models

Traditional two-dimensional (2D) cell culture models have long been utilized to study PCa biology and to evaluate potential therapeutic interventions. While these models have provided valuable insights, they often fail to recapitulate the complex three-dimensional (3D) architecture and microenvironment of prostate tumours, limiting their ability to mimic the *in vivo* behaviour of cancer cells accurately.

In recent years, the beginning of advanced technologies and the growing appreciation for the importance of tumour microenvironment components have encouraged the emergence of more sophisticated and physiologically relevant 3D models for PCa research. These 3D models offer the potential to bridge the gap between conventional 2D cultures and *in vivo* animal models, providing a platform that more faithfully represents the intricate interactions between cancer cells and their surrounding stromal elements.

This chapter aims to explore and compare the utility of both 2D and 3D models for investigating PCa pathogenesis, tumour progression, and therapeutic responses. By investigating these models in parallel, a comprehensive understanding of their respective strengths and limitations can be gained, leading to improved translational relevance and enhanced drug discovery efforts.

2D models

In 2D cell cultures, cells are grown on plastic flat surfaces such as tissue culture dishes or plates, where they adhere and form a monolayer. It is still the most frequent model for studying cellular and molecular mechanisms, drug response and high-throughput screening based on its multiple advantages such as highly reproducibility and easy handling[37].

PCa cell lines can be categorized by different characteristics based on their site of origin, histopathology and androgen dependency. Here, we focus on the classification based on their androgen dependency. Thus, PCa cells lines could be into differentiated into three primary groups mainly: androgen-dependent (AD), androgen-independent but androgen-sensitive (AI/AS), and androgen-independent (AI) cell lines. The AD cell lines rely on androgens for their growth. LNCaP is the classical representative, and PC346C and LAP-C4 also belong to this category[38]. In contrast, AI/AS cell lines are responsive to androgens whereas androgens are not necessary for their growth. This group includes several cell lines, such as MDA PCa 2a, MDA PCa 2b, 22RV1, VCaP, DuCaP, and CWR-R1[38]. The AI cell lines that neither require

androgens nor are affected by their presence comprises well-known PCa cell lines like PC-3 and DU145, along with 1013 L, UM-SCP-1, NCI-H660, MDA PCa 1, PSK-1, as well as LNCaP derivatives LNCaP-C4 and LNCaP-C4-2[38].

An exception to the general behavior is observed in the ARCaP cell line, where androgens repress cell growth and it is not included in this chapter[38].

In most cases, these cell lines behave aligns with the presence or absence of androgen receptor (AR) expression at both mRNA and protein levels (**Table 1**). Specifically, AD cells typically exhibit significant AR expression, while AI cells demonstrate either negligible or very weak AR expression. Meanwhile, AR alteration such as mutation and variant should be considered carefully while choosing the models due to their crucial role in drug resistance and disease progression (see the chapter 7) (**Table 1**).

Cell line	Origin	AR			Classification
		expression	mutation	splice	
LNCaP	lymph node metastasis from patients	AR positive with mutation	T878A	AR-V7 variant	
PC346C	mouse xenograft of untretaed primary tumor patient	wild type			
LAPC4	mouse xenograft of lymph node metastasis patient	wild type			AD
MDA PCa 2a	bone metastasis from patients whose cancer exhibited androgen-independent growth	AR positive with mutation	L702H; T878A		
MDA PCa 2b	bone metastasis from patients whose cancer exhibited androgen-independent growth	AR positive with mutation	L702H; T878A		
22Rv1(CWR22RV-1)	mouse xenograft of human primary prostatic carcinomas	AR positive with mutation	H875Y	AR-V7 variant	
VCaP	mouse xenograft of a a patient with hormone refractory prostate cancer and spin cord metastatic	wild type		AR-V7 variant	
DuCaP	mouse xenograft of spin cord metastatic patient	wild type		AR-V7 variant	
CWR-R1	Recurrent CWR22 human xenograft tumors that were harvested from nude mice 140-160 days after castration	AR positive with mutation	H875Y	AR-V7 variant	AI/AS
PC-3	bone metastasis from patients	AR negative			
DU 145	brain metastasis from patients	AR negative			
1013 L	a rare non-acinar subtype of prostate carcinoma from patients	AR negative			
UM-SCP-1	primary squamous cell carcinoma of prostate cancer from patients	AR negative			
NCI-H660	Lymph node metastasis extrapulmonary small cell carcinoma originating in the prostate gland	AR negative			
MDA PCa 1	Ascites from patient with metastatic disease origin	AR negative			
PSK-1	primary squamous cell carcinoma of prostate cancer from patients	AR negative			
LNCaP-C4	mouse xenograft of LNCaP co-incubated with fibroblasts	AR negative			
LNCaP-C4-2	mouse xenograft of LNCaP-C4	express mRNA but not protein			AI

Table 1. **Prostate carcinoma cell lines classification, origin and their AR status**. (adapted from Sailer et al., Nature Reviews Urology, 2022.)

Until now PCa cell lines are scarce compared with other common malignancies. For example, the Cancer Cell Line Encyclopedia comprises 83 breast cell lines, while only 13 prostate cell lines are included[39]. In my thesis, we chose to use LNCaP, 22RV-1, DU145 and PC3 respectively from these 3 groups. These cell lines are recognized as models for castration-resistant prostate cancer (CRPC) despite their response to androgens[40] and they are all derived

from metastatic patients. Consequently, they serve as valuable representations of advanced and higher-grade PCa.

Whereas it should be noticed that 2D cell lines do not capture patient tumour heterogeneity and do not recapitulate key characteristics of primary tumour, they have undergone the transcriptomic alterations due to the adaption to the *in vitro* cell culture environment, possibly deviating from a complete representation of the primary tumours' properties[41].

3D models

Three-dimensional (3D) culture systems have emerged as powerful platforms for studying tumorigenesis and drug response in PCa without the need for *in vivo* experiments by incorporating various aspects of the tumour microenvironment and architecture, such as nutrient gradients, hypoxia, pH, and interstitial pressure[42,43]. 3D models could be categorized into scaffold-free and scaffold-based systems, encompassing monocellular and multicellular tumor spheroids, organoids, tissue slices, and tumor-on-a-chip systems[37].

Spheroids

Cell spheroids or tumour spheroids formation could be achieved in the absence of extracellular matrix support by using low-adhesion plates, suspension cultures in appropriate devices, or the hanging-drop technique. These methods lead to cellular aggregation rather than attachment to solid surfaces[44,45].

Various PCa cell lines and patient-derived cells were investigated for their ability to form spheroids. Specific cell population $CD49b^{hi}CD29^{hi}CD44^{hi}$cells, displayed tumour-initiating characteristics, implying their potential in tumorigenicity, clonogenicity, migration, and invasion.

One study introduced "tumor histoids" by co-culturing stromal cells with epithelial cells such as fibroblast spheroids with the addition of PC3 cells, resulting in structures resembling tumour tissue architecture[46]. Another model employed a two-layer microfluidic system to mimic metastatic PCa, incorporating multiple cell type including fluorescently labeled PC3 cells, osteoblasts, and endothelial cells to replicate the tumor microenvironment in bone[47]. The proliferation rates of PC3 cells in this model closely resembled *in vivo* PCa cell growth in bone metastasis compared to classical 2D culture[47].

The formation of patient-derived spheroids was found to be dependent on the Gleason score, with higher scores showing reduced efficiency[48]. Larger spheroids exhibited central necrosis, indicating hypoxia, which influenced their properties and heterogeneity and demonstrated the role of size in the model[48].

However, there exist some limitations for each of these models. For example, there is no vasculature in monocellular and multicellular tumour spheroids. And tissue availability is restricted in patient-derived spheroid[37].

Organoids

Patient-derived organoids (PDOs) could be derived from healthy human or murine prostate tissues, as well as primary prostate tumours or metastatic lesions[49]. PDOs preserve the molecular alterations *in vivo*, which renders them an excellent model for personalized *in vitro* research[50] especially in CRPC where alteration occur due to selective pressure from various therapies[51]. PDOs exhibited the ability to reproduce the molecular mutational landscape resembles that of primary prostate with a prevailing occurrence of alterations in the TP53 and RB tumor suppressor pathways[51]. Thus, PDOs hold promise for discovering therapeutic targets and validating them in a high-throughput approach in PCa research.

However, establishing continuously propagated organoid lines from metastatic PCa is challenging, with a success rate of only about 15-20%[51]. The improved selection strategy of isolate tumour cells from the contaminating non-malignant cells could be helpful to increase the success rate. Recently, Clémentine Le Magnen's group, succeeded in developing a new organoid model, P20-11-Lg, obtained from a patient with metastatic hormone-naïve disease which recapitulates phenotypic and molecular traits commonly observed in PCa and also responds to androgen deprivation[52].

Scaffold-based systems

Spheroid and organoid models can be extended to scaffold-based systems using extracellular matrix (ECM)-like gels such as matrigel, collagen, and alginate. These gels made with hydrophilic polymers material promote spontaneous aggregation of prostate cell cultures with cell-cell and cell-matrix interactions, making them valuable for PCa research[53,54]. Recently, other synthetic or semi-synthetic matrices, such as hyaluronic acid-modified polyethylene glycol (HA-PEG) with the tripeptide RGD, have been successfully employed for cultivating PDXs-derived PCa cells[55]. These systems have increased resistance to chemotherapy compared

to traditional 2D cell cultures, which can better mimics the actual tumour regression *in vivo*. And they recreated the vascularization found in prostate tumours, making it capable to study the effects of anti-angiogenic therapies[56]. In addition, prefabricated scaffolds made from natural polymers such as medical-grade polycaprolactone can be engineered to simulate osseous metastasis, offering a mineralized model platform for studying PCa growth in bone and evaluating responses to therapies for metastasis CPRC[57,58,59]. Moreover, they have been utilized to cultivate primary patient-derived cancer-associated fibroblasts (CAFs), mimicking microenvironment around prostate epithelial cells[60].

Tissue cultures and microfluidic platforms

Tissue slice models have been successfully established by using samples from patients who undergo radical prostatectomy[61] or transurethral resection of the prostate, as well as PCa bone metastases[62,63]. One of the remarkable advantages of tissue slice cultures over primary cell cultures and traditional 2D or 3D models is their ability to preserve the original tumor's morphology and microenvironment. The intricate interactions between cancer cells and stromal components are retained, offering a more comprehensive representation of *the in vivo* tumor environment in these models[61,64]. The thin, precision-cut tissue slices and their transplantation under the renal capsule of immunodeficient mice, followed by androgen deprivation therapy (ADT) and analysis of the recovered tissue slices, has been successfully generated[61].

However, the limitation of these models exists as a result of lack of enough samples available after tissue processing for diagnostic purposes especially in metastatic and castration-resistant specimens. To address the challenge, microfluidic platforms have been employed to cultivate tissue slices. Fluid flows through micrometer-sized domains in these platforms, facilitating the culture of micro-dissected tissue sections from surgical or biopsy samples. An intricately optimized cancer-on-chip platform was developed to effectively preserve the viability and continuous proliferation of prostate patient-derived xenograft (PDX)-derived tissue slices over 7 days[65]. Micro-dissected tumor tissue has been demonstrated to better preserve tumor cell viability and proliferation compared to tissue slice cultures[66]. Combining microfluidic devices with micro-electro-mechanical systems allows the integration of multiple components of the tumor environment[67].

5.2 In vivo models

a. Tumour xenografts

Tumour xenograft animal models play a pivotal role in facilitating translational research by complementing *in vitro* model systems. These models involve the engraftment of PCa cells or tissues into experimental animals, typically mice, and are categorized based on the site of implantation as subcutaneous, subrental, or orthotopic xenograft model[37].

Subcutaneous xenografts

Subcutaneous xenografts are established by either injecting cultured PCa cells, or co-injecting cultured these cells along with stromal cells directly into the mice under skin[68,69]. These models are valuable for basic research but have limited predictive ability for drug efficacy in clinical settings due to their high homogeneity, transcriptome alterations, and lack of human tissue architecture[70,71]. Nevertheless, subcutaneous xenograft experiments exhibit key characteristics of *in vivo* tumour growth, including androgen-dependent and androgen-independent proliferative responses, providing valuable data beyond *in vitro* cultures[37].

Subrenal xenografts

Subrenal grafting represents a procedure wherein PCa cells are merged with rat urogenital sinus mesenchymal cells, followed by the transplantation of this amalgamated tissue beneath the kidney capsule of immunodeficient mice. The primary objective of this approach is to examine the proliferative behaviour and potential of putative basal-like prostate stem cells derived from both non-malignant mouse prostate and mouse PCa tissues in generating prostatic tissue[72].

Orthotropic xenografts

Orthotopic xenografting involve the injection of malignant cells or the transplantation of tumours into the same anatomical location, in this case, it can represent the prostate in its actual pathophysiological[73]. Through the faithful recapitulation of the organ-specific microenvironment, these models facilitate in-depth analyses concerning tumour-stromal interactions, which play a crucial role in the development of next-generation cancer therapies. Furthermore, these models allow for the monitoring of tumour progression and the development of metastases[74,75,76].

Patient-derived xenografts

Patient-derived xenografts (PDXs) involve direct transplantation of freshly isolated tumour tissue from a patient's primary or metastatic lesion into mice. PDX models aim to retain the original tumour's mutational profile and heterogeneity, offering potential for personalized treatment[77]. More than 300 PCa PDXs across laboratories of the world has been established including a multitude of PDXs representing AR positive castration-sensitive PCa (CSPC) and CRPC[78] . These models have the same limitations as patients-derived material such as long time period and complex handling process and also tumour tissue availability.

Meanwhile, further endeavours are warranted to enhance their utilization in research, such as the establishment of novel PDXs for less represented PCa subtypes, integration of data from diverse cohorts, and facilitation of collaborative efforts among research laboratories[79].

Genetic models

Genetic mouse models, also known as genetically engineered mouse models (GEMMs), are mice that have been genetically modified to carry specific genetic mutations or alteration. Plenty of GEMMs with phenotypic similarities to human PCa have been reported such as the TRAMP (transgenic adenocarcinoma of the mouse prostate), CDCP1 (UB domain-containing protein 1), PTEN (Phosphatase and TENsin homolog) and Hi-Myc models, offering valuable opportunities to study different stages of PCa progression in mice[80,81]. However, the use of these models could be time consuming and costly and ethical issues should also be considered.

b. Drosophila model

Drosophila melanogaster, commonly known as the fruit fly, has emerged as a prominent genetic model organism in cancer biology due to its numerous advantages such as short life cycle, high offspring production, well-characterized anatomy, and abundant genetic tools[82]. Moreover, Drosophila exhibits minimal redundancies and maintains conservation of fundamental biological mechanisms and signalling pathways, which has facilitated the identification and characterization of several intracellular signalling pathway regulators and new genes associated with tumorigenesis and the tumour microenvironment[83,84].

Drosophila model has been used for investigation of early prostate carcinogenesis. Studies have shown that the activation of Ras/MAPK and PI3K/AKT/mTOR pathways in Drosophila's prostate-like gland leads to the extrusion of basal epithelial cells, mirroring the initial stages of tumour invasion. This finding may have relevance to human PCa[85]. Moreover, PTOV1 (Prostate tumour overexpressed gene 1 protein) was found as a negative regulator of Notch signalling in

PCa and it was confirmed in drosophila[86]. Moreover, Drosophila cell line was used to perform the genome-wide RNA interference screen to identify new regulators of the AR[87]. These studies shed light on the importance of Drosophila as a complementary model in elucidating PCa development.

Notably, Drosophila model in PCa research also has limitations such as lacking of an equivalent of AR. Additionally, Drosophila cannot fully replicate the complexity of the prostate microenvironment, limiting its ability to model certain aspects of PCa progression[82].

6. Prostate cancer treatments

Prostate cancer treatment options are diverse and are chosen based on individual factors such as cancer grade and stage, patient age, overall health, and more. The available treatment options include active surveillance, surgery (prostatectomy), radiotherapy, High-Intensity Focused Ultrasound (HIFU) Therapy, Hormone therapy, Chemotherapy and Vaccination.

Active surveillance involves closely monitoring the cancer's progression through regular check-ups, PSA tests, and biopsies. Currently, medical guidelines recommend active surveillance for patients diagnosed with low-risk localized prostate cancers (characterized by being T1-T2 stage, PSA levels below 10, and a Gleason score of 6). Under active surveillance, these patients are regularly monitored through periodic PSA tests every 3 to 6 months, digital rectal examinations every 6 to 12 months, and follow-up biopsies performed between 3 and 24 months after the initial biopsy. This approach allows healthcare providers to closely monitor the cancer's progression and determine if any treatment intervention becomes necessary over time[28].

Surgery stands as one of the standard treatment options for localized prostate cancers that are confined to the prostate gland. A **radical prostatectomy** is commonly performed, involving the complete removal of the prostate and surrounding tissues, including the seminal vesicles. In modern practice, this operation is often conducted laparoscopically, with the assistance of a surgical robot, offering precise and minimally invasive approaches[28]. Clinical studies have demonstrated the effectiveness of prostatectomy in patients diagnosed with localized cancer at intermediate or high risk of metastasis. Randomized trials have shown that prostatectomy leads to significant improvements in both overall and specific survival outcomes[88]. However, despite its success in treating localized prostate cancer, prostatectomy is associated with notable side effects such as urinary incontinence, sexual impotence, and sterility that can impact the quality of life for patients[89].

Radiotherapy employs high-energy beams to target and destroy cancer cells. It can be delivered externally (external beam radiotherapy) or internally (brachytherapy), depending on the cancer stage and patient characteristics. External radiotherapy involves precisely targeted irradiation of the tumour region. While it has comparable side-effects to prostatectomy, it also carries the risk of secondary tumour development[90]. Brachytherapy involves placing radioactive iodine seeds directly into the prostate. These seeds emit radiation locally over a few millimetres. Brachytherapy is primarily recommended for low-risk localized cancers, where it has demonstrated remarkable efficacy[91]. Radiotherapy is often used as a first-line treatment combined with hormone therapy for localized, low-risk cancers. Additionally, radiotherapy is employed in cases where cancer has spread locally or as a treatment for cancer recurrence after prostatectomy. Furthermore, it can be used to alleviate the symptoms of highly advanced cancers[28].

High-intensity focused ultrasound (HIFU) treatment is a potential option for elderly patients or those with significant co-existing health issues that may render them unsuitable candidates for surgery. It is specifically considered for patients diagnosed with localized PCa at low risk of progression[28]. However, the use of HIFU treatment varies across different countries, and a clear consensus is lacking. This is primarily due to the scarcity of randomized controlled trials[92]. HIFU is precisely targeted at the prostate, leading to its destruction along with the tumour cells and the induction of secondary fibrosis. Compared to prostatectomy, HIFU is considered less invasive. Nevertheless, it is essential to note that the side effects associated with HIFU treatment are similar to those seen in prostatectomy, including urinary incontinence and erectile dysfunction[93,94].

Hormone Therapy aims to lower androgen levels or block their effects, as androgens fuel PCa growth, which is the major medical treatment used for PCa. **Chemotherapy** uses chemical drugs to kill or inhibit the growth of rapidly dividing cancer cells. It is typically used for advanced PCa or when other treatments have failed. These therapies will be detailed in chapter 7 with a special emphasis on hormone therapy since the resistance to this treatment is the main focus on my PhD.

Vaccination: PCa vaccines, such as sipuleucel-T, stimulate the immune system to target PCa cells, which can slow cancer growth[95].

The selection of the most appropriate treatment depends on various factors, including the cancer's aggressiveness, extent of spread, the patient's overall health, and personal preferences.

Recently, one 15-year follow-up study showed that there were no significant differences in prostate cancer-specific mortality among the groups receiving active monitoring, prostatectomy, or radiotherapy. The study suggests that the choice of treatment for localized prostate cancer should consider the balance between benefits and potential harms associated with each treatment. The results emphasize the importance of personalized treatment decisions for patients[96]. Thus, a multidisciplinary approach involving the collaboration of urologists, radiation oncologists, medical oncologists, and other specialists is essential to develop a tailored treatment plan for each patient.

7. Hormonal treatment and mechanisms of its resistance in PCa

The AR signalling pathway and the intricate process of androgen biosynthesis are pivotal components in the development and progression of normal prostate and also PCa. The AR, a nuclear transcription factor, mediates the effects of androgens on prostate cell growth, differentiation, and survival. Furthermore, the biosynthesis of androgens, primarily from the testes, adrenal glands, and even within prostate tumour tissues, sustain AR activation and the proliferation and maintenance of prostate cells. This is evidenced not only by the major growth of this organ during puberty but also by the fact that men with congenital 5α-reductase deficiency or treated with 5α-reductase inhibitors (treatment of BPH) show prostatic regression and reduced PSA production[96,97]. The two next chapters (7.1 and 7.2) will elucidate the crucial role of AR signalling and androgen biosynthesis in PCa, shedding light on their intricate interplay and implications for therapeutic targeting.

7.1 Androgen synthesis by the hypothalamic-pituitary-testicular (HPT) axis

Testosterone is the main circulating male sex hormone, synthesized mainly by Leydig cells in the testes (90%) and in some extend by adrenal glands (10%) (**Figure 7**). The production of testosterone is tightly regulated by a complex interplay of hormones known as the hypothalamic-pituitary-testicular (HPT) axis. The HPT axis is a sophisticated endocrine system that involves communication between the hypothalamus, pituitary gland, and the testes. The process begins with the hypothalamus, a region in the brain that produces gonadotropin-releasing hormone (GnRH). GnRH serves as the initial trigger for the HPT axis by stimulating the pituitary gland's release of luteinizing hormone (LH). Of particular significance for testosterone production is LH, which binds to specific receptors on the Leydig cells within the testes. This binding event stimulates the Leydig cells to synthesize and secrete testosterone into the bloodstream or be used by prostate cells. The tight regulation of testosterone production

within the HPT axis is achieved through a negative feedback loop. As testosterone levels rise in the bloodstream, the hypothalamus and pituitary gland sense this increase and subsequently reduce the release of GnRH and LH. Conversely, when testosterone levels decline, the HPT axis is stimulated to increase the production of these hormones, thereby maintaining testosterone homeostasis[98]. Also, adrenocorticotropic hormone (ACTH), secreted by the pituitary gland, stimulates androgen synthesis in the adrenal gland[99] **(Figure 7**).

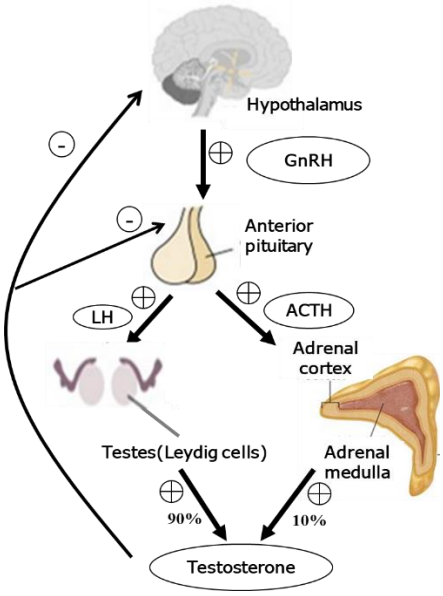


Figure 7. **Schematic representation of the hypothalamic-pituitary-testicular axis**. ⊕ = stimulates; ⊖ = inhibits; GnRH = gonadotropin-releasing hormone; LH = luteinizing hormone; ACTH =Adrenocorticotropic hormone, adapted from S Hiller-Sturmhöfel et al., Alcohol Health Res World, 1998

Understanding the intricacies of the HPT axis and testosterone production is crucial in the context of PCa treatment.

7.2 Androgen Receptor (AR) function and activity

AR belongs to steroid hormone nuclear receptor family and serves as a nuclear ligand-activated transcription factor. The coding gene for AR is situated on the X chromosome at the Xq11-Xq12 locus. AR comprises four major structural domains: the N-terminal transactivation domain (NTD) comprising, the central DNA-binding domain (DBD), and the C-terminal ligand-binding domain (LBD) and the hinge region[100]. AR binds both testosterone and DHT, but with greater affinity for DHT[101]. Upon interaction with the bioactive androgens (testosterone and DHT), AR forms a complex that functions as a transcriptional activator. In the absence of androgens, AR remains in an inactive state in the cytoplasm combined with heat shock proteins (HSPs). Upon androgen binding, a conformational alteration occurs in the AR, leading to the dissociation of HSPs from AR. Subsequently, the AR dimers translocate into the

nucleus, where it binds to androgen responsive elements (AREs) present on the genomic DNA. At the same time, factors of the transcriptional machinery are recruited, including chromatin remodelling complexes (SWI/SNF), factors with histone acetyl transferase activity (e.g. CBP), coactivators (e.g. SRC) and RNA polymerase II (PolII)[102]. The chromatin is remodelled, allowing for the assembly of a fruitful transcriptional initiation complex leading to the activation of specific AR targeted genes such as for example KLK3, FKBP5 and TMPRSS2[103] that promote cell growth and differentiation[104,105] (**Figure 8**).

Meanwhile, a lot of other signalling pathway including Wnt signalling, growth factor receptor signalling, MAPK signalling and cytokine signalling have been shown to modifyAR signalling even without androgen or in the presence of a small quantity of androgens (**Figure 8**). Firstly, in Wnt signalling pathway, the β-catenin protein could promote androgen signalling through DNA binding of AR, AR gene is also a direct target of the β-catenin coactivator LEF-1/TCF[106]. Secondly, several growth factors, such as insulin-like growth factor (IGF)-1, keratinocyte growth factor (KGF) and epidermal growth factor (EGF), were found to increase the transactivation potential of AR[107]. Binding of these ligands to the receptor tyrosine kinases (RTK) triggers the activation of the phosphatidylinositol 3-kinase (PI3K) and subsequently phosphorylation of phosphatidylinositol (3,4,5)-trisphosphate (PIP3) which then activates Akt kinase and further increases transcriptional activity of AR[108]. The PI3K/Akt signal transduction pathway is negatively regulated by the phosphatase PTEN which has been reported to negatively regulates AR stability[109,110]. Thirdly, the interaction between tumour necrosis factor alpha (TNFα) and its cell surface receptor results in the activation of IκB kinase (IKK). This activation leads to the phosphorylation and subsequent degradation of IκB, a pivotal inhibitor of the nuclear factor-kappa B (NF-κB) pathway. Additionally, TNFα-mediated signalling pathway could induce the activation of the transcription factor c-Jun by means of the c-Jun N-terminal kinase (JNK) pathway[102]. A reciprocal inhibitory association exist between AR and the activated JNK and NF-κB signalling pathway[111]. Finally, the mechanisms underlying the activation of AR induced by interleukin-6 (IL-6) involves both the activated mitogen-activated protein kinase (MAPK) pathway and the signal transducer and activator of transcription 3 (STAT3) pathway[112,113].

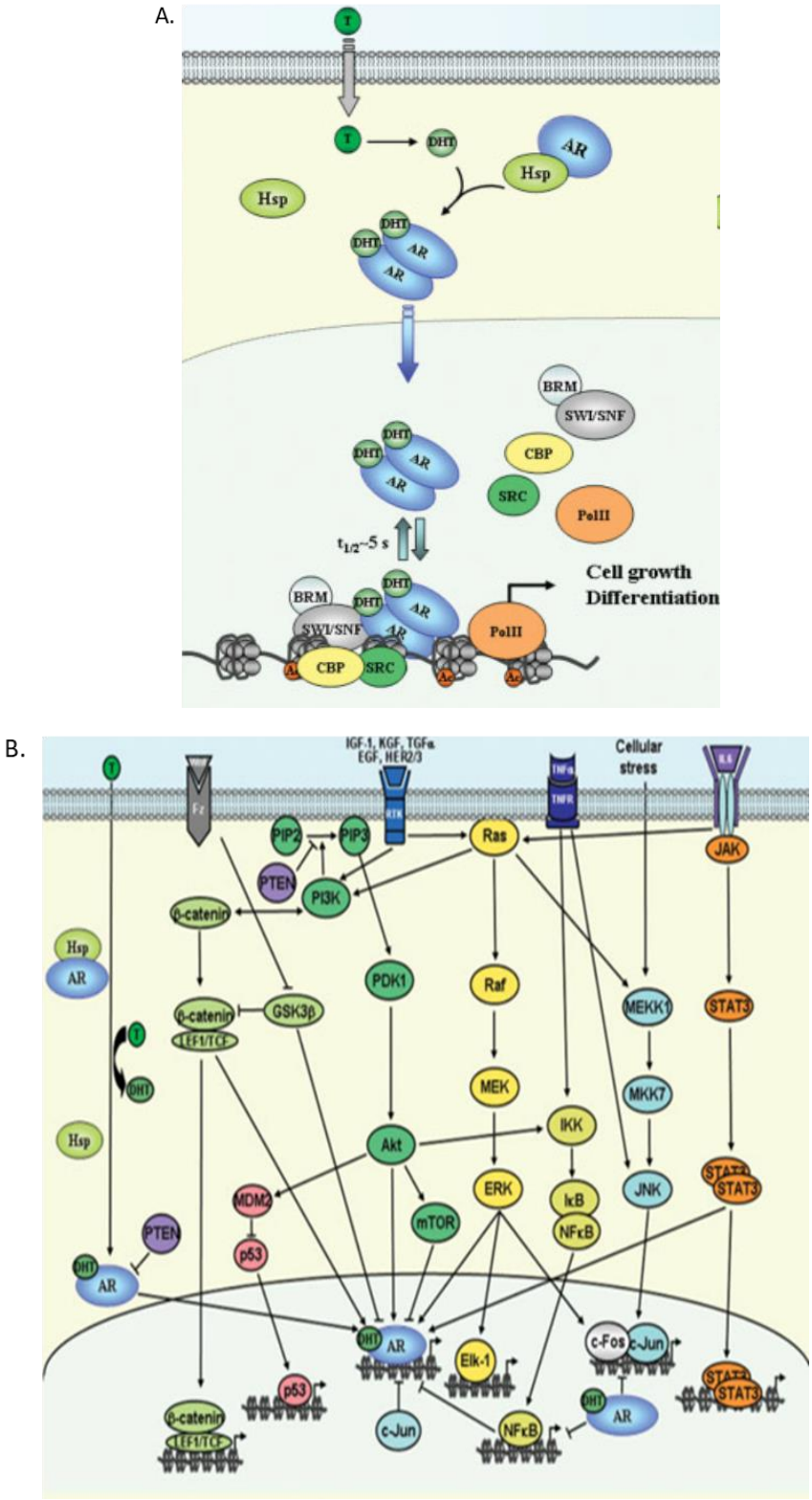


Figure 8. **Androgen receptor (AR) action model (A) and major signalling pathways interacting with AR in Prostate cancer (B).** Adapted from Mari Kaarbø et al., Bioessays. 2007

7.3 First generation hormonal treatment: androgen deprivation therapy (ADT)

C. Huggins demonstrated that the PCa was hormone-dependent, leading to the establishment of androgen suppression as the fundamental principle in treating metastatic and also locally advanced PCa[114]. Surgical castration by removal of the testicular pulp which is responsible for the production over 90% of circulating testosterone, effectively reduces the secretion threshold of testosterone below 50 µg/ml, where castration was considered to be achieved[115]. However, its use has decreased significantly due to the advent of more effective and less invasive treatments for PCa. The surgical castration was gradually replaced by chemical castration which was achieved by blocking the hypothalamic-pituitary-testis feedback system with LHRH (Luteinizing Hormone-releasing Hormone) analogues due to their comparable efficacy and side effect caused by surgical castration[116]. The first LHRH analogue was synthesized by A Schally and R Guillemin (Nobel Prize in Medicine and Physiology 1977) to induce androgenic suppression[117].

Currently, the available LHRH agonists including leuprolide, goserelin, triptorelin, and histrelin require monthly to yearly administration via injection or implantation. These agonists disrupted hypothalamic–pituitary–testicular axis and reduced testosterone production by triggering an initial release of luteinizing hormone and then downregulation of LHRH receptors in the hypothalamus[118]. However, the testosterone suppression typically only occurs within 10–20 days after administration but a significant number of patients treated with LHRH agonists fail to achieve castrate levels of testosterone[119].

Moreover, there is an initial release of luteinizing hormone in the first 72h which transiently increase testosterone and PSA levels[120]. This phenomenon is named biochemical flare and can induce several side effects such as spinal cord compression, bladder outlet obstruction and even death[121,122]. Subsequently, LHRH antagonists were developed with rapid chemical castration and less risks for cardiovascular diseases as for LHRH agonists[123,124,125,126.] The approach by surgical or chemical castration represents the first-line hormone therapy, also be known as **androgen deprivation therapy (ADT).** Due to the evolving understanding and usage of different treatment approaches over time, the addition of anti-androgen medications to block the androgens synthesis from adrenal gland and the action of androgens by blocking the AR (described in the next chapter 7.5) combining ADT has become a common practice in more recent years and recommended by Current EAU guidelines [127,128].

7.4 Mechanisms of resistance to first generation hormonal treatments

Although ADT initially provides a period of remission, in the vast majority of cases, the cancer eventually returns and is then referred to as castration-resistant PCa (CRPC)[129]. In my thesis manuscript, the term CRPC therefore defined the patients that are resistant to this fist-line treatment. Several molecular mechanisms have been described to explain castration resistance to this first-line of treatment, especially the influence of the presence of other sources than the testis of active androgens or androgen precursors which will be described in this chapter. Meanwhile, the mechanisms also involves the modification of AR receptor and AR activation independently of ligand binding, which will be described in chapters 7.6.

a. The role of adrenal-derived androgens in CRPC

Most of CRPC remains androgen dependent and partially activated by intracrine androgen synthesis via androgen precursors from adrenal gland or tumour microenvironment or inside the tumour. Potential androgens DHT remain detectable in castrated patient as ADT is not able to remove the influence of extra-gonadal androgens. The intra-tumoral conversion of extra-gonadal especially adrenal androgen precursors into active androgens has been universally recognized as the primary source of residual intra-tumoral androgens[130]. The adult human adrenal gland synthesizes various adrenal androgen precursors, such as DHEA and its sulphate (DHEA-S), 5-androstenediol and its 3-sulphate, androstenedione, and 11β-hydroxy androstenedione contributing to the pool of precursor molecules[131,132,133,134,135,136,137,138]. Among these, DHEA-S, as the predominant serum steroid, exhibits an overwhelming abundance compared to all other circulating steroids[139]. These precursors could be readily metabolized to DHT via a series of enzymes within prostate tissue or cancer cells[139,140]

b. Androgen metabolism pathways in adrenal gland and PCa cells

Within adrenal gland, cholesterol is transferred from the outer mitochondrial membrane to the inner mitochondrial membrane mediated by the steroidogenic acute regulatory protein (StAR). Thus, *de novo* sex steroidogenesis starts (**Figure 9**). Then, cholesterol undergoes conversion to pregnenolone, the precursor of all sex steroid hormones, through the activity of cytochrome P450 side-chain cleavage (CYP11A1). Subsequently, pregnenolone is transformed into 17α-OH pregnenolone by cytochrome P450 17α-hydroxylase/17,20-lyase (CYP17A1). The CYP17A1 subsequently converts the C21 steroid 17α-hydroxylase to the C19 steroid DHEA[141, 142,143,144]. Although adrenal glands can produce testosterone via DHEA directly, the level of testosterone is quite lower than those produced by testes[145] (**Figure 7**). Thus, the main C19

steroids produced by the adrenal gland are in the form of inactive androgen precursors. Moreover, adrenal gland is capable to produce 11β-hydroxy androstenedione, one precursor for new potential androgens 11-ketotestosterone and 11β-hydroxy dihydrotestosterone (11-keto-DHT) via androstenedione[136,146].

In PCa, there exist several steroidogenesis pathways contributing to active androgen 5α-DHT. In the **canonical pathway** (**Figure 9, in blue**), DHEA can be converted to androstenediol by type 5 17β-hydroxysteroid dehydrogenase (AKR1C3), and then transformed to testosterone by the hydroxy-delta-5-steroid dehydrogenase, 3 beta- and steroid delta-isomerase 1 (HSD3B1) which has both 3β-hydroxysteroid dehydrogenase activity and ketosteroid isomerase activity. Meanwhile, DHEA can also be transformed into androstenedione by HSD3B1. There are 2 ways for conversion from androstenedione to 5α-DHT. In the canonical pathway, androstenedione can be converted to testosterone by AKR1C3 and type 7/3 17β-hydroxysteroid dehydrogenase (HSD17B7 and HSD17B3) and then reduced by 5α-reductase (mainly SRD5A2[147]) to 5α-DHT[148,149]. In the **5α-androstanedione pathway** (**Figure 9, in purple**), androstenedione can be converted to 5α-androstanedione by 5α-reductase (mainly SRD5A1[147]) then reduced by AKR1C3/HSD17B7/3 to DHT. The role of SRD5A3 in this conversion has not been fully described[150]. **Backdoor pathway** (**Figure 9, in orange**) represents the conversion from pregnenolone to androsterone by multiple reaction involving intermediates such as progesterone, dihydro-progesterone, allopregnanolone and 17α-OH-allopregnanolone. The pathway also includes the conversion of 5α-androstanedione into androsterone by the reduction of 3α-hydroxysteroid dehydrogenase (3α-HSD, AKR1C2)[151]. AKR1C3 further reduces androsterone to 5α-androstane-3α, 17β-diol (one isoform of Androstanediol)[152] which is then oxidized by type 6 17β-hydroxysteroid dehydrogenase (HSD17B6) to DHT[153,154]. More recently, it has been described that the **11-oxygenated androgen pathway** (**Figure 9, in green**) involves the generation of 11-keto-testosterone and 11-keto-DHT, which can be used as bona fide AR agonists in PCa[155] as introduced before. In this pathway, 11β-OH-androstenedione from adrenal gland could be converted into 11-keto-androstenedione by type 2 11β-hydroxysteroid dehydrogenase (11β HSD2) in PCa[156,157, 158]. 11-keto-androstenedione could be further transformed into 11-keto-testosterone via AKR1C3. Finally, 11-keto-testosterone is reduced into 11-keto DHT via catalysis of 5α reductase[130]. Notably, the active androgens as well as androstenediol could be converted back into upstream inactive androgens via type 2 17β-hydroxysteroid dehydrogenase (HSD17B2) and type 4 17β-hydroxysteroid dehydrogenase (HSD17B4) (**Figure 9**).

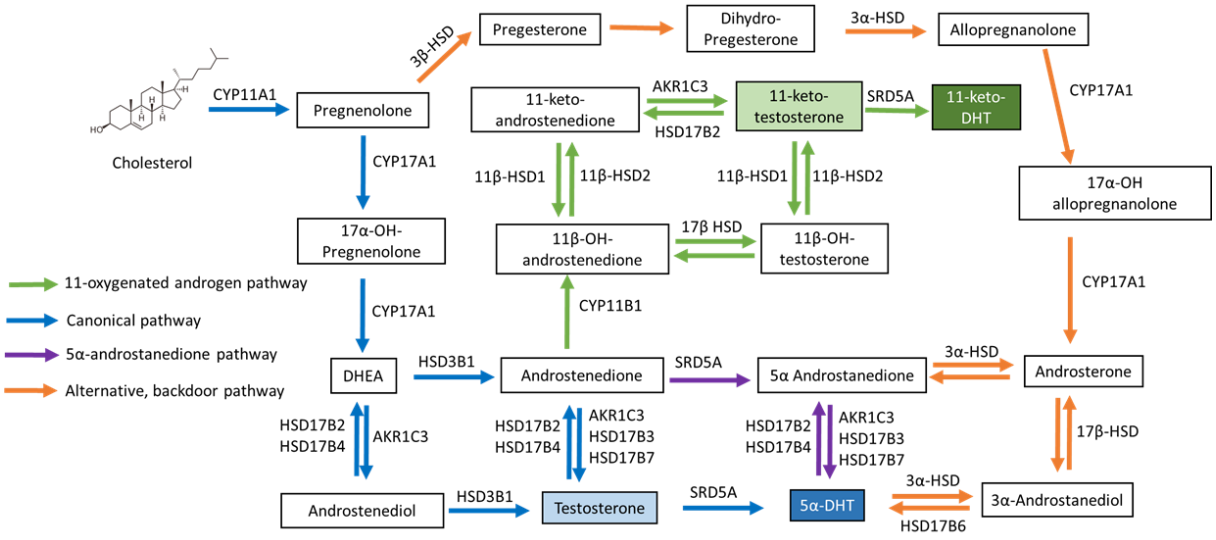


Figure 9. **Several key pathways of steroidogenesis contributing to DHT biosynthesis**. The canonical pathway of DHT synthesis through testosterone (blue), the 5α-androstanedione pathway, which is the primary route of DHT biosynthesis from adrenal precursors in PCa (purple), the 11-oxygenated androgen pathway which can serve as AR agonists in PCa (green) and the alternative, backdoor pathway (orange). DHEA, dehydroepiandrosterone; DHT, dihydrotestosterone; HSD, hydroxysteroid dehydrogenase; HSD17B2/HSD17B3/HSD17B4/AKR1C3/HSD17B6/HSD17B7, type 2/3/4/5/6/7 17β-hydroxysteroid dehydrogenase respectively; SRD5A, 5α-reductase; CYP11A1, cytochrome P450 side-chain cleavage; CYP17A1, cytochrome P450 17α-hydroxylase/17,20-lyase (Adapted from Dai et al., Journal of Clinical Oncology, 2023).

c. Intra-tumoral steroids synthesis in CRPC

In CRPC human cell lines, metastatic tissue biopsies and xenografts (described in chapter 5), the **alternative 5α-androstanedione pathway** bypassing testosterone has been shown to be the preferred pathway compared with the canonical pathway[147] and was confirmed to be predominant in hormone refractory cancer[159]. Androstenedione exhibits a higher substrate preference towards SRD5A1, whereas testosterone serves as the primary substrate for SRD5A2[147]. The decrease in SRD5A2 expression in cancerous prostate tissues compared to benign and the notable shift in both expression and enzymatic activity from SRD5A2 towards SRD5A1 in primary and recurrent prostate tumours also emphasise the importance of the alternative 5α-androstanedione pathway in the development of CRPC[160,161]. Besides that, androstenedione was demonstrated to be a poor substrate for AKR1C3, therefore, upon the efficient catalysation of androstenedione by SRD5A1, the 5α-androstanedione pathway is favoured for DHT synthesis[147].

11-oxygenated androgens pathway in CRPC

11-oxygenated androgens accumulation in PCa tissue and plasma compared to the canonical C19 steroids revealed the potential mechanism in CPRC[156]. It was demonstrated that AKR1C3

catalyzes the conversion of 11-keto-androstenedione with 8 and 24-fold greater efficiency than that of androstenedione and 5α-androstanedione, respectively[162]. In parallel, PCa cell lines were found to exhibit a lower inactivation rate of 11 keto-testosterone and 11-keto DHT in comparison to testosterone and 5α-DHT[155]. Furthermore, an increased ratio of AKR1C3 to 17βHSD2 was observed to favour the flux of 11-oxygenated androgens over the canonical or 5α-androstanedione pathway. Notably, the ratio was found to be elevated in PCa patients received ADT compared to benign tissues, with a further increase seen in CRPC patients[162]. Importantly, 11 keto-testosterone and 11-keto DHT exhibit the comparable affinities for AR and similar efficacy in activating AR compared to testosterone and 5α-DHT[155]. Collectively, these studies underscore the pivotal role of accumulated 11-oxygenated androgens in AR activation and the development of CRPC.

In CRPC, all C19 precursors could be used as androgens precursors for 5α-DHT synthesis. It is reported the existence of the synthesis from 5α-androstane-3α, 17β-diol (3α androstanediol) conversion to 5α-DHT via HSD17B6 directly as introduced before (**Figure 9**) and 5α-androstane-3β, 17β-diol (3β androstanediol) conversion to 5α-DHT via other potential intermediate metabolites such as epiandrosterone and 5α-androstanedione (**Figure 10**) within the CRPC cell lines LNCaP and VCaP. Meanwhile, HSD17B6 expression was increased in patients who received long-term ADT, which indicates the crucial role of **the back door pathway** in CRPC progression[163].

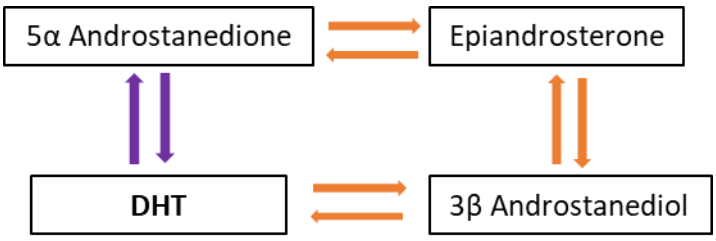


Figure 10. **Complement for the alternative backdoor pathway** (orange)

In LNCaP xenografts, the tumour testosterone and 5α-DHT levels increased after castration during the progression of CRPC and no androgen precursors were detected in the adrenal glands of these xenografts suggesting intratumoral androgen synthesis[164]. Indeed, the tumour explants expressed all steroidogenic enzymes and were capable of *de novo* synthesis of DHT. They could uptake [^{3}H] progesterone to synthesize upstream steroids of 5α-DHT[164].

Other study reported that *de novo* androgen synthesis from cholesterol via CYP17A1 within PCa also contribute to the relapse of CRPC. In CRPC VCaP tumour xenografts, CYP17A1

expression was comparable with clinical samples and AR activity was dependent of CYP17A1 and AKR1C3 involved in tumour androgen synthesis[165].

It is not clear whether adrenal precursor's conversion is more important than intra-tumour or not. One study reported that wild-type AR PCa cell lines PC346C and VCaP mainly responded to adrenal precursors like DHEA and androstenedione rather than pregnenolone and progesterone, showing that conversion of adrenal precursors is more prone to activate cell growth than *de novo* steroidogenesis[166]. However, in LNCaP displaying the AR mutation T8$_7$8A, all androgen precursors could stimulate cell growth and AR targeted gene expression[166].

d. Altered steroidogenic enzymes expression in CRPC

A significant characteristic of CRPC is the dysregulated expression of steroidogenic enzymes. These enzymes play a crucial role in furnishing the tumour with the necessary enzymatic machinery for synthesizing potent androgens from adrenal androgen precursors or tumour microenvironment.

AKR1C3

AKR1C3 emerges as one of the most highly expressed steroidogenic genes in CRPC, consistently demonstrated through RT-PCR and Affymetrix microarray analyses[160]. Notably, androgen deprivation induces the up-regulation of AKR1C3 in PCa cell lines, xenografts and patient tumour samples[167,168,169]. More than ten independent studies have consistently replicated the finding of AKR1C3 overexpression in CRPC. Approximately 30% of CRPC patients are estimated to overexpress this enzyme, prompting its consideration as a potential biomarker for CRPC[170].

HSD3B1

The HSD3B1 1245A→C variant have appeared to be a hot biomarker of predicting recurrence after ADT. This variant has been identified in CRPC tumours, with an allelic population frequency ranging between 15% and 35% reported in most cohorts[171,172] and the frequency varied in different ethnic group[173]. This mutation does not influence the function of enzymes but instead is more resistant to ubiquitination and degradation and leads to a more stable protein. The mutation accelerates DHEA conversion to 5α-DHT and provides the necessary 5α-DHT to activate the AR[172]. For example, LNCaP cells expressed higher HSD3B1 protein due to the presence of the variant than LAPC-4 cell line, leading to a more efficient conversion of DHEA into androstenedione[172]. Clinical studies show that the HSD3B1 variant (1245C) was found to

be associated with an accelerated development of metastases in men undergoing ADT for biochemical recurrence after primary radiation therapy for PCa[174]. The patients carrying the HSD3B1 variant (1245C) have a higher incidence to develop CRPC without difference in time to biochemical recurrence, survival time, or risk of mortality[175].

HSD17B4

HSD17B4 is a potential biomarker to predict poor prognosis in CRPC. Testosterone and 5α-DHT are inactivated to weaker upstream androgens precursors by HSD17B4 (**Figure 9**). Five spliced isoforms of HSD17B4 with differing activities has been reported and among them, only HSD17B4 isoform 2 functionally catalyse the reaction. The expression of this isoform was suppressed during the development of CRPC whereas the expression of other isoforms was increased. Genetic knockdown of HSD17B4 in CRPC xenograft model increased the production of active androgens and enhanced tumour progression[176].

HSD17B2

Similarly, HSD17B2 also catalyses the inactive reaction from testosterone and 5α-DHT to upstream androgens precursors (**Figure 9**). Its expression was decreased as PCa progresses. The benign tissue adjacent to the tumour exhibited a comparatively higher expression of HSD17B2 when compared to the corresponding cancerous tissue[177]. However, the expression of this enzyme was increased in CRPC clinical samples compared with low-degraded PCa[178]. Thus, more investigation needs to be performed for its role in CRPC. Other study reported an alteration in genes encoding steroidogenic enzymes in castration-resistant metastases when compared to primary prostate tumours. These included increased expression of CYP17A1, HSD3B1, HSD17B3, AR, AKR1C3, SRD5A1 and AKR1C2 in along with decreased expression of SRD5A2. These changes suggested the adaption of PCa to androgen deprivation by intracrine steroidogenesis in castration-resistant metastases PCa[179,160].

e. Others alternate sources of androgen precursors for PCa

Tumour macro or microenvironment such as gut microbiota or cancer-associated fibroblast can also provide androgen precursors for PCa development. For example, Pernigoni et al. showed that commensal gut microbiota contributes to endocrine resistance in CRPC by providing an alternative source of androgens. Indeed, CRPC mice and patients have an increase of species in their microbiota capable of converting pregnenolone and 17α-OH-pregnenolone from circulation into DHEA and testosterone and thus sustaining androgen-dependant PCa growth. Fecal microbiota transplantation from CRPC samples could lead to the rapid emergence of

CRPC and promote tumour cell proliferation. Thus, gut microbiota could represent a promising target in treating resistance in CRPC[180].

3β-hydroxysteroid dehydrogenase (3β-HSD) is the rate-limiting enzyme in the conversion of the nonactive androgen DHEA to the bioactive androgen DHT. Cancer-associated fibroblast conditioned medium (CAF-CM) induced 3β-HSD expression and activity in PCa cell lines by secreted glucosamine. Through this mechanism, CAF-CM increased DHEA conversion to downstream androgens and then activate the AR signalling pathway in PCa cells[181].

Interestingly, osteoblasts represent another source of androgens to fuel PCa bone metastasis. For example, DHEA-treated murine osteoblast conditioned medium containing androstenedione, testosterone and androstenediol could activate AR signalling pathway and promote cell growth of LNCaP and C42B[182]. Moreover, co-culture with pre-osteoblast cell line MC3T3 could increase 5α-DHT-regulated cell number of MDA-PCA-2B cells in a Wnt dependent manner[183]. Meanwhile, conditioned medium from the pre-osteoblast cell line MC3T3 increased the expression of steroidogenic enzymes such as HSD3B1, AKR1C3 and SRD5A1 and expression of AR in the CRPC cell line LNCAP-19[184]. These evidences suggested that bone microenvironment with the capacity to create a rich source of androgens could offer a plausible explanation for the preferential invasion and growth of PCa in the skeletal system, particularly when intra-tumoral androgen production by PCa cells is limited or absent.

7.5 Second generation hormonal treatments

a. Inhibition of adrenal and intracellular androgen synthesis

As described above in chapter 7.4, one of castration resistance mechanisms in PCa cells is the increase in intracellular androgen levels within the tumors. Thus, inhibition of enzymes involved in androgen synthesis could be an efficient way to overcome this resistance. Some inhibitors based on this mechanism have been developed.

CYP17A1 enzyme inhibitors

Abiraterone acetate (Zytiga®) is a molecule structurally similar to pregnenolone. It selectively and irreversibly blocks the intra-tumoral androgen biosynthesis by inhibiting cytochrome P450 17A1 (CYP17A1)[185]. As shown in **Figure 9** (Chapter 7.4b), the primary function of the CYP17A1 enzyme is to convert pregnenolone to dehydroepiandrosterone. Thus, by inhibiting CYP17A1, the production of androgens precursors was significantly reduced, ultimately

leading to a decrease circulating androgens or intratumor androgens available to activate the AR[186]. After demonstrating efficacy in clinical trials involving both chemotherapy treated and chemotherapy-naive metastatic CRPC patients, the drug was approved by the Food and Drug Administration (FDA) and the European Medicines Agency (EMA) for the treatment of metastasis CRPC[187,188]. Recent research has shown that abiraterone (steroidal) could exerts its mechanism of action through AR binding and inhibition, providing further insights into its therapeutic properties[189] (**Figure 11**).

New CYP17A1 inhibitors

It has been shown that abiraterone inhibits both C17,20-lyase activity and the 17α-hydroxylase activity. And the latter inhibition can cause symptoms of mineralocorticoid excess, which make the use of prednisone necessary to manage those side effects[190,191]. Galeterone, also known as TOK-001 or VN/124-1, selectively inhibits the 17,20-lyase activity of CYP17A1, thus offering potential advantages compared to abiraterone. It is a steroidal multitargeted inhibitor with a unique mechanism of action, leading to not only decreased androgen production, while also the degradation of AR and antagonizing its function[190,191]. It exhibited efficient anti-tumour inhibitory activity *in vitro* [192] and in phase I and II clinical trials in both non-metastatic treatment –naïve CRPC and metastatic treatment-naïve CRPC patients[193]. However, it was discontinued in phase III as it was not likely to meet the primary endpoint of improved overall survival[194].

Another outstanding CYP17A1 inhibitor is Seviteronel (INO-464), which has even higher selective inhibition of the 17,20-lyase activity of CYP17A1[195] and could also target AR[196]. Currently, phase II trial about oral Seviteronel in CRPC patiently treated with anti-androgen enzalutamide (**See 7.5b**) is on ongoing[197]. Other enzyme inhibitiors as new treatment for PCa will be introduced in chapter 7.7.

b. Anti-androgens or AR Inhibitors (ARI)

The anti-androgen drugs, also called AR Inhibitors (ARI), hinder androgen's biological activity by directly binding to and blocking the AR LBD (ligand-binding domain), thereby inducing repressive activity. They are mainly used in combination with LHRH agonists or antagonists to

achieve complete androgen blockade[127,128].

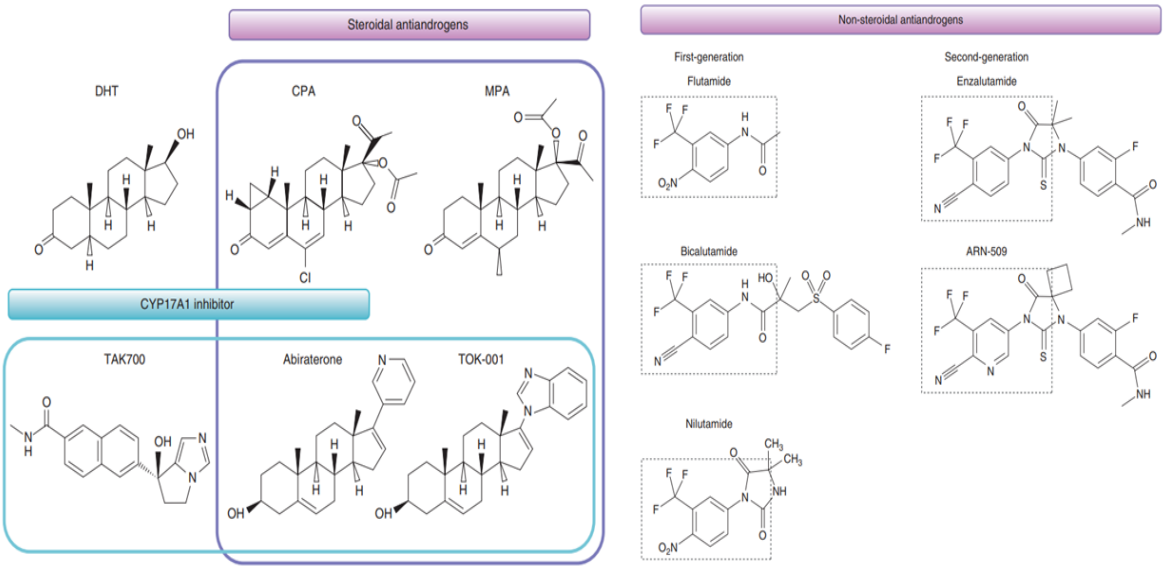


Figure 11. Chemical Structure of steroidal anti-androgens and non-steroidal anti-androgens. From Christine Helsen et al., Endocr Relat Cancer, 2014.

Steroidal anti-androgens

Drawing inspiration from the structure of androgens, the initial anti-androgens featured a steroidal skeleton to ensure receptor binding (**Figure 11**). Among them, cyproterone acetate (CPA), megestrol acetate, and medroxyprogesterone acetate were employed to achieve maximal androgen blockade in patients. However, their clinical use was restricted due to significant drawbacks, including hepatotoxicity, interference with libido and potency, cardiovascular side effects, and low efficacy[198,199,200,201].The side effects associated with these drugs were attributed to their interactions with other steroid receptors, particularly the progesterone receptor and the glucocorticoid receptor, where they act as weak or partial agonists[202,203].

Non-steroidal anti-androgens

Non-steroidal anti-androgens (NSAAs) were first introduced into clinical practice in 1989 as a treatment for advanced and metastatic PCa. The first-generation anti-androgens include flutamide, bicalutamide, and nilutamide whereas the second-generation compound is enzalutamide (previously known as MDV3100). In first-generation drugs, bicalutamide stands out as the best tolerated and most stable anti-androgen currently used in clinical practice[204,205]. Bicalutamide binds to the ligand-binding pocket of AR but fails to induce the correct

conformational change. The resultant platform formed cannot recruit coactivators but instead recruits corepressors, leading to the formation of an inactive AR–DNA complex[206]. (**Figure 12**).

Enzalutamide, first introduced in 2009 as a second-generation anti-androgen to overcome the limitations of bicalutamide such as suboptimal clinical results due to its low affinity for the AR and partial agonist activity[207,208]. Enzalutamide is a stronger AR antagonist by three mechanisms of action. First it blocks androgen binding as classical anti androgens, but also inhibits the translocation of the AR to the nucleus and impairs AR binding to DNA thus inhibiting the transcription of target genes[207] (**Figure 12**). Enzalutamide has been approved by the FDA and EMA for the treatment of patients with chemo-resistant CRPC[209]. It prolongs the overall survival from 4.8 months in metastatic CRPC patients after chemotherapy[210].

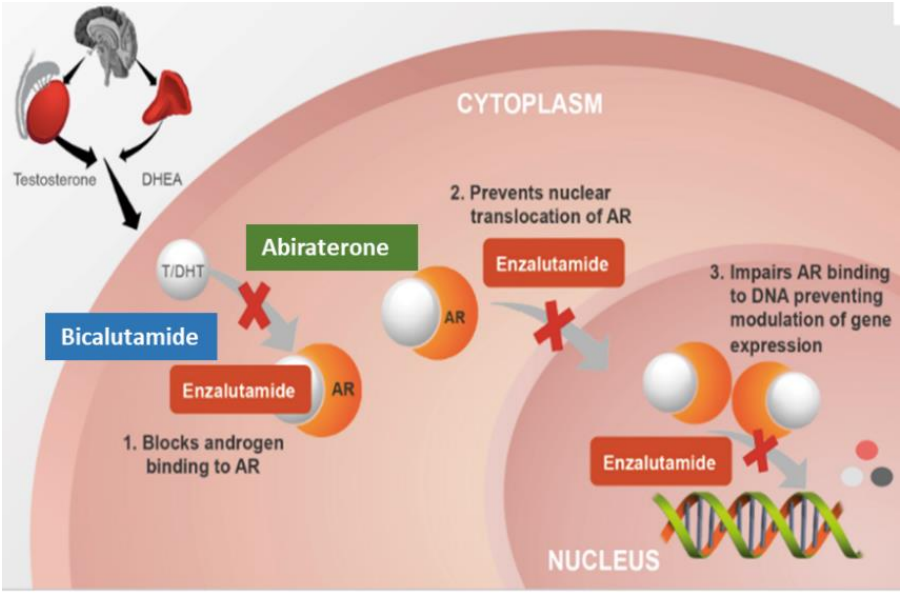


Figure 12. **Mechanisms of bicalutamide, abiraterone and enzalutamide actions on AR** (adapted from Audenet F, Progrès en Urologie, 2016)

7.6 Mechanisms of resistance to second-line treatment and part of first-line treatment

Several molecular mechanisms have been described to explain resistance to anti-androgens or ARI in PCa cells. Most of them have been associated with the reactivation of the AR-axis and these mechanisms can be categorized into three groups: (1) those that concern AR ligands (Pre-receptor) (2) those that directly modify the AR protein (Receptor), (3) those leading to AR activation independently of ligand binding (Post-receptor) [211]. Both receptor mechanism and post-receptor mechanism has also been shown to be involved in first-line treatment resistance (CRPC), which will be described with second-line treatment at the same time in this chapter.

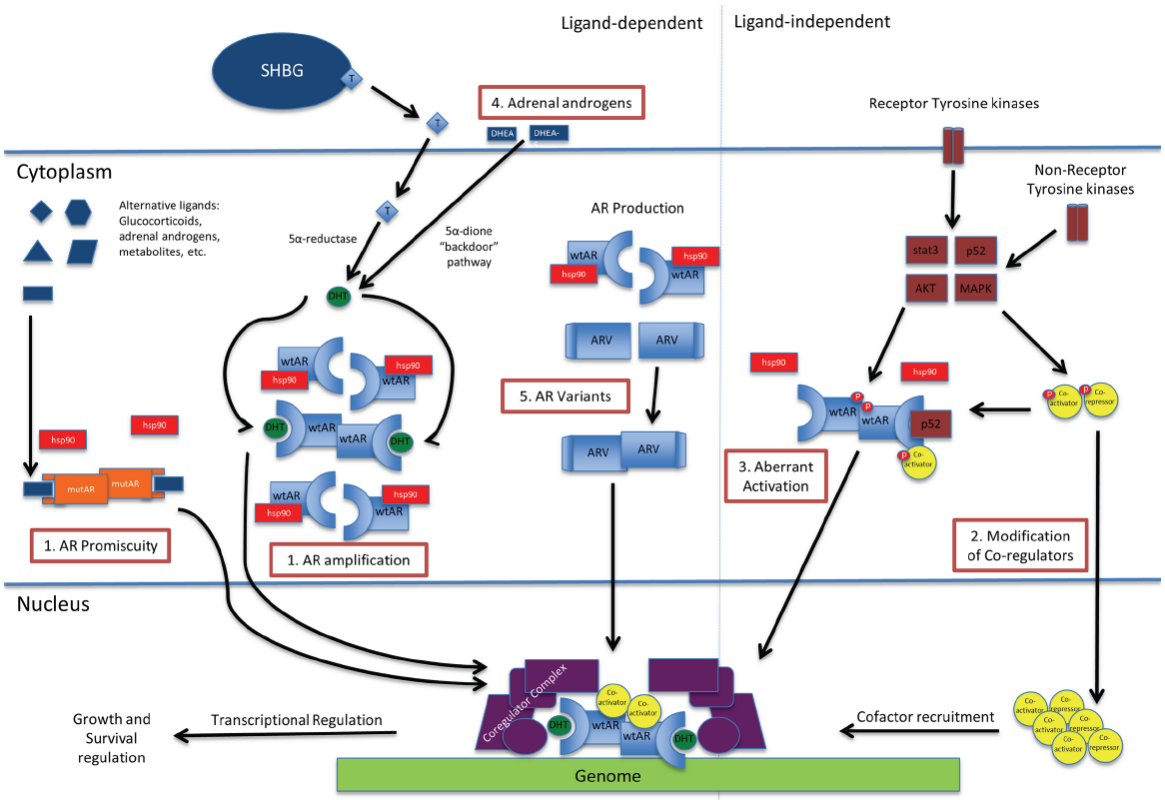


Figure 13. Androgen receptor-dependent mechanisms of resistance in hormone-naive prostate cancer leading to castration-resistance. wtAR, wild-type androgen receptor; ARV, androgen receptor variant; mutAR, mutated androgen receptor; T, testosterone; DHT, dihydrotestosterone; SHGB, sex hormone binding globulin (from Chandrasekar et al., Transl Androl Urol, 2015)

a. Availability of steroids ligands for AR (Pre-receptor mechanism)

As described above (in 7.4c), the intra-tumoral synthesis of steroids is involved in the resistance to the first line treatment of PCa with ADT. In the second line treatment this mechanism can also be involved since steroids could compete with ARI as ligands for AR.

Steroidogenic enzymes gene such as CYP17A1, HSD3B1, HSD3B2, HSD17B3, SRD5A1, AKR1C1/2 and AKR1C3 expression and androgen precursors such as cholesterol, DHEA and progesterone are upregulated in enzalutamide-resistant PCa cells compared to parental cells. For example, AKR1C3 activation, which favour the accumulation of steroids ligand for AR (testosterone or DHT), is one of crucial mechanism for enzalutamide resistance[212]. These results provide a new insight for overcoming enzalutamide resistance and improving their survival by targeting AKR1C3. Similarly, overexpression or genomic changes in CYP17A1 gene (involved in upstream androgen precursor's synthesis, **Figure 9**) contribute to abiraterone acetate resistance[165]. Also, HSD3B1 (involved in androgen synthesis from adrenal precursors,

Figure 9) mutation (1245C) plays a significant role in promoting abiraterone acetate resistant progression to CRPC. It is due to that the A/B steroid ring (Δ5,3β-hydroxyl) structure of abiraterone (**Figure 11**) could be metabolized by HSD3B1 and produce 5α-abiraterone, an agonist for AR which counteract the beneficial effect of CYP17A1 inhibition[213].

b. Modifications of the AR protein

AR amplification

Amplification of the AR occurs in approximately 60%-70% of cases and is the most commonly observed molecular alteration in metastasis CRPC[214]. It involves mainly the increased histone acetylation/phosporylation at enhanced sites[215]. AR gene amplification has been implicated in driving resistance to enzalutamide and abiraterone[216,217,218].

AR mutations

AR mutations are typically detected in PCa upon the treatment with anti-androgens. Most of the mutations occur in the LBD of AR. T877A point mutation within LBD has been discovered as the first mutation for its resistance to hydroxyflutamide treatment, a first-generation antiandrogen[219,220.221]. Subsequently, four common mutations in the LBD, including L702H, W742C/L, H875Y, and T878A/S, were revealed in a significant proportion of 10%-25% of CRPC due to the development of contemporary next-generation sequencing methods[222,223,224]. These mutations make AR possible to be activated by various noncanonical ligands or even antagonists in an inappropriate manner[225,226]. For example, T877A point mutation renders hydroxyflutamide into a potent agonist[227]. Both T878A/S and H875Y mutations enhance AR activation in response to various noncanonical steroidal ligands such as progesterone, estradiol, and DHEA, as well as to anti-androgens like flutamide[228,229,230,231]. W742C/L mutation confers bicalutamide agonist activity[232,233]. FF877L mutation which has been described recently confers the second ARIs enzalutamide and apalutamide agonist activity in *in vitro* tests[234]. Moreover, clinical studies have shown patients who have experienced disease progression on abiraterone therapy (targeting CYP17A1 involved in upstream androgen precursors synthesis, **Figure 9**) exhibited AR mutations, including T878A, H875Y, and L702H. These mutations may enable AR to be activated by the steroids synthesised upstream of CYP17A1 (for instance progesterone), which cannot be inhibited by abiraterone and thus decreased the efficacy of the drug[216,217,235]. Notably, some mutations in the NTD and DNA-binding domain were also identified[236].

AR-variants

Another additional adaptive mechanism that occurs in ARIs resistance involves the expression of AR splice variants (AR-Vs). AR-Vs is commonly described as lacking of LBD and maintaining AR signalling activation in a constitutive and ligand-independent manner[237]. More than 20 AR-Vs have been identified to date and AR-V7 seems to be the predominant variant in CRPC with the pivotal role in resistance to second line treatment[238,239]. For example, enzalutamide treatment enhanced AR-V7 expression leads to PCa cell resistance to enzutamide. Subsequent AR-V7 depletion re-establishes CRPC cell sensitivity to enzalutamide[240]. AR-V7 protein is rarely expressed in primary PCa whereas detected frequently after ADT treatment with further increase after abiraterone acetate or enzalutamide treatment[241]. Moreover, AR-V7 correlated with poor clinical outcomes in CRPC patients after abiraterone and enzalutamide therapies[242]. In addition, other AR-Vs has also been described such as the potential role of AR-V9 in CRPC biopsies to predict resistance to abiraterone therapy[243]. Although, the expression of AR-V7 and AR-V9 generally correlate with full-length AR (AR-FL), it is still uncertain whether AR-Vs play a role in driving CRPC independently of AR-FL and whether AR-Vs activate similar or different transcriptional programs compared to AR-FL[244,245,246,247].

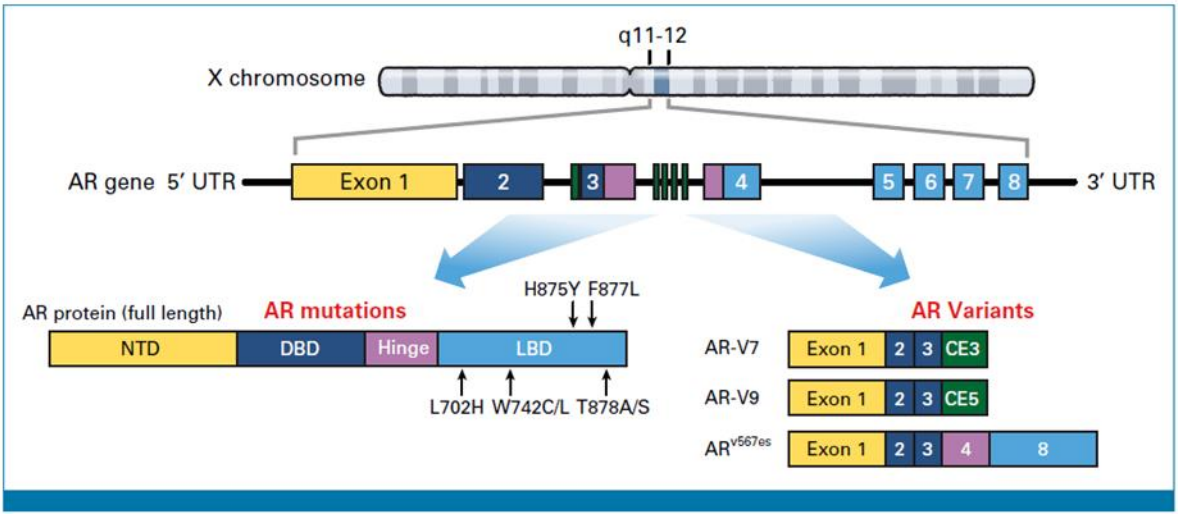


Figure 14. **The AR gene locus and protein**. The mRNA transcript encoding the full-length AR protein encompasses eight exons, which consists of four major functional protein domains. AR mutations most frequently occur in the LBD. Several AR-Vs including AR-V7, AR-V9, and AR-V12/ARv567es are depicted as well, including their corresponding exons. AR, androgen receptor; AR-Vs, AR variants; DBD, DNA-binding domain; LBD, ligand-binding domain; NTD, N-terminal domain; UTR, untranslated region (from Dai et al., Journal of Clinical Oncology, 2023)

AR-Co-regulators

The AR transcriptional activity is regulated by diverse co-regulator complexes, including chromatin remodels, co-activators, and co-repressors, which are recruited by AR to chromatin effectively controlling gene expression[248]. Maintaining an appropriate balance of co-activators and co-repressors is crucial for adjustment AR-mediated transcription. Nevertheless, imbalances in these co-regulators can lead to increased AR activity in PCa and diminished antagonism by anti-androgens[248,249,250,251]. The AR's binding to androgen response elements (ARE) can be regulated by diverse factors. Recent study indicates that the loss of CHD1, an ATP dependent chromatin remodeler and one prostate-specific tumour suppressor gene, leads to heterogeneous drug resistance mechanisms to enzalutamide *in vivo*[252]. Additionally, the AR co-regulator transcription factor HOXB13 interacts with AR and modulates AR target loci, which is involved in the development and maintenance of PCa and also progression to CRPC[253,254]. HOXB13's expression is decreased or even lost while the transformation from CRPC to more aggressive neuroendocrine PCa, an aggressive subtype of CRPC that typically does not respond to AR pathway inhibition[255]. Other pioneering factors, FOXA1 and GATA2, act as chromatin factors at enhancer sites, increasing AR expression and activity of AR and AR-V7 in metastatic CRPC[256,257,258]. Isolated circulating tumour cells (CTC) from patients with abiraterone- or enzalutamide-resistant metastasis demonstrated FOXA1 gene amplification in over 30% of CRPC patients, highlighting FOXA1's critical role in emerging drug resistance[258]. Also, ACK1 an epigenetic regulator of AR, impacts androgen-independent growth and induces CRPC drug resistance by mediating phosphorylation of histone H4 and then leading to epigenetic upregulation of AR expression[259]. CREB5, another AR co-activator amplified and overexpressed in CRPC, is associated with enzalutamide resistance, suggesting a potential therapeutic target[260].

c. Ligand independent resistance mechanism (Post-receptor mechanism)

In addition to pre-receptor and receptor-level resistance mechanisms involving ligand-dependent AR activity, post-receptor mechanisms include aberrant signalling pathways inducing AR activation inside the cytosol independently of ligands[211,261].

PI3K-Akt-mTOR pathways

The PI3K-Akt-mTOR pathways play pivotal roles in regulating essential cellular processes, including cell growth, development, proliferation, protein synthesis regulation, and programmed cell death[222]. Dysregulation of the PI3K-Akt pathway has been linked to PCa

development and progression, and its activation may contribute to anti-androgen drug resistance[262]. AR interact with the tumour suppressor gene PTEN and PI3K[263,264,265]. Preclinical model studies have shown the activation of PI3K-AKT pathway is crucial in CRPC development[263]. The loss of PTEN, which negatively regulates the PI3K/Akt pathway occurs mainly in metastatic PCa[264,265]. A phase II randomized clinical trial demonstrated promising trends of improvement in patients with PTEN loss when treated with an AKT inhibitor in combination with abiraterone acetate[266]. These findings underscore the critical role of PI3K/Akt pathway dysregulation in PCa progression and suggest that targeting the PI3K/Akt pathway could be a promising therapeutic approach for CRPC.

NF-kB signalling

The NF-kB family proteins play a significant role in the oncogenic pathways of various cancers[267]. Among the five distinct NF-kB proteins, the p65/p50 heterodimer has been found to be constitutively active in PCa[268]. The activation of the NF-kB/p52 pathway has been associated with the development of resistance in PCa[179]. And also, increased expression of p52 has been found to enhance glucose uptake and lead to higher levels of ATP and lactate, contributing to enzalutamide resistance in CRPC cells[269]. Suppressing NF-kB downregulates AR-Vs expression, leading to restored sensitivity of CRPC to second-generation anti-androgen therapy and decreased cellular responsiveness to androgens[270].

Moreover, NF-kB has a regulatory role in the expression of IL-6 in cancer cells. In CRPC, IL-6 is highly expressed and lead to increased transcriptional activity of the AR in a ligand-independent manner. IL-6 mediates its effects through the Janus kinase (JAK)-signal[271]. Interestingly, the treatment of PCa cells with the JAK inhibitor AG490 has been shown to re-sensitize cells to enzalutamide, and co-treatment of the inhibitor and enzalutamide lead to an inhibitory effect on cell growth and induction of apoptosis[272]. Additionally, a combination therapy of antiandrogens with NF-kB inhibitors efficiently inhibits tumour growth in human CRPC xenografts[272].

Autophagy

Autophagy is a dynamic and catabolic process essential for maintaining cellular homeostasis through the degradation and recycling of cellular components[273]. It serves as an adaptive mechanism to respond to various stressors and metabolic demands, allowing cells to efficiently eliminate damaged organelles and proteins, through lysosomes, thereby ensuring their proper

functionality and survival[274]. In cancer cells, the balance between autophagy and apoptosis may be disrupted[275]. Metabolic stress and hypoxia can lead to increased autophagy, providing nourishment to highly proliferative tumour cells[276]. Androgen deprivation has been shown to induce autophagy, but the exact mechanism remains unknown. Inhibiting autophagy by siRNA led to cell death in PCa cells exposed chronically to enzalutamide or androgen deprivation, indicating that autophagy plays a crucial role in the survival of CRPC cells[277]. *In vivo* studies using mice engrafted with enzalutamide-resistant PCa cells showed that the combination of enzalutamide with autophagy inhibitors significantly reduced tumour growth compared to control groups[277]. The study emphasis the therapeutics potential of autophagy inhibitors combined with anti-androgens in CRPC treatment.

Glucocorticoid Signalling

Glucocorticoid receptor (GR), a member of the steroid hormone nuclear receptors family whose structure and mechanism of action is similar to AR. Both AR and GR possess similar DBD structures and exhibit similar transcriptomes and response elements profile in their target genes, suggesting a degree of functional overlap and crosstalk between these receptors[278,279,280]. GR expression is initially low in primary PCa tissue but undergoes significant upregulation during prolonged exposure to enzalutamide in both PCa cell lines and patients, demonstrating that GR overexpression contributes to enzalutamide resistance[281,282]. This upregulated GR signalling mediated resistance mechanism is named as "glucocorticoids receptor take-over" pathway[283].

TMPRSS2-ERG fusion

TMPRSS2-ERG gene fusion (T-E fusion) is the most prevalent fusion event linked to CRPC. Two studies detected T-E fusion in 9 out of 15 (9/15) and 14 out of 19 (14/19) CRPC tumour samples[284,186]. Additionally, T-E fusion positive samples were found to be more aggressive than T-E fusion negative samples[285]. T-E fusion leads to upregulation of ERG, one of the most common genomic dysregulations in PCa. Interestingly, ERG has also been found to regulate the expression of the steroidogenic enzyme AKR1C3, which is highly expressed in enzalutamide-resistant cells[286]. Further investigation demonstrated that the presence of the ERG/AKR1C3/AR feed-forward loop contributes to androgen synthesis, AR signalling, and resistance to AR targeting agents in CRPC[287].

Other androgen independent mechanisms

The development of resistance to anti-androgens involves other multiple mechanisms, including epithelial-mesenchymal transition (EMT), neuroendocrine differentiation, and immune resistance. EMT, induced by ADT, promotes tumour progression and drug resistance by altering transcription factors like Snail and Twist, and reducing E-cadherin expression[262,288,289]. As described above in chapter 7.6.b**,** neuroendocrine PCa arises after hormonal therapies[290]. The loss of AR signalling during the neuroendocrine trans-differentiation leads to resistance to enzalutamide treatment[291]. PD-L1 (Programmed Death-Ligand 1) and PD-1 (Programmed Cell Death Protein 1) which play a crucial role in regulating the immune system are implicated in immune resistance to enzalutamide *in vitro* and *in vivo* animal models[292]. Clinical trials exploring immunotherapy in CRPC are undergoing and will help to better understand primary resistance mechanisms.

7.7 Newest treatment for PCa

a. AR signalling inhibitors

Given to the presence of various resistance mechanisms that prevent effective targeting of the LBD (Ligand binding domain) of the AR, there has been a growing interest in exploring alternative approaches to inhibit AR signalling. Proteolysis-targeting chimeras (PROTACs) and selective AR degraders (SARDs) have emerged as promising therapeutic strategies. PROTACs are composed of two ligands connected by a linker, where one ligand binds to AR and the other recruits an E3 ubiquitin ligase, promoting ubiquitination and proteasome-mediated degradation. Among these, ARV-110, a first-in-class PROTAC, has shown encouraging clinical activity in heavily pre-treated metastasis CRPC patients, particularly those with T878A/S and H875Y mutations. Additionally, several SARDs have demonstrated activity in preclinical models for CRPC, including against AR-V7, offering a potential new class of AR-directed therapies[293,294].

b. Steroidogenic enzyme inhibitors

As introduced before, in recent years, substantial research has focused on identifying inhibitors that selectively target enzymes involved in DHT synthesis as a promising strategy for PCa therapy. Firstly, the key enzyme 5α-reductase, which converts testosterone to DHT, has been a primary target for therapeutic interventions. Different generations of 5α-reductase inhibitors, including finasteride (SRD5A1inhibitor) and dutasteride (dual SRD5A1/SRD5A2 inhibitor), have demonstrated clinical efficacy in inhibiting PCa growth; however, they have also been associated with an increase Gleason score in small patient group as side effects observed in clinical studies[295,296]. Thus, the use of them have been warned by FDA.

AKR1C3 inhibitors act by blocking the enzymatic activity of AKR1C3, thus reducing the conversion of non-active androgens, such as androstenedione and 5α-androstanedione, to the potent androgen DHT. By inhibiting AKR1C3, these inhibitors aim to decrease ligands availability for AR and to disrupt the androgen signalling pathway, which is critical for PCa growth and survival. For example, indomethacin has been advanced into clinical trials for patients who experience progression while on enzalutamide. However, the prolonged use of this nonsteroidal anti-inflammatory drug (NSAID) is associated with gastrointestinal side effects. The development of indomethacin analogues exhibiting greater potency and selectivity for AKR1C3, holds promise as potential replacements for indomethacin[297]. Some other AKR1C3 inhibitors did not progress very well in clinical trials because of their lower efficacy such as ASP9521[298] or hepatic toxicity such as Bay1128688[298]. Two outstanding and promising inhibitors BMT4-158 and GTx-560 exhibited excellent AKR1C3 function inhibition and acted as AR antagonists as well[298]. Although AKR1C3 inhibitors hold promise as a therapeutic strategy, further research and clinical trials are needed to evaluate the efficacy and safety of these inhibitors as a therapeutic option for PCa patients. Additionally, understanding the resistance mechanisms that may arise during treatment with AKR1C3 inhibitors is crucial for the development of effective combination strategies.

Finally, emerging strategies have focused on combining multiple inhibitors to achieve synergistic effects and overcome potential resistance mechanisms. Combinatorial approaches involving 5α-reductase inhibitors with CYP17A1 inhibitors or anti-androgens have shown encouraging results, offering improved clinical outcomes and prolonged disease control[299]. Understanding the intricate mechanisms of these inhibitors and their impact on DHT levels and tumour growth will aid in the development of more effective treatment strategies, ultimately improving patient outcomes and quality of life.

c. Chemotherapy

Chemotherapy is commonly used in advanced or metastatic cases, especially when the cancer has spread beyond the prostate gland. The most widely used chemotherapy drug for PCa is docetaxel, which has shown effectiveness in extending survival and improving quality of life in certain patients. In recent years, another chemotherapy drug called cabazitaxel has emerged as a treatment option for PCa that has progressed despite initial chemotherapy with docetaxel. Cabazitaxel has demonstrated improved outcomes in terms of overall survival in patients with advanced PCa. In this phase, chemotherapy with taxanes and 2nd generation hormone therapies

targeting the AR or CYP450 enzyme (CYP11A1 and CYP17A1) will be offered[300,301, 302]. Soon PARP inhibitors (poly (ADP-ribose) polymerase inhibitors) will come on the market while the results are inconclusive and immature for immune checkpoint inhibitor immunotherapies[303],[304]. In recent years, the concept of optimizing the first line of treatment, by combining 1st generation hormone therapies (ADT) + chemotherapy or 2nd generation hormone therapy (ARI), at the hormone-sensitive metastatic stage has made it possible to further improve the oncological results of patients[305,306]. In conclusion, PCa is a disease with a very heterogeneous prognosis allowing active surveillance for low-risk forms or requiring a sequence of palliative systemic treatments for metastatic diseases.

Part 2 Adipose tissue

1. The white adipose tissue

White adipose tissue (WAT) is a vital and dynamic component of the human body, primarily recognized for its role in energy storage and metabolic regulation. It is the most abundant type of adipose tissue (AT) in mammals and serves as a critical reservoir for triglycerides (TG), enabling efficient energy storage in the form of lipid droplets. These last 20 years, researches in AT have revealed the role of WAT as an endocrine organ[307]. WAT is distributed throughout the body, with the two mains adipose depots located in subcutaneous regions (SAT) and around internal organs (visceral AT, VAT) **Figure 15**.

SAT is located under the skin, in an area called the hypodermis. It is actually made up of two distinct layers: the superficial and deep subcutaneous AT. It is distributed throughout the body, the main deposits being the femoral, gluteal, abdominal as well as the mammary TA in women[308,309]. It represents 80% of the total fat mass in normal weight individuals. VAT is made up of deeper deposits that surround the organs enclosed in the large cavities of the body. The main deposits are the omental and mesenchymal. Despite constituting a smaller proportion (5-10% in women and 10-20% in normal weight men), this AT displayed the highest metabolic activity. Moreover, it plays a pivotal role in the pathogenesis of cardiovascular and metabolic complications associated with obesity[310,311].

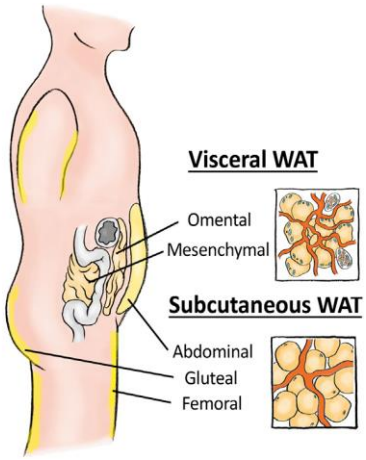


Figure 15. **The important visceral and subcutaneous white AT depots in human.** (adapted from Emma Börgeson et al., Front. Cell Dev. Biol, 2022)

Adipocytes, the primary cell type in WAT, play a pivotal role in lipid storage, as well as in the synthesis and secretion of bioactive molecules that modulate various physiological processes, including appetite regulation, insulin sensitivity, and inflammation. Normally, visceral adipocytes have smaller size than subcutaneous adipocytes in normal weight individuals[312]. The

cellular composition also shows more proportion of macrophages in VAT[313,314]. Secretions profile are also different with adiponectin and leptin mainly released by SAT while VAT produces more pro-inflammatory cytokines such as TNFα, IL6, MCP-1, VEGF and PAI1[315].

Other fat deposits are found dispersed throughout the body, such as periprostatic, mammary, bone marrow, perivascular, pericardial, and retroperitoneal AT including peripancreatic and perirenal depots. More and more studies show that all these deposits have a certain independence and specificities that mean that AT can no longer be considered as a homogeneous entity but as a heterogeneous set of tissues[316].

2. Composition of white adipose tissue

The WAT is a connective tissue composed of adipocytes and stroma-vascular fraction (SVF) including adipose-derived stem cells (ADSCs) progenitors, endothelial cells, fibroblasts and immune cells[317].

2.1 White adipocytes

The adipocytes are organized into lobules, which are supported by the connective extracellular matrix. Morphologically, white adipocytes take the form of a large, unilocular lipid droplet, which occupies approximately 90% of the cell volume. This prominent lipid droplet pushes the organelles, including the mitochondria that are relatively small and few in number, and mitochondria, granular and smooth endoplasmic reticulum, golgi apparatus the nucleus, towards the periphery of the cell[318]. The size of adipocyte is around 80 to 200 µm and the size of the lipid droplet varies from 30 to 150 µm, depending on depot and its lipid load[319]. The adipocyte possesses all the machinery needed to store TG and release free fatty acids (FFA) as required. In addition, the adipocyte performs the endocrine function of the AT through the secretion and release of adipokines, which will be described in detail later.

2.2 SVF

Immune cells play a pivotal role in the regulation of energy homeostasis through a paracrine communication with surrounding adipocytes. Moreover, beyond interactions with adipocytes, they also actively shape the microenvironment by interacting with other cell types within AT. The physiological and pathophysiological roles of the immune system in the regulation of metabolism are being studied in a new field of metabolic diseases: immunometabolism[320]. These immune cells play a beneficial role. For instance, in metabolically healthy individuals, they participate in tissue homeostasis maintenance. Conversely, in obesity, the accumulation of

specific immune cells contributes to a chronic inflammatory state associated with AT dysfunction[320].

In physiological situations, normal-weight individuals, immune cells participate in tissue homeostasis maintenance by clearing apoptotic cells, extracellular matrix remodelling, and angiogenesis. In this condition, the immune fraction of AT is primarily composed of macrophages, eosinophils (part of the innate immune system), and T lymphocytes (part of the acquired immune system).

Macrophages account for up to 10% of SVF in normal-weight individuals. Traditionally, AT macrophages (ATM) were distinguished into two types: "M1" macrophages, predominantly pro-inflammatory and characterized by TNFα secretion and NOS (Nitrite Oxide Synthase) expression; and "M2" macrophages, exhibiting an anti-inflammatory phenotype, expressing the surface marker CD206 and predominantly secreting IL10 and TGFβ[321]. Macrophages display plasticity, and their polarization towards which phenotype depends on their microenvironment. It was described that Th2 cytokines like IL4 and IL13 direct them towards the "M2" phenotype, while Th1 cytokines such as IFNγ tend to induce an "M1" phenotype. Accumulating evidences have shown that AT are populated by mixed forms between M1 and M2 types, capable of repolarization under the influence of cytokines towards a certain phenotype depending on the circumstances[322,323] (**Figure 16**).

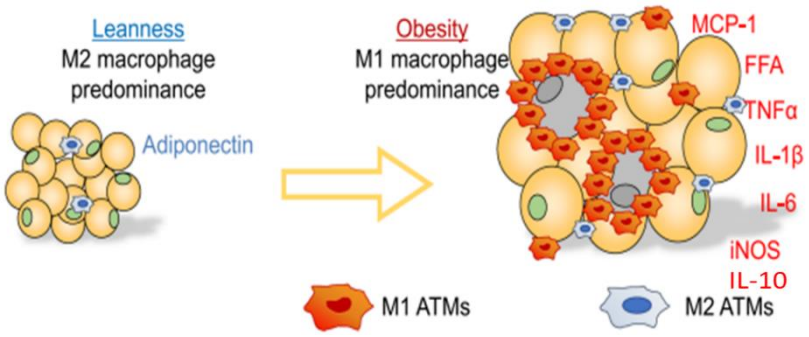


Figure 16. **General characteristics of M1/M2 AT macrophages (ATM).** (from Shiho Fujisaka et al., Diabetol Int, 2020.)

More recently, the M1/M2 classification was updated regarding to the current understanding of macrophage diversity in AT. Resident ATM expressing CD206, CF163 and TIM4 were found in lean mice whereas obesity favour a population of macrophages expressing CD11c, CD9 and TREM called metabolically activated macrophages or lipid associated macrophages (LAM) (Figure 17). In contrast, human AT is composed of mixed population; resident macrophages

CD206+ and CD11c- and LAM and obesity triggers the accumulation of resident macrophages with few CLS[324].

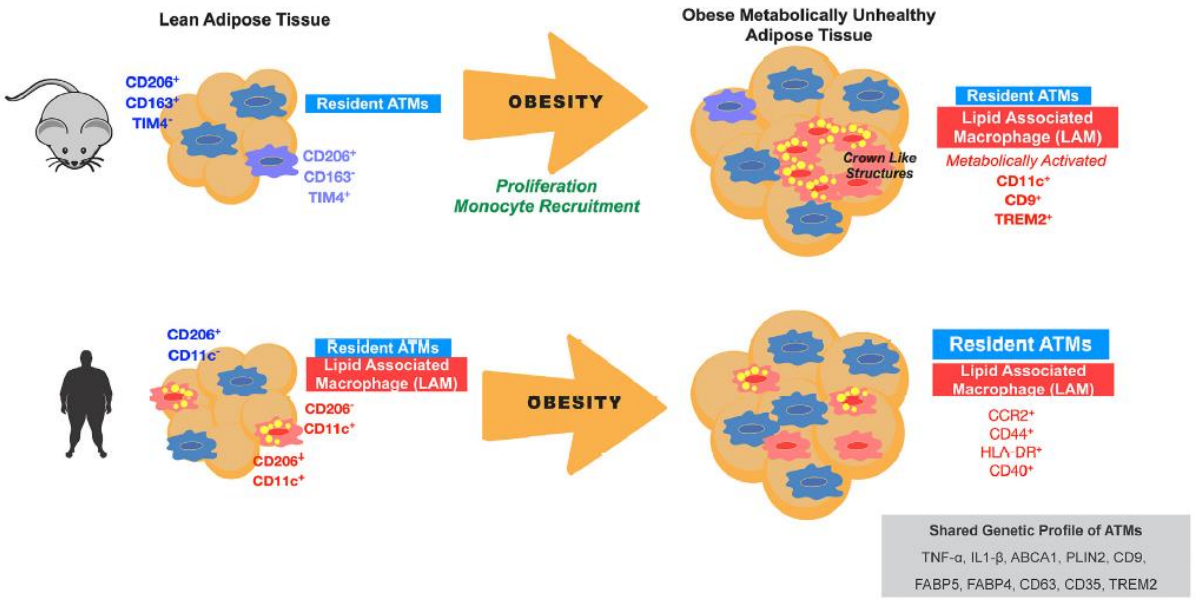


Figure 17. **New classification of ATM**: **Comparison of mouse and human adipose tissue macrophage diversity during obesity.** For mice, lean states are dominated by a resident ATM pool that can be divided into at least two subtypes. With diet induced obesity, lipid associated ATMs (LAM) accumulate in crown like structures (CLS) and are maintained via proliferative and recruitment mechanisms. In humans, LAM ATMs are part of the resident tissue pool along with CD206+ ATMs. With obesity and metabolic disease, CD206+ ATMs expanded in adipose tissue in contrast with mouse models of obesity. In addition, CLS are much less abundant in human adipose tissue. **(**from Nance et al, Molecular metabolism, 2022).

Granulocytes (neutrophils, eosinophils, and basophils) are poorly represented in SVF. However, eosinophils have been found to play a significant role in maintaining healthy AT by regulating formation of macrophages[322]. Foxp3+ regulatory T-lymphocytes (Tregs) are more abundant in AT than in other lymphoid organs. These Tregs in AT have a specific phenotype, expressing high levels of IL-10 and unusual PPARγ (Peroxisome Proliferator-activated Receptor gamma). They play a role in polarizing macrophages towards an M2 phenotype[325,326].

These findings highlight that immune cells in healthy AT contribute to tissue homeostasis and metabolic regulation by secreting factors. However, the underlying mechanisms are not fully elucidated, and they may act through their anti-inflammatory properties or by secreting insulin-sensitizing factors that improve glucose homeostasis.

Adipocyte progenitors

White AT (WAT) undergoes continuous renewal throughout life (approximately 10% turnover each year)[327] and maintains an expansion capacity that allows it to respond to energy excesses.

The development of AT undergoes two processes: hypertrophy, characterized by an increase in adipocyte size, and hyperplasia, involving the recruitment and differentiation of new progenitors, resulting in an increased number of adipocytes[328]. Adipose-derived stem cells (ADSCs) play the crucial role in this adipocyte differentiation process, known as adipogenesis. This multipotent mesenchymal precursor is capable to differentiate into a variety of cell lineages, including myogenic, chondrogenic, osteogenic, or endothelial depending on culture conditions[312,313,314]. During adipocyte differentiation, ADCSs are initially committed into preadipocytes through BMP4 (Bone morphogenetic protein-4) influence, followed by their growth arrest and their transformation into differentiating preadipocytes and then into mature adipocytes (terminal differentiation), under the major influence of PPARγ and transcription factors of the C/EBP (CCAAT/enhancer binding proteins) family. PPARγ and C/EBP represent the early differentiation markers with AP2 and GLUT4 whereas the mature adipocyte markers are adiponectin, leptin, ATGL (Adipose triglyceride lipase), LPL (Lipoprotein lipase) and perilipin[316] (**Figure 18**).

The endothelial cells involved in vascular network formation and its role will be discussed in the chapter 4.

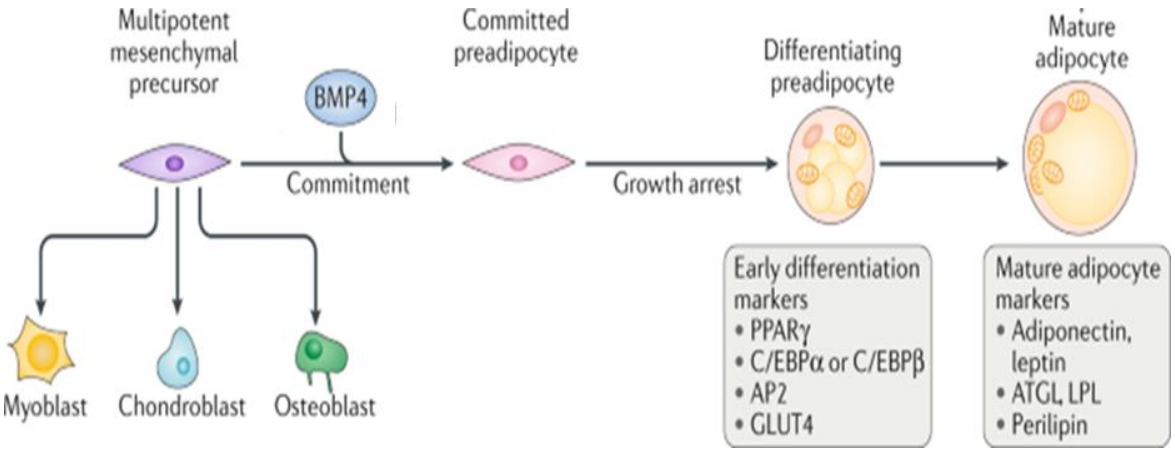


Figure 18. **Key regulators of adipogenesis**: the differentiation of adipose-derived stem cells (ADSCs) into mature adipocytes involves a complex integration of cyto-architectural modifications, signaling pathways and transcriptional factors (adapted from Alexandra L. Ghaben and Philipp E. Scherer, Nature Reviews Molecular Cell Biology volume 2011)

3. Extra-cellular matrix (ECM)

As in all connective tissues, AT cells are embedded in an extracellular matrix (ECM) composed of both structural proteins, collagens, and adhesion proteins such as fibronectin, laminin, elastin and proteoglycans[329]. While the ECM in AT shares similarities with other connective tissues, it also exhibits specific features

3.1 Main components of the ECM

The primary structural proteins in the ECM are **collagens,** which form trimers of α polypeptide chains linked by hydrogen and covalent bonds in a triple helix structure[330]. To date, 28 types of collagen have been identified[331]. Format contains fibrillary collagens (collagens type I, III, V, XI, XII, XIV, XVI) and so-called non-fibrillary collagens (basement membrane type IV, short-chain type VIII, filament type VI and XV, XVIII multiplexin type)[329]. Collagen VI stands out as a particularly crucial component of the ECM in AT. It is highly abundant and more strongly expressed in AT than in other tissues like the liver, muscle, pancreas, and heart[332,333]. While fibroblasts are typically a major source of collagens, mature adipocytes seem to be the primary source of collagen VI in AT[334].

Scherer's group identified that the cleavage product of the C-terminal domain of the α chain of Collagen VI, called endotrophin, stimulated fibrosis, endothelial cell activation and macrophage infiltration in breast tumours[334]. The same team described endotrophin as an adipokine with a major influence on AT, involved in increased secretion of pro-inflammatory cytokines and insulin resistance[335].

Elastin is also a structural protein. But unlike collagens, they confer elasticity to the tissues, enabling them to stretch and then return to their basal state. The ECM also contains **glycoproteins** like fibronectin, which, by binding to both collagen fibers and cell surface integrins, enable cell migration through the matrix. Laminins, another kind of glycoproteins, associate with collagens to reinforce the structure of the cell's basement membrane[336]. The ECM also contains proteoglycans such as heparan sulphate, capable of binding to numerous ligands, protecting them from degradation and facilitating their specific sequestration and release [337,338] Finally, SPARC (Secreted Protein Acidic and Rich in Cystein) do not have a structural function but "supervise" the turnover and organization of other matrix proteins[339]. Overall, the complex composition of the ECM in AT plays a critical role in regulating tissue integrity, elasticity, cell mobility, and ligand sequestration, contributing to the overall function and physiological processes of AT.

3.2 Organization of ECM around adipocytes

In AT, each adipocyte is surrounded by a thin basement membrane composed of collagen IV associated with laminin and heparin sulfate[340]. Thicker collagen I fibers surrounding several adipocytes form a lobular architecture. Type V and VI collagen fibers form microfiber bridges between collagen I fibers, as well as between the cell and collagen I fibers. Fibronectin, located

very close to collagen I fibers, influences cell shape and tissue contraction. Other proteins such as SPARC and thrombospondin regulate collagen I formation[341] (**Figure 19**).

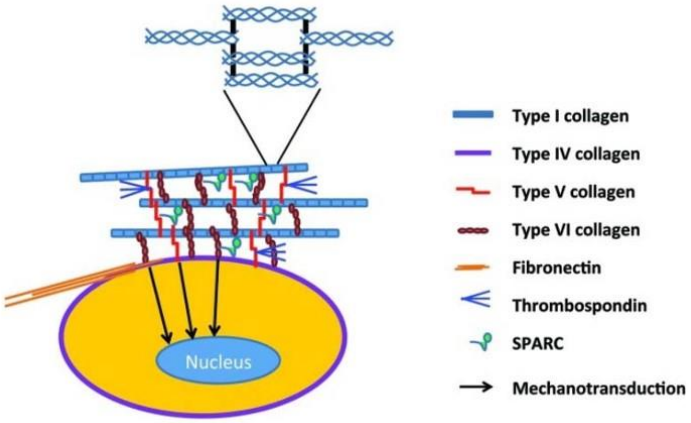


Figure 19. Peri-adipocyte extracellular matrix (SPARC = Secreted protein, acidic and rich in cysteine). (from Chun, Adipocyte 2012).

3.3 Degradation or remodelling of ECM

The ECM of AT is constantly remodelled by the action of metalloproteinases, the two main families being MMPs (Matrix Metalloproteinases) and ADAMTSs (A Disintegrin And Metalloproteinase with Thrombospondin Motifs)[342].

The MMP, as a family of enzymes that degrade ECM includes 23 enzymes, each capable of targeting various types of collagen and ECM proteins with different affinities and efficiencies depending on the target. Most MMPs are initially secreted in an inactive form either in the extra cellular space or in a transmembrane situation. Cleavage of a peptide at the N-terminal part allows the activation of these enzymes. Once activated, their function is restrained by endogenous inhibitors known as TIMPs (Tissue Inhibitors of Metalloproteinases). The TIMP family consists of 4 molecules, each capable of inhibiting specific MMPs with varying degrees of affinity. This intricate regulatory system ensures precise control over ECM degradation[342]

In AT, MMP-14 is the predominant matrix and its levels increase with obesity[343]. Moreover, it can regulate biological processes such as angiogenesis, tumour invasion, immunity and inflammation[344] PMID: 12781798. MMP-9 causes a release of VEGF after the cleavage of collagen IV and stimulates angiogenesis[345].

Similarly, the ADAMTS family comprises 19 members capable of degrading ECM proteins, particularly proteoglycans[346]. The activity of these enzymes is highly regulated.

3.4 Role of the ECM in AT

In addition to its role in maintaining the architecture of the AT, the ECM also performs biological functions. In particular, it plays a major role in the development and maintenance of the AT, as well as in the availability of growth factors. The ECM plays a crucial role in adipogenesis, since adipocyte differentiation requires specific collagen remodelling such as the accumulation of collagen IV which forms the adipocyte basement membrane and also replacement of fibrillar and sparse collagens I by thicker, cohesive collagen V and VI fibers[347]. Furthermore, inhibition of collagen V and VI synthesis or MMPs prevents adipocyte differentiation[348]. Adipocyte secretions are modified during this process, in particular with an increase in MMP2, 9 and 14, which enable the proteolysis of fibrillar collagens and the expansion of adipocyte size due to lipid accumulation[349,350,351]. The remodelling of the ECM extends beyond adipocyte differentiation and persists in mature adipocytes. Notably, a study analysing secretions from mature 3T3-L1 adipocytes revealed the presence of various ECM components, such as COL1A1, COL1A2, and calreticulin. Collagens represented the most abundant proteins in the secretome, suggesting substantial ECM turnover in mature adipocytes[352].

The ECM also acts as a reservoir for growth factors. ECM proteins can bind to several growth factors, protecting them from degradation and storing them for release by proteases. For example, the proangiogenic growth factor VEGF (Vascular Endothelial Growth Factor) sequestered in the ECM in heparin sulphate-bound is under the control of proteases[338].

The ECM serves as a reservoir of peptides derived from ECM macromolecules, known as matrikines and matricryptines, which also regulate cellular functions[353]. These peptides are inactive and require proteolysis for activation[354]. Several matrikines and matricryptines have been described in AT, but they have been studied in the context of obesity and their physiological role is still unknown. The upregulated level of Elastin-Derived Peptides (EDP) in obesity results in enhanced expression of PPARγ and lipogenesis enzymes, thereby promoting insulin resistance and adipocyte hypertrophy[355] by binding to their receptor ECR (Elastin Receptor Complex). Moreover, Endostatin, a cleavage fragment of collagen XVIII known to inhibit angiogenesis, has shown weight-reducing effects through regulation of fat

mass in obese mice[356]. Furthermore, as previously mentioned, endotrophin, a cleavage fragment of collagen VI, amplifies fibrosis, angiogenesis and inflammation through the recruitment of macrophages and endothelial cells to the TA in obesity[335] and promotes tumor progression in breast cancer by increasing cell proliferation, the EMT phenomenon and also resistance to cisplatin treatment[334,357].The underlying mechanisms are poorly described, as neither the protease responsible for this cleavage nor the receptor(s) on which endotrophin acts are known.

4. Vascular organization of AT

AT possesses a rich vascular network, with each adipocyte surrounded by a blood capillary[358,359]. Both endothelial cells and non-endothelial stromal fraction in SVF play a crucial role in formation of vascular modelling. The endothelial cells expressing CD34 and CD31, are capable of self-organization into tubal structures, forming the vascular network[360]. They also adapt the vascular network to the metabolic and functional requirements of AT under the influence of various growth factors, cytokines, and adipokines[361]. The non-endothelial stromal fraction of the SVF is involved in the mature and functional vascular system formation[360]. For example, collagen IV production promotes rapid development of endothelial tube-like structures[362]. The presence of lactate (product of glycolysis in adipocytes and pre-adipocytes), adenosine, and interleukin IL-8 (by macrophages in the extracellular space) stimulate angiogenesis from mesenchymal stem cells and endothelial cells[363].

Moreover, the vascular and adipose compartments interacted closely during adipogenesis. Studies have shown that cells located in the vascular wall provide precursor cells from pericytes which eventually differentiate into preadipocytes and adipocytes[364, 365]. Angiogenic factors, such as FGF-2 and VEGF, increase during different stages of adipogenesis[366]. These studies supported the endothelial and perivascular origin of pre-adipocytes and highlighting the tightly regulated coordination between angiogenesis, adipogenesis, and AT remodelling.

5. AT functions

The main role of WAT is to keep the body's energy balance by storing excess FFA from food in the form of TG and releasing FFA into the circulation to meet the energy needs of different organs. More recently, WAT has been described as an endocrine organ that are able to secrete numerous molecules referred to as adipokines[367].

5.1 Lipogenesis

AT, an essential component of the human body, serves as a major reservoir for storing energy in the form of TG. TG are synthesized within adipocytes by combining three esterified fatty acid (FA) molecules with one glycerol-3-phosphate (G3P) 368 (Figure 20).

The storage of lipids in AT occurs through two primary pathways. In the first pathway, the main source of FA comes from dietary intake, and they are incorporated into lipoproteins such as very low-density lipoprotein (VLDL) in the liver or chylomicrons in the intestines before being transported in the bloodstream. LPL hydrolyses these lipoproteins to release the non-esterified FA[369] (**Figure 20**). The uptake of non-esterified FA into adipocytes through transporters like CD36 (Fatty Acid Translocase, FAT) or by passive diffusion. Once inside the adipocyte, non-esterified FA undergo conversion to acyl-coA by acyl-coA synthase-1 and reesterification into TGs in the presence of G3P subsequently[368]. The glycerokinase, responsible for the synthesis of G3P from ATP and glycerol, being relatively inactive in adipocytes, leads to G3P production either from glucose during the early stages of glycolysis or from glucose metabolites (lactate, pyruvate) through glyceroneogenesis[368].

The second pathway, known as *de novo* lipogenesis, involves the synthesis of FA from glucose within adipocytes. Glucose is taken up by adipocytes through glucose transporters (GLUT-1 and 4) and is converted into pyruvate through glycolysis. Pyruvate is further transformed into FA by acetyl-CoA carboxylase (ACC), which are then esterified to form TGs[368].

Overall, the intricate process of lipid storage in AT is tightly regulated and plays a pivotal role in maintaining energy homeostasis and metabolism.

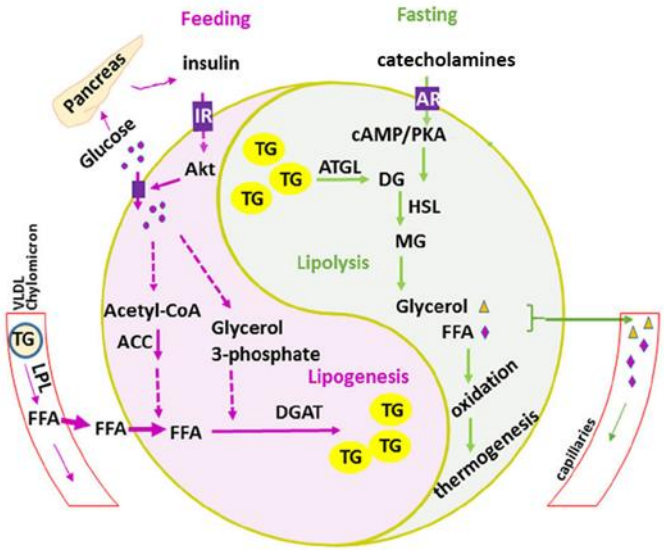


Figure 20. Lipid metabolism and mobilization controlled by AT. AR, adrenergic receptor; cAMP, cyclic adenosine monophosphate; IR, insulin receptor; PKA, protein kinase A. (from Liping Luo, J Endocrinol, 2016)

5.2 Lipolysis

Lipolysis occurs in several successive steps of TG hydrolysis, first into diacylglycerol (DG), then into monoacylglycerol (MG), and finally into glycerol, with each step accompanied by the release of a molecule of non-esterified FA. Three enzymes are responsible: ATGL, HSL (Hormone-Sensitive Lipase), and MAGL (Monoacylglycerol Lipase)[370]. Adipocytes, having very low glycerokinase activity, release glycerol into circulation, making it available for use in other tissues. In contrast, the non-esterified FA, which are toxic and insoluble in the cytosol, will either be taken up by transport proteins called FABP (Fatty Acid Binding Protein) 4 and 5 and released into circulation or re-esterified and stored again in the lipid vacuole[371,372].

Among the three enzymes involved, HSL plays a prominent role in lipolysis, displaying a preferential activity toward DG[373]. Lipolysis is stimulated by catecholamines through β-adrenergic receptors, which activate the adenylyl cyclase/cAMP/PKA signaling pathway[374]. PKA, in turn, phosphorylates HSL, translocating it from the cytoplasm to the lipid droplet surface, where it exerts its lipolytic activity[375] (**Figure20**). Conversely, lipolysis can be inhibited by catecholamines through their α-adrenergic receptors and by insulin, which is the main anti-lipolytic hormone[372]. Lipolysis is tightly controlled to meet the metabolic demands of the body. Under basal conditions, lipolysis is maintained at a low level, preserving the triglyceride (TG) stores for future demands. Conversely, during energy-demanding scenarios, such as fasting, exercise, or stress, lipolytic stimulation occurs, facilitating the release of free FFA to serve as a principal fuel source for diverse tissues[376] (**Figure20**).

5.3 Secretions

The adipokines secreted from AT play a pivotal role in regulating a wide range of physiological processes, including energy homeostasis, inflammation, insulin sensitivity, and appetite control. Through their secretion into the bloodstream, adipokines exert both local and systemic effects, influencing various tissues and organs throughout the body.

Leptin was the first adipokine to be discovered (along with TNFα) in 1994[377]revolutionizing the view of TA as a simple, relatively inert energy reservoir. It is mainly (but not exclusively) secreted by adipocytes and AT is the major source in the body[378]. It plays a key role in regulating metabolism and controls weight by regulating the sensations of hunger and satiety in the hypothalamus[379].

Adiponectin, as the most abundant adipokine, is secreted exclusively by AT. It plays a crucial role in maintaining metabolic balance[380]. For example, it helps to maintain an anti-inflammatory microenvironment by inducing the secretion of IL10 by macrophages[381]. It also enhances insulin sensitivity in peripheral tissues, such as skeletal muscle and liver by increasing β-oxidation and decreasing liver production of glucose[382].

Conversely, some adipokines have been implicated in promoting insulin resistance and inflammation.

Tumor necrosis factor-alpha (TNF-α) is the first pro-inflammatory cytokine secreted by AT that has been discovered[383]. With **interleukin-6 (IL-6)**, both adipokines are upregulated in obesity. They have a pro-atherogenic role by increasing inflammation of the vessels and pro-diabetic role by inhibiting insulin signalling pathways[384,385]. In PCa, elevated IL-6 levels are also associated with the aggressiveness and progression of PCa as described in chapter 7.2 and 7.6.b.

Resistin has been associated with insulin resistance in obese rodents, although its role in humans remains controversial[386]. Visfatin, also known as nicotinamide phosphoribosyl transferase (NAMPT), has been linked to insulin resistance and inflammation in metabolic disorders[387].

In addition, other adipokines have been described in AT such as PAI-1 (Plasminogen Activating Inhibitor-1), angiotensinogen, RBP-4 (Retinol Binding Protein-4) but I will not explain them here in detail[388]. Beyond their systemic action, adipokines can play an autocrine or paracrine role in AT because adipocytes have receptors for leptin, adiponectin, IL-6 and TNFα[388].

5.4 AT modification in obesity

Obesity, a prevalent and complex health condition, is fundamentally defined by the excessive accumulation of AT in the body[389]. This condition is a consequence of an intricate interplay between genetic predisposition, environmental factors, and lifestyle choices[389]. Two primary mechanisms contribute to the expansion of AT in obesity: hypertrophy which corresponds to the increase of adipocyte size, and hyperplasia, which corresponds to the increase of adipocytes number formed by recruitment, multiplication and differentiation of adipocyte progenitors[389]. Genetic factors and diet as well as the location of deposit play significant roles in determining how much these two mechanisms contributes to the expansion of AT during obesity[389]. For example, adipocyte precursor cells from SAT differentiate better, whereas ADSCs from VAT

have a relative "resistance" to differentiation, which may explain why, in obesity, VAT develops mainly by hypertrophy and SAT by hyperplasia[390,391,392].

Obesity-induced irreversible remodelling of AT function not only inhibits AT healthy expansion but also exert systemic effects that contribute to the pathogenesis of metabolic disorders such as insulin resistance, type 2 diabetes, and cardiovascular diseases[393,394,395].

Three main mechanisms involved in this AT remodelling including inflammation, hypoxia and the angiogenic response and fibrosis will be further described in detail.

Inflammation

In obese individuals, AT undergoes a phenotypic shift characterized by immune cell infiltration and elevated levels of pro-inflammatory cytokines as described below.

It has been demonstrated that adipocyte hypertrophy is accompanied by an increased release of pro-inflammatory cytokines such as TNFα and IL-6, as well as chemoattractant like MCP-1, which promote chemoattraction of pro-inflammatory M1 macrophages into the AT via the MCP-1/CCR2 pathway[396,397]. Extreme adipocytes hypertrophy exposed to an abundance of lipid toxins undergo structural changes like organelle expansion and plasma membrane disruption. It is observed that these deteriorating adipocytes are surrounded by macrophages forming "Crown-like structures, CLS" ultimately resulting in the phagocytosis of these adipocytes[398,399]. Moreover, obese AT activates CD8 (+) T cells, which, in turn, promote the recruitment and activation of macrophages in this tissue[400]. However, early lymphocyte infiltration might protect against AT inflammation during obesity and insulin resistance[401] (**Figure 21**).

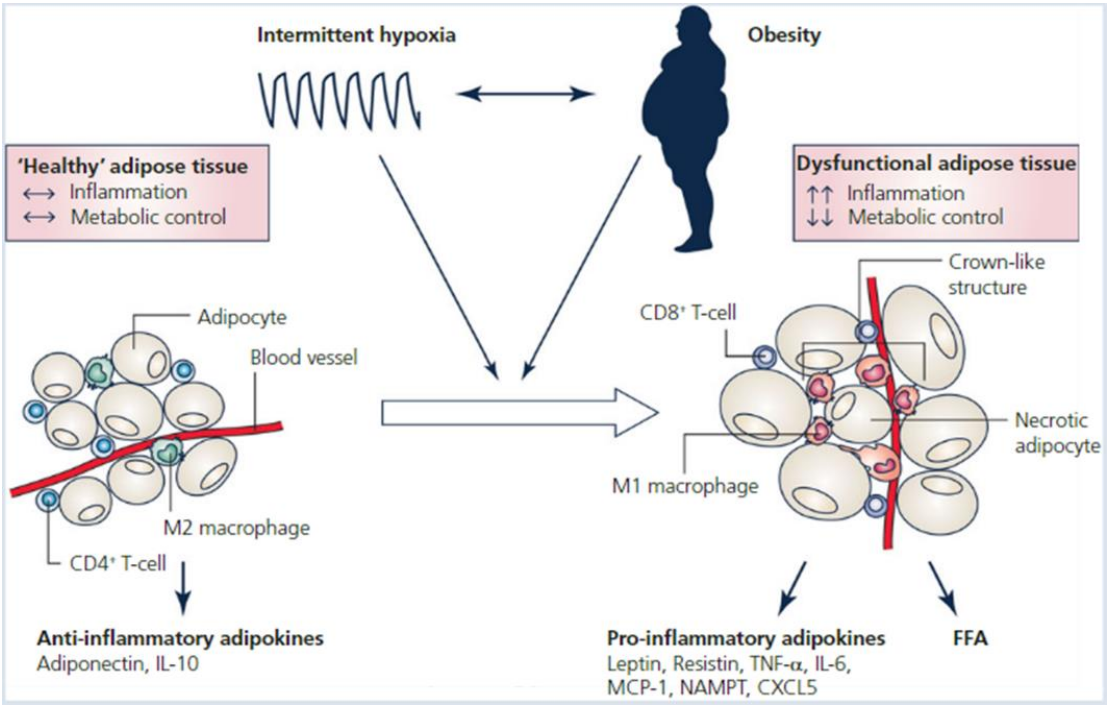


Figure 21. Inflammation in obesity in AT. (from Silke Dyan, J Physiol, 2017)

Hypoxia and the angiogenic response

Obese AT becomes hypoxic due to the inability of the vasculature to keep space with tissue growth[402]. Adipocyte hypertrophy could be the initial cause of AT hypoxia. As adipocytes increase rapidly in size in hypertrophy status, they outgrow their existing blood supply. This results in regions of AT becoming distanced from functional blood vessels, creating pockets of hypoxia within the tissue[403]. The AT response to hypoxia is not as adapted in obesity as in physiological situations. HIF-1α pathway is upregulated in hypoxia associated with inflammation, notably by the NO (nitric oxide) pathway activated by macrophages[404]. Furthermore, hypoxia affects the process of pre-adipocytes maturing into mature adipocytes by regulating the C/EBP-α and PPARγ pathways"[405]. This has direct consequences for the organization of the AT, with increased angiogenesis, as pre-adipocytes secrete a pro-angiogenic factor, β-FGF[406]. Finally, increased secretion of leptin, pro-inflammatory cytokines (e.g. PAI-1, IL-6) and decreased secretion of adiponectin is observed in hypoxia which leads to a disruption of the secretory homeostasis of the AT[407] (**Figure 22**).

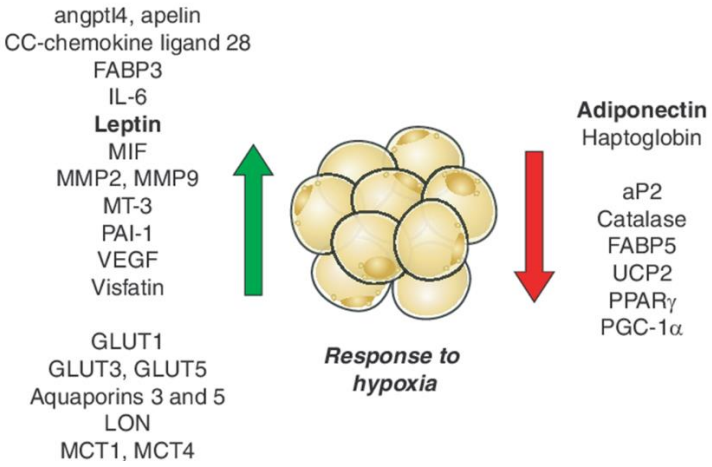


Figure 22. Presentation of genes whose expression is increased (green arrow) or decreased (red arrow) in response to the hypoxic state in AT (genes are presented by their protein name for consistency with the text) (from Trayhurnet al., Biology Physiological reviews, 2013)

Fibrosis

The hypoxic state in obese AT activate HIF-1α pathway promoting AT fibrosis, with an associated increase in local inflammation[408]. Fibrosis involves the excessive deposition of ECM components, particularly collagen, altering the AT architecture and impairing its plasticity[409]. This local inflammation in obesity leads to a remodelling of the ECM by increasing fibrillary collagen fibers production[332]. These fibers form dense clusters around adipocytes, which may restrict expansion of adipocytes[332]. It has been reported that Type VI collagen (Col6) is involved in the fibrosis of obese AT. Adipocytes expansion in mice lack of Col6 are no longer limited. And they present a less inflammatory state compared to that from wild-type mice[332]. Meanwhile, the expression of genes encoding ECM proteins such as collagen type I α1 (COL1A1), collagen type VI α3 (COL6A3), luminance (LUM) and tenascin C (TNC) is increased in obesity in humans. Moreover, in obesity, saturated FA-activated toll-like receptor 4 (TLR4) plays an important role in the development of fibrosis by stimulating macrophages which in turn secrete TGFß1 involved in the pro-fibrotic pathway[410,411] (**Figure 23**).

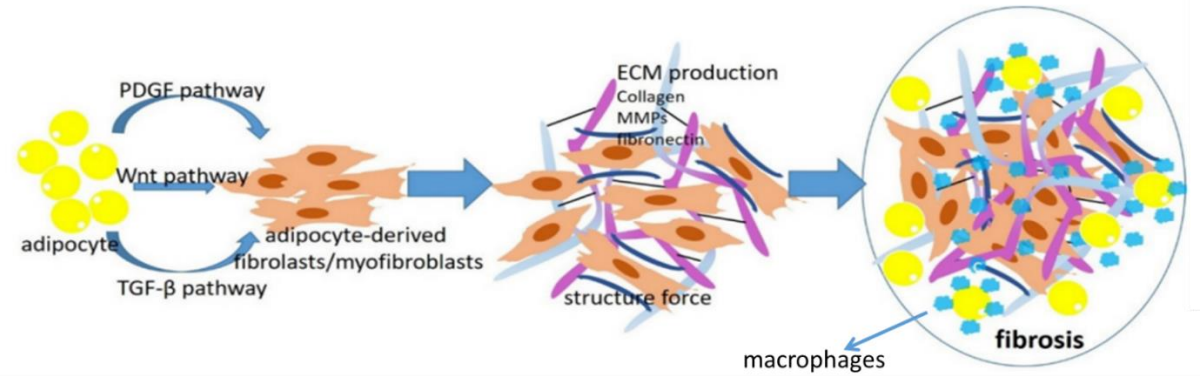


Figure 23. The mechanism underlying obesity-associated fibrosis. During obesity development, adipocyte-derived fibroblasts/myofibroblasts deposit significant amounts of ECM and ECM-related enzymes, including collagen, fibronectin, and MMPs. (from Junyan Li et al., Cancers, 2022)

These changes have been mainly described for "classical" adipose depots such as SAT and VAT. However, it is important to note that the "minor" adipose depots might behave differently as we will see below for the periprostatic adipose tissue which is fibro-inflammatory already in lean patients. Furthermore, my team have also demonstrated that in MAT there is an increase in resident macrophages without any occurrence of fibro-inflammation (Fallone et al, in prep).

Part 3 Periprostatic adipose tissue (PPAT)

The prostate gland is surrounded by a fat depot called periprostatic AT (PPAT). As a new player in PCa, the anatomic of PPAT and its role in PCa will be described in this chapter.

1. Anatomical description of PPAT

PPAT is situated in the sub-peritoneal region, limited anteriorly by the pubic symphysis, posteriorly by the recto-prostatic fascia, and laterally by the obturator muscles[412]. The prostate gland and adjacent PPAT are separated by a fibromuscular sheet known as the prostate fascia or "capsule," which varies in thickness and predominantly exists on the lateral faces of the prostate gland. Notably, approximately one third of the anterior surface of prostate gland is directly in contact with PPAT since the anterior zone lacks a capsule[412]. The sagittal and axial magnetic resonance imaging (MRI) sections of PPAT location is shown in **Figure 24A**. Therefore, vascularization of the prostate could cross PPAT which favours molecular exchanges between PPAT and cancer cells (**Figure 24B**). The extra prostatic extension into PPAT is a significant clinical prognostic indicator for negative outcomes[413] that will be explained in detail in the next chapter.

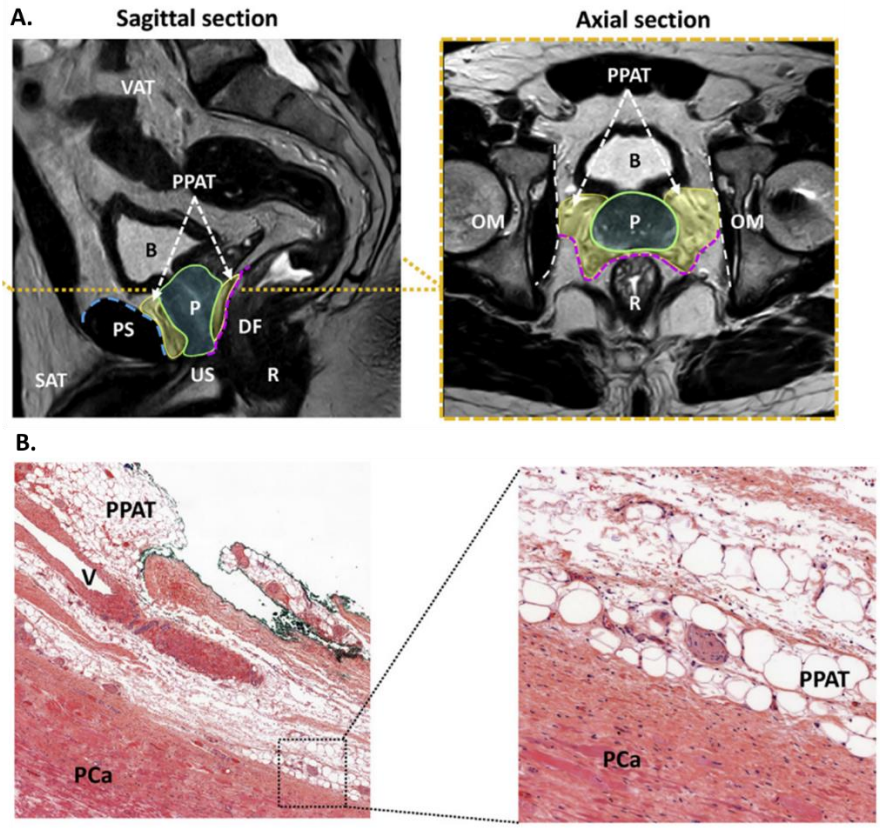


Figure 24. A. **Periprostatic AT (PPAT) surrounds the prostate**. Prostate (P); Bladder (B); Urethral sphincter (US); Pubicsymphysis (PS, blue dotted line) and Denonvilliers' fascia (DF, purple dotted line), obturator muscles (OM). DF separates PPAT and rectum (R). SAT and VAT, respectively, are indicated to highlight the anatomical

distance between these fat depots and the prostate. MRI, magnetic resonance imaging**. B. PPAT and the prostate are in close proximity.** Hematoxylin eosin staining of PCa and adjacent PPAT on histological section. The blood vessels (V) responsible for nourishing the prostate traverses the periprostatic AT (PPAT). (from Esteve et al., Current Opinion in Endocrine and Metabolic Research, 2020)

In mice, the prostate is an intricate organ constituted by four distinct lobes circumferentially around the urethra. Perigonadal fat as the largest proximal WAT is situated within the peritoneal cavity with the prostate[414] Considering the heterogeneity of the perigonadal fat anatomy between mice and human, cautions should be taken in studies using mice models.

2. Characterization of PPAT

The specific morphological and functional characteristics of PPAT has been revealed in several studies. First, compared to SAT: (i) PPAT adipocytes are smaller (ii) they have the same basal lipolysis but (iii) PPAT are more sensitive to isoproterenol-stimulated lipolysis[415]. Secondly, PPAT has a significantly higher amount of adipose derived stem cells than paired VAT, independently of body mass index and prostatic disease[416]. Recently, a study of our group, in which I took part, shows that unlike the general AT, PPAT secretes high level of pro-inflammatory cytokines even in lean individuals and its volume does not increase in obesity. PPAT exhibits hypoxic state with a sparse vascular network found in it compared with that in abdominopelvic AT (APAT), an extra peritoneal adipose depot, whose accumulation is correlated to body mass index. Meanwhile, in this chronic hypoxic state, inflammation and fibrosis were observed, and were not further up-regulated by obesity (Article presented in the Result's part 1). These traits make PPAT a specific AT whose regulation of accumulation is unique, independent of obesity. Its close proximity to the prostate indicates that the accumulation of PPAT could be coordinated with the growth of the prostate which evolves from puberty under the influence of steroid hormones.

3. The interplay between PPAT and PCa

The AT in close contact with specific organs has attracted considerable interest due to its potential paracrine functions such as mammary AT surrounding breast tissue. PPAT is capable to secrete diverse factors including pro-inflammatory cytokines, chemokines, lipid, hormones, and so on. Some studies evaluated the role of these secreted factors from PPAT on normal prostate function[417,418]. However, in this chapter, I will only focus on the studies which reveal the interplay between PPAT and PCa and are resumed in a review written by our group[419].

3.1 The influence of PPAT on PCa development

Adipokine

Adiponectin is shown to have an anti-tumour effects in PCa *in vivo* whereas leptin has proliferative effects in these cells. However, their level does not correlate with PCa aggressiveness in 30 PPATs from patients underwent radical prostatectomy[420]. The **pro-inflammatory factors** such as IL-6 and TNF-α play a more positive role in PCa progression. One study showed that IL-6 in PPAT-conditioned medium was around 375 times abundant than in patient matched serum and levels correlated with pathological grade[421]. Furthermore, cell signalling analysis demonstrated that STAT3 regulated by IL-6 exhibited greater phosphorylation in PPAT with higher gleason score[421]. Another study also demonstrated that intensity of IL-6 expression in PPAT was associated with PCa aggressiveness[421]. Immunostaining of TNF-α in PPAT showed a positive correlation with high-grade PCa[422]. In addition, PPAT inflammation, reflected by the amount of crown-like structure (CLS) was identified in half of patients and associated with higher BMI and Gleason grade. Interestingly, the relationship between PPAT inflammation and high Gleason grade remained significant after adjusting for BMI[423]. Meanwhile, PPAT obtained from PCa patients demonstrates an increased expression of inflammation-associated genes compared to those from BPH[424].

Comparison of PPAT transcriptome data in patients at higher risk and lower risk revealed that genes involved in inflammation and immune responses predominated the differences between the two groups[425,426]. Thus, PPAT inflammation could be seen as a key factor in PCa progression more than obesity.

Chemokines

Chemokines secreted by PPAT exert the crucial role in PCa local dissemination. The two most widely investigated axis in human are the CCL7-CCR3 axis and CCL2-CCR2 axis. Both *in vitro* and *in vivo* studies demonstrated that secretion of C-C motif ligand 7 (CCL7) by PPAT adipocytes, amplified in obesity, promoted directed migration of CCR3-positive PCa cells (**Figure 25A**). Moreover, clinical data showed that expression of CCR3 receptors was associated with the risk of aggressive disease with extended local dissemination and biological recurrence[427]. CCL2, also named MCP1 (monocyte chemoattractant protein 1) secreted by differentiated adipocytes, promote the invasive capabilities of PCa via the activation of metalloprotease 2 (MMP2) and increase of CCR2 receptor expression *in vitro*[428]. In addition, CXCL12 secreted by stromal cells from PPAT and upregulated by obesity, activates the

invasiveness of PCa cells in a manner of CXCR4 /CXCR7 receptors dependent way in mice[429] (**Figure 25B**). Meanwhile, prostate tumour cells promote the migration of PPAT ASCs to tumours *in vivo* in a CXCR1/CXCR2-dependent manner by secreting the chemokines CXCL1 and CXCL8[430].

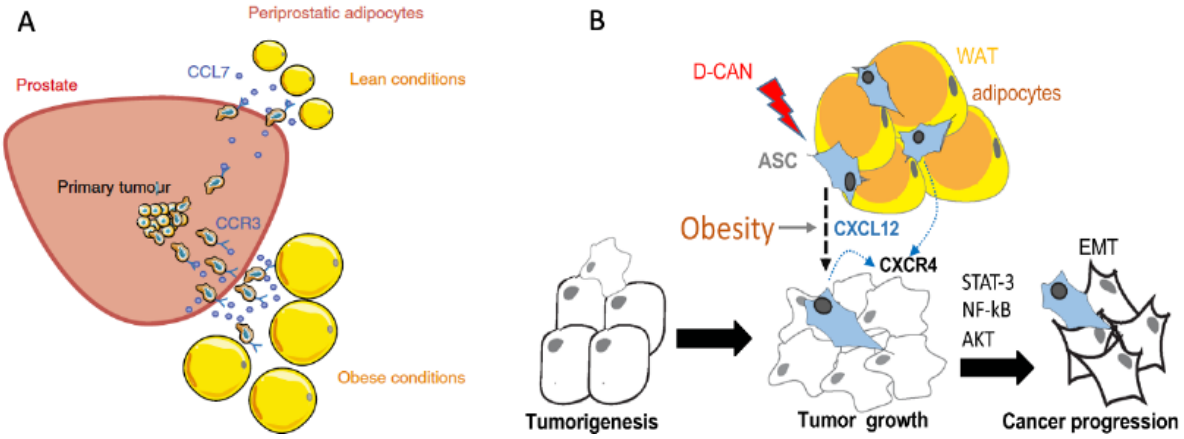


Figure 25. Role of chemokines secreted by the PPAT under lean and obese conditions in tumor proliferation. A/ Role of the CCL7-CCR3 axis in extra prostatic migration of tumor cells according to Laurent et al., Nature Com, 2016. B/ Role of the CXCL12-CXCR4 axis in the activation of signaling pathways involved in tumor progression according Su et al., NPJ Precision Oncology, 2021.

Lipid

Another important aspect of the dialogue between PPAT and PCa is the involvement of lipids. Some cancer cells such as breast and ovarian cancer are able to induce lipolysis in tumor-surrounding adipocytes and then uptake liberated FA for their own progression[431,432]. FA has been shown to be a dominant energetic substrate for PCa[433]. Our group showed that PCa cells induce lipolysis of PPAT adipocytes. Consequently, FFA liberated from PPAT are further used by PCa cells to increase their oxidative stress and then promote invasiveness. The signalling pathways described involve NOX5, an isoform of the pro-oxidant enzyme NADPH oxidase, which leads to the expression of MMP14 via reactive oxygen species production. Expression of NOX5 and MMP14 is upregulated at the invasive front of human tumours, where cancer cells are found close to adipocytes compared to that at the centre of the tumour. The characteristic is amplified in the context of obesity[434].

Notably, different species of lipid differentially influence PCa progression with anti-migratory effect of n-6 PUFAs linoleic acid but pro-migratory effects of saturated FA[435].

It was confirmed in one study conducted in African-caribbeans. Their FA profile associated with PCa aggressiveness was characterised by low level of linoleic acid but high levels of

saturated FA. Moreover, *in vitro* migration potential was increased with FA extracted from PPAT whose linoleic acid content is lower[436].
In addition, FA uptaken by PCa cells could be stored and incorporated into intracellular lipids mainly TG and cholesterol esters in the form of lipid droplets (LDs)[437]. The LDs marker Perilipin were increased in extraprostatic areas where cancer cells are in contact with PPAT compared to intraprostatcic areas[438]. The esterified cholesterol accumulation in LDs is associated with high-grade PCa and metastases which related to loss of tumour suppressor PTEN and activation of PI3K/AKT pathway in PCa cells[439].

In PPAT from high-risk PCa patients, the expression of genes involved in *de novo* FA synthesis, such as FASN (Fatty Acid Synthase) and ACACA (Acetyl-CoA Carboxylase), is lower compared to those from low-risk PCa patients. Besides, co-cultured PPAT explants with PCa cell lines exhibit downregulation of lipid metabolic-related genes (CD36, FASN, PPARγ, and CPT1A), whereas the co-cultured PCa cell lines exhibit an opposite trend. A consequential augmentation in lipid uptake and accumulation and also the expression of tumor-related genes in gene expression in PCa cell lines was observed[440] (**Figure 26**).

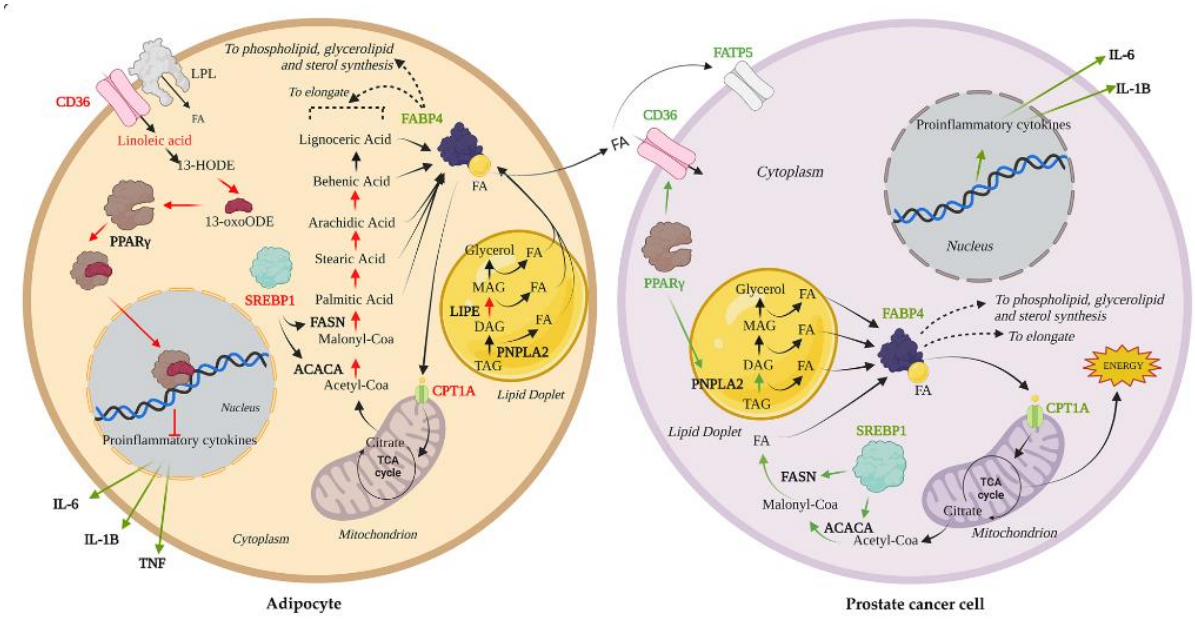


Figure 26. Scheme illustrating lipid metabolite alterations, related pathways, and implicated genes in human PPAT and PCa cell lines. 13-HODE, 13 hydroxy-octadecadienoic acid; 13-oxoODE, 13-oxo-octadecadienoic; PPARG, peroxisome proliferator-activated receptor gamma; IL-6, interleukin 6; IL-1B, interleukin 1 B; TNFα, tumor necrosis factor alpha; FASN, fatty acid synthase; SREBP-1, sterol regulatory element binding transcription factor 1; ACACA, acetyl-CoA; CPT1A, carboxylase alpha; Carnitine Palmitoyl transferase 1A; LIPE, hormone-sensitive lipase; MG, monoglyceride; DG, diglyceride; TG, triglyceride; FABP4, fatty acid binding protein 4; FA, fatty acid; PNPLA2, patatin-like phospholipase domain containing 2; CD36, CD36 molecule; LPL, lipoprotein lipase (from Altura-Coy et al., BMC Medicine, 2022)

Osteopontin

Osteopontin is a protein involved in inflammation and immune responses. The expression of osteopontin was increased in PPAT upon conditioned medium treatment of PCa cell line PC3[434]. Moreover, in mice model genetically modified to be prone to PCa, when the signaling adaptor p62 was inactivated specifically in adipocytes, it leads to a general shutdown of energy-utilizing pathways in adipocytes whereas activates the energy utilization in PCa. This effect is linked to an increase in osteopontin, which reveals a central role of osteopontin in the symbiotic AT-tumor collaboration that enables PCa metabolic fitness[441].

Hormones

Free Cholesterol as the initial substrate for steroid biosynthesis, its content in PPAT from Afrian-Carbbean is associated with PCa aggressiveness[442]. However, whether it triggers downstream sex steroids change is not clear. Indeed, WAT is capable of synthesis and metabolize steroid hormones which I will review later. Several evidences demonstrated androgens precursors supported PCa growth as described in 7.4.e. But sex steroid quantification of PPAT and their role in this interplay with PCa has never been elicited thus my thesis work holds great significance. It is noticeable that there exists some relationship between adipokines and hormone metabolism. For example, leptin increased the expression of aromatase and ERα in PC-3[443], which could be taken into consideration while investigating the role of sex hormones.

As described in this chapter, all these studies show that PPAT acts on tumour progression via numerous actors secreted by both adipocytes and adipocyte progenitors. These data are summarized in **Figure 27**.

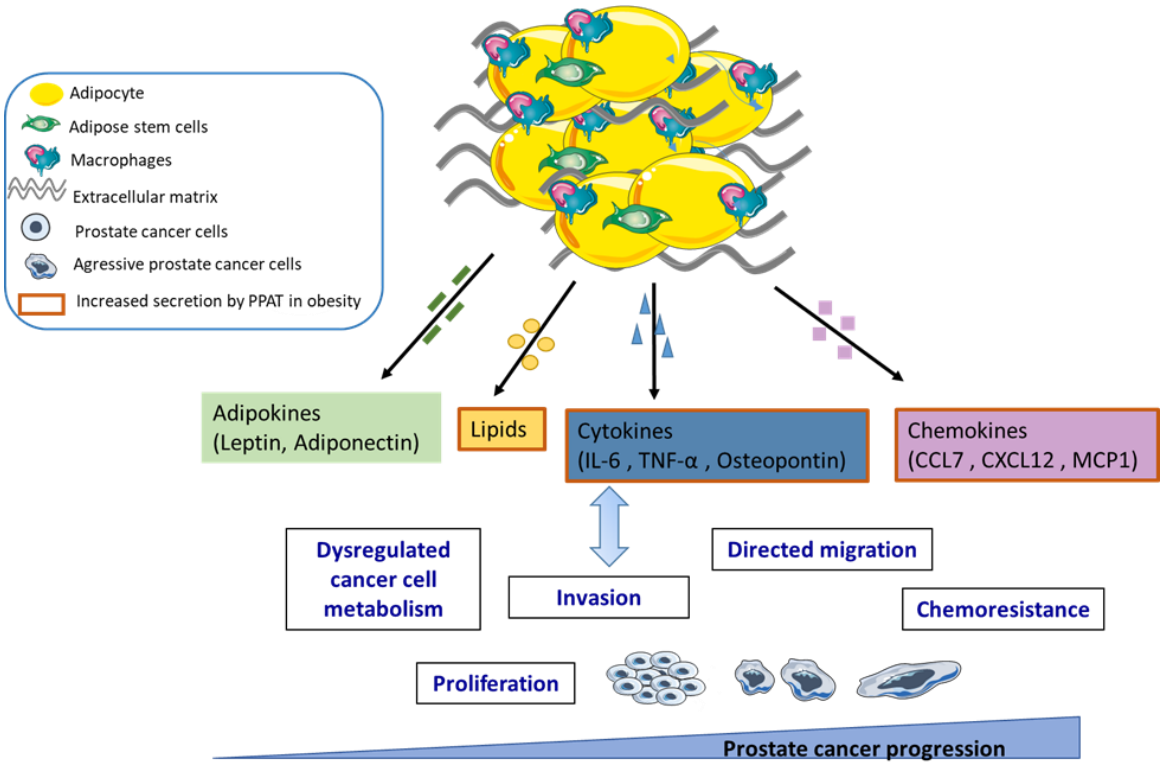


Figure 27 Bidirectional crosstalk between PPAT and tumor cells promotes prostate cancer progression: a process amplified in obesity Secretions emanating from PPAT (blue squares) are able to modify cancer cell behavior and promote tumor progression. The effect of some secretions (chemokines, proinflammatory cytokines) or the released lipids has been validated using coculture between human PPAT and cancer cells, animal models and/or human samples (solid arrows) while the effect of leptin and adiponectin has only been demonstrated in vitro (dotted arrows). Secretion levels of the factors upregulated in PPAT from obese patients are underlined with red squares (adapted from Esteve et al., Current Opinion in Endocrine and Metabolic Research, 2020).

3.2 The influence of PCa cells on PPAT behavior

It's not only PPAT that influences the progression of PCa; Conversely, PCa cells also exerts an impact on the remodelling of PPAT, which may trigger a more pronounced impact on the PCa progression. Cancer-Associated Adipocytes (CAAs), which exhibit a specific phenotype because of the interaction with tumour cells was first introduced in 2011 by my group[444]. CAAs are smaller than naïve adipocytes and their lipid content is decreased due to delipidation. Adipokines secreted by CAAs exhibit an increased pro-inflammatory phenotype compared with naïve adipocytes[444]. CAAs are also observed in the co-culture of mature adipocytes with PCa cells[445]. Moreover, the expression of adipokines associated with cancer progression such as osteopontin, TNF-α and IL-6 from PPAT explants is increased upon the stimulation with PCa PC3 conditioned medium whereas the expression of the protective adipokine, adiponectin, is decreased[434].

3.3 Beyond obesity

Numerous studies (including our work) have found that unlike all other visceral ATs, there is lack of correlation between PPAT accumulation and BMI[446,447,448] even though obesity has an influence on PPAT function. Interestingly, PPAT accumulation, have been shown to be correlated positively with the aggressiveness of the PCa defined by Ash, D'Amico scores[449,450] or high Gleason score on prostatectomy pieces[451,447]. Moreover, the abundance of PPAT is associated with worsened progression-free survival in men with PCa on active surveillance[452] and could predict occurrence of castration resistance for patients who have been received ADT[453,454]. Although measurement methods for defining abundance are widely varied, consistent results showed the link between PPAT abundance and PCa aggressiveness which has been reviewed by Zeyad D Nassar et al[455]. However, the mechanisms that explain PPAT accumulation and the contribution of abundant PPAT to PCa progression remain unknown. Recently, the study of our group, in which I took part brings some answers to this question (Article presented in the Result's part 2). Briefly, we employed a statistical methodology to define abundant PPAT by standardizing PPAT volume to prostate volume, within a cohort comprising 351 patients with a linear regression model. Then we found patients with abundant PPAT exhibit several hallmarks of aggressiveness, suggesting that PPAT abundance might be used to improve risk stratification. Furthermore, our investigation demonstrates that the occurrence of abundant PPAT is associated with adipocytes hypertrophy whereas unaccompanied with the inflammatory state as in obesity. This inflammation-free hypertrophy is due to a reduction in mechanical stress as seen by the extensive extracellular matrix remodelling, notably of the collagen framework, coupled with a downregulation of mechanic-sensing proteins in adipocytes. Moreover, collagen VI degradation in abundant PPAT is associated with production of endotrophin, a matrikine that promotes cancer progression. Notably we find high levels of endotrophin specifically in the urine of patients with abundant PPAT, thus underscoring the clinical relevance and translational potential of our findings.

In addition, some studies suggest that PPAT accumulation might be regulated by androgens. PPAT volume is correlated to prostate size which indicates a coordinated development of these two tissues under the control of sexual steroids[451]. Patients exposed to treatment with 5α-reductase inhibitor, blocking the transformation of testosterone into DHT, exhibited a decreased PPAT volume compared to control[456].

Taken together, all these studies highlight the importance of PPAT in prostate cancer progression. Although androgens are key to PCa progression, none of the studies have investigated the role of androgens secreted by PPAT in this crosstalk despite the fact that AT are known reservoir of androgens as I will described in the next chapter.

Part 4 Steroid hormones and AT

This aim of this chapter is to provide an overview of our current knowledge on sex steroids and AT with a more in-depth focus on androgens. It summarizes the steroid metabolism of AT, the functional effects of androgens on AT and the potential effects of androgens from AT on general and/or androgen homeostasis in physiology and pathology. We are planning to publish this chapter as a review.

1. Steroids quantification and synthesis capacity in AT

1.1 Production of sex steroids by different AT in humans and other species

a. WAT

The fact that steroid hormones including androgens are detectable in AT has been known from physiologists for a long time. Initially, it has been described that a large fraction of the peripheral conversion of androgens to estrogens occurs in AT[457]. Rapidly a growing interest occurs to decipher if AT is an important steroid reservoir and potentially a site of steroid metabolism. In general, due to the major role of estrogen in the development of breast cancer, a large number of studies has dosed these sex steroid hormones in the mammary adipose tissue (MAT) whose large amounts can be obtained from mastectomy. Meanwhile, there are many studies done in women with Polycystic Ovary Syndrome (PCOS), which is a common hormonal disorder that characterized by a combination of irregular menstrual cycles, high levels of androgens (male hormones) inducing an excess of VAT, and the presence of small cysts on the ovaries[458]. Several mains results have been obtained from these studies.

Firstly, DHEA is the most abundant sex steroid in WAT. For example, DHEA was found thousands of times more elevated than other metabolites detected such as androstenediol, androstenedione, testosterone, estradiol and estrone in both MAT and abdominal subcutaneous AT (SAT) from postmenopausal women[459]. In another study in MAT, DHEA represented the highest percentage (35%) in 31 measured metabolites including 27 androgens, progestogens and 4 estrogens[460]. Other studies also showed that DHEA concentration was highest in women MAT independently of menopausal status and in abdominal SAT from both men and women[461,462,463,464]. DHEA accounts for 70% of the total five metabolites including androstenedione, testosterone, estrone, 5α-DHT quantified in both omental (OM) AT and SAT in obese men[465].

Secondly, the concentration of the precursors stored in AT are higher than their downstream metabolites and in particular the active form of androgens or estrogens. Androstenedione and 17β testosterone are the precursors for the synthesis of estrone and estradiol respectively (**Figure 27**). Several papers showed the following concentration order in women MAT independently of menopausal status: androstenedione >> estrone > testosterone > 17β-estradiol[463,464] in accordance with another study showing that the active androgen testosterone levels are higher than 17β-estradiol in MAT[462]. Estrogens represented only 1% whereas upstream precursors including pregnenolone, androstenedione and 17α-hydroxypregnenolone as well as DHEA, accounted for 80% of the total steroid hormone profile in MAT[460]. The most active form of androgen, 5α-DHT was dosed in omental (OM) AT from obese men but it was the metabolite with the lowest concentration compared to other four metabolite concentrations following this order: androstenedione >testosterone>estrone>5α-DHT[465]. Compare to rodents, **The sex steroid dosage profile in human AT are not really depot nor sex dependent.** For example, in one study, the mean concentrations of DHEA, DHEA-sulfatase (DHEA-S), androstenedione, androstenediol, estrone, and 17β-estradiol were similar in OM AT and SAT from 15 patients including both men and women with the only exception of testosterone concentration which were higher in men than in women[462]. Another study including female and male subjects and using radio immunological methods showed that the concentration of steroids followed the same order (DHEA > androstenedione > progesterone > testosterone > 17α hydroxyprogesterone > 17β-estradiol and estrone) in both MAT and abdominal AT obtained from surgery in patients with cholelithiasis and hernia inguinalis[461]. Another study showed that MAT and abdominal SAT from postmenopausal women displayed a similar profile with slightly higher content of DHEA and androstenediol in MAT, and slightly higher testosterone, 17β-estradiol and estrone in SAT[459].

Since most of these studies used MAT coming from mastectomies for breast cancer, it was interesting to evaluate if there is a change in hormone content between the proximal and the distant MAT from the tumours. In one study, among the 14 metabolites detected out of 31 measured in 51 patients, only 17β-estradiol concentration was increased in the proximal compared to the distant MAT[460] whereas another group only found a slight decrease of estrone concentration[463]. Interestingly, differences have been observed between types of breast cancer. The concentrations of androstenedione, testosterone, androsterone, estrone and 17β-estrodiol were significantly higher in estrogen receptor and progesterone receptor positive (ER+/PR+) samples than in estrogen receptor and progesterone receptor negative (ER−/PR-) samples

despite BMI being slightly higher in the latter group[464]. Among them, the testosterone change was the most obvious with almost 40% higher content in women with ER+/PR+ compared to ER−/PR− tumours[463].

Moreover, changes in steroid content could be observed in women with pathological conditions such as PCOS or with obesity in both women and men. DHEA, androstenedione, and testosterone were significantly increased in abdominal SAT of PCOS women compared to the healthy women[466]. 5α-DHT was also detected with its content being 5 times higher in abdominal SAT from PCOS women than in the healthy women[466]. Androstenedione and 5α-DHT levels were higher in SAT and VAT of obese women compared to lean women but this increase was not significant due to the small sample size and strong inter individual variation. There was, however, a significant 7.9-fold increase of testosterone in VAT of obese women compared to lean one[467]. The obese patients including women and men weighing over 10 kg more than normal weight patients had 10-20 times higher concentrations of metabolites including DHEA, androstenedione, progesterone, testosterone, 17α hydroxyprogesterone, 17β estradiol and estrone in MAT and abdominal AT[461]. Furthermore, some depot difference could be seen in obesity. For example, OM AT contains more DHEA, androstenedione and 5α-DHT levels than SAT in obese men[465].

Also, age has an influence on sex steroid production. Androgens decreased with age (>60-year-old) in men and women abdominal SAT[462].

Even though only a few sex steroids species were able to be detected in rodents compared to human, the sex and depot differences concerning sex steroids contents are more obvious in rodents than in human (**Figure 28**).

Sex-specific differences have been reported in WAT from rodents. For example, in mice, testosterone and its sulphated form testosterone-S was detected in male inguinal white AT (iWAT), epididymal white AT (eWAT), but not in female mice tissues[468]. Free DHEA was detected only in iWAT and eWAT of male high fat diet (HFD)-fed mice and parametrical white AT (pmWAT) of female mice (no detection of conjugated DHEA in those tissues)[468]. 17β estradiol was only detected in female WAT in one study[469]. In rat, testosterone levels were higher whereas progesterone levels were lower in male AT than in female AT in all the investigated AT including inguinal, retroperitoneal, gonadal and mesenteric AT[470].

Depot and age-specific differences can be found in AT from rats. For example, testosterone levels were higher in retroperitoneal compared to inguinal AT[470]. High amounts of testosterone were measured in periovarian and inguinal AT of young and adult female rats and in supernatants of isolated preadipocytes and adipocytes[471]. The testosterone concentration in the periovarian AT was 4 times higher than in the inguinal depot of young animals whereas it was similar between depots in adult animals[471]. The testosterone level was decreased 6 times in periovarian AT and 2 times in inguinal AT in old rats compared with young rats[471]. 17β-estradiol was detected in male and female inguinal, retroperitoneal, gonadal and mesenteric WAT with no sex differences but inguinal WAT contains higher levels of this metabolite compared to the other adipose depots[470].

Furthermore**,** like in human**,** testosterone concentration was 3 times higher than the more active form 5α-DHT in male mice WAT[469]. Whereas, the contents for testosterone and testosterone-S were not affected by obesity[468].

b. Brown Adipose Tissue (BAT)

Brown AT (BAT) is a specialised type of AT located in the cervical, supraclavicular, axillary, peri-aortic, paravertebral and suprarenal regions in adult humans[472]. It plays a role in thermogenesis and energy expenditure due to its unique expression of UCP1, which enables the release of energy as heat[473]. There exists a sex dimorphism when it comes to BAT activation in humans as women generally have a higher prevalence of active BAT than men, as observed in positron emission tomography–computed tomography (PET/CT) scans[474,475].

Very few studies investigated the steroid content and metabolism in BAT. Androsterone was identified in BAT of the alp-marmot, badger and rat for the first time[476]. Testosterone and testosterone-S was detected in male mice BAT[468]. In BAT from female mice, both DHEA-S and free DHEA were identified. DHEA-S levels were found to be higher than those of free DHEA[468]. However, others studies were unable to detect any steroid production or steroid enzyme expression in BAT of normal mice[477,469,478].

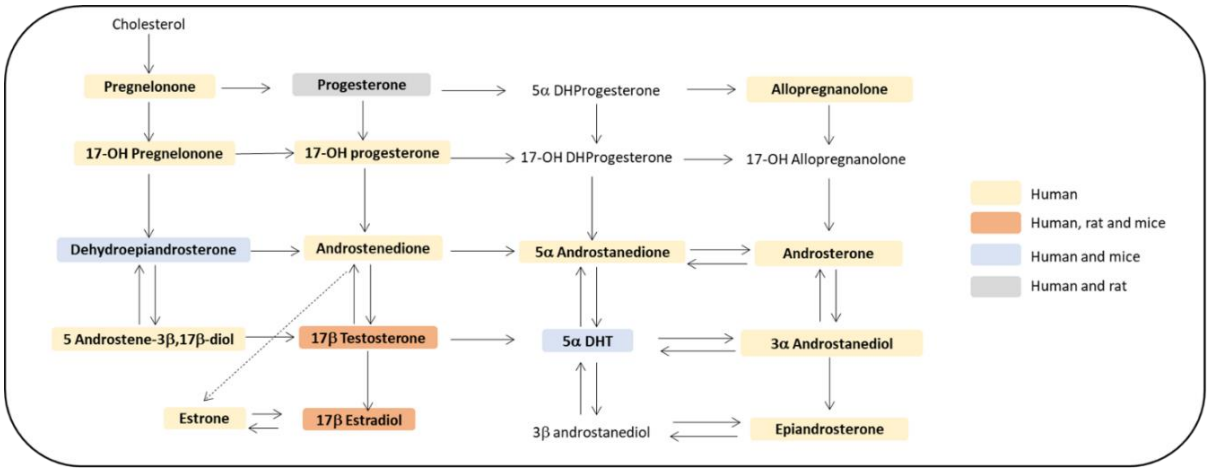


Figure 28. Sex steroids present in AT in humans, rats and mice. Representation of the sex steroid metabolism. Sex steroids identified in AT are in bold. Highlighted in red are the metabolites which have been detected in human, rat and mice adipose tissue; in yellow only identified in human; in blue in human and mice and in grey in human and rat.

1.2 Sex steroid storage in AT

Sex steroids from circulation could be stored partially in AT. This is highlighted by the positive correlations between AT and plasma sex hormone dosage. For example, in women with breast cancer, the concentrations of estrone and testosterone in MAT were positively correlated with those in plasma (r=0.75 and r=0.57 respectively) and this was also the case in the non-cancer group. There was also a positive correlation for estrone (r=0.79) and 5 androstene-3β,17β-diol (r=0.63) concentrations between abdominal AT and plasma[459]. Another study showed that the relative concentrations of adipocytes sex hormones were found to be consistent with their respective rankings in serum. In the follicular and luteal phases of menstrual cycle, the average serum levels of androstenedione were 20 to 30 times higher than estrone, while testosterone levels were 3 to 8 times higher than 17β-estradiol. In accordance with these results, the androstenedione level was 10-fold higher than estrone in AT, the testosterone level was about 2 times higher than 17β-estradiol in premenopausal AT and 7-fold higher in the postmenopausal group[463]. In men, there was a positive significant association between circulating levels and concentrations in OM AT and SAT for estrone, testosterone and 5α-DHT. Plasma DHEA-S was also positively correlated to the level of DHEA in OM AT ($r = 0.56$, $p < 0.01$) as well as SAT ($r = 0.38$, $p = 0.05$)[465].

Gonadal organs and adrenal glands being the main producers of sex steroids in the body, AT might contribute to a small amount in circulation[98]. **Thus, all these studies suggest that AT**

might play a more important role in storage of steroids as seen by the correlation between sex steroid concentration between AT and serum.

AT is also involoved in local sex steroid synthesis. Comparison of sex steroid concentrations between AT and serum brings some arguments. However, the comparison of sex steroid concentrations between AT and serum should be considered carefully since different matrix or units are used in these two parts (per gram of oil vs per ml of serum), some studies try to compare directly taken these technical issues into considerations. Their conclusion is that sex steroid concentration in AT in general is higher than in serum. For example, the levels of androstenedione, estrone, testosterone and 17β-estradiol in AT were approximately 10-times greater than in serum in women with breast cancer independently of the type of breast cancer considered[464]. In another article, in which the hormone levels were measured by radioimmunoassay, the authors showed that the concentration of estrone, estradiol, androstenedione and DHEA were higher in MAT or abdominal SAT than in plasma with the exception of testosterone[459]. The ratio of tissue to plasma showed that the concentrations of DHEA, androstenedione, estrone and 17β-estradiol in fat tissue were 3-17 times higher than in the plasma concentration with the exception of DHEA-S. Moreover, the total amount of steroids within men SAT and women MAT was found to be 40–400 times greater than in plasma[462]. One study in mice showed that, about 60% of HFD-male mice had conjugated testosterone below the limit of detection (LOD) in the serum, but their AT levels of free and conjugated testosterone were all above the LOD[468]. **These studies showed a higher level of sex steroid in AT than in serum which strongly suggests that steroid synthesis occurs in AT**.

The relative comparison of concentrations between AT and serum could be more convincing. For example, androstenedione as the precursor for estrone was at least 23 times more represented than testosterone in women adipocytes, however, there was only a 3-5-fold increase in serum, showing that adipocytes have an important capacity for estrogen synthesis from androstenedione compared to the serum[463]. Moreover, testosterone was 4-fold higher than 17β-estradiol in MAT, but 30 times higher than 17β-estradiol in serum independently of the type of breast cancer. The observed reduction of the ratio of testosterone to 17β-estradiol in AT compared to serum levels, suggests that AT acts as a dynamic reservoir of androgens, actively metabolizing them into estrogens within breast tissue of cancer patients[464]**.**

Meanwhile, the involvement of AT in local sex hormones synthesis may be amplified in obesity and PCOS than in normal conditions. In one study including women and men, the tissue/serum

ratio for the steroids DHEA, androstenedione, testosterone, 17β-estradiol and estrone, progesterone, and 17α OH progesterone ranged from 2.2 to 13.2. Whereas the ratios for all these metabolites were 2.4-86.5 times higher in obese subjects, especially for DHEA and androstenedione with ratios of 53.7 and 86.5 respectively[461]. In another study, in healthy group, testosterone and 5α-DHT levels were similar between serum and abdominal SAT, whereas both androgen levels were higher in AT than serum in PCOS women[466]. Moreover, obese male subjects exhibited lower total circulating testosterone compared with the normal weight group; however, their SAT contained a higher concentration of testosterone and 17β-estradiol[465].

In conclusion, AT seems to be both an important site for both the storage of circulating sex steroid but also a site of in situ biosynthesis. In pathological conditions such as obesity or PCOS, the sex steroid storage and synthesis could be enhanced. In order to understand how and why sex steroid is produced and stored in AT, it is worthwhile to learn more about AT capacity to synthesis sex steroid and also their function on AT.

1.3 Mechanisms of sex steroids biosynthesis in AT

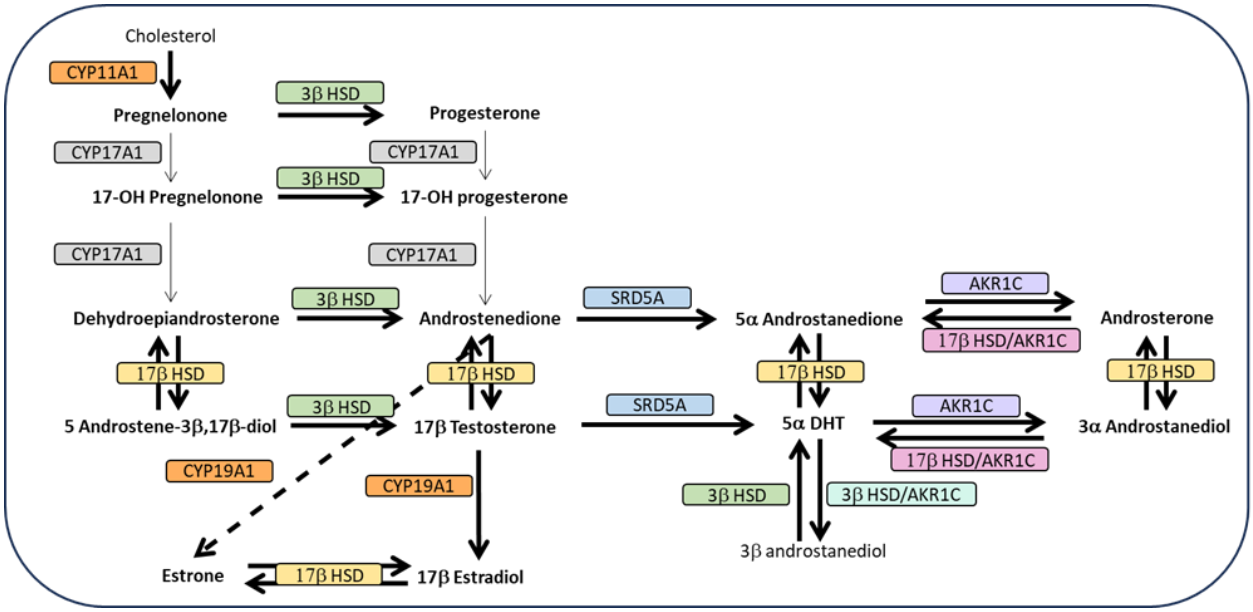


Figure 29. Schematic representation of sex steroid metabolism in AT. Steroid metabolism for the production of progestagens, androgens and estrogens in AT. Enzymes and pathways identified in AT are highlighted and represented by bold arrows (respectively). CYP11A1: cytochrome P450 family 11; CYP17A1: cytochrome P450 family 11; CYP19A1: cytochrome P450 family 19 also called aromatase; 3β HSD: 3β-hydroxysteroid dehydrogenase; SRD5A: 5α-reductases; 17β HSD: 17β-hydroxysteroid dehydrogenase; AKR1C: aldo-keto reductase family 1. CYP17A1 enzyme expression indicated in grey is not confirmed in AT

CYP11A1 and CYP17A1

AT could be classified as a steroidogenic tissue by its ability to convert endogenous cholesterol to pregnenolone (a precursor of sex steroids in the gonads) through CYP11A1 activity (**Figure 29**). Indeed, several studies reported CYP11A1 gene expression in women OM and SAT and CYP11A1 protein expression and activity in differentiated mouse 3T3-L1 adipocytes[479,480,481,467,482]. 17α-hydroxylase encoded by CYP17A1 is also crucial for steroid biosynthesis as it catalyses the conversion of pregnenolone and progesterone to downstream androgen metabolites such as DHEA and androstenedione respectively (**Figure 29**). However, the expression of CYP17A1 in human AT remains controversial. Whereas some studies reported CYP17 gene expression and activity in women SAT and VAT[480,483,484,467], other studies could not detect CYP17A1 gene expression in women AT[479,482].Thus, *de novo* synthesis of androgen from pregnenolone in human AT needs to be confirmed. On the contrary, in female rat AT, all steroidogenic enzymes are expressed[471]. Moreover, CYP11A1 and CYP17A1 mRNA levels increased in AT of obese rats[485].

In fact, human AT contains other enzymes (described below) needed for active androgen synthesis from DHEA. Generally, around 95% of the active estrogens and androgens are inactivated locally before being released in the blood as inactive metabolites thus avoiding inappropriate exposure of the other tissues[486,487]. AT follows this rule since enzymes involved in inactivation of metabolites were detected in it[488,489].

3β-HSD

Two distinct isoforms of 3β-hydroxysteroid dehydrogenase (3β HSD) encoded by HSD3B1 and HSD3B2 have been identified in humans. It can catalyse the conversion from pregnenolone, 17α-hydroxypregnenolone, and DHEA to progesterone, 17α-hydroxyprogesterone, and androstenedione, respectively (**Figure 29**). It also has the capacity to convert 5 androstane-3β,17β-diol to 5α-DHT in the presence of NAD^+[490,491,492]. HSD3B1 and HSD3B2 gene expression levels were higher in SAT compared to OM AT[479,493] and significantly increased in SAT of women with PCOS compared with healthy control[482]. 3β HSD activity has also been demonstrated in breast adipose stromal cells from women undergoing reduction mammoplasty[494].

In mice VAT, gene expression levels of HSD3B1 were decreased with a high fat diet[495] whereas in female rats, HSD3B2 gene expression was higher in VAT from obese samples compared to

lean ones[471]. While in mice and rats 3β HSD expression was modulated by obesity, in human, the precise role of 3β HSD in AT physiology and homeostasis remains to be elucidated.

17β-HSD enzymes:

17β-hydroxysteroid dehydrogenase (17β HSD) control the synthesis of 17β testosterone, 5α-DHT, androstenediol, 3α androstanediol and also 17β estradiol (**Figure 29**). These enzymes were found widely spread in human tissues and in AT[496]. Different isoforms of 17β-HSD enzymes have different functions and could be differentially expressed within the different AT depots.

17β-HSD type 1 encoded by HSD17B1 can catalyse the conversion from estrone to 17β estradiol (**Figure 29**). The expression of HSD17B1 in AT is controversial. Most studies were unable to detect significant levels of mRNA or detected predominantly incompletely spliced mRNA not associated with 17βHSD1 protein expression in women SAT and OM AT[482,497,498]. However, one study reported an increased expression of HSD17B1 in VAT compared to SAT in obese men[499].

17β-HSD type 2 encoded by HSD17B2 can catalyse the conversion of active androgens and estrogens to fewer active metabolites such as the conversion of testosterone to androstenedione and estradiol to estrone (**Figure 29**). In men, the activity and expression of 17β-HSD2 was higher in OM AT compared with SAT [500],[501]. 17βHSD2 was detected in the blood vessels of both OM AT and SAT with no detection in adipocytes[501]. The authors also showed a positive correlation between BMI or subcutaneous adipocyte diameter and 17β-HSD2 activity in whole AT[501]. These results suggest a role of 17βHSD2 in testosterone availability in AT in obesity.

The expression of this enzyme is controversial in women AT. Some studies found that, 17β-HSD2 localized in blood vessels as in men AT and its expression was higher in OM than in SAT of women[493,502]. 17βHSD2 was also expressed in the abdominal SAT and intra-abdominal AT[497]. However, in other studies, no relevant expression was detected in paired OM and SAT from healthy women[498,482].

17β-HSD type 3 encoded by HSD17B3 can catalyse the conversion from DHEA to androstenediol, from androstenedione to testosterone, from 5α androstanedione to 5α-DHT, and the conversion of androsterone to 3α androstanediol (**Figure 29**). HSD17B3 was expressed in SC abdominal and intra-abdominal AT of women[497,493]. MacKenzie et al, reported higher expression of HSD17B3 mRNA in SAT compared to OM AT in women[479]. However, like

17βHSD2, other studies did not detect HSD17B3 expression in paired OM and SAT from healthy women[498,482]. Moreover, the increased expression of this enzyme was associated with the differentiation process of adipocytes isolated from SAT in women[493].

HSD17B3 played a role in obesity. The ratio of HSD17B3 mRNA to aromatase (conversion from androgens to estrogens) mRNA in intra-abdominal women AT correlates positively with BMI and waist circumference whereas the situation is contrary in abdominal SAT[503]. Accordingly, in female rats, HSD17B3 gene expression was higher in AT from obese compared to lean animals[471]. No relevant studies were found in men AT.

17β-HSD type 4 degrades 17β estradiol into estrone and 5 androstene-3β,17β-diol into DHEA[504] (**Figure 29**). Its expression was higher in OM than in SAT from women[498] whereas in another publication, the enzyme was not detected in women SAT[482].

17β-HSD type 5, also called aldoketoreductase encoded by AKR1C3 is preferentially involved in forming testosterone from androstenedione[505] (**Figure 29**). Blouin et al, first found that female SAT and OM AT expressed this enzyme with a higher expression in SAT[489] and later it was confirmed in men[500]. AKR1C3 mRNA expression in SAT was increased in PCOS women compared to the normal group and the ratio of testosterone to androstenedione, reflective of AKR1C3 activity, was significantly higher in AT than in circulation in PCOS women but not in the control group[466,482].

AKR1C3 may participate in the obesity regulation. Its mRNA expression was positively correlated with BMI and trunk fat mass in women SAT and with central obesity (identified by the waist to hip ratio) in men and women SAT[498,506,507]. Moreover, AKR1C3 expression decreased with diet-induced weight-loss in men and women SAT[498,508] and was positively correlated with serum leptin levels and expression in obese subjects supporting a connection with adiposity. Also, the expression was lower in obese men with an abnormal metabolic profile compared to healthy obese subjects[508].

AKR1C3 may also participate in the adipocyte differentiation process since predominant expression was found in OM and subcutaneous (SC) mature adipocytes[498,493]. As SC preadipocytes differentiate, the balance of androstenedione conversion shifts in favour of testosterone production. However, AKR1C3 displayed other enzymatic activities and has an inhibitory effect on the prostaglandin, 15d-PGJ2, which is an endogenous ligand for PPARγ, whose expression is important in adipocyte differentiation[509,510]. The regulation of

prostaglandin synthesis explained a contrary role of AKR1C3 in obesity and adipocyte differentiation. During diet induced weight-loss, the expression of this enzyme decreased, potentially causing an increase in PPARγ ligand, which may help to explain the observed improvement in PPARγ regulated AT insulin sensitivity.

17β-HSD type 12 is encoded by HSD17B12 and can participate in the conversion of estrone to 17β-estradiol in adipocytes (**Figure 29**). The protein and mRNA expression of this enzyme was increased in differentiated adipocytes compared with preadipocytes in women from both OM and SAT. At the same time, conversion from estrone to 17β-estradiol increased 5-fold in differentiated adipocytes, which demonstrated the role of HSD17B12 in this reaction[511].

AKR1C isoenzymes

AKR1C enzymes (AKR1C1, AKR1C2, AKR1C3, and AKR1C4) are homologous with different substrate specificities. Like 17β HSD, AKR1C enzymes have a hydroxysteroid dehydrogenase activity. They are ketosteroid reductases, which catalyse NADPH dependent reductions at the C3, C5, C17, and C20 of steroids[512].

They were strongly expressed in both SAT and OM AT in women when compared with other mRNAs measured including 3β HSD 1, 17β HSD1/3, 5α reductase and aromatase[500]. AKR1C enzyme expression was correlated with adiposity and PCOS risk. For example, AKR1C1 and AKR1C2 gene expression was higher in isolated adipocytes and AT from heavier men and women compared to their leaner twins[513,514]. Also, AKR1C1/2 gene expression was increased significantly in SAT of PCOS women compared with healthy control[482]. AKR1C2 was the predominant isoform in human SAT, followed by AKR1C3 and then AKR1C1 whereas AKR1C4 mRNA was not detected[507,506]. All AKR1C enzymes were expressed in SVF but their expression was lower than in adipocytes[493].

AKR1C1

AKR1C1 mainly inactivates progesterone into 20α-hydroxyprogesterone through its 20α HSD activity, but also forms testosterone from androstenedione (3–4 % of its 20α-HSD activity) and inactivates 5α-DHT into 3α androstanediol (8% of its 20α-HSD activity) and 3β androstanediol. (**Figure 29**). It could be responsible for 30% of 3α androstanediol and 40-60% of 3β androstanediol production[500]. AKR1C1 expression and activity was higher in SAT than in OM AT of men and women[500,515]. While obesity did not affect AKR1C1 activity in SAT, in OM AT, 20α-hydroxylation of progesterone was higher in women with visceral obesity than those with

less VAT area[515]. AKR1C1 expression was also significantly higher in differentiated adipocytes than pre-adipocytes isolated from women SAT[516].

AKR1C2

AKR1C2 is responsible for converting 5α-DHT into inactive metabolites androstanediols. It is responsible for the production of approximately 70% of the 3α androstanediol and 40–60% of the 3β androstanediol as AKR1C2 inhibition reduced the formation of these metabolites[500] (**Figure 29**). Higher 3α HSD activity to form 3α androstanediol was found in SAT compared to OM AT in men[500]. AKR1C2 expression was found to be more abundant in adipocytes than in SVF for severely obese patients. Within the different cell populations of SVF, AKR1C2 expression was higher in adipocytes precursor cells who expressed apolipoprotein E (APOE), Fatty Acid Binding Protein 4(FABP4) and CCAAT/enhancer binding protein β (CEBPB)[506]. AKR1C2 expression was increased in differentiated adipocytes compared to preadipocytes[493].

In addition, the expression of AKR1C2 was higher than AKR1C3 in men AT. Correspondingly, the conversion from 5α-DHT to 3α androstanediol was largely predominant in comparison to the conversion from androstenedione to testosterone[500].

AKRIC2 enzyme is associated with obesity. For example, higher OM 5α-DHT inactivation rates were found in obese compared to lean men and correlated with adiposity in women[500,488]. Moreover, AKR1C2 3α-HSD activity in VAT was positively associated with its area, BMI and adipocyte size[489,488,500]. Central obesity (determined by the waist to hip ratio in men and trunk fat mass in women) was associated with AKR1C2 mRNA expression[507,506].

The strong genetic regulation of AKR1C2 was identified to be located on the binding sites of two nuclear transcription factors: retinoid acid-related orphan receptor alpha and GR[506]. AKR1C2 drived basal and glucocorticoid-induced androgen inactivation to 3-diol in human preadipocyte of obese men[517]. Upon transfection with AKR1C2 siRNA, the lipid accumulation, Glyceraldehyde 3-phosphate dehydrogenase (G3PDH) activity, and FABP4 mRNA expression in differentiated preadipocytes exposed to DHT were further decreased[517]. These results show that AKR1C2 could be a potential therapeutic target for the management of obesity-related complications.

AKR1C2 may have functional effects on AT. For example, higher 3α HSD activity was found in mature adipocytes than preadipocytes in the SAT from men. The increasing 5α-DHT inactivation during differentiation could prevent mature adipocytes' exposure to 5α-DHT[500].

Moreover, there was a positive mRNA level correlation between AKR1C2 and leptin in SAT from both diagnosed PCOS patients and healthy patients[482]. Cortisol production was positively correlated with androgen inactivation in both SAT and OM AT[517].

AKR1C3 - see section 17β-HSD type 5.

Aromatase encoded by **CYP19A1** controls the conversion from androgens to estrogens (**Figure 29**). The expression of aromatase in gluteal AT is higher than in abdominal SAT in women[518]. This higher expression was found in postmenopausal women versus premenopausal women along with the fact that the aromatization in peripheral AT is a main source of circulating estrogens in post-menopausal women[518]. The expression of aromatase was higher in SVF than in mature adipocytes in breast AT and women abdominal AT. However, the estrogen receptor alpha (ERα) was more expressed in adipocytes compared to SVF[519,520]. The basal aromatase activity was higher in SAT SVF than VAT SVF[521].

Aromatase expression is implicated in breast cancer. The enzyme is overexpressed in breast AT of cancer patients[522]. Moreover, multiple studies found that aromatase activity and mRNA levels were increased in breast AT adjacent to the tumour compared to distal or disease-free breast AT[523].

This enzyme is also strongly associated with obesity. For example, aromatase mRNA in SAT was positively associated with BMI and the percentage of body fat in men and women[507]. This difference remained significant when women were excluded from the data[507]. The volume of SC, intra-abdominal fat and liver fat were positively correlated with CYP19A1 gene expression in obese men[513]. BMI and waist circumference were positively associated with the ratio of 17β HSD3 mRNA levels to CYP19A1 mRNA levels measured in women intra-abdominal AT, suggesting that androgen formation (through 17β HSD3) may be higher than its inactivation through aromatization[503]. However, it is contrary in abdominal SAT[503].

Aromatase may also be associated with PCOS occurrence as there is a lower mRNA level of aromatase in SAT of PCOS women compared to the normal control[482].

In mice, Hong et al, found for the first time that male but not female gonadal AT expressed aromatase mRNA. The expression didn't change as the gonadal fat pad weight increased. Neither SAT nor BAT contained detectable CYP19A1 mRNA[524,525]. Also, there was 2 or 3-fold higher 17β estradiol to testosterone ratio in rat inguinal (SC) AT than other adipose depots, suggesting that aromatase activity is higher in inguinal AT[470].

5α-reductases

5α-reductases are microsomal enzymes responsible for the formation of 5α-DHT, either through conversion of androstenedione to 5α androstanedione and subsequent 17-oxoreduction, or through direct conversion of testosterone to 5α-DHT[526]. In some tissues, 5α-DHT formation likely results mostly from androstenedione transformation rather than direct transformation of testosterone[527] and in human preadipocytes, androstenedione serves as the primary source of 5α-DHT[528]. There exist different expression levels of the three isoforms of this enzyme, SRD5A1, SRD5A2, SRD5A3 in different adipose depots. SRD5A1 was found to be expressed in OM and SAT from men and women[482,528,493]. SRD5A3 was also expressed in OM and SAT of men, with its mRNA level being higher than SRD5A1 mRNA level in both of these tissues, however, no such difference was observed for their protein expression[528]. One study found that SRD5A2 was not expressed SAT and OM AT of men[528] whereas another study detected SRD5A2 mRNA at similar levels in 8 paired women OM and SAT[479]. SRD5A1 and SRD5A3 mRNA were expressed in both pre-adipocytes and in adipocytes after differentiation induction[493,528].

The expression of the 5α reductase enzymes is correlated with obesity and PCOS. Indeed, SRD5A1 mRNA expression in whole SAT was positively correlated with BMI[528]. The ratio of 5α-DHT to testosterone, reflective of 5α reductase activity, was higher in SAT than in serum in PCOS women[529]. Moreover, SRD5A1 expression and activity decreased in SAT of PCOS women compared with the normal group[482,466]. The mRNA abundance of SRD5A1tended to decrease with adipogenesis in both OM and SAT and decrease in SAT of PCOS women compared with the normal group[493,482].

2. General influence of androgens on AT

2.1 Body fat distribution regulation by androgens in women and men

One of the biggest differences between women and men is that they have different fat distribution. Women tend to accumulate their fat in the gluteal and femoral regions, which gives them a pear-like morphology[530]. Men tend to accumulate their fat in the abdomen, giving them an apple-like shape (**Figure. 30**). The difference in reginal body fat deposition in males versus females suggests a causal role for sex steroid hormones including androgens and estrogens in human body fat distribution patterning.

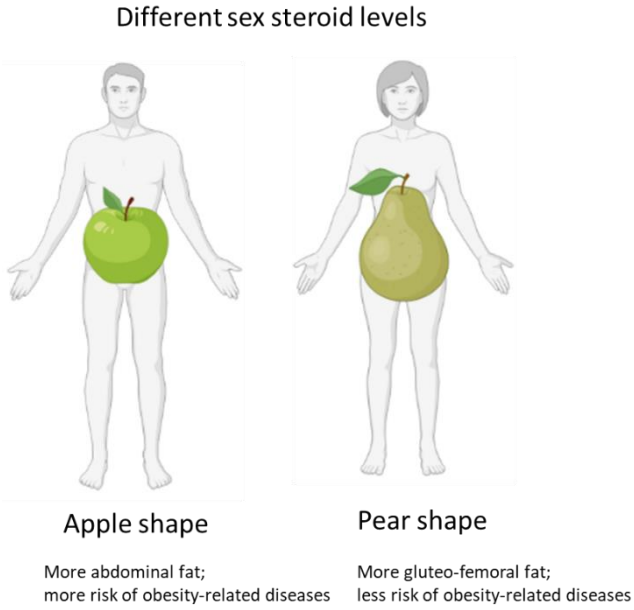


Figure 30. Fat distribution between men and women

Men

Testosterone was negatively associated with multiple anthropometric markers in men, especially BMI and waist-to-hip-ratio (central adiposity)[531]. Increasing obesity, particularly central obesity, is associated with decreasing serum total testosterone and sex hormone-binding globulin (SHBG)[532]. A large number of studies have confirmed that low total plasma testosterone concentrations were often found with elevated VAT accumulation[533,534,535]. Additionally, lower concentrations of adrenal C19 steroids like androstenedione and DHEA were also correlated with obesity[533,534]. Furthermore, positive associations were found between active androgen 5α-DHT inactivation and VAT accumulation in men[536].

Women

The effect of androgens on women adiposity is not really clear in the literature, and the results were contradictory between free testosterone levels and abdominal fat or VAT accumulation. For example, D J Evans et al, reported that in premenopausal women, the enlargement of abdominal adipocytes with an increased size and WHR (waist to hip girth ratio) is related to the decreased plasma SHBG and increased free testosterone. And the change in androgens is also accompanied by localization of fat in the upper body (a more androgenic profile) and an imbalance in the glucose-insulin homeostasis[537]. Whereas in some studies, some negative correlations or no correlation between plasma testosterone levels and abdominal AT accumulation were reported with varied protocol[536]. One study reported that, as in men, VAT accumulation is also positively associated with 5α-DHT inactivation rate[536]. However, it is

noticeable that women tend to accumulate more visceral fat after menopause with the increased ratio of androgen to estrogen, displaying a man-like fat distribution.

Androgens were inversely with BMI, waist-circumference and leptin content in women SAT in one study[531]. Almost all the studies found no relationship between circulating androstenedione levels and abdominal fat in women. Heavier women had a higher gene expression of steroid sulfatase and enzymes involved in androgen metabolism in abdominal SAT and isolated adipocytes but lower serum levels of DHEA, 5α-DHT, and SHBG compared to their leaner co-twins, with no differences in serum testosterone or androstenedione levels[514].

2.2 Hormone therapy influence on male AT

The side effects of ADT induced an increase in fat mass of PPAT and other fat masses such as SAT and VAT reflecting androgen influence on male AT indirectly[538]. It was reported that there was an 8.9% increase of SAT area compared to the baseline scan in SATpatients treated with neoadjuvant chemo-hormonal therapy and ADT after 3 months and 18.9% increase after 12 months[539]. Also, ADT-treated patients with degaelix and abiraterone acetate displayed several upregulated genes involved in the cholesterol metabolism and inflammation of PPAT[540]. Antoun et al, measured body composition in patients with mCRPC who had been treated with abiraterone acetate and enzalutamide and found that there was a slight decrease for the SAT index and increase for the VAT index from baseline to 3 months[541].

3. Functional effect of androgens on AT

3.1 AR expression

As AT expresses AR, it is not surprising that androgens have an effect on AT function. Moreover, due to its capacity to produce sex steroids and synthesize sex steroid enzymes, AT could have an impact on its own local steroid metabolism that would be independent of the plasma levels of sex hormones[542].

Androgens exert their effects through the AR which is a nuclear hormone receptor, broadly expressed in various tissues, including AT[543,544]. The mechanism of AR action involves the formation of a complex between the receptor, its corresponding ligands, and coregulator proteins, which interacts with basal transcription factors to regulate transcription of target genes[545].

Human WAT

AR expression seems to be higher in VAT than SAT. One study reported more AR mRNA expression in visceral than in SC preadipocytes[544]. Intra-abdominal preadipocytes contained 2-fold more androgen binding sites than SC preadipocytes quantified by using the synthetic radioligand [*3H*]-*R1881*, with no difference for the same adipose depot between men and women[543]. AR gene and protein expression decreased in mature adipocytes compared to preadipocytes during differentiation, suggesting that preadipocytes are more active than mature adipocytes in regards to steroid signaling[543]AR mRNA expression was not different in SAT of women with PCOS compared to healthy control[482]. Moreover, in women SAT, AR protein expression was negatively correlated with 5α-DHT concentration, which was seen as AR desensitization which is a protective mechanism[546].

WAT of other animals

Similarly, to humans, a lower AR expression was found in male rats inguinal (SAT) and retroperitoneal depots (non-SAT, non-VAT) than in VAT (gonadal and mesenteric depots). However, these differences were not observed in female rats[470],[543]. Nuclear AR binding assay was negatively correlated with lipid accumulation in different AT from castrated rats, suggesting that AR activity inhibit lipid uptake[547]. Testosterone, but not 5α-DHT can induce the formation of new AR in adipose precursors cells from male rat fat pad[548]. In contrast, in 3T3-L1 adipocytes, testosterone did not have any effect on AR mRNA levels, however, estradiol significantly upregulated and progesterone slightly downregulated AR mRNA expression[470].

BAT of rat

Higher AR mRNA was found in male BAT than in female rats[549] . AR mRNA expression tended to decrease upon testosterone treatment of BAT culture whereas treatment with 17 β estradiol or progesterone had no significant effect on AR expression[549]. This is contrary in WAT, which indicates that different factors can regulate the response to androgens in WAT and BAT[470].

3.2 Effect of androgens on WAT

a. Adipocytes differentiation

As described in previous chapter, adipogenesis is the process of differentiation of ADSC into mature adipocytes. It is a well-regulated process requiring different transcription factors, the

most extensively studied being the CCAAT/enhancer-binding protein (C/EBP) gene family and peroxisome proliferator activated receptor-γ (PPAR-γ)[550]. To date most of the results obtained suggest that androgens have a negative effect on adipogenesis.

In human, 5α-DHT and testosterone can inhibit primary preadipocytes proliferation and differentiation in SAT and VAT in both men and women, with stronger effects observed in women[551,552]**.** In SAT of non-obese women, testosterone can inhibit the commitment of human adipose-stem cells to preadipocytes and early differentiation of preadipocyte into adipocytes[553]. Androgen inhibition of early-stage adipocyte differentiation was shown to be mediated in part through AR action by decreasing PPARγ, C/EBPα and C/EBPβ mRNA levels in SAT through BMP4 signalling[553] (**Figure 31**).

In mice, transcriptome analysis on retroperitoneal AT by RT-qPCR revealed an upregulation, in the response to 5α-DHT, of four genes CDKN1Ad (Cyclin Dependent Kinase Inhibitor 1A), FKBP5 (FK506 binding protein 5), GADD45 (Growth Arrest and DNA Damage protein), and MT1A (Metallothionein 1A) involved in negative regulation of adipogenesis[554]. Differentiation of murine preadipocyte cell lines 3T3-L1 was inhibited by testosterone and 5α-DHT via an AR-dependent pathway, which was partially reversed by AR antagonists flutamide or bicalutamide[555].

As the most abundant androgen in AT, DHEA also exerts some effects on AT adipogenesisand the effects are depot-specific and concentration dependent but not influenced by sex. For example, 10^{-8}M DHEA inhibited the adipogenesis of human primary OM preadipocytes with decreased LPL transcripts (terminal differentiation marker)[556]. Additionally, 10^{-7}M DHEA was necessary to inhibit the proliferation of human subcutaneous preadipocytes whereas only 10^{-8} M DHEA impeded the proliferation of OM preadipocytes[556]. Moreover, this study mixed both women and men samples, showing the effect of DHEA is not affected by sex[556]. Similarly, DHEA has been shown to impede the differentiation and proliferation of human subcutaneous preadipocytes derived from the Chub-S7 cell line[557]. This effect on proliferation was shown to be mediated through an arrest in the G1 phase of the cell cycle but this was independently of AR[557].

Different studies showed the inhibitory effect of DHEA on adipocytes differentiation[558]. In mice, DHEA can inhibit white (3T3-L1) and brown (PAZ6) preadipocyte cell line proliferation by blocking G1/S or G2/M phase cell cycle respectively[556]. Also, DHEA blocked 3T3-F442A preadipocyte differentiation into adipocytes as well as 3T3-L1 preadipocyte proliferation and

differentiation[559,560]. After castration, male rats exhibited increased proliferative capacity of preadipocytes in epididymal and perirenal fat, but the differentiation capacity was enhanced only in epididymal fat and decreased in perirenal fat whereas no significant effect was observed in the SAT[558].

Whether DHEA relies on the conversion to other hormones or not, to display these effects, is still needed to be validated. One study showed that DHEA conversion into estrogen or androgen was not involved[557] but in another, DHEA effects on 3T3-F442A / L1 cell and differentiation could be inhibited by 3β-HSD inhibitors indicating that conversion to androgens or other steroids is necessary to elicit an effect of DHEA in these cells[556].

b. Lipolysis and lipogenesis

As described in previous chapter, Lipogenesis converts FFAs and glycerol into TG. LPL plays a key role in this process as it hydrolyses triglyceride-rich lipoproteins found in circulation into FFAs and glycerol, which are taken up by adipocytes and used as substrates for lipogenesis[561]. lipolysis is hydrolysis of triglycerides (TG) into glycerol and free fatty acids (FFA) which can then be used by peripheral organs to produce energy. The hydrolysis of TG involves 3 steps and different lipases (ATGL, HSL and MAGL). HSL involved in the hydrolysis of DG into 2 FFAs and one glycerol, is the rate limiting enzyme for lipolysis[562].

Although it is known that androgens can modulate fat distribution in humans, the role of androgens in lipolysis and lipogenesis remains controversial and seems to be gender and AT depot-specific[542,563].

FA uptake and TG storage

Some studies indicate that androgens inhibit FA uptake and storage in AT and decrease fat mass. The castrated rats exhibited higher FA uptake in retroperitoneal and mesenteric AT compared to non-castrated group and testosterone administration reduced FA uptake[564]. In rat adipocytes, higher AR nuclear binding was associated with lower FA-uptake[547]. Testosterone inhibited FA uptake in human intra-abdominal AT depots but not in SAT[565] (**Figure 31**). Furthermore, the VAT in obese men with diabetes was more specifically decreased upon testosterone treatment with undecanoate for 3 months[566]. Thus, VAT seems to have a higher responsiveness to androgen than the SAT.

Controversial effects were reported in simian animals. For example, testosterone reversed the small and multilocular adipocytes formation induced by castration in male Japanese macaques and 5α-DHT treatment stimulated FA uptake in retroperitoneal AT from female macaques[567]. In another publication, FA uptake and insulin signalling in OM AT were increased by chronic testosterone treatment. However, this effect was only observed in the menstrual period and not in the luteal phase, suggesting that the balance between androgens and estrogens plays a vital role in the function of AT[568].

LPL activity and lipolysis

Testosterone and 5α-DHT can inhibit lipogenesis and stimulate lipolysis mainly in men and male rats. For example, 6-week oral testosterone treatment to obese middle-aged men decreased waist/hip circumference and LPL activity and also increased lipolytic response to norepinephrine specifically in abdominal VAT but not in femoral SAT[569]. 5α-DHT and testosterone inhibited LPL activity in subcutaneous and OM primary preadipocytes cultures in men. However, in women OM AT, higher 5α-DHT concentrations were necessary to inhibit LPL activity[551]. In rats, several studies indicate a lipolytic effect of androgens. In adipose precursors cells and isolated adipocytes from castrated male rats, testosterone, but not 5α-DHT, promoted lipolysis induced by catecholamines (isoproterenol and norepinephrine) through the stimulation of synthesis or externalization of β-adrenoceptors. These effects were mediated by binding to AR without conversion to estrogens[570,571] (**Figure 31**).

DHEA displays a lipolytic effect in different location of AT in men, women and rats. Serum DHEA-S was inversely correlated with VAT area in obese men and women and *in vitro,* DHEA-S increased lipolysis specifically in SAT explants from women and in VAT explants from men[572]. This result could explain the gender specificity of fat distribution observed in humans. Also, oral administration of DHEA reduced adiposity and stimulated lipolysis from rats by enhancing the response to adrenergic stimulation in isolated epididymal adipocytes[573]. (**Figure 31**)

Other indirect evidence suggests a role of androgens in stimulating lipolysis when the use of obese humans and rodents' samples are considered. In insulin resistant 3T3 L1 adipocytes and SAT explants from obese male patients, testosterone release was inhibited compared with lean subjects, inducing an increase of intracellular testosterone. The expression of androgen-responsive genes involved in the lipolytic and anti-adipogenic response, such as AR, FKBP, GADD45, LIPE (Hormone-sensitive lipase), and MT1A (Metallothionein 1A), was lower in

obese compared to lean patients[574]. The molecular mechanism involved in late-onset obesity developed by AR-KO male mice relies on decreased lipolysis associated with a decrease of HSL transcription level in WAT whereas markers for *de novo* lipid synthesis, like fatty acid synthase (FAS), acetyl-CoA carboxylase and the lipogenic transcriptional factor sterol regulatory element binding protein-1C (SREBP-1C) were unchanged compared with AR wild type mice[575].

In PCOS women, it has been reported an increase of catecholamines stimulated lipolysis in VAT[576]and lower LPL activity in abdominal subcutaneous adipocytes compared to normal androgenic women[577]. However, except these two studies in women with PCOS, the regulation of lipolysis and lipogenesis by androgens in women AT seems to be opposite to what is observed in men. In women SAT, 5α-DHT treatment of isolated adipocytes stimulated LPL and decreased HSL protein expression and basal lipolysis. Flutamide reduced 5α-DHT induced-LPL protein expression showing that LPL expression could be mediated by AR[546]. In differentiated preadipocyte from women SAT, the reduction of catecholamine stimulated lipolysis by testosterone was associated with a decrease of β2-adrenoreceptor and HSL protein expression[578]. In women with PCOS plasma testosterone and DHEA-S were positively correlated with VAT accumulation in lower or upper half body part suggesting a positive effect on lipogenesis[579]. Also, lower HSL and increase CD36 protein expression has been found in OM AT from women with PCOS compared to control group[580] (**Figure. 31**).

Finally, findings from female rhesus macaques indicate that the regulation of lipolysis by sex hormones is intricate. During the luteal phase of the menstrual cycle, characterized by elevated levels of estrogen and progesterone, basal lipolysis and HSL expression were observed to be higher specifically in VAT compared to menstruating controls. Administration of testosterone supplementation during the prepubertal period was found to alleviate the impact of the luteal phase on basal lipolysis. Interestingly, these hormonal effects were not observed during stimulated lipolysis induced by the β-adrenergic agonist isoproterenol[568].

In conclusion, androgens are prone to diminish the fat mass by inhibition of adipogenesis and lipogenesis and stimulation of lipolysis mainly in men whereas in women androgens seems to have opposing effect (**Figure 31**) Indeed, tissue specific and sex specific effects should be considered, and local synthesis and inactivation of androgens as described in 1.3 in this chapter could explain these specialities[581].

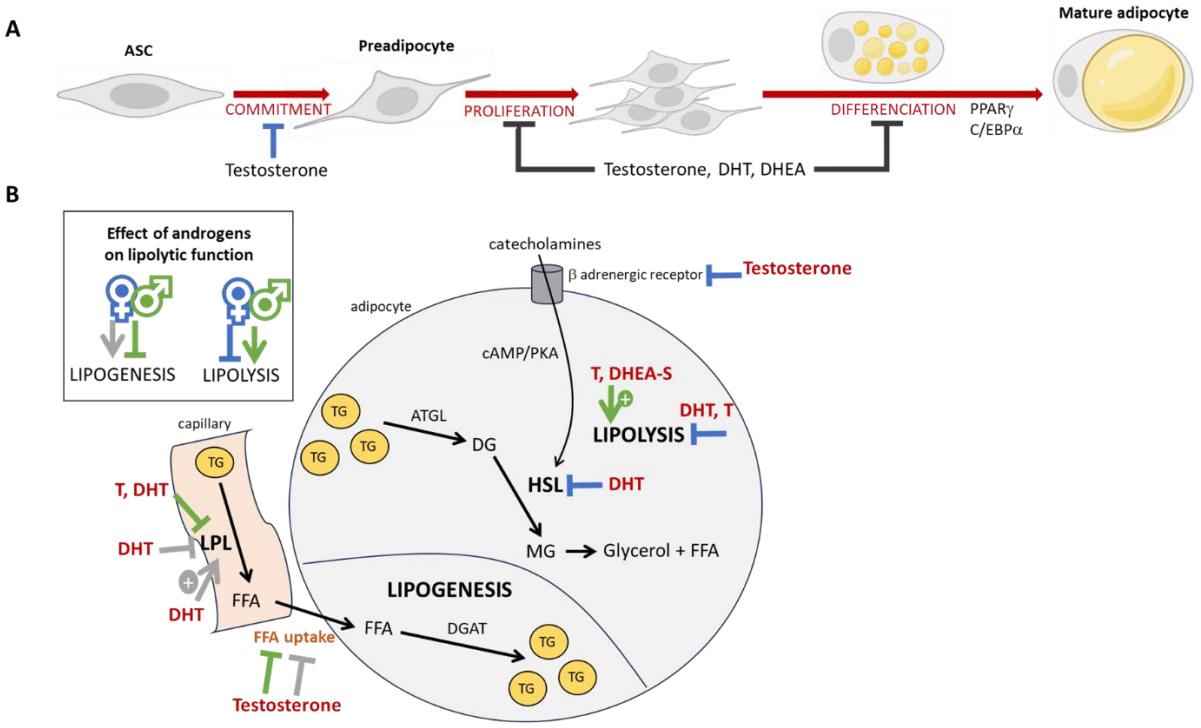


Figure 31. Effect of androgens on human WAT. **A- Effects of testosterone, 5α-DHT and DHEA on adipogenesis**. Androgens inhibit adipogenesis through inhibition of commitment of adipose stem cells (ASC) and proliferation and differentiation of preadipocytes into mature adipocytes. In blue are the effects only mediated by testosterone. **B- Effects of androgens on lipolysis and lipogenesis.** In blue are the effects of androgen on women AT, in green on men AT. In general, androgens have opposite effects on men and women AT. They tend to inhibit lipogenesis and stimulate lipolysis in men AT and vice versa in women. However, the effect of androgens on LPL are controversial in women AT (represented by a grey arrow). LPL: lipoprotein lipase. FFA: free fatty acid, DGAT: Diglyceride acyltransferase, DG: diacylglycerol, MG: monacylglycerol, ATGL: Adipose triglyceride lipase; HSL: Hormone-sensitive lipase; cAMP/PKA: cyclic adenosine monophosphate/protein kinase A; T: testosterone.

c. Adipokines secretion and function

Adiponectin

In vitro, 3T3-L1 adipocytes had a reduced adiponectin secretion upon treatment with testosterone[582]. One study found that testosterone reduced rat differentiated adipocyte secretion of high molecular weight adiponectin (but not the low or middle molecular weight forms)[583]. However, testosterone had no effect on adiponectin expression in SGBG adipocytes (at early and late differentiation stage) and human SAT primary in vitro differentiated adipocytes nor on adiponectin secretion by SGBG adipocytes[584]. Moreover, 5α-DHT and testosterone had no significant effect on adiponectin secretion by primary human cultures of SC and OM adipocytes[551].

Castrated mice had an increase in adiponectin serum levels and testosterone treatment decreased these levels[582]. Similarly, serum levels of adiponectin were inversely correlated with serum testosterone levels in young male and female rats and androgens reduced total circulating

adiponectin concentrations in a dose dependent manner in young male rats[585]. Moreover, adiponectin serum levels decreased with puberty in boys[586] and compared to eugonadal men, hypogonadal men have higher adiponectin concentration in serum and this was reduced by testosterone replacement therapy[587].

Thus, in general, androgens seem to have a negative effect on adiponectin levels.

Leptin

5α-DHT and testosterone treatment reduced leptin mRNA levels and secretion in 3T3-L1 adipocytes and reduced leptin secretion in women differentiated SAT adipocytes[588,589]. SAT and OM adipocytes had a reduced leptin secretion upon testosterone treatment[578]. Treatment of OM AT with 5α-DHT, DHEA-S and androstenedione reduced leptin secretion only in female patients, however contrary to other studies, testosterone treatment effect[590]. Castration decreased leptin concentrations in serum in pigs[591]. On the other hand, in macaques, testosterone increased leptin mRNA levels in retroperitoneal WAT but had no effect on leptin serum levels[567].

There are conflicting results in the literature, but it seems that the consensus is that androgens decrease leptin secretion.

3.3. Effects of androgens on BAT

Androgens can display some effects on UCP1 expression since an androgen response element in the UCP1 promoter has been described[575]. However, the function of androgens on brown AT is controversial.

Most of the literature reported that in rodent brown adipocytes, androgens can inhibit mitochondrial biogenesis and respiration, isoproterenol-stimulated UCP1 gene expression, adipocyte differentiation, lipolysis and downregulate PGC1 α (peroxisome proliferative activated receptor gamma coactivator 1, alpha) mRNA expression[592,593,594,595]. First, results have been observed *in vitro*. When brown adipocytes from rodents were differentiated in culture, exposure to testosterone led to not only a reduction in UCP1 mRNA expression but also the presence of fewer, smaller lipid droplets compared to untreated cells. These effects were observed in a dose-dependent manner and were amplified by adrenergic stimulation with norepinephrine. These effects can also be reversed by co-treatment with the AR antagonist flutamide, which indicates that they are mediated at least in part, by AR[595].

In human, women with PCOS exhibited lower BAT activity, as indicated by a decrease in supraclavicular skin temperature which was inversely correlated with testosterone levels compared to healthy groups[596]. This suggests that testosterone inhibits thermogenesis *in vivo* but the inhibitory effect of androgens on thermogenesis remains controversial especially in animal models as described in the next paragraph.

One study showed that the protein expression of UCP1 was increased after orchidectomy (surgical removal of the testes) in murine BAT and that 5α-DHT treatment reversed this effect[597]. Whereas in another study, mRNA expression of UCP1 was unchanged in BAT of orchidectomized mice when exposed to long-term 5α-DHT treatment[598]. Also, the expression of thermogenic genes was reduced in BAT of AR-KO male mice[575]. Furthermore, the expression of UCP1 and its upstream regulators, β-3 ARA, PGC-1 and also UCP-3 decreased in BAT of prediabetic and obese rats compared to lean rats[599]. A 17-day long DHEA administration significantly increased the expression of these thermogenic genes in BAT of prediabetic and obese rats indicating that the inefficient energy utilization and obesity in these rats caused by decreased expression levels of UCP-1 and its upstream regulators could be corrected by DHEA treatment[599].

Furthermore, androgens can exert indirect effects on BAT through central mechanisms, in addition to direct effects. For example, chronic exposure to DHT in female mice has been shown to diminish hypothalamic leptin sensitivity and inhibit leptin-induced BAT thermogenesis via alterations to the melanocortin system[600]. It is worth noting that some of the observed effects of testosterone may actually be ER-mediated because of the intra-tissue aromatization of androgens into estrogens, especially as it is the case in WAT[601]. However, additional research is needed to provide further insights in the androgen effect in BAT.

In conclusion, data from the literature clearly show that AT is able to store and to metabolize androgens and that androgens (either synthetize from AT and or emanating from the general circulation) affect AT accumulation through regulation of differentiation and metabolic function (lipogenesis and lipolysis) of adipocyte, this effect being both depot and sex-dependent. Androgen from AT might represent a small amount compared to the production from testis (90%) and adrenal (10%)[602]. However, in the case of men with PCa who underwent ADT by inhibiting testosterone secretion from testis, a majority of patients still relapse and this is, in part, due to the intratumoural androgen production from other sources of androgen precursors than the testes. The sources of precursors from extra gonadal sites are mainly produced by the

adrenal gland[130] but as we discussed in previous chapter other unexpected sources of androgens have been recently uncovered such as the microbiota[180]. The capacity of AT to contain and secrete androgens as well as the role of PPAT into tumor progression lead to hypothesize that androgen from PPAT could play an important role in CRPC occurrence. This hypothesis and the experimental results obtained are presented in the next chapter of my thesis.

RESULTS

1. Periprostatic Adipose Tissue Displays a Chronic Hypoxic State that Limits Its Expandability

As described in the introduction, recent studies have shown that the fatty deposit surrounding the prostate gland, known as periprostatic adipose tissue (PPAT), is a major component of the prostate microenvironment that may play a role in the progression of prostate cancer (PCa), particularly in the context of obesity[427,445]. PPAT is a unique adipose deposit with distinct characteristics compared to other WAT, such as VAT. These characteristics includes its accumulation is not dependent on body mass index (BMI)[455]. It is located in the pelvis in an extraperitoneal position and in close proximity to the prostate, separated by a fibromuscular capsule. PPAT secretes large quantities of pro-inflammatory cytokines, such as IL-6 and TNFα[455,423]. In the beginning of my thesis, I took part to the thesis project of Mathieu Roumiguié which was to define the structural and functional characteristics of PPAT to understand the mechanisms involved in the progression of PCa. To achieve this, PPAT obtained from patients who underwent total prostatectomy for PCa was compared to control abdominal-pelvic adipose tissue (APAT). The volumes of these adipose tissues were measured using preoperative prostate MRI, revealing that the accumulation of PPAT was independent of BMI, unlike the control tissue (APAT), which behaved like SAT. Subsequent analyses, including confocal microscopy with anti-CD31 staining, showed that PPAT was less vascularized than APAT, suggesting that PPAT is hypoxic. Unsupervised comparisons of the transcriptomes of PPAT and APAT revealed that most differentially expressed genes were related to the response to hypoxia. Elevated levels of the hypoxia-inducible factor HIF-2α confirmed the presence of an adaptive response to hypoxia in PPAT. This chronic state of hypoxia was associated with an inflammatory response, including macrophage recruitment, secretion of pro-inflammatory cytokines, and increased collagen fibers in PPAT compared to APAT. While obesity promoted fibrosis in APAT, in PPAT, this fibrosis was already present in non-obese patients. This part of our research suggests that the specific vascularization of PPAT leads to chronic hypoxia, resulting in fibrosis and inflammation, which may explain the lack of PPAT expansion in obesity and its potential contribution to prostate pathologies.

The American Journal of Pathology, Vol. 192, No. 6, June 2022

ELSEVIER

The American Journal of
PATHOLOGY

ajp.amjpathol.org

METABOLIC, ENDOCRINE, AND GENITOURINARY PATHOBIOLOGY

Periprostatic Adipose Tissue Displays a Chronic Hypoxic State that Limits Its Expandability

Check for updates

Mathieu Roumiguié,*† David Estève,* Cécile Manceau,*† Aurélie Toulet,* Jérôme Gilleron,‡ Chloé Belles,§ Yiyue Jia,* Cynthia Houël,* Sarah Pericart,¶ Sophie LeGonidec,‖ Philippe Valet,‖ Mireille Cormont,‡ Jean-François Tanti,‡ Bernard Malavaud,† Anne Bouloumié,§ Delphine Milhas,* and Catherine Muller*

From the Institut de Pharmacologie et de Biologie Structurale (Equipe Labélisée Ligue Nationale contre le Cancer), Université de Toulouse, Centre national de la recherche scientifique, Toulouse; Département d'Urologie,† Institut Universitaire du Cancer, Toulouse; the Université Côte d'Azur,‡ INSERM, Centre Méditerranéen de Médecine Moléculaire, Team Cellular and Molecular Pathophysiology of Obesity, Nice; the Institut des Maladies Métaboliques et Cardiovasculaires,§ Université de Toulouse, INSERM, Toulouse; the Département d'Anatomo-Pathologie,¶ Institut Universitaire du Cancer, Toulouse; and the Institut RESTORE,‖ Université de Toulouse, Centre national de la recherche scientifique U-5070, Etablissement Français du Sang, Ecole Nationale Vétérinaire de Toulouse, INSERM U1301, Toulouse, France*

Accepted for publication March 8, 2022.

Address correspondence to Catherine Muller, M.D., Ph.D., or Delphine Milhas, Ph.D., Institut de Pharmacologie et de Biologie Structurale, Centre national de la recherche scientifique, UMR 5089, 205 Rte de Narbonne, 31077 Toulouse, France.
E-mail: muller@ipbs.fr or delphine.milhas@ipbs.fr.

White adipose tissue accumulates at various sites throughout the body, some adipose tissue depots exist near organs whose function they influence in a paracrine manner. Prostate gland is surrounded by a poorly characterized adipose depot called periprostatic adipose tissue (PPAT), which plays emerging roles in prostate-related disorders. Unlike all other adipose depots, PPAT secretes proinflammatory cytokines even in lean individuals and does not increase in volume during obesity. These unique features remain unexplained because of the poor structural and functional characterization of this tissue. This study characterized the structural organization of PPAT in patients compared with abdominopelvic adipose tissue (APAT), an extraperitoneal adipose depot, the accumulation of which is correlated to body mass index. Confocal microscopy followed by three-dimensional reconstructions showed a sparse vascular network in PPAT when compared with that in APAT, suggesting that this tissue is hypoxic. Unbiased comparisons of PPAT and APAT transcriptomes found that most differentially expressed genes were related to the hypoxia response. High levels of the hypoxia-inducible factor 2α confirmed the presence of an adaptive response to hypoxia in PPAT. This chronic hypoxic state was associated with inflammation and fibrosis, which were not further up-regulated by obesity. This fibrosis and inflammation explain the failure of PPAT to expand in obesity and open new mechanistic avenues to explain its role in prostate-related disorders, including cancer. *(Am J Pathol 2022, 192: 926–942; https://doi.org/10.1016/j.ajpath.2022.03.008)*

In mammals, white adipose tissue (WAT) accumulates at various sites throughout the body. Visceral adipose tissue (VAT), the most important and well-studied fat deposit, occurs in subcutaneous regions and in the abdominal cavity that surrounds key internal organs such as the intestines.[1] WAT comprises metabolically active adipocytes and other cell types in the stroma vascular fraction, including adipose progenitor cells, fibroblasts, mural, endothelial, and immune cells, all of which are embedded in the extracellular matrix (ECM).[1] Studies of these 2 fat depots primarily centered on their role in controlling energy homeostasis in response to systemic nutritional and metabolic needs have highlighted metabolic differences between them.[2] Other adipose depots, such as mammary, epicardial, perivascular, and bone marrow adipose tissues, are distributed throughout the body.[1] These adipose tissues are frequently closely associated with other anatomic structures, and emerging evidence

Supported by the Ligue Nationale Contre le Cancer (Équipe labélisée), the French National Cancer Institute grant INCA PL-BIO 2016-176 (P.V., B.M., and C.M.), the Fondation Toulouse Cancer Santé (P.V., B.M., and C.M.), Fondation ARC (Association de Recherche contre le Cancer) Programmes labelisés 2016 (P.V., B.M., and C.M.), and postdoctoral fellowship SPF201809007124 from the Fondation pour La Recherche Médicale (D.E.).

M.R. and D.E. contributed equally to this work.

Disclosures: None declared.

Copyright © 2022 American Society for Investigative Pathology. Published by Elsevier Inc.
This is an open access article under the CC BY-NC-ND license (http://creativecommons.org/licenses/by-nc-nd/4.0).
https://doi.org/10.1016/j.ajpath.2022.03.008

shows that they play a paracrine role in proximal organ−specific functions during pathologic processes, such as regenerative or infectious disorders as well as cancers.[1,3] However, despite their increasing importance, their biology remains poorly described.

Periprostatic adipose tissue (PPAT) is one such adipose depot. PPAT surrounds the prostate gland and is separated from it by a fibromuscular sheet of varying thickness called the prostate capsule. Nearly one-third of the anterior surface of the glandular tissue, however, is in direct contact with the PPAT.[4,5] PPAT is often considered to be VAT, although it is located in the pelvic region. Characterization of this tissue in any species remains poor, but at least two characteristics of PPAT indicate that it is distinct from other WAT. First, it does not increase in volume even when other forms of WAT (including VAT) are present in excess in obesity.[6] Second, it secretes large amounts of proinflammatory cytokines, such as IL-6 and tumor necrosis factor (TNF)-α.[6−8] Although this chronic inflammatory state is usually observed in WAT of patients with obseity,[9] in PPAT it is independent of the state of obesity of the individual.[10−12] PPAT has received increasing attention in recent years because of reports that PPAT plays a paracrine role in prostate cancer (PCa) progression, implicating soluble factors (such as proinflammatory cytokines and chemokines) as well as lipid mediators.[4,13,14] Molecules released by PPAT could also impact normal prostate development and contractility and contribute to benign prostatic hyperplasia and related symptoms.[15] A better understanding of PPAT biology is mandatory to provide a foundation for further mechanistic inquiries on its paracrine role on prostate.

Accordingly, the initial goal of this study was to characterize the structural organization of PPAT in patients, which led to new functional insights. The study showed that PPAT has a sparse vascular network responsible for a chronic hypoxic state, leading to inflammation as well as fibrosis independent of obesity. These structural and functional characteristics explain the failure of PPAT to expand in obesity and open new mechanistic avenues to explain its role in prostate disorders, including cancer.

Materials and Methods

Patients and Fat Measurements

Between September 2016 and March 2021, patients with localized PCa diagnosed by prostate biopsies who had opted for radical prostatectomy were recruited. Patients with metastatic PCa (as assessed by computed tomography and/or bone scan) and patients who had received radiotherapy, hormonal treatment, or high-intensity ultrasonography were excluded. As controls for the experiments to investigate the three-dimensional vasculature (see below), PPAT samples were obtained from two patients undergoing radical cystoprostatectomy for muscle-invasive bladder cancer and who lacked PCa according to the pathologist's report. The study was conducted in accordance with the guidelines and with the full approval of the national ethics committee (AC-2020-4031). Written informed consent was received from participants before inclusion in the study, which was conducted in accordance with the Declaration of Helsinki principles as revised in 2000.

All the patients underwent pre-operative 1.5-T multiparametric magnetic resonance imaging (mpMRI) after injection with 20 mg of butyl scopolamine (Buscopan; Boehringer-Ingelheim, Paris, France). Anatomic three-dimensional fast spin echo T2-weighted MRI, functional diffusion-weighted MRI, and dynamic contrast-enhanced MRI data were acquired. After anonymization of the mpMRI data, the subcutaneous fat thickness (SFT) and the PPAT and abdominopelvic adipose tissue (APAT) volumes were measured in 54 patients with a semiautomated segmentation technique on contiguous 3-mm T2-weighted axial slices (except for SFT for which one slice was used) and Olea Sphere software version 3.0 (Olea Medical, La Ciotat, France). Baseline demographic characteristics [age and body mass index (BMI)], disease-specific parameters (Gleason score and histopathologic stage of radical prostatectomy specimens), and mpMRI data were acquired from the medical records of the patients. The clinical characteristics of the cohort are presented in Supplemental Table S1. One observer (M.R.), trained by a senior experienced radiologist and blind to the clinical and pathologic data, performed all segmentations and measurements. The PPAT was segmented from the level of the prostate base to the apex (Figure 1A) (mean of 14 slices per patient). The following anatomic boundaries were used to define PPAT limits on each slice: pubic symphysis at the front, obturator muscles on the lateral sides, and Denonvilliers' fascia at the back. APAT was measured by segmenting the fat located above the pubic symphysis, in front of the bladder and behind the abdominal muscles, and included between each spermatic cordon on the lateral sides (mean of 3 slices per patient). SFT was determined by measuring the perpendicular distance between the skin and the anterior upper border of the symphysis pubis on a selected T2-weighted axial slice.

Tissue Collection and Tissue Processing

Paired anterior PPAT and APAT from patients undergoing radical prostatectomy were removed and the samples were anonymized. Charred samples and those weighing <300 mg were excluded from the study. Samples were immediately put in 50-mL tubes that contained 10 mL of Dulbecco's modified Eagle's medium (Thermo Fisher Scientific, Courtaboeuf, France) and were transported to the research laboratory within 1 hour, except for the Western blotting experiments for which the samples were immediately placed in 100 μL of radioimmunoprecipitation assay lysis buffer that contained phosphatases and proteases inhibitors (all

from Sigma-Aldrich, St Quentin Fallavier, France) in the operating theatre. The samples were weighed and used for several preparations. For quantitative real-time PCR analysis and dosage of hydroxyproline content, paired PPAT and APAT were immediately frozen in liquid nitrogen and stored at −80°C for later use. For three-dimensional microscopy and lobule size analysis, samples were embedded in paraffin for measuring adipocyte size as previously described[16] and for Masson's trichrome stain or were fixed with 4% paraformaldehyde solution at room temperature for 24 hours. Lobules were dissected as previously described.[17] Some of the samples were also used to isolate the stroma vascular fraction after collagenase digestion (see below). Finally, samples were used to prepare PPAT- or APAT-conditioned medium as previously described.[13] Briefly, 1 g of tissue was incubated overnight in 8 mL of Dulbecco's modified Eagle's medium supplemented with 1% bovine serum albumin in a humidified incubator at 37°C and with 5% CO_2, and the medium was collected after filtration through a 0.2-μmol/L filter. The conditioned media were immediately stored in small aliquots at −80°C.

RNA Extraction and Quantitative Real-Time PCR

For RNA extraction, 100 mg of frozen tissue was mixed with 500 μL of QIAzol lysis reagent (Qiagen, Hilden, Germany) and homogenized with a Precellys tissue homogenizer (two cycles of 45 seconds at 7500 rpm at 4°C) using the Cryolys cooling system (Bertin Technologies, Montigny le Bretonneux, France). RNA was extracted using the Qiagen RNeasy minikit, and cDNA was reverse transcribed from 250 ng of purified RNA by using the ReverAid H Minus First Strand cDNA synthesis kit (Thermo Fisher Scientific) with hexamer random primers according to the supplier's recommendations. Gene expression was quantified by quantitative real-time PCR with TaqMan primers (*VEGFA*: Hs00900055_m1, *VEGFB*: Hs00173634_m1; Thermo Fisher Scientific) and Fast Advanced TaqMan Master Mix (Thermo Fisher Scientific) with a CFX96 real-time PCR system (BioRad, Marnes la Coquette, France). Results were normalized to the amount of 18S rRNA.

RNA Sequencing and Data Preprocessing

RNA sequencing libraries were generated from 400 ng of total RNA by using the TruSeq Stranded mRNA LT Sample Preparation Kit (Illumina, San Diego, CA), according to the manufacturer's instructions. The cDNA libraries were sequenced on an Illumina HiSeq 4000 system using single-read 50 bp following Illumina's recommendations. Preprocessed reads were mapped onto the *Homo sapiens* genome assembly hg38 by using STAR version 2.5.3a (Massachusetts Institute of Technology, Cambridge, MA).[18] Gene expression was quantified from uniquely aligned reads by using HTSeq-Count version 0.6.1p1 (Python Software Foundation, Fredericksburg, VA) with annotations from Ensembl version 91 (European Bioinformatics Institute, Heidelberg, Germany) and "union" mode2. Only unambiguously assigned reads were retained for further analyses. Data sets generated during this study have been deposited in the Gene Expression Omnibus database (*https://www.ncbi.nlm.nih.gov/geo*; accession number GSE196442).

Normalized gene expression was $\log_2$ transformed and used to perform principal component analysis with the FactomineR package version 1.42 within R software version 3.6 (R Foundation for Statistical Computing, Vienna, Austria). Statistical analysis of differentially expressed genes was performed with the Limma package version 3.40.2 (WEHI Bioinformatics, Bundoora, VIC, Australia). Gene expression was considered significantly different if $P < 0.05$ and the $\log_2$ fold-change was >2 or <-2. Pathway enrichment analysis was performed with Gene Set Variation Analysis package version 1.46.0 (Broad Institute, Cambridge, MA) using the official gene symbols and hallmark gene sets in the Molecular Signatures Database version 7.3 (*www.gsea-msigdb.org*, last accessed May 28, 2021). Overlap between differentially expressed genes and curated gene sets or hallmark gene sets were computed. Heatmaps were made with Ward's hierarchical clustering method by using the gplots package version 3.0.1.1. Protein-protein interaction networks were created by using Cytoscape version 3.7.1 and ClueGo plugin (Institute for Systems Biology, Seattle, WA).

Tridimensional Vasculature Imaging of Adipose Tissues

To study the tridimensional vasculature of adipose tissues, a clearing method suited to investigate the morphology of WAT by fluorescence imaging was used, which was described recently.[19] Briefly, the tissues were stained with anti-CD31−Alexa Fluor 647 antibody (Miltenyi Biotech, Paris, France), DAPI (5 μg/mL), and phalloidin−Alexa Fluor 488 (Invitrogen, Courtaboeuf, France). The three-dimensional image stacks were acquired in a mosaic with a Nikon-A1R confocal microscope equipped with a 20× long-distance air objective and analyzed with Imaris software version 9.2.1 (Bitplane, Gometz la Ville, France).

Hydroxyproline Quantification

Fragments of adipose tissue of approximately 100 mg were weighed precisely and then placed in 500 μL of deionized water in a Precellys 2-mL soft tissue homogenizing ceramic beads kit (CK14) and extracted by using the Precellys tissue homogenizer with 2 cycles of 45 seconds at 7500 rpm at room temperature. Samples were then centrifuged for 10 minutes at 5000 × *g* at room temperature to remove lipids floating on the top layer by pipetting. Lipid-free supernatants were vortex mixed, and then 150 μL was mixed with an equal volume of 10 mol/L sodium hydroxide and heated at 105°C for 1 hour to fully digest collagens. The reaction was stopped by adding 150 μL of 10 mol/L hydrochloride.

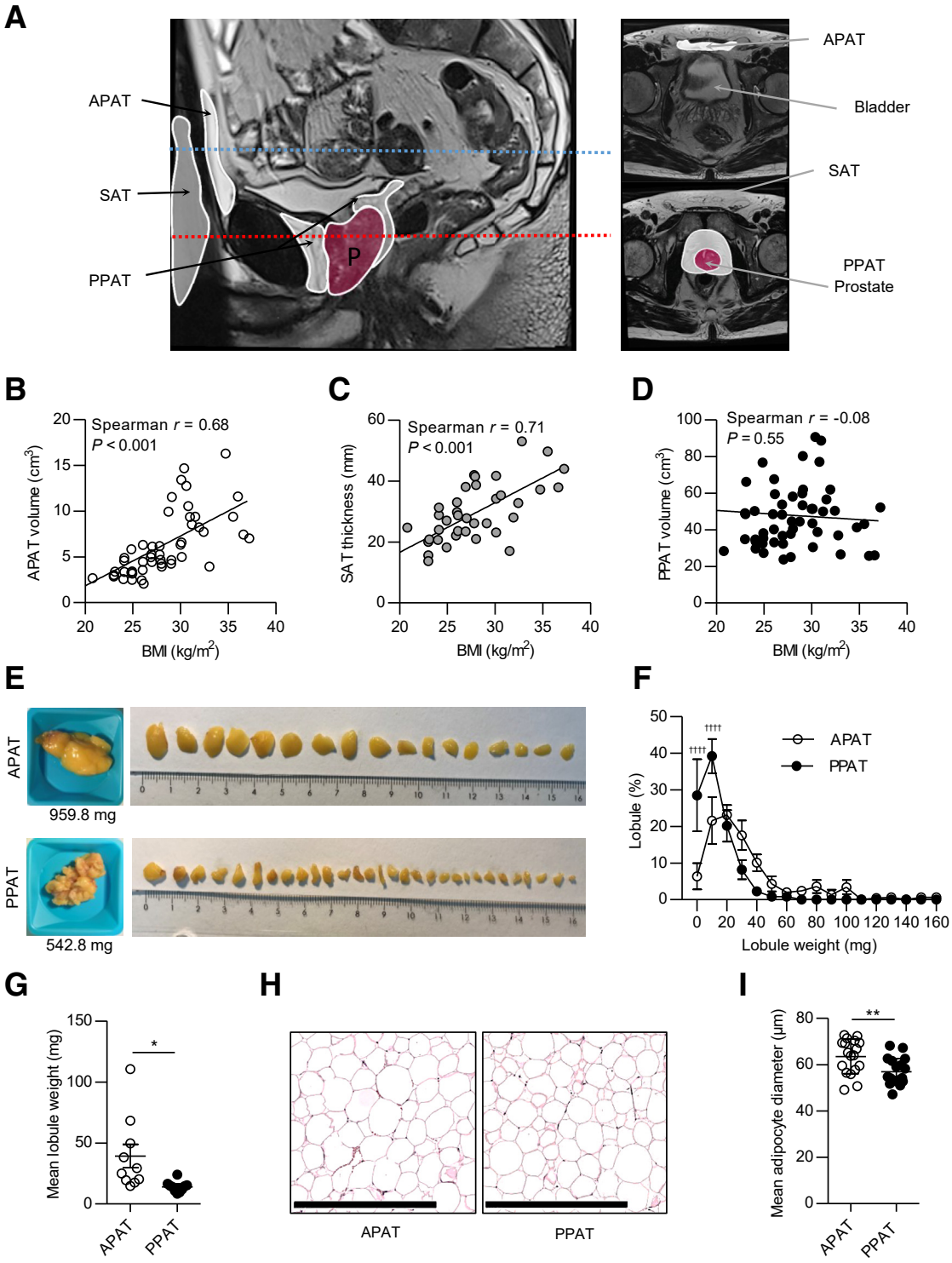


Figure 1 The accumulation of periprostatic adipose tissue (PPAT) is independent of body mass index (BMI), and its morphology differs from abdominopelvic adipose tissue (APAT). **A:** Sagittal (**left panel**) and axial (**right panel**) sections of the midbody of a man as seen by T2-weighted magnetic resonance imaging. The locations of PPAT, APAT, and subcutaneous adipose tissue (SAT) are shown. Dotted lines on the sagittal section indicate the position of axial sections represented. **B**–**D**: Correlations between the BMI of each patient and APAT volume (**B**), SAT thickness (**C**), and PPAT volume (**D**). **E:** Representative images of the size of the lobules obtained after dissection of the indicated amounts of APAT and PPAT (scale in centimeters). **F:** Lobule weight distribution in paired PPAT and APAT samples. **G:** Mean lobule weight in paired APAT and PPAT samples. **H:** Representative images of hematoxylin and eosin–stained, paraffin-embedded APAT and PPAT tissue sections. **I:** Mean diameter of adipocytes in paired APAT and PPAT tissue sections as in **H**. Data are expressed as means ± SEM (**F**, **G**, and **I**). $n = 54$ (**B**); $n = 40$ (**C**); $n = 56$ (**D**); $n = 10$ (**F** and **G**); $n = 18$ (**H**). $^{*}P < 0.05$, $^{**}P < 0.01$ (two-way analysis of variance followed by Bonferoni posttest); $^{\dagger\dagger\dagger\dagger}P < 0.0001$ (*t*-test). Scale bar = 500 µm.

Hydroxyproline was quantified in duplicate by using a hydroxyproline assay kit (Perchlorate-Free; Biovison, Milpitas, CA) as recommended by the supplier and normalized to the precise tissue weight initially digested.

Masson's Trichrome Stain, Collagen Staining with Picrosirius Red, and Three-Dimensional Collagen Fiber Quantification

For Masson's trichrome staining, adipose tissues were deparaffinized with xylene for 5 minutes, dehydrated in 100% alcohol for 5 minutes, and then rehydrated in running tap water for 5 to 10 minutes. The tissues were stained in Mayer's hemalum solution for 20 minutes and washed in distilled water and in ammonia water each for 30 seconds. Then they were stained in Ponceau S solution for 1 minute and washed in distilled water. They were differentiated in 1% phosphomolybdic solution for 5 minutes, transferred to aniline blue solution, and stained for an additional 5 minutes. The tissues were rinsed briefly in distilled water and differentiated in 1% acetic acid solution for 4 minutes, then dehydrated rapidly through alcohol and cleared in xylene. For collagen staining with Picrosirius Red, fixed adipose tissues were incubated for 3 hours in Picrosirius Red solution (1 g/L Sirius red in 1.3% picric acid). After two washes in acidified water followed by fixation and dehydration steps in 100% ethanol, images were taken with a Zeiss LSM710 confocal microscope (Zeiss International, Oberkochen, Germany) equipped with a 40× oil-immersion inverted objective with a numerical aperture of 1.3. The samples were excited at 560 nm, and fluorescence emission was collected above 580 nm. Pinhole was setup at 0.7 Airy (ZEN imaging software version 6.0.0.485; Zeiss International) to increase resolution. Three-dimensional reconstructions and analyses of collagen fiber organization were performed with Imaris software version 9.7.2 and the filament tracer module. The data generated were normalized to the tissue volume obtained after tissue surface reconstruction with Imaris.

Western Blotting

For Western blotting, 100-mg samples of PPAT or APAT were immediately incubated with 100 μL of radioimmunoprecipitation assay lysis buffer that contained phosphatases and proteases inhibitors (Sigma-Aldrich, St. Louis, MO) before transportation to the research laboratory. Proteins were extracted using the Precellys tissue homogenizer and soft tissue homogenizing ceramic beads (CK14) with two cycles of 45 seconds at 7500 rpm at room temperature. The samples were then centrifuged 10 minutes at 10,000 × *g* at room temperature to separate the lipids. The extract was recovered without the lipid layer and centrifuged again 10 minutes at 10,000 × *g* at 4°C. In some experiments, proteins were extracted from the PCa cell line PC3 before or after treatment with 200 μmol/L cobalt chloride for 16 hours, as previously described.[14] Proteins in the extracts (40 μg for tissues and 20 μg for PC3 cells) were separated by electrophoresis on a 4% to 10% gradient SDS-PAGE gel (Bio-Rad) and transferred to a nitrocellulose membrane. After incubation in blocking buffer containing 1× tris-buffered saline (Tris, 20 mmol/L; sodium, 150 mmol/L) and 5% skimmed milk, the membranes were incubated with primary antibodies in blocking buffer at 4°C overnight [anti− hypoxia-inducible factor (HIF)-1α (clone 54, 1/1000, BD Biosciences, Le Pont de Claix, France), anti−HIF-2α (1/400, Novus Biologicals, Noyal Châtillon sur Seiche, France), anti−HIF-1α (clone 29, 1/1000, BD Biosciences), anti−glucose transporter (GLUT)-1 (1/1000, Abcam, Cambridge, UK), and anti−β-actin (clone AC-15, 1/5000, Sigma-Aldrich)]. The membranes were then washed with tris-buffered saline that contained 1% Tween and incubated with secondary antibodies conjugated to horseradish peroxidase (1/5000, Santa Cruz Biotechnology, Dallas, TX). The immunoreactive protein bands were revealed by using the ECL Prime Western Blotting Detection Reagent (Amersham, Amersham, UK) and detected with a ChemiDoc Imaging System (Bio-Rad). Densitometry quantification was performed using ImageJ version 1.53-j (NIH, Bethesda, MD; *http://imagej.nih.gov/ij*).

Isolation of Adipose Tissue Stroma—Vascular Fraction

Digestion of fresh PPAT and APAT was performed as previously described.[17] Briefly, adipose tissues were digested with 250 U/mL of type I collagenase (Sigma-Aldrich) in phosphate-buffered saline that contained 2% bovine serum albumin for 30 minutes at 37°C, with shaking. After digestion, the cell suspension was filtered through a 250-μm strainer and centrifuged at 300 × *g* for 10 minutes. Erythrocytes were lysed by incubation at room temperature in erythrocyte lysis buffer (155 mmol/L NH_4Cl, 5.7 mmol/L K_2HPO_4, 0.1 mmol/L EDTA, pH 7.3) for 10 minutes followed by successive filtration through 100-, 70-, and 40-μm strainers. The viable recovered cells were counted and analyzed by flow cytometry.

Flow Cytometry Analysis

Flow cytometry was performed as initially described with minor modifications.[20] A total of 100,000 stroma-vascular cells were incubated for 30 minutes at 4°C in phosphate-buffered saline supplemented with 0.5% bovine serum albumin and 2 mmol/L EDTA that contained the following fluorescent labeled antibodies: Brilliant Violet 510 anti-human CD45 Antibody (clone HI30, dilution 1/20, Biolegend, San Diego, CA), APC anti-human CD206 (clone 19.2, dilution 1/10, BD Biosciences), and PE-Vio 770 anti-human CD14 (clone TÜK4, dilution 1/50, Miltenyi Biotec). As control, a panel of appropriate isotype antibodies was used. The labeled cells were washed with phosphate-buffered saline and analyzed in a FACS Canto II

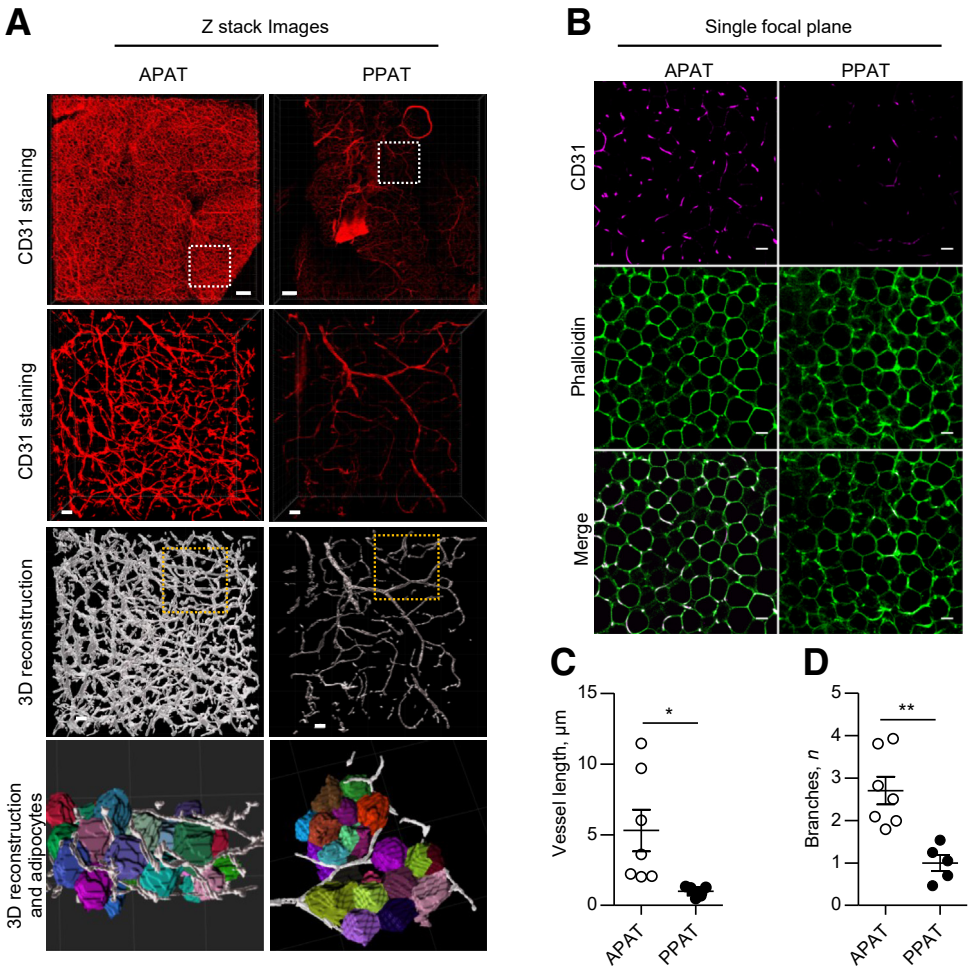


Figure 2 The microvasculature of periprostatic adipose tissue (PPAT) suggests a hypoxic state. **A:** Representative Z stack confocal images of cleared PPAT and abdominopelvic adipose tissue (APAT) stained with anti-CD31 showing the capillary networks (**upper panels**). The zones indicated by the dotted squares are shown in higher magnification in the images below. Three-dimensional (3D) reconstructions of the microvasculature (gray) and adipocytes (randomly color coded to identify each adipocyte) were made using Imaris software version 9.7.2. **B:** A representative single focal plane (thickness, 8 µm) extracted from 3D confocal images of paired APAT and PPAT samples stained with anti-CD31 (magenta, **upper panel**) and phalloidin (green, **middle panel**) and the merge images (**lower panel**). **C** and **D:** Quantification after 3D reconstruction of the total length of the vessels (**C**) and the number of branches (**D**) in APAT and PPAT. Data are expressed as means ± SEM (**C** and **D**). $n = 7$ APAT samples (**C** and **D**); $n = 5$ PPAT samples (**C** and **D**). $^{*}P < 0.05$, $^{**}P < 0.01$ (*t*-test). Scale bars: 300 µm (**A**); 50 µm (**enlargements of box areas**).

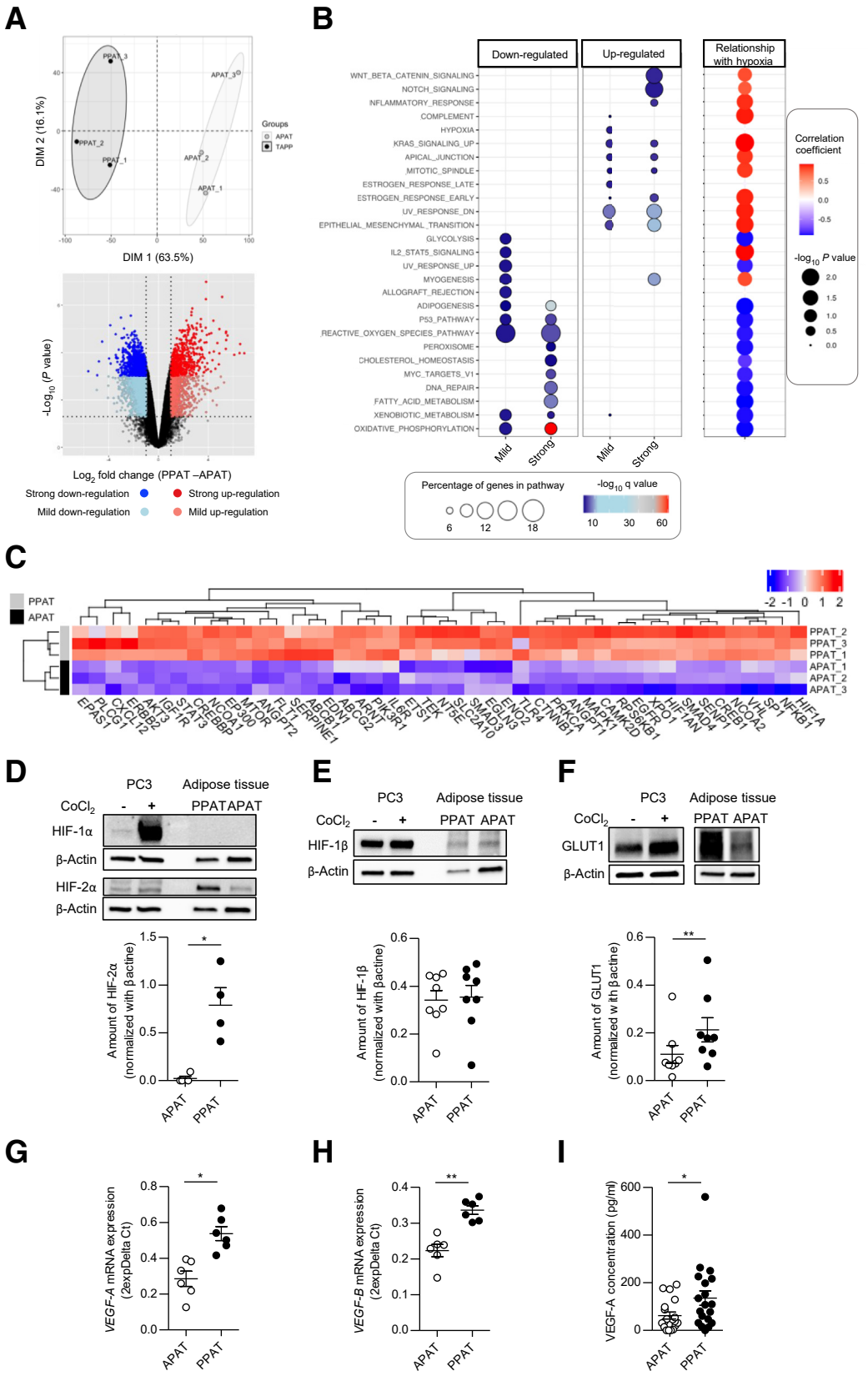
flow cytometer using Diva Pro software version 9 (BD Biosciences). Cell debris, dead cells, and doublets were excluded based on scatter signals. Compensation was established using compensation particles set (BD Biosciences) and single staining, and flow cytometer calibration was performed with rainbow calibration particles (BD Biosciences).

ELISA Assays

Vascular endothelial growth factor (VEGF)-A in the conditioned medium from APAT and PPAT samples was quantified with an enzyme-linked immunosorbent assay (ELISA) kit (DVE00, R&D Systems, Noyal Châtillon sur Seiche, France) according to the protocol provided by the manufacturer. Optical density was determined at 450 nm using a µQuant microplate reader (Agilent-BioTek Instruments, Les Ulis, France). A panel of secreted adipokines were quantified likewise with an ELISA kit (LXSAHM-08, R&D Systems) and a mixture of antibodies against adiponectin/Acrp30, IL-6, IL-1β, leptin, plasminogen activator inhibitor (PAI)-1/serpin E1, and TNF-α, according to the protocol provided by the manufacturer.

Statistical Analysis

Statistical analyses were performed with GraphPad Prism version 5.04 (GraphPad Software, San Diego, CA). The univariate relationship between fat measurement and BMI was performed with Spearman's correlation. Frequency distribution was calculated for fat lobule size and the mean diameter of collagen fibers, and two-way analysis of variance was performed followed by the Bonferroni posttest. Comparisons between APAT and PPAT were performed


A
DIM 2 (16.1%)
DIM 1 (63.5%)
Groups
APAT
TAPP
-Log10 (P value)
Log2 fold change (PPAT –APAT)
Strong down-regulation
Strong up-regulation
Mild down-regulation
Mild up-regulation
B
Down-regulated
Up-regulated
Relationship with hypoxia
WNT_BETA_CATENIN_SIGNALING
NOTCH_SIGNALING
INFLAMMATORY_RESPONSE
COMPLEMENT
HYPOXIA
KRAS_SIGNALING_UP
APICAL_JUNCTION
MITOTIC_SPINDLE
ESTROGEN_RESPONSE_LATE
ESTROGEN_RESPONSE_EARLY
UV_RESPONSE_DN
EPITHELIAL_MESENCHYMAL_TRANSITION
GLYCOLYSIS
IL2_STAT5_SIGNALING
UV_RESPONSE_UP
MYOGENESIS
ALLOGRAFT_REJECTION
ADIPOGENESIS
P53_PATHWAY
REACTIVE_OXYGEN_SPECIES_PATHWAY
PEROXISOME
CHOLESTEROL_HOMEOSTASIS
MYC_TARGETS_V1
DNA_REPAIR
FATTY_ACID_METABOLISM
XENOBIOTIC_METABOLISM
OXIDATIVE_PHOSPHORYLATION
Mild
Strong
Correlation coefficient
-log10 P value
Percentage of genes in pathway
-log10 q value
C
PPAT
APAT
PPAT_2
PPAT_3
PPAT_1
APAT_1
APAT_2
APAT_3
D
PC3
Adipose tissue
CoCl2
PPAT APAT
HIF-1α
β-Actin
HIF-2α
Amount of HIF-2α (normalized with β actine)
E
HIF-1β
Amount of HIF-1β (normalized with β actine)
F
GLUT1
Amount of GLUT1 (normalized with β actine)
G
VEGF-A mRNA expression (2expDelta Ct)
H
VEGF-B mRNA expression (2expDelta Ct)
I
VEGF-A concentration (pg/ml)

using a paired *t*-test or *U*-test when data are not normally distributed. Comparisons between lean patients and patients with obesity were performed using the *t*-test. Normal distribution of the data was determined using the Kolgomorov-Smirnov test.

Results

Differences between PPAT and APAT

To investigate how PPAT might differ from other adipose depots depending on the BMI of the individual, a cohort of 54 patients awaiting prostatectomy for PCa was examined by using preoperative mpMRI of PPAT, subcutaneous adipose tissue (SAT), and APAT (Figure 1A). The SFT at the upper border of the pubic symphysis was used as an indicator of the accumulation of SAT.[21] The volume of the APAT, which is located in front of the bladder and behind the abdominal muscles (Figure 1A), was measured on contiguous axial slices. This fat depot was chosen because, like PPAT, it is located in the extraperitoneal area and can be removed easily during surgery for further biological comparisons. The volume of PPAT was measured on successive slices from the base to the apex of the prostate. Both APAT volume (Figure 1B) and SAT thickness (Figure 1C) correlated with BMI, consistent with a previous study.[6] By contrast, PPAT volume was independent of BMI (Figure 1D), also in accordance with several previous studies as outlined by Nassar et al.[6] These data confirm that PPAT differs from other adipose depots in its regulation by obesity and show that APAT can be used as a control tissue because it behaves like typical adipose tissue.

WAT comprises distinct lobules that contain clusters of adipocytes separated from each other by fibrous septa.[17] On dissection, the lobules in PPAT were smaller and more numerous than those in APAT (Figure 1E). The weight distribution of the lobules indicated a significantly larger proportion of small lobules (<20 mg) in PPAT when compared with those in APAT (Figure 1F), and the mean lobule weight in PPAT was smaller than in APAT (Figure 1G). The adipocytes in PPAT were also slightly smaller than those in APAT (Figure 1H-I). These findings indicate that the two adipose tissues differ in their organization, with smaller lobules in PPAT when compared with those in APAT.

Microvasculature of PPAT Suggests a Hypoxic State

To investigate the vasculature of PPAT and compare it with that of APAT, cleared tissues were immunostained with an antibody against the endothelial marker CD31 and the stained tissue was visualized by three-dimensional confocal imaging. In WAT, classically, each fat lobule in adipose tissue is supplied by a vascular bundle of arterioles and venules, which in turn are subdivided into capillaries that surround individual fat cells.[22] At low magnification, the vascular network of PPAT appeared much less dense than that of APAT (Figure 2A), and this was more evident at higher magnification and on three-dimensional reconstruction of the vasculature (Figure 2A). Three-dimensional reconstruction of the adipocytes and associated capillaries showed a generally less dense structure in PPAT, with capillaries surrounding groups of adipocytes, whereas the capillaries in APAT surrounded individual adipocytes (Figure 2A). This distinct organization could be seen also by analyzing representative focal planes from three-dimensional images of APAT and PPAT (Figure 2B) stained with an antibody against CD31, the endothelial cells marker, and with phalloidin (an actin stain) that delineated the adipocytes. Merging of these images showed fewer adipocytes contacting endothelial cells in PPAT in contrast to those in APAT. Quantification of the vascular network after three-dimensional reconstruction showed that the total length of the vessel network as well as the number of branches were significantly smaller in PPAT than in APAT (Figure 2, C and D). Similar analyses of PPAT from patients

Figure 3 Transcriptomics reveals a hypoxic signature in periprostatic adipose tissue (PPAT) associated with an increased expression of hypoxia-inducible factor (HIF)-2α. **A:** Principal component analysis performed on the whole transcriptomics data set. Ellipses represent the CI for the PPAT group and the abdominopelvic adipose tissue (APAT) (**upper panel**). Volcano plot representing the mean $\log_2$ fold change (PPAT/APAT) versus $-\log_{10}$ *P* value (**lower panel**). Vertical dotted lines indicate the limits for genes that were twofold overrepresented or underrepresented (ie, $\log_2$ fold change >1 or <−1, respectively). Horizontal dotted line indicated genes that reached the cutoff *P* value ($P < 0.05$). Dark blue dots show highly underrepresented (ie, strong down-regulation) genes (ie, adjusted $P < 0.01$ and $\log_2$ fold change <−1). Light blue dots show mildly underrepresented (ie, mild down-regulation) genes (ie, $P < 0.05$ and $\log_2$ fold change <−1). Dark red dots show highly overrepresented (ie, strong up-regulation) genes (ie, adjusted $P < 0.01$ and $\log_2$ fold change >1). Light red dots show mildly overrepresented (ie, mild up-regulation) genes (ie, $P < 0.05$ and $\log_2$ fold change >1). **B:** Balloon plots representing the pathways enriched in each gene category according to the hallmark collection in the Molecular Signatures Database. The size of each balloon is setup according to the percentage of genes belonging to each pathway enriched and the color according to $-\log_{10}$ of the q value. The relationship between hypoxia hallmark and other enriched hallmarks was evaluated as Pearson correlation of enrichment score determined with the single-sample Gene Set Enrichment Analysis algorithm. **C:** Heatmap and hierarchical clustering of sample based on up-regulated genes belonging to the hypoxia hallmark. **D:** Representative Western blots of HIF-1α, HIF-2α, and β-actin in paired samples of PPAT and APAT (**upper panel**) and quantification of HIF-2α (**lower panel**). **E:** Representative Western blots of HIF-1β and β-actin in paired samples of PPAT and APAT (**upper panel**) and quantification (**lower panel**). **F:** Representative Western blots of anti−glucose transporter (GLUT)-1 and β-actin in paired samples of PPAT and APAT (**upper panel**) and quantification (**lower panel**). **D**—**F:** PC3 cells treated or not with cobalt (II) chloride ($CoCl_2$) were used as controls. **G** and **H:** *VEGF-A* (**G**) and *VEGF-B* (**H**) mRNA expression was determined by quantitative real-time PCR in paired samples of PPAT and APAT. **I:** Secreted vascular endothelial growth factor (VEGF)-A was measured by enzyme-linked immunosorbent assay in conditioned media from paired samples of PPAT and APAT. Data are expressed as means ± SEM (**G**—**I**). $n = 3$ per group (**A**); $n = 6$ (**C**); $n = 4$ (**D**); $n = 8$ (**E** and **F**); $n = 6$ (**G** and **H**); $n = 19$ (**I**). $^*P < 0.05$, $^{**}P < 0.001$ (*t*-test). DIM, dimension.

without PCa also found a low-density vasculature in PPAT when compared with APAT (Supplemental Figure S1A). The vascular organization in PPAT suggests that this tissue might be hypoxic.

Transcriptomics Reveals a Hypoxic Signature in PPAT that Exhibits an Increased Expression of HIF-2α

The transcriptomes of paired PPAT and APAT were sequenced to study the biological consequences of the structure of PPAT. Unsupervised principal component analysis of the whole transcriptome data sets showed that the first dimension, which accounted for 63.5% of the data set variance, separated samples according to their anatomic location, whereas the second dimension, which accounted for 16.1% of data set variance, discriminated between samples according to the identity of the patient (Figure 3A). These strong differences distinguish PPAT from APAT.

To investigate further the differences between PPAT and APAT, differential gene expression was evaluated using a linear modeling fitted for a small number of samples.[23] Among the 3935 differentially expressed genes identified, 1479 were up-regulated in PPAT, of which 604 were strongly up-regulated (ie, adjusted $P < 0.01$ and fold change >2), whereas 2456 were down-regulated, of which 817 were strongly downregulated (Figure 3B and Supplemental Table S2). Genes that were considered to be only mildly differentially expressed could discriminate between samples according to their anatomic location, albeit less well than genes that were strongly differentially expressed (Supplemental Figure S2A–D). To identify key features and a molecular signature specific to PPAT, pathway analysis was performed on the differentially expressed genes by using the Molecular Signatures Database. Most of the pathways associated with up-regulated and down-regulated genes were related to the hypoxia response (Figure 3C). A large set of genes that were down-regulated were associated with metabolic pathways, such as fatty acid metabolism, cholesterol homeostasis, and oxidative phosphorylation, with oxidative phosphorylation being the most strongly down-regulated pathway (Figure 3C). Adipogenesis, which is down-regulated in hypoxic adipose tissue,[24] was among the pathways down-regulated in PPAT when compared with APAT (Figure 3C; see Supplemental Figure S3A for the heatmap with a detailed list of genes). Among the up-regulated pathways, most were associated with hypoxia (Figure 3C). Single-sample Gene Set Enrichment Analysis confirmed the up-regulation of genes in the hypoxia pathway (Supplemental Figure S4A) and the positive correlation between hypoxia enrichment scores and other hallmarks up-regulated in PPAT (Figure 3C and Supplemental Figure S4B). By contrast, pathways down-regulated in PPAT correlated negatively with hypoxia hallmark enrichment scores (Figure 3C and Supplemental Figure S4B). In addition to up-regulation of genes related to hypoxia (see Figure 3D for the heatmap with detailed list of genes), genes related to several signaling pathways that are known downstream effectors in hypoxia signaling, including the β-Catenin and Notch signaling pathways,[25–27] were strongly up-regulated in PPAT (Figure 3C). In addition, genes related to the inflammatory response and the epithelial-to-mesenchymal transition (including ECM proteins), which are key hallmarks of the hypoxic microenvironment, were up-regulated in PPAT (Figure 3C). Together, this unbiased comparison of PPAT and APAT transcriptomes reveals hypoxic traits in PPAT consistent with the low-density vasculature of this tissue.

The cell's response to hypoxia is mediated by two heterodimeric HIFs, which comprise an α-subunit (HIF-1α or HIF-2α) whose expression is regulated by oxygen, and an oxygen-insensitive β-subunit.[28] Hypoxia prevents hydroxylation of the HIF-α subunits by prolyl hydroxylases, thereby inhibiting their degradation and promoting HIF-dependent up-regulation of genes involved in cell survival, angiogenesis, metabolism, inflammation, and the ECM and its remodeling.[28] In normoxic conditions, by contrast, degradation of the HIF-α subunits occurs within minutes.[28]

If PPAT is indeed a hypoxic tissue, it may have relatively high levels of HIFs. To test this prediction, HIF subunits were analyzed in samples of PPAT and APAT taken from patients and immediately incubated in lysis buffer in the operating theatre to avoid exposure of the tissue to ambient oxygen, and then rapidly transferred to the research laboratory for protein extraction. Immunoblotting of the protein extracts revealed more HIF-2α in samples of PPAT than in paired APAT samples, whereas HIF-1α was undetectable in both tissues (Figure 3E). By contrast, similar amounts of the oxygen-insensitive β-subunit were found in the two tissues (Figure 3F). When the tissue samples were transferred from the operating theatre to research laboratory in culture medium, only the stable HIF-1α subunit was detected by immunoblotting, indicating the importance of immediate lysis of the samples to detect the HIF-α subunits (Supplemental Figure S5).

To investigate whether the large amount of HIF-2α in PPAT was associated with an adaptive response to hypoxia, the expression of target genes of HIF-2α involved in metabolism and angiogenesis were harvested. Immunoblotting indicated significantly larger quantities of the glucose transporter protein GLUT-1, an HIF target gene product in adipocytes,[29] in PPAT than in APAT (Figure 3G). Similarly, as determined by quantitative real-time PCR, there was more *VEGF-A* and *VEGF-B* mRNA in PPAT than in APAT (Figure 3H-I) and, as determined by ELISA, more secreted VEGF-A protein in the conditioned medium of PPAT than in that of APAT (Figure 3I). Thus, consistent with the hypoxic nature of PPAT, more HIF-2α and its target gene products were found in this tissue than in the control APAT.

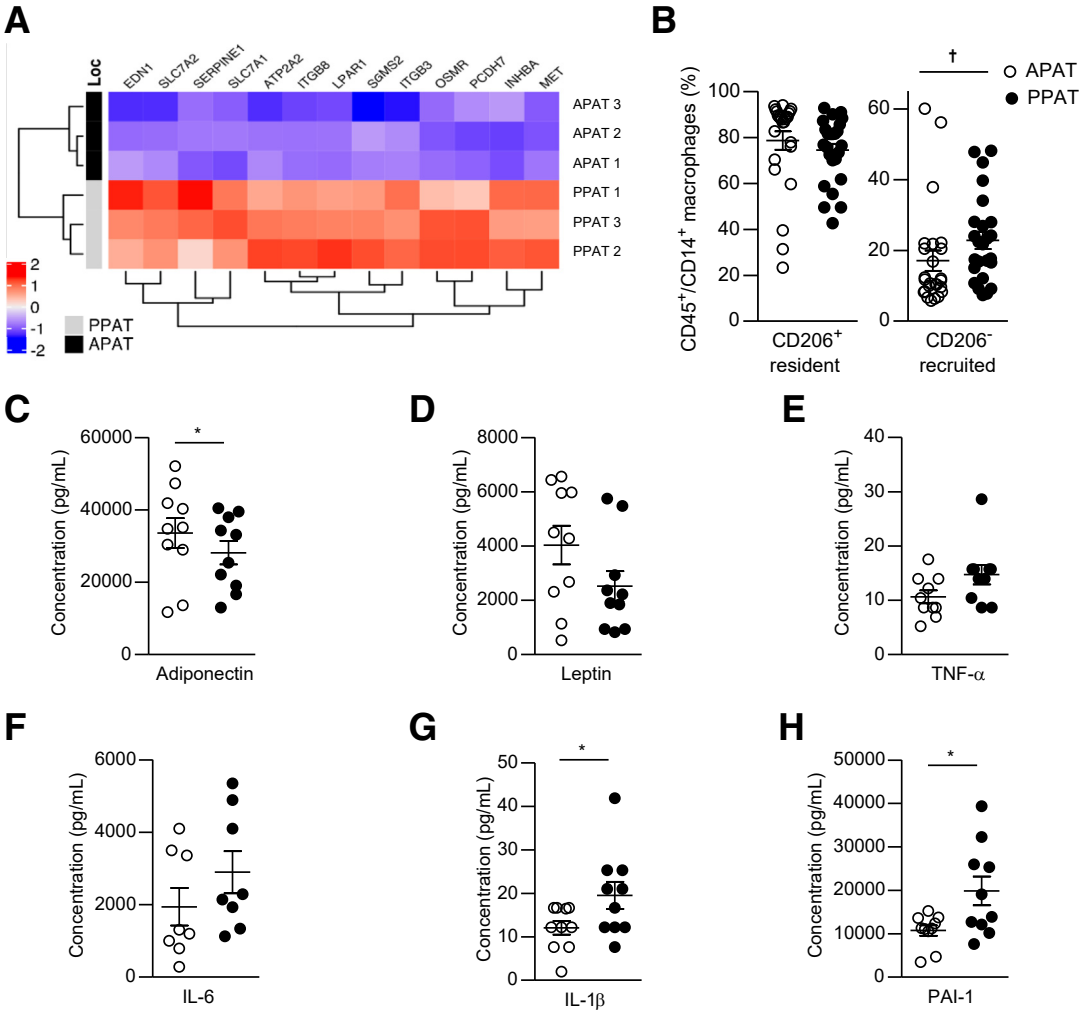


Figure 4 Periprostatic adipose tissue (PPAT) displays features of inflammation in lean patients. **A:** Heatmap and hierarchical clustering of PPAT and abdominopelvic adipose tissue (APAT) samples based on up-regulated genes belonging to the inflammatory response hallmark. **B:** Quantification of resident macrophages ($CD206^+$) and recruited monocytes ($CD206^-$) in the $CD45^+/CD14^+$ population in the stroma vascular fractions of paired PPAT and APAT samples. **C**—**H:** Adiponectin/Acrp30 (**C**), leptin (**D**), tumor necrosis factor (TNF)-α (**E**), IL-6 (**F**), IL-1β (**G**), and plasminogen activator inhibitor (PAI)-1 (**H**) in conditioned media from paired PPAT and APAT samples were quantified by enzyme-linked immunosorbent assay. Data are expressed as means ± SEM (**B**—**H**). $n = 6$ (**A**); $n = 25$ (**B**); $n = 10$ adiponectin/Acrp30 samples (**C**), leptin samples (**D**), TNF-α samples (**E**), IL-1β (**F**), and PAI-1 (**H**) samples; $n = 8$ IL-6 samples (**F**). $^*P < 0.05$ (*U*-test); $^\dagger P < 0.05$ (*t*-test).

PPAT Displays Features of Inflammation in Lean Patients

Accumulating evidence indicates that the chronic hypoxia observed in WAT from individuals with obesity leads to tissue inflammation. It is characterized by infiltration of immune cells, including macrophages, increased secretion of proinflammatory cytokines, and decreased secretion of the anti-inflammatory adipokine adiponectin[24,30] and is tightly associated with interstitial fibrosis.[9,24] The transcriptomics analysis of PPAT found a significant increase in the expression of many genes involved in inflammation. The genes related to the inflammatory response hallmark overexpressed in PPAT were also present in the heatmap, which discriminated PPAT from APAT (Figure 4A). To explore further the possibility that the hypoxic state of PPAT might be associated with chronic inflammation, adipose tissue macrophages in the stroma vascular fractions of PPAT and APAT samples from 25 patients were analyzed by using FACS. These macrophages are characterized by their expression of the common leukocyte antigen CD45 and the monocyte differentiation antigen CD14. In both PPAT and APAT, $CD45^+$ $CD14^+$ macrophages comprised two populations based on the mannose receptor CD206 expression with $CD206^+$ macrophages, predominant in both adipose tissues as resident macrophages with a remodeling phenotype[31] and $CD206^-$ macrophages identified as proinflammatory recruited population. The proportion of the proinflammatory $CD206^-$ macrophages was larger in PPAT than in APAT, whereas no significant difference was found in the proportions of $CD206^+$ macrophages in the two tissues (Figure 4B). The

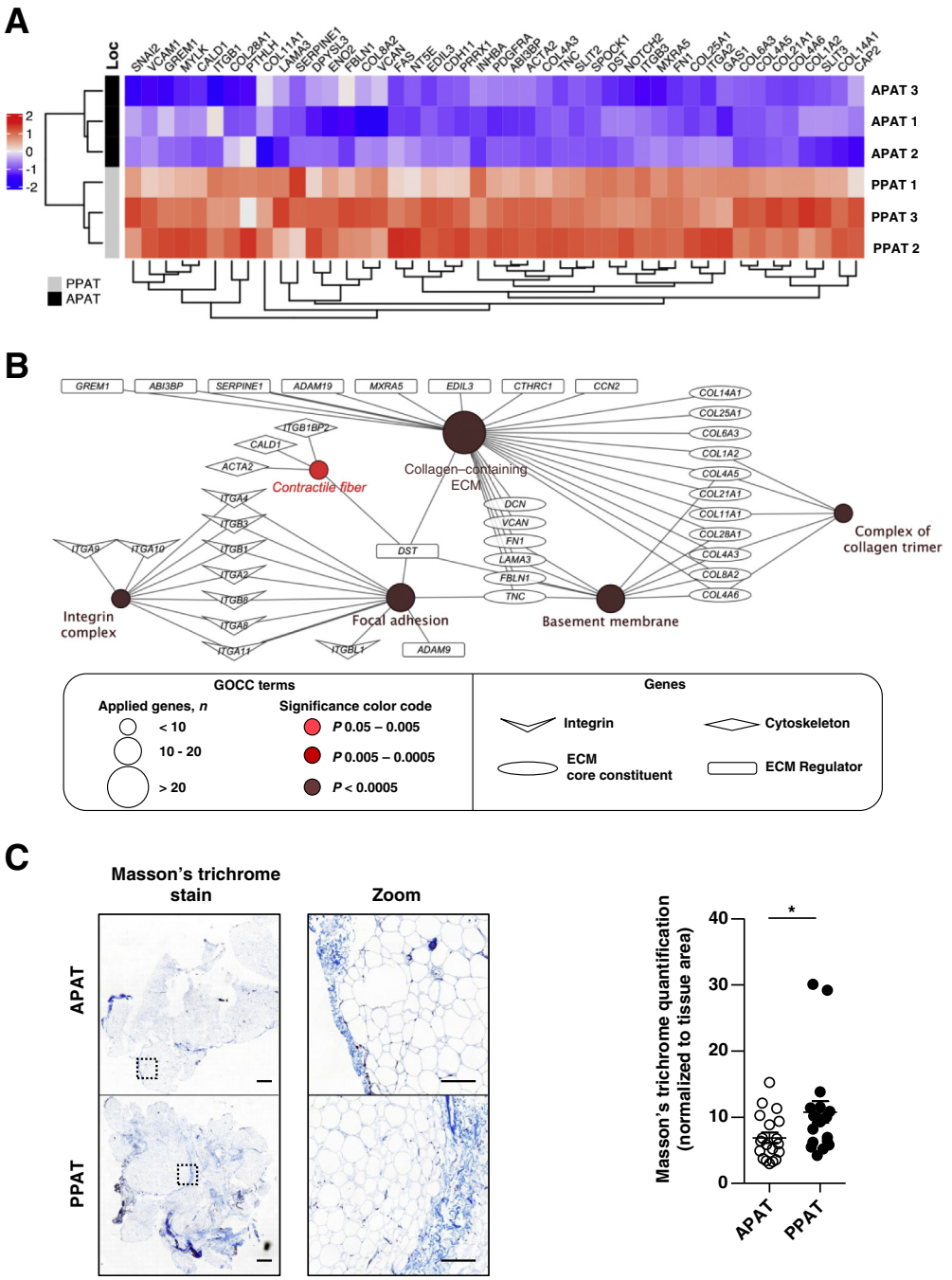


Figure 5 Increased expression of extracellular matrix (ECM) genes in periprostatic adipose tissue (PPAT) from lean patients. **A:** Heatmap and hierarchical clustering of PPAT and abdominopelvic adipose tissue (APAT) samples based on up-regulated genes belonging to the epithelial-to-mesenchymal transition (EMT) hallmark. **B:** Protein-protein interaction network showing the relationship of genes up-regulated in the EMT to the biological processes as indicated by gene ontology analysis. Clear circles indicate genes and brown circles indicate biological processes. Edges indicate interactions with a confidence score >0.7. **C:** Representative images of paraffin-embedded tissue sections of paired APAT and PPAT samples after Masson's trichrome stain (**left panels**), and the zones indicated by the **dotted squares** in higher magnification (**right panels**). Quantification of staining (**right panel**) was performed on whole tissue sections. $n = 6$ (**A**); $n = 19$ (**C**). $^*P < 0.05$ (*t*-test). Scale bars: 500 μm (**C**); 100 μm (**insets**). GOCC, Gene Ontology Cellular Component.

mean concentration of adiponectin was significantly lower in the conditioned medium from PPAT than in that from APAT (Figure 4C), whereas that of leptin was not (Figure 4D). The mean concentrations of the proinflammatory cytokines TNF-α, IL-6, and IL-1β (Figure 4E–G) and PAI-1 (Figure 4H), whose expression in adipose tissues is up-regulated by inflammation,[9,32] were all higher in PPAT than in APAT. Thus, PPAT exhibits hallmarks of chronic inflammation in accordance with its hypoxic state.

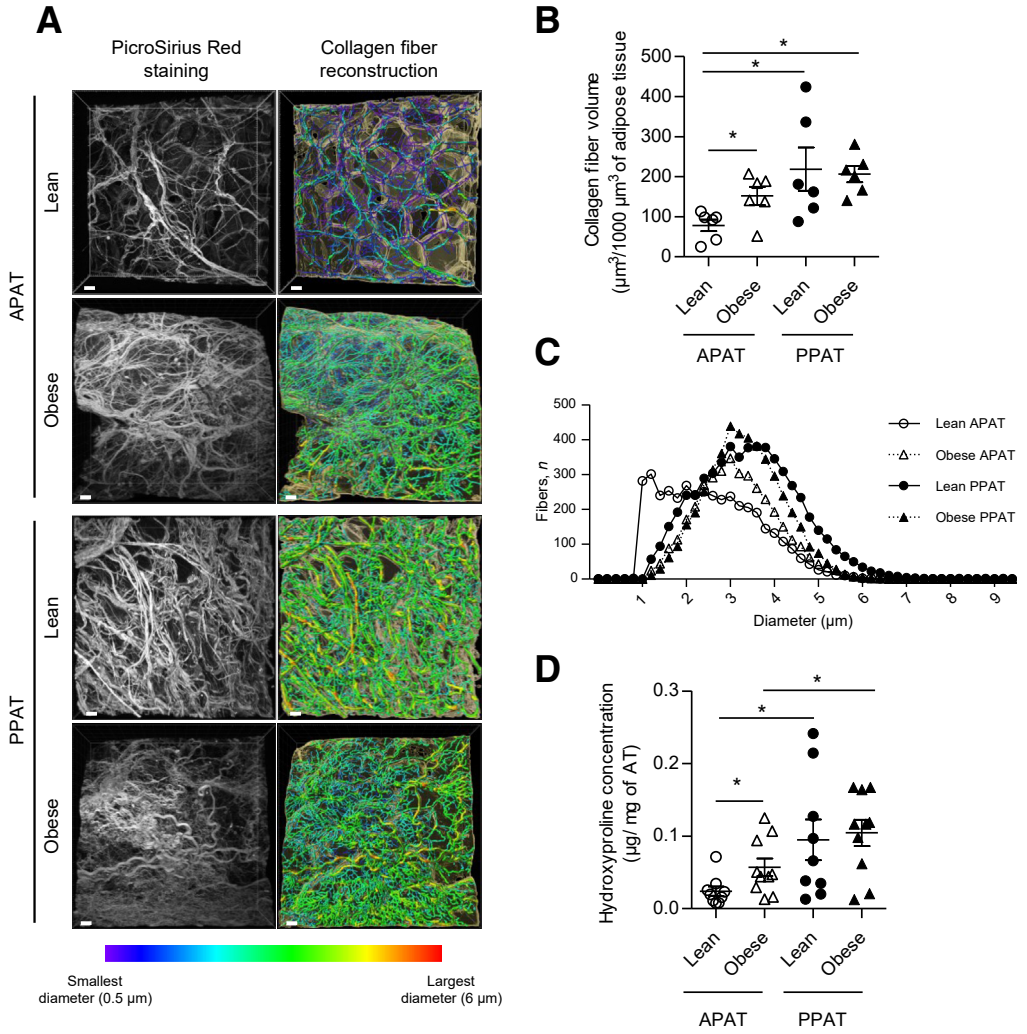


Figure 6 An obesity-like extracellular matrix (ECM) phenotype in periprostatic adipose tissue (PPAT) independent of body mass index (BMI). **A:** Representative three-dimensional (3D) confocal images of Picrosirius Red staining (**left panel**) and 3D reconstruction of collagen fibers (**right panel**) in paired abdominopelvic adipose tissue (APAT) and PPAT samples from lean patients (means ± SD BMI = 24.5 ± 0. 6 kg/m^2, means ± SD age = 65.4 ± 2.2 years) and patients with obesity (means ± SD BMI = 32.4 ± 1.2 kg/m^2, means ± SD age = 66.2 ± 2.2 years). Reconstructed collagen fibers are color-coded according to their mean diameter as shown below. **B:** Quantification of collagen fiber volume in Picrosirius Red–stained paired APAT and PPAT samples from lean patients and patients with obesity. **C:** Distribution of the number of collagen segments according to their diameter measured after 3D reconstruction in paired APAT and PPAT samples from lean patients and patients with obesity. **D:** Hydroxyproline concentrations in paired APAT and PPAT samples from lean patients and patients with obesity. Data are expressed as means ± SEM (**B**–**D**). n = 6 lean patients and 6 patients with obesity (**B** and **C**); n = 9 lean patients and 10 patients with obesity (**D**). *P < 0.05 (t-test). Scale bars = 50 µm.

Increased Expression of ECM Genes in PPAT

Fibrosis is one of the hallmarks of adipose tissue hypoxia in obesity.[9,24] The transcriptomics study showed increased expression of many genes involved in ECM organization in PPAT, consistent with fibrosis. Genes that encode several collagen isoforms, including *COLIA2* and type VI and IV collagens, were more highly expressed in PPAT than in APAT (Figure 5A). In addition, genes that encode certain markers of ECM-producing myofibroblasts,[33] such as *SNAIL*, or regulators of myofibroblast activation, such as *INHBA* or *GREM1*, were highly expressed in PPAT (Figure 5A). Analysis of the protein-protein interaction network of the products of ECM-related genes that were differentially expressed in PPAT and APAT showed the likely importance of collagen-containing ECM assembly in the differences observed (Figure 5B).

To investigate collagen deposition in PPAT and APAT, sections of paraffin-embedded PPAT and paired APAT samples were stained with Masson's trichrome, which stains blue the fibrillar collagens.[34] Whereas the staining of APAT showed sparse and thin collagen sheets, the staining of PPAT revealed large areas of staining and fibrotic bundles of various thickness running along the adipose tissue lobules (Figure 5C). Quantification of the staining indicated enhanced collagen deposition in PPAT when compared with APAT (Figure 5C). Together, these data indicate that the ECM is more extensive in PPAT than in APAT.

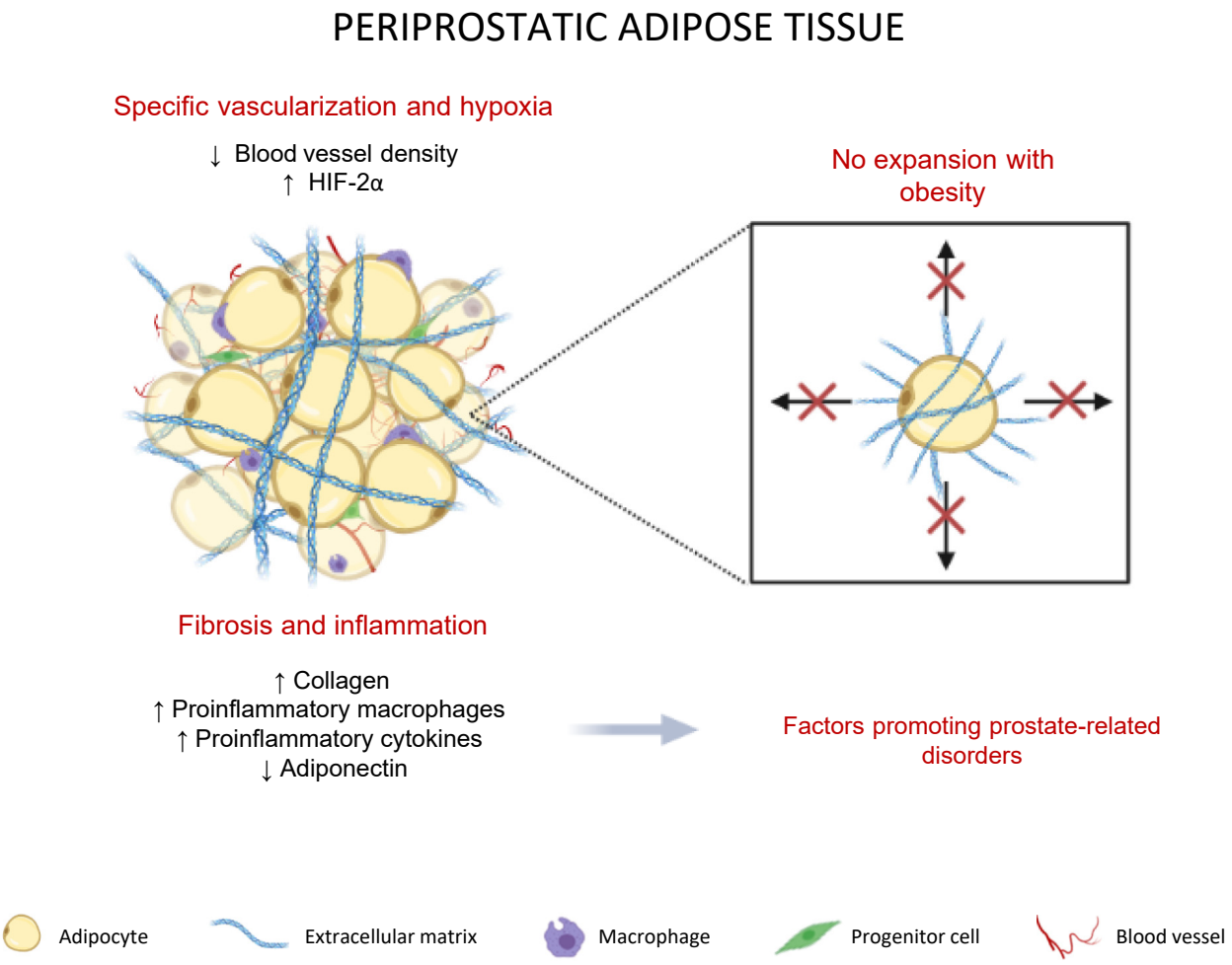


Figure 7 The chronic hypoxic state of periprostatic adipose tissue (PPAT) limits its expansion in obesity and favors tumor progression. PPAT has an atypical vascular organization when compared with other adipose tissues, with a sparse vascular network surrounding clusters of adipocytes rather than individual cells. In our working model, this finding contributes to a chronic hypoxic state, leading to the overexpression of hypoxia-inducible factor (HIF)-2α. In accord with its hypoxic state, PPAT exhibits hallmarks of chronic inflammation, such as the presence of proinflammatory macrophages, increased secretion of proinflammatory cytokines, and decreased secretion of the anti-inflammatory adipokine adiponectin. In addition, PPAT has more extracellular matrix and, specifically, more collagen, another hallmark of hypoxia. This chronic hypoxic state in PPAT probably limits its expansion in individuals with obesity and results in features known to favor prostate-related disorders.

An Obesity-like ECM Phenotype in PPAT Independent of BMI

The volume of PPAT is independent of BMI, yet ECM gene expression and protein levels are higher in this tissue than in APAT, suggesting obesity-like fibrosis. We hypothesized that, in contrast to APAT, obesity would not further increase the fibrosis seen in PPAT. To investigate this hypothesis, the collagen networks were examined in PPAT and APAT tissues from lean patients and patients with obesity with three-dimensional confocal microscopy followed by reconstruction of the observed collagen fiber network. No difference was observed in this network in PPAT from lean individuals and individuals with obesity, whereas the network in APAT was substantially more dense in patients with obesity than it was in lean ones (Figure 6A). The collagen fiber network in PPAT from lean patients, however, was much denser than that in APAT. These conclusions were verified by quantifying the volume of collagen fibers seen in the three-dimensional reconstructions (Figure 6B) and their diameters (Figure 6C) by using Imaris software version 9.7.2.

To confirm the finding that obesity has no influence on the collagen content in PPAT, a different approach was used based on quantification of hydroxyproline, a component of collagen that comprises approximately 13.5% of its amino acid composition.[35] Consistent with the analysis of the collagen fiber network, significantly more hydroxyproline was found in PPAT than in paired APAT from lean patients, whereas there was more hydroxyproline in APAT from patients with obesity than in the same tissue from lean patients, but no differences in PPAT from lean patients and patients with obesity (Figure 6D). Together, these data confirm that there is more ECM in PPAT than in APAT

from individuals without obesity, but the ECM of PPAT in lean individuals and individuals with obesity resembles that of APAT in obese individuals irrespective of the BMI of the patients.

Discussion

In this study, structural organization of PPAT in humans was characterized as a way to understand its biology better. The findings revealed the distinctive tissue organization of PPAT and showed, in particular, that it has a sparse vascular network. Consistent with this, PPAT exhibited hallmarks of chronic hypoxia, including inflammation and a dense collagen network typical of fibrosis. These features may explain its failure to expand in individuals with obesity and its contribution to prostate-related disorders.

The present study of a cohort of 54 patients with PCa showed that, unlike other adipose depots, the volume of PPAT is independent of BMI. This also confirmed the observations of several previous studies,[6] which used computed tomography or MRI to measure PPAT volume. The results corroborated previous studies[6] showing that although not correlated with BMI, PPAT accumulated at a wide range as indicated by the variation in the PPAT volume from 23.77 to 90.72 cm^3. Thus, the limited PPAT expandability with BMI was not attributable to anatomic constraints but rather to active biological processes. A large number of recent studies have demonstrated that there is a correlation between PPAT accumulation and PCa aggressiveness (reviewed in the article by Nassar et al[6]). Characterization of the mechanisms that drive PPAT development independently of BMI remains to be deciphered to explain the role of abundant PPAT in PCa progression. These studies will certainly benefit from the extensive characterization of the structural organization of PPAT presented here. In the present study, APAT was used as a control tissue against which to compare PPAT because both adipose tissues are located in the extraperitoneal area and can be removed easily during surgery. Like in the other WAT, the volume of APAT correlated with BMI, offering an appropriate control tissue for additional studies of PPAT.

Human WAT is highly vascularized, and its expansion in obesity depends on its well-defined vascular network structure with each adipocyte surrounded by one or more capillaries,[22,36] as observed in APAT. This close contact between cells and capillaries allows the circulation to provide the nutrients, oxygen, and soluble factors (hormones, growth factors, and cytokines) required for tissue homeostasis.[36] By comparison, the vasculature of PPAT is less dense, with fewer capillaries surrounding groups of adipocytes. This atypical organization is most probably the physiologic state of the normal PPAT rather than a consequence of its proximity to PCa because a similar vascular organization was observed in PPAT samples from patients devoid of cancerous lesions in the prostate. Moreover, tumors generally stimulate angiogenesis,[37,38] so it is unlikely that the observed decrease in vascularity would be due to secretions from the nearby tumor. The physiologic function of this atypical vascular organization is unclear but may be related to its response to steroid hormones. One study reported that the volume of PPAT is reduced by 5α-reductase inhibitors,[39] which inhibit conversion of testosterone into dihydrotestosterone in the prostate gland and decrease the volume of the prostate due to apoptosis of epithelial cells.[40] Consistent with this idea, androgen- and estrogen-responsive genes were up-regulated in PPAT when compared with those in APAT. Sex hormones influence the metabolism, endocrine functions, and angiogenesis of certain other adipose tissues,[41,42] so these findings raise the interesting possibility that they might also influence PPAT physiology and development, an avenue that deserves further investigation.

The unusual organization of the vasculature in PPAT led us to postulate that this tissue might be hypoxic. Unbiased comparison of PPAT and APAT transcriptomes indeed revealed a hypoxic signature in PPAT. Many of the biological pathways relevant to hypoxia were differentially represented in the transcriptome of PPAT when compared with that of APAT. Moreover, there was a specific increase in expression of the oxygen-labile HIF-2α, but not of HIF-1α, in PPAT, indicating an adaptive response of this tissue to hypoxia. Both HIF-1α and HIF-2α form heterodimers with the constitutive HIF-1β subunit to form the transcription factors HIF-1 and HIF-2 to mediate the hypoxic response.[28] Although HIF-1 and HIF-2 have common target genes, such as *VEGFA* and *GLUT1*, they also have specific target genes, depending on the tissue, as well as differences in their temporal regulation.[43] These differences might explain why HIF-2α, but not HIF-1α, was overexpressed in PPAT and the consequences of its overexpression in this tissue. Indeed, in some systems HIF-1α drives the initial response to hypoxia, whereas chronic hypoxia involves HIF-2α.[43–45] In addition, HIF-2 is active under mild hypoxia (<5% oxygen) with a long-lasting response, whereas HIF-1 is most active during short periods of intense hypoxia or anoxia (<0.1%).[43,45] This distinct temporal regulation might explain why HIF-2 overexpression occured in PPAT, which is likely to exhibit chronic mild hypoxia. The importance of chronic HIF-2α overexpression in adipose tissue inflammation is illustrated by mice with an adipose tissue–specific deletion of the gene encoding Von Hippel–Lindau protein, which is required for degradation of both HIF-1α and HIF-2α by the proteasome.[28] In these mice, long-term activation of HIFs causes adipose tissue inflammation characterized by overexpression of proinflammatory cytokines, such as IL-6 and TNF-α, and chemokines.[46] Genetic deletion of *HIF-2α*, but not *HIF-1α*, abrogates this inflammation, demonstrating that this isoform is key to the inflammatory response of adipose tissue to chronic hypoxia.[46] Consistent with the findings from the *VHL* gene knockout mice, anti-inflammatory adipokine

adiponectin[30] were down-regulated and the proinflammatory cytokines IL-6, TNF-α, and IL-1β were overexpressed. Like inflammation, enhanced ECM deposition, or fibrosis, is a hallmark of the hypoxic response in adipose tissue.[47,48] To our knowledge, the role specifically of HIF-2α in the induction of fibrosis in hypoxic adipose has not been investigated, but studies have shown that HIF-2 can induce transcription of genes that encode ECM components, leading to fibrosis in the liver[49] and lungs.[50]

The higher level of VEGF secretion by PPAT when compared with APAT may promote angiogenesis; however, it was not sufficient to counteract the hypoxic state of PPAT. This might be due to the lower level of adiponectin secreted by PPAT as well as the overexpression of PAI-1 when compared with APAT, which have been shown to inhibit new vessel formation and may counterbalance any VEGF-induced angiogenesis.[51] A resulting suboptimal level of angiogenesis might be sufficient to limit the dysfunctional state of PPAT but not to resolve hypoxia.

In addition to explaining the high basal inflammatory state of PPAT, these findings also provide a likely explanation for why PPAT did not expand in obesity: the extensive ECM and fibrosis seen in this tissue may prevent any expansion of PPAT in individuals with obesity. Previous studies of human and rodent adipose tissues show that fibrosis alters the plasticity of the tissue and places a physical constraint on its expansion.[48,52] The current study found that obesity causes no increase in ECM deposition in PPAT beyond that seen in the PPAT of lean individuals, but the ECM of PPAT resembles that of WAT in obesity. We propose that this obesity-like organization of the ECM in PPAT does not adapt to external signals but provides an important physical constraint on PPAT expansion. A recent study demonstrated that obesity was not associated with adipocyte hypertrophy in PPAT,[53] consistent with the idea that PPAT is in a state of maximum expandability in lean individuals. Moreover, the genes related to adipogenesis were down-regulated in PPAT compared with those in APAT, which might also contribute to its failure to expand during obesity. The basal inflammatory state of PPAT might also contribute to the inability of this tissue to expand during obesity because inflammation of adipose tissue contributes to perpetuating fibrosis[48,51] and interferes with adipocyte differentiation,[54,55] which may explain the inhibition of adipogenesis.

The present study opens new mechanistic avenues to explain the role of PPAT in prostate disorders. The hallmarks of PPAT identified in this study might favor benign prostatic hyperplasia and related lower urinary tract symptoms. In fact, chronic inflammation as well as fibrosis have been associated with this frequent disorder.[56] The etiology of this chronic inflammation is probably multifactorial, but the current study highlights that PPAT needs to be considered as an important contributor of this process as also proposed by a recent review.[15] Clinical studies have established evidence of a link between PPAT inflammation, independent of obesity, and the occurrence of high-grade PCa.[10–12] There is accumulating evidence that proinflammatory cytokines contribute through multiple signal transduction pathways to PCa initiation and in established tumors to growth, survival, metastasis, and resistance to therapy.[57] The current study deciphered the mechanism by which PPAT, as an important source of proinflammatory molecules, may promote PCa initiation and progression. The present work highlights that PPAT might also contribute to PCa progression through fibrosis. In fact, the large amounts of ECM in PPAT might directly affect tumor progression by increasing ECM stiffness, which in proximal mammary adipose tissue promotes mammary tumor progression *in vivo*.[58,59] In addition, these changes in ECM might promote tumor progression directly by ECM components functioning as signaling molecules. In breast cancer, for example, a bioactive fragment of adipocyte-derived collagen type VI, called endotrophin, contributes to tumor progression.[60] The consequences of these biological features, including the biomechanical specificities in the ECM of PPAT, open a new avenue to explain the role of PPAT in prostate-related disorders that deserves further investigation. All the data reported here and the remaining questions are summarized in Figure 7.

Acknowledgments

This work benefited from the Toulouse Réseau Imagerie RIO Optical Imaging Platform at the Institute of Pharmacology and Structural Biology (Genotoul, Toulouse, France). Sequencing was performed by the GenomEast platform, a member of the France Génomique consortium (ANR-10-INBS-0009). We acknowledge Life Science Editors for professional scientific editing during the preparation of the manuscript.

Author Contributions

M.R., D.E., C.M., A.T., J.G., C.B., Y.J., C.H., S.P., S.L., and D.M analyzed data; M.R., D.E., C.M., A.T., J.G., C.B., Y.J., C.H., S.P., P.V., M.C., J.-F.T., B.M., A.B., D.M., and C.M. conducted experiments and acquired data; M.R., D.E., A.T., J.G., A.B., D.M., and C.M. designed research studies; M.R., D.E., D.M., and C.M. wrote the manuscript; D.E., A.T., J.G., P.V., M.C., J.-F.T., B.M., and A.B. edited the manuscript; D.M. and C.M. supervised the study.

Supplemental Data

Supplemental material for this article can be found at *http://doi.org/10.1016/j.ajpath.2022.03.008*.

References

1. Zwick RK, Guerrero-Juarez CF, Horsley V, Plikus MV: Anatomical, physiological, and functional diversity of adipose tissue. Cell Metab 2018, 27:68–83

2. Tchkonia T, Thomou T, Zhu Y, Karagiannides I, Pothoulakis C, Jensen MD, Kirkland JL: Mechanisms and metabolic implications of regional differences among fat depots. Cell Metab 2013, 17:644−656
3. Wang YY, Lehuédé C, Laurent V, Dirat B, Dauvillier S, Bochet L, Le Gonidec S, Escourrou G, Valet P, Muller C: Adipose tissue and breast epithelial cells: a dangerous dynamic duo in breast cancer. Cancer Lett 2012, 324:142−151
4. Estève D, Roumiguié M, Manceau C, Milhas D, Muller C: Periprostatic adipose tissue: a heavy player in prostate cancer progression. Curr Opin Endocr Metab Res 2020, 10:29−35
5. Ishidoya S, Endoh M, Nakagawa H, Saito S, Arai Y: Novel anatomical findings of the prostatic gland and the surrounding capsular structures in the normal prostate. Tohoku J Exp Med 2007, 212:55−62
6. Nassar ZD, Aref AT, Miladinovic D, Mah CY, Raj GV, Hoy AJ, Butler LM: Peri-prostatic adipose tissue: the metabolic microenvironment of prostate cancer. BJU Int 2018, 121(Suppl 3):9−21
7. Bandini M, Gandaglia G, Briganti A: Obesity and prostate cancer. Curr Opin Urol 2017, 27:415−421
8. Gucalp A, Iyengar NM, Zhou XK, Giri DD, Falcone DJ, Wang H, Williams S, Krasne MD, Yaghnam I, Kunzel B, Morris PG, Jones LW, Pollak M, Laudone VP, Hudis CA, Scher HI, Scardino PT, Eastham JA, Dannenberg AJ: Periprostatic adipose inflammation is associated with high-grade prostate cancer. Prostate Cancer Prostatic Dis 2017, 20:418−423
9. Kahn CR, Wang G, Lee KY: Altered adipose tissue and adipocyte function in the pathogenesis of metabolic syndrome. J Clin Invest 2019, 129:3990−4000
10. Zhang Q, Jiang SL, Yang ZG, Zhang GM, Huo RC: Influence of adipocytokines in periprostatic adipose tissue on prostate cancer aggressiveness. Cytokine 2016, 85:148−156
11. Finley DS, Calvert VS, Inokuchi J, Lau A, Narula N, Petricoin EF, Zaldivar F, Santos R, Tyson DR, Ornstein DK: Periprostatic adipose tissue as a modulator of prostate cancer aggressiveness. J Urol 2009, 182:1621−1627
12. Dahran N, Szewczyk-Bieda M, Vinnicombe S, Fleming S, Nabi G: Periprostatic fat adipokine expression is correlated with prostate cancer aggressiveness in men undergoing radical prostatectomy for clinically localized disease. BJU Int 2019, 123:985−994
13. Laurent V, Guérard A, Mazerolles C, Le Gonidec S, Toulet A, Nieto L, Zaidi F, Majed B, Garandeau D, Socrier Y, Golzio M, Cadoudal T, Chaoui K, Dray C, Monsarrat B, Schiltz O, Wang YY, Couderc B, Valet P, Malavaud B, Muller C: Periprostatic adipocytes act as a driving force for prostate cancer progression in obesity. Nat Commun 2016, 7:10230
14. Laurent V, Toulet A, Attané C, Milhas D, Dauvillier S, Zaidi F, Clement E, Cinato M, Le Gonidec S, Guérard A, Lehuédé C, Garandeau D, Nieto L, Renaud-Gabardos E, Prats AC, Valet P, Malavaud B, Muller C: Periprostatic adipose tissue favors prostate cancer cell invasion in an obesity-dependent manner: role of oxidative stress. Mol Cancer Res 2019, 17:821−835
15. Passos GR, Ghezzi AC, Antunes E, de Oliveira MG, Mónica FZ: The role of periprostatic adipose tissue on prostate function in vascular-related disorders. Front Pharmacol 2021, 12:626155
16. Vaysse C, Lomo J, Garred O, Fjeldheim F, Lofteroed T, Schlichting E, McTiernan A, Frydenberg H, Husoy A, Lundgren S, Fagerland MW, Richardsen E, Wist EA, Muller C, Thune I: Inflammation of mammary adipose tissue occurs in overweight and obese patients exhibiting early-stage breast cancer. npj Breast Cancer 2017, 3:19
17. Estève D, Boulet N, Belles C, Zakaroff-Girard A, Decaunes P, Briot A, Veeranagouda Y, Didier M, Remaury A, Guillemot JC, Ledoux S, Dani C, Bouloumié A, Galitzky J: Lobular architecture of human adipose tissue defines the niche and fate of progenitor cells. Nat Commun 2019, 10:2549
18. Dobin A, Davis CA, Schlesinger F, Drenkow J, Zaleski C, Jha S, Batut P, Chaisson M, Gingeras TR: STAR: ultrafast universal RNA-seq aligner. Bioinformatics 2013, 29:15−21
19. Gilleron J, Méziat C, Sulen A, Ivanov S, Jager J, Estève D, Muller C, Tanti J-F, Cormont M: Exploring adipose tissue structure by methylsalicylate clearing and 3D imaging. J Vis Exp 2020, 162: e61640
20. Curat CA, Miranville A, Sengene C, Diehl M, Tonus C, Busse R, Bouloumie A: From blood monocytes to adipose tissue−resident macrophages. Diabetes 2004, 53:1285−1292
21. Wang H, Chen YE, Eitzman DT: Imaging body fat techniques and cardiometabolic implications. Arterioscler Thromb Vasc Biol 2014, 34:2217−2223
22. Wassermann F: The development of adipose tissue. Handbook of Physiology. Hoboken, NJ: Wiley, 1965. pp. 87−100
23. Ritchie ME, Phipson B, Wu D, Hu Y, Law CW, Shi W, Smyth GK: Limma powers differential expression analyses for RNA-sequencing and microarray studies. Nucleic Acids Res 2015, 43:e47
24. Trayhurn P: Hypoxia and adipose tissue function and dysfunction in obesity. Physiol Rev 2013, 93:1−21
25. Park YK, Park B, Lee S, Choi K, Moon Y, Park H: Hypoxia-inducible factor-2α-dependent hypoxic induction of Wnt10b expression in adipogenic cells. J Biol Chem 2013, 288:26311−26322
26. Marignol L, Rivera-Figueroa K, Lynch T, Hollywood D: Hypoxia, notch signalling, and prostate cancer. Nat Rev Urol 2013, 10:405−413
27. Skuli N, Majmundar AJ, Krock BL, Mesquita RC, Mathew LK, Quinn ZL, Runge A, Liu L, Kim MN, Liang J, Schenkel S, Yodh AG, Keith B, Simon MC: Endothelial HIF-2α regulates murine pathological angiogenesis and revascularization processes. J Clin Invest 2012, 122:1427−1443
28. Lee P, Chandel NS, Simon MC: Cellular adaptation to hypoxia through hypoxia inducible factors and beyond. Nat Rev Mol Cell Biol 2020, 21:268−283
29. Wood IS, Wang B, Lorente-Cebrián S, Trayhurn P: Hypoxia increases expression of selective facilitative glucose transporters (GLUT) and 2-deoxy-d-glucose uptake in human adipocytes. Biochem Biophys Res Commun 2007, 361:468−473
30. Ohashi K, Shibata R, Murohara T, Ouchi N: Role of anti-inflammatory adipokines in obesity-related diseases. Trends Endocrinol Metab 2014, 25:348−355
31. Bourlier V, Zakaroff-Girard A, Miranville A, De Barros S, Maumus M, Sengenes C, Galitzky J, Lafontan M, Karpe F, Frayn KN, Bouloumié A: Remodeling phenotype of human subcutaneous adipose tissue macrophages. Circulation 2008, 117: 806−815
32. Kaji H: Adipose tissue-derived plasminogen activator inhibitor-1 function and regulation. Compr Physiol 2016, 6:1873−1896
33. Bourlier V, Sengenès C, Zakaroff-Girard A, Decaunes P, Wdziekonski B, Galitzky J, Villageois P, Esteve D, Chiotasso P, Dani C, Bouloumié A: TGFbeta family members are key mediators in the induction of myofibroblast phenotype of human adipose tissue progenitor cells by macrophages. PLoS One 2012, 7:e31274
34. Halberg N, Khan T, Trujillo ME, Wernstedt-Asterholm I, Attie AD, Sherwani S, Wang ZV, Landskroner-Eiger S, Dineen S, Magalang UJ, Brekken RA, Scherer PE: Hypoxia-inducible factor 1α induces fibrosis and insulin resistance in white adipose tissue. Mol Cell Biol 2009, 29:4467−4483
35. Neuman RE, Logan MA: The determination of hydroxyproline. J Biol Chem 1950, 184:299−306
36. Christiaens V, Lijnen HR: Angiogenesis and development of adipose tissue. Mol Cell Endocrinol 2010, 318:2−9
37. Folkman J: Tumor angiogenesis: therapeutic implications. N Engl J Med 1971, 285:1182−1186
38. Kerbel RS: Tumor angiogenesis. N Engl J Med 2008, 358: 2039−2049
39. Taussky D, Barkati M, Campeau S, Zerouali K, Nadiri A, Saad F, Delouya G: Changes in periprostatic adipose tissue induced by 5α-reductase inhibitors. Andrology 2017, 5:511−515
40. Bass R, Perry B, Langenstroer P, Thrasher JB, Dennis KL, Tawfik O, Holzbeierlein J: Effects of short-term finasteride on apoptotic factors

and androgen receptors in prostate cancer cells. J Urol 2009, 181: 615−620
41. Karastergiou K, Smith SR, Greenberg AS, Fried SK: Sex differences in human adipose tissues: the biology of pear shape. Biol Sex Differ 2012, 3:131
42. Volat F, Bouloumié A: Steroid hormones and the stroma-vascular cells of the adipose tissue. Horm Mol Biol Clin Investig 2013, 15:5−10
43. Koh MY, Powis G: Passing the baton: the HIF switch. Trends Biochem Sci 2012, 37:364−372
44. Koh MY, Lemos R, Liu X, Powis G: The hypoxia-associated factor switches cells from HIF-1α- to HIF-2α-dependent signaling promoting stem cell characteristics, aggressive tumor growth and invasion. Cancer Res 2011, 71:4015−4027
45. Holmquist-Mengelbier L, Fredlund E, Löfstedt T, Noguera R, Navarro S, Nilsson H, Pietras A, Vallon-Christersson J, Borg Å, Gradin K, Poellinger L, Påhlman S: Recruitment of HIF-1α and HIF-2α to common target genes is differentially regulated in neuroblastoma: HIF-2α promotes an aggressive phenotype. Cancer Cell 2006, 10:413−423
46. Lin Q, Huang Y, Booth CJ, Haase VH, Johnson RS, Celeste Simon M, Giordano FJ, Yun Z: Activation of hypoxia-inducible factor-2 in adipocytes results in pathological cardiac hypertrophy. J Am Heart Assoc 2013, 2:e000548
47. Marcelin G, Silveira ALM, Martins LB, Ferreira AVM, Clément K: Deciphering the cellular interplays underlying obesity-induced adipose tissue fibrosis. J Clin Invest 2019, 129:4032−4040
48. Sun K, Tordjman J, Clément K, Scherer PE: Fibrosis and adipose tissue dysfunction. Cell Metab 2013, 18:470−477
49. Qu A, Taylor M, Xue X, Matsubara T, Metzger D, Chambon P, Gonzalez FJ, Shah YM: Hypoxia-inducible transcription factor 2α promotes steatohepatitis through augmenting lipid accumulation, inflammation, and fibrosis. Hepatology 2011, 54:472−483
50. Shimoda LA, Semenza GL: HIF and the lung: role of hypoxia-inducible factors in pulmonary development and disease. Am J Respir Crit Care Med 2011, 183:152−156
51. Crewe C, Aaron An Y, Scherer PE: The ominous triad of adipose tissue dysfunction: inflammation, fibrosis, and impaired angiogenesis. J Clin Invest 2017, 127:7−82
52. Khan T, Muise ES, Iyengar P, Wang ZV, Chandalia M, Abate N, Zhang BB, Bonaldo P, Chua S, Scherer PE: Metabolic dysregulation and adipose tissue fibrosis: role of collagen VI. Mol Cell Biol 2009, 29:1575−1591
53. Miladinovic D, Cusick T, Mahon KL, Haynes AM, Cortie CH, Meyer BJ, Stricker PD, Wittert GA, Butler LM, Horvath LG, Hoy AJ: Assessment of periprostatic and subcutaneous adipose tissue lipolysis and adipocyte size from men with localized prostate cancer. Cancers (Basel) 2020, 12:1385
54. Estève D, Boulet N, Volat F, Zakaroff-Girard A, Ledoux S, Coupaye M, Decaunes P, Belles C, Gaits-Iacovoni F, Iacovoni JS, Rémaury A, Castel B, Ferrara P, Heymes C, Lafontan M, Bouloumié A, Galitzky J: Human white and brite adipogenesis is supported by msca1 and is impaired by immune cells. Stem Cells 2015, 33:1277−1291
55. Hammarstedt A, Gogg S, Hedjazifar S, Nerstedt A, Smith U: Impaired adipogenesis and dysfunctional adipose tissue in human hypertrophic obesity. Physiol Rev 2018, 98:1911−1941
56. Bushman WA, Jerde TJ: The role of prostate inflammation and fibrosis in lower urinary tract symptoms. Am J Physiol Ren Physiol 2016, 311:817−821
57. Archer M, Dogra N, Kyprianou N: Inflammation as a driver of prostate cancer metastasis and therapeutic resistance. Cancers (Basel) 2020, 12:1−24
58. Iyengar P, Espina V, Williams TW, Lin Y, Berry D, Jelicks LA, Lee H, Temple K, Graves R, Pollard J, Chopra N, Russell RG, Sasisekharan R, Trock BJ, Lippman M, Calvert VS, Petricoin EF, Liotta L, Dadachova E, Pestell RG, Lisanti MP, Bonaldo P, Scherer PE: Adipocyte-derived collagen VI affects early mammary tumor progression in vivo, demonstrating a critical interaction in the tumor/stroma microenvironment. J Clin Invest 2005, 115:1163−1176
59. Seo BR, Bhardwaj P, Choi S, Gonzalez J, Eguiluz RCA, Wang K, Mohanan S, Morris PG, Du B, Zhou XK, Vahdat LT, Verma A, Elemento O, Hudis CA, Williams RM, Gourdon D, Dannenberg AJ, Fischbach C: Obesity-dependent changes in interstitial ECM mechanics promote breast tumorigenesis. Sci Transl Med 2015, 7:301ra130
60. Park J, Scherer PE: Adipocyte-derived endotrophin promotes malignant tumor progression. J Clin Invest 2012, 122:4243−4256

2. Collagen remodeling leads to inflammation-free expansion of periprostatic adipose tissue and promotes prostate cancer progression through endotrophin production.

Recently, a new concept of abnormal PPAT accumulation or abundant PPAT, unrelated to BMI, has emerged in the literature. Despite variations in measurement techniques, different studies confirmed an association between PPAT abundance and the aggressiveness of PCa, as assessed by the Gleason score and d'Amico classification but the mechanism remains unexplained.

The research conducted by our group on the link between PCa and PPAT in obese individuals and the organization of PPAT in non-obese subjects has identified a patient population with PPAT accumulation in a cohort of 351 patients. I took part of this project conducted by David Estève and initiated by Aurélie Toulet and Mathieu Roumiguié which was focused on the molecular mechanisms underlying abundant PPAT development and its secretory modifications that may be involved in PCa progression. The main hypothesis was that specific features of abundant PPAT could be associated with a worse prognosis for PCa. Futhermore, abundant PPAT may not exhibit the same inflammatory, fibrotic, and hypoxic signatures as non-abundant PPAT since these characteristics are limiting factors for adipose tissue expansion. We found that tumors specifically from patients with abundant PPAT exhibited several hallmarks of aggressiveness such as undifferentiated tumors, and changes in the tumor microenvironment including increased fibrosis (Masson's trichrome staining), angiogenesis (CD31 staining), and macrophage infiltration (CD68 staining). We showed that abundant PPAT expanded by adipocyte hypertrophy but this did not result in inflammation as defined by the infiltration of pro-inflammatory macrophages or the secretion of pro-inflammatory cytokines. Collagen VI degradation and decreased expression of mechano-sensing proteins and cytoskeletal contractile force generation in abundant PPAT adipocytes could explain its inflammation-free expansion by decreasing the mechanical constraints on the adipocytes. Moreover, collagen VI degradation likely by MMP9 in abundant PPAT was associated with endotrophin production, a matrikine already known to promote breast cancer progression. We found high levels of endotrophin specifically in the urine (obtained after prostatic massage) of patients with abundant PPAT, indicating the clinical relevance of our findings. Interestingly, endotrophin production in abundant PPAT could be linked to PCa aggressiveness.

3. Role of androgen metabolites from the periprostatic adipose tissue in the development of castration resistance of prostate cancer

PCa is a hormone dependent cancer, androgens being essential to its development and progression. The testis produce testosterone which is converted into its active form 5α-dihydrotestosterone (5α-DHT) by the prostate to activate the androgen receptor (AR) signaling[97]. Androgen deprivation therapy is the first-line treatment of locally advanced PCa and consists in inhibiting the production of testosterone by the testis[114,115,118]. However, the disease will progress into castration resistant PCa (CRPC) after a few years[603]. One major mechanism of resistance is based on androgen synthesis at the tumour level through alternative pathways and increased expression of enzymes involved in steroidogenesis. As seen in the introduction of the manuscript, emerging evidence in the literature have demonstrated that the tumour environment could also contribute to CRPC occurrence that is defined by the androgen-dependent growth of the tumors despite the efficient inhibition of the production of androgens by the testis[180,181]. Pernigoni et al, showed that commensal gut microbiota favours PCa tumour growth and progression to CRPC by producing androgens from androgen precursors[180]. Cui et al, recently found that cancer associated fibroblasts (CAFs) promote intratumoural production of androgens from extragonadal sources through the increase in expression of steroidogenic enzymes[181]. Among PCa microenvironment, periprostatic adipose tissue (PPAT) is a white adipose tissue (AT) that surrounds the prostate gland. My team and others have demonstrated that PPAT is a key player in PCa progression through its ability to secrete soluble factors such as chemokines, proinflammatory cytokines and lipid metabolites[419]. It is tempting to speculate that PPAT could also contribute to the occurrence of CPRC. As depicted in the review presented in the introduction, AT is described as a reservoir of sex steroids capable of locally synthesizing steroid precursors *de novo* from cholesterol and/or converting steroids captured from the bloodstream through the expression of biosynthesis (CYP11A, CYP17A) and conversion (3βHSD, 17βHSD, SRD5A) enzymes enabling the production of androgens such as DHEA, androstenedione, testosterone and 5α-DHT[604]. Moreover, we performed an extensive structural and functional characterization of PPAT compared to a control tissue, the abdominopelvic adipose tissue (APAT). Among the obtained results, we have shown that PPAT displays an increased androgenic signaling using transcriptomic approaches (Article presented in Result's part 1). All these indirect arguments suggest that PPAT might possess a specific steroid metabolism that could be involved in regulating both physiological and pathophysiological processes in the prostate. Accordingly, **the aim of my PhD project was to determine if PPAT**

bioRxiv preprint doi: https://doi.org/10.1101/2023.01.05.522843; this version posted January 6, 2023. The copyright holder for this preprint (which was not certified by peer review) is the author/funder. All rights reserved. No reuse allowed without permission.

Collagen remodeling leads to inflammation-free expansion of periprostatic adipose tissue and promotes prostate cancer progression

David Estève[1], Aurélie Toulet[1], Mathieu Roumiguié[1,2], Dawei Bu[3], Sarah Pericart[4], Chloé Belles[5], Cécile Manceau[1,2], Cynthia Houël[1], Manuelle Ducoux-Petit[1,6], Nathalie Van Acker[4], Stéphanie Dauvillier[1], Yiyue Jia[1], Camille Franchet[4], Nicolas Doumerc[2], Mathieu Thoulouzan[2], Sophie Le Gonidec[7], Philippe Valet[7], Bernard Malavaud[2], Odile Burlet-Schiltz[1,6], Anne Bouloumié[5], Philipp E. Scherer[3], Delphine Milhas[1], Catherine Muller[1]

[1]Institut de Pharmacologie et de Biologie Structurale (IPBS), Université de Toulouse, CNRS, Université Toulouse III - Paul Sabatier (UPS), Toulouse, France. Équipe Labélisée Ligue Nationale contre le Cancer.
[2]Department of Urology and Renal Transplantation, Toulouse University Hospital ; Institut Universitaire du Cancer de Toulouse, Oncopole, Toulouse, France.
[3]Touchstone Diabetes Center, Department of Internal Medicine and Department of Cell Biology, University of Texas Southwestern Medical Center, Dallas, TX, USA.
[4]Department of Pathology, Institut Universitaire du Cancer de Toulouse, Oncopole, Toulouse, France.
[5]Institut des Maladies Métaboliques et Cardiovasculaires, Université de Toulouse, INSERM, UPS, Toulouse, France
[6]Infrastructure Nationale de Protéomique, ProFI, FR 2048, Toulouse, France
[7]Institut RESTORE, Université de Toulouse, CNRS U-5070, EFS, ENVT, INSERM U1301, UPS, Toulouse, France.

Address correspondance to : Catherine Muller, IPBS CNRS UMR 5089, 205 route de Narbonne, 31077 Toulouse, France. Phone: 33.561.17.59.32; E-mail: muller@ipbs.fr or to: Delphine Milhas, IPBS CNRS UMR 5089, 205 route de Narbonne, 31077 Toulouse. Phone: 33-561-17-58-66 ; E-mail: milhas@ipbs.fr

Summary
The abundance of periprostatic adipose tissue favors prostate cancer aggressiveness. The increase in extracellular matrix remodeling that occurs in expanded periprostatic fat allows adipocyte hypertrophy without tissue inflammation and generates a matrikine, endotrophin, which favors tumor progression.

Abstract

Periprostatic adipose tissue (PPAT) abundance correlates with prostate cancer progression, but the mechanism remains unexplained. Here, we used a statistical approach to define abundant PPAT by normalizing PPAT volume to prostate volume in a cohort of 351 patients with a linear regression model. Applying this definition, we find tumors specifically from patients with abundant PPAT exhibit several hallmarks of aggressiveness, suggesting that PPAT abundance might be used to improve risk stratification. We show that abundant PPAT expands by adipocyte hypertrophy but this does not result in inflammation. Extensive extracellular matrix remodeling, notably of the collagen network, and decreased expression of mechano-sensing proteins in adipocytes explains this inflammation-free expansion by decreasing the mechanical constraints on the adipocytes. Moreover, collagen VI degradation in abundant PPAT is associated with production of endotrophin, a matrikine that promotes cancer progression. We find high levels of endotrophin specifically in the urine of patients with abundant PPAT, indicating the clinical relevance of our findings.

bioRxiv preprint doi: https://doi.org/10.1101/2023.01.05.522843; this version posted January 6, 2023. The copyright holder for this preprint (which was not certified by peer review) is the author/funder. All rights reserved. No reuse allowed without permission.

Introduction

Prostate cancer (PCa) is the second most common form of solid tumor in men worldwide and the fifth leading cause of death from cancer (Pernar et al., 2018). It is a highly heterogeneous disease, ranging from slow-growing indolent tumors to fatal metastatic carcinomas (Pernar et al., 2018). Risk stratification is, therefore, the cornerstone for selecting the most appropriate treatment for these men. Progression from indolent to aggressive PCa depends on endocrine signaling (mainly through the androgen receptor) and genetic alterations leading to cancer cell-autonomous progression (Pernar et al., 2018) ; however, paracrine signaling from the tumor microenvironment also plays a role (Shiao et al., 2016). The adipose tissue (AT) surrounding the prostate, called periprostatic adipose tissue (PPAT), has emerged recently as an important factor in the progression of the disease (Estève et al., 2020). Like other white adipose tissue (WAT), PPAT comprises mainly adipocytes and other cell types in the stromal vascular fraction, including adipose progenitor cells, fibroblasts, endothelial and immune cells, all of which are embedded in the extracellular matrix (ECM) (Zwick et al., 2019). Also, as a WAT, PPAT is an active metabolic and secretory organ (Zwick et al., 2019; Nassar et al., 2018).

Both clinical and fundamental biological studies have shown that PPAT contributes to the progression of PCa. Extension of the prostate tumor into PPAT is an important indicator of a poor prognosis (Kapoor et al., 2013). PPAT promotes prostate tumor aggressiveness and local dissemination by secreting soluble factors such as chemokines (Laurent et al., 2016), pro-inflammatory cytokines (Gucalp et al., 2017) and lipid mediators (Laurent et al., 2019) (for review, (Estève et al., 2020). Also, in obese patients, the secretory and metabolic dysfunctions of PPAT amplify the involved mechanisms (Estève et al., 2020; Gucalp et al., 2017; Laurent et al., 2016, 2019). Several meta-analyses have established an association between obesity and increased risk of PCa recurrence, progression to advanced cancer, and PCa-related mortality (Cao and Ma, 2011; Harrison et al., 2020). The increased risk of advanced disease and PCa-specific mortality ranges from 6-12 % with every 5 kg/m^2 increase in body mass index (BMI) (Cao and Ma, 2011; Harrison et al., 2020). Although changes in PPAT function occur in obesity (Estève et al., 2020), many studies have shown that, unlike all other WAT, the volume of PPAT, as measured by multiparametric magnetic resonance imaging (mpMRI), does not correlate with BMI (Woo et al., 2015; Roumiguié et al., 2022; Zhang et al., 2014). This failure of PPAT to expand in obese individuals may be explained by the chronic hypoxic state of PPAT, which induces fibrosis (Roumiguié et al., 2022).

Although the volume of PPAT in an individual does not correlate with his BMI, it does vary considerably between individuals (Zhang et al., 2014; Woo et al., 2015; Roumiguié et al., 2022). Recent clinical studies have demonstrated that patients with large amounts of PPAT have more aggressive PCa than the patients with low amounts (Nassar et al., 2018), suggesting that the abundance of PPAT might be used to stratify patients' risk. PPAT abundance correlates with prostate tumors with high Gleason

bioRxiv preprint doi: https://doi.org/10.1101/2023.01.05.522843; this version posted January 6, 2023. The copyright holder for this preprint (which was not certified by peer review) is the author/funder. All rights reserved. No reuse allowed without permission.

scores and local dissemination (Nassar et al., 2018; Zhang et al., 2014; Woo et al., 2015; Van Roermund et al., 2011; Zhai et al., 2021), which are indicators of high risk progression**.** Measurement of PPAT abundance may be used in the early management of PCa patients since it predicts PCa aggressiveness in patients undergoing radical prostatectomy (RP) for localized disease (Dahran et al., 2019; Zhai et al., 2018) and predicts progression-free survival in men with indolent PCa who are under active surveillance (Gregg et al., 2021)**.** Moreover, in advanced PCa, the abundance of PPAT may be a predictor of the cancer's resistance to castration (Salji et al., 2018; Sasaki et al., 2020; Huang et al., 2019). Considered together, these studies suggest that the expansion of PPAT might be far more important than obesity in determining the progression of PCa and its outcome for the patient.

The recognition of an important relationship between PPAT abundance and PCa raises several important issues (Dahran et al., 2017). First, no consensus has emerged from the literature about the most appropriate way to quantify PPAT abundance, making it difficult to compare directly the findings of different studies and potentially limiting translation of this concept from clinical studies into practice. Several methods have been reported, including measuring the area of PPAT in a single slice image obtained by computed tomography (Van Roermund et al., 2011) or mpMRI (Zhang et al., 2014), and simply measuring the thickness of PPAT by mpMRI (Woo et al., 2015). More recently, calculating the whole PPAT volume from successive mpMRI slices by using appropriate software has been proposed as a more accurate method (Dahran et al., 2019; Zhai et al., 2018; Gregg et al., 2021; Salji et al., 2018) . As PPAT volume is reported to correlate with prostate volume (Dahran et al., 2017; Tan et al., 2016), several studies have used the ratio of PPAT volume to prostate volume in an individual – the normalized periprostatic fat volume (NPFV) (Dahran et al., 2017; Tan et al., 2016) – to compare PPAT abundance between individuals. Second, the biological mechanisms that result in expansion of PPAT and the role of abundant PPAT in PCa progression are still unknown.

In this study, we developed a more refined definition of abundant PPAT that might be applicable both in basic research and for risk stratification in the clinic. Using this definition, we characterize the differences between abundant PPAT and less abundant PPAT in PCa patients to shed light on the role of abundant PPAT in the aggressiveness of PCa. We find that tissue expansion in abundant PPAT is due to adipocyte cell enlargement, or hypertrophy, which, unlike expansion of other WAT, does not drive inflammation. This inflammation-free expansion of PPAT is explained by extensive remodeling of the ECM, in particular degradation of collagen, which reduces the mechanical constraints on the adipocytes, and generates a matrikine, endotrophin, which promotes tumor progression.

bioRxiv preprint doi: https://doi.org/10.1101/2023.01.05.522843; this version posted January 6, 2023. The copyright holder for this preprint (which was not certified by peer review) is the author/funder. All rights reserved. No reuse allowed without permission.

Results

A new statistical approach to defining abundant PPAT relative to prostate volume

To define PPAT abundance more precisely, we wanted to develop a measure that expresses the volume of PPAT with respect to the volume of the prostate normalized to a population rather than to an individual. To do so, we examined a cohort of 351 patients awaiting prostatectomy for PCa by using pre-operative mpMRI, from which we measured prostate and PPAT volume within well-defined anatomical limits (Table S1 and Fig. 1A). We found a strong correlation between the volume of the prostate determined by mpMRI before prostatectomy and its weight after prostatectomy (Fig. 1B), thus validating the accuracy of the measurement method. A group of 20 patients that underwent mpMRI for non-oncological pathologies were also included in the study. In the cohort of PCa patients, PPAT volume was independent of BMI (Fig. 1C), as we reported previously for a smaller cohort (Roumiguié et al., 2022); this was true also for the patients without PCa (Fig. 1C). In both groups of patients, subcutaneous AT area (Fig. S1A) and perirectal AT area (Fig. S1B) both correlated with BMI. PPAT volume correlated with prostate volume in both groups of patients (Fig. 1D), thus this relationship is independent of the presence of PCa. Based on this strong correlation between PPAT volume and prostate volume, we modeled the expected PPAT volume according to the prostate volume by using a linear regression model and calculated PPAT abundance with the residual values from this model. The residual values are a measure of the difference between the volume of PPAT quantified by mpMRI and the amount of PPAT predicted by the model (Fig. 1E). The cohort was divided into quartiles according to residuals values allowing to identify patients with the least PPAT in the 1st quartile (low PPAT) and patients with the most PPAT in the 4th quartile (high PPAT) (Fig. 1 E-F). Patients in the 2nd and 3rd quartile were classified as having a mid PPAT abundance (Fig. 1 E-F). No differences were observed between patients in the four quartiles when we analyzed prostate volume (Figure 1G), BMI (Figure 1H) or age (Figure 1I).

In our PCa cohort, NPFV only partially reflected PPAT abundance as calculated by our model (Fig. S2A). When we ranked our patients according to ascending NPFV, some patients with the highest NPFVs fell into our mid PPAT group, whereas others with relatively low NPFVs fell into our high PPAT group (Fig. S2A). Overall, nearly 30% of patients fell into different groups when analyzed by the two methods (Fig. S2A). To investigate further the differences between the two methods, we assigned the individuals in our cohort to quartiles based on ascending NPFV: 1st quartile (low NPFV), 2nd and 3rd quartile (mid NPFV) and 4th quartile (high NPFV). When we plotted the PPAT volumes of the individuals in each quartile, we saw no difference between the mean PPAT volumes of the quartiles (Fig. S2B), whereas prostate volume decreased as NPFV increased (Fig. S2C). Thus, large NPFVs are due primarily to small prostate volumes rather than large PPAT volumes, unlike our model.

bioRxiv preprint doi: https://doi.org/10.1101/2023.01.05.522843; this version posted January 6, 2023. The copyright holder for this preprint (which was not certified by peer review) is the author/funder. All rights reserved. No reuse allowed without permission.

Abundant PPAT is associated with aggressive tumors

To evaluate the relationship between PPAT abundance, as defined above, and PCa aggressiveness, we compared abundance to the clinical and pathological parameters of the patients in our cohort (Table S2). This cohort included only patients who underwent prostatectomy, because we wanted to perform histological and biochemical analyses on the excised tissues. The cohort was rather homogenous in the aggressiveness of their cancers, according to current prostatectomy indications (Costello, 2020). The Gleason score, one of the main criteria to evaluate the prognosis of a PCa, is based on hematoxylin and eosin (HE) staining of tumor sections and evaluate the differentiation and architecture of the tumor; it is used to determine the ISUP (International Society of Urological Pathology) grade (1-5). Most patients in our PCa cohort were graded 2 or 3 on the ISUP scale (Table S2). Nevertheless, the proportion of patients with an ISUP grade ≥ 3 increased with PPAT abundance and was significantly different between the low PPAT and high PPAT groups (Fig. 2A and Table S3). In addition to the ISUP score, the percentage of undifferentiated cancer cells in the tumors of patients in the high PPAT group was significantly greater than it was in the patients in the low PPAT group (Fig. 2B and Table S3). Moreover, there was a significant association between the abundance of PPAT and the concentration of prostate-specific antigen in the blood of patients with PCa prior to surgery (Table S3). Taken together, these data indicate that abundant PPAT, as defined by our method, correlates with more aggressive tumors, suggesting that it might play a role in PCa progression.

To evaluate the potential value of our PPAT abundance measure for predicting the ISUP score, we compared the ISUP grade of tumor tissue obtained after prostatectomy with that determined on pre-operative biopsied tissue in a subset of patients with ISUP grades < 3 (i.e. less aggressive prostate cancer), then determined the percentage of patients in low, mid and high PPAT groups whose ISUP scores were upgraded after surgery (Fig. 2C). The proportion of patients whose ISUP scores were upgraded increased from 15% in the low PPAT group to 39% in the high PPAT group, suggesting that PPAT abundance might be a useful criterion to improve risk stratification. Multivariate analysis using a logistic regression model found that PPAT abundance was an independent risk factor for PCa with an ISUP score ≥ 3 (Fig. 2D), whereas NPFV was not (Fig. S2D). In addition, NPFV was not associated to PCa aggressiveness (Table S4).

Accumulating evidence indicates that mechanisms underlying the progression of PCa are not confined to epithelial cells but also involve the tumor microenvironment (Shiao et al., 2016). We found above that the abundance of PPAT correlated with the occurrence of tumors with a high Gleason grade, but this grade considers only the epithelial component of the tumor. To investigate whether the microenvironment differs in tumors associated with abundant PPAT when compared to those with less

bioRxiv preprint doi: https://doi.org/10.1101/2023.01.05.522843; this version posted January 6, 2023. The copyright holder for this preprint (which was not certified by peer review) is the author/funder. All rights reserved. No reuse allowed without permission.

abundant PPAT, we used histochemistry and immunohistochemistry of sections of paraffin-embedded tumors to analyze ECM deposition (Masson's trichrome staining; Fig. 2E), angiogenesis (anti-CD31 staining, Figure 2F) and macrophage infiltration (anti-CD68 staining, Fig. 2G); all three are hallmarks of cancer aggressiveness. Quantification of Masson's trichrome staining, which stains fibrillar collagens blue, indicated enhanced collagen deposition in tumors from patients in the high PPAT group when compared with that of patients in the low PPAT group (Fig. 2D). Likewise, immunostaining with anti-CD31 and anti-CD68 antibodies showed greater blood vessel density and macrophage infiltration, respectively, in tumors from patients in the high PPAT group than in those in the low PPAT group (Fig. 2E-F). Overall, the tumors from patients in the high PPAT group exhibited several hallmarks of aggressiveness including modifications of glandular architecture and dedifferentiation of the epithelial compartment as reflected in the ISUP score, fibrosis, dense vascularization and high levels of macrophage infiltration into the tumors.

PPAT expands by adipocyte hypertrophy with no associated inflammation

AT expands in response to surplus energy by two main mechanisms: adipocyte enlargement, or hypertrophy, and adipocyte hyperplasia, in which new adipocytes are recruited by adipogenesis from progenitors (Pellegrinelli et al., 2016). The balance between hypertrophy and hyperplasia depends on the adipose depot concerned (Pellegrinelli et al., 2016). To distinguish between these two mechanisms of expansion in PPAT, we stained paraffin-embedded PPAT sections with HE and measured the diameters of the adipocytes by a semi-automated method, Adiposoft© (Fig. 3A). The adipocyte size distribution curve was shifted towards larger cells in PPAT from patients in the high PPAT group when compared with those in the low PPAT group, and the mean adipocyte diameter was larger (Fig. 3B), indicating adipocyte hypertrophy. To analyze whether adipocyte hyperplasia was also occurring, we digested PPAT with collagenase to separate adipocytes from the stromal vascular fraction, which contains the adipose progenitors. The cells in the stromal vascular fraction were immunostained with antibodies against the markers CD45, CD34 and CD31 and analyzed by flow cytometry. The percentage of cells in this fraction that were progenitor cells (defined as CD45-/CD34+/CD31- cells) was similar in PPAT from patients in the various groups (Fig. 3C). Furthermore, when additional markers (MSCA1 and CD271) were used to characterize the sub-populations of adipose progenitors (Estève et al., 2019), the proportions of the various progenitor subsets (the adipogenic, MSCA1+; myofibrogenic MSCA1-/CD271+, and immature MSCA1/CD271- subsets), were similar in all groups (Fig. S3A), indicating no increased adipogenesis from progenitors in abundant PPAT. We conclude that adipocyte hypertrophy rather than hyperplasia is the mechanism of PPAT expansion in patients with abundant PPAT.

bioRxiv preprint doi: https://doi.org/10.1101/2023.01.05.522843; this version posted January 6, 2023. The copyright holder for this preprint (which was not certified by peer review) is the author/funder. All rights reserved. No reuse allowed without permission.

Adipocyte hypertrophy during AT expansion is usually associated with changes in secretion related to AT dysfunction (Ouchi et al., 2011). Key among these changes is increased secretion of leptin and, in parallel, decreased secretion of adiponectin (Frühbeck et al., 2019). The decrease in the ratio of adiponectin/leptin secretion has been proposed as a marker of dysfunctional AT in metabolic disorders and inflammation (Frühbeck et al., 2019; Zhao et al., 2021). Despite the adipocyte hypertrophy we saw in PPAT from patients in the high PPAT group, more adiponectin was secreted by this PPAT than by PPAT from patients in the low PPAT group (Fig. 3D), whereas leptin secretion by both tissues was similar (Fig. 3E). Accordingly, the adiponectin/leptin secretion ratio was greater in high than in low PPAT (Fig. 3F). Thus, the adipocyte hypertrophy observed in high PPAT is not associated with the changes in secretion that are usually observed in dysfunctional AT.

The proportion of immune system cells in AT generally increases as the tissue expands and this is associated with the onset of chronic low-grade inflammation (Ouchi et al., 2011). We measured the proportion of immune cells in PPAT from patients in the three groups by immunostaining the cells in the stromal vascular fraction with antibodies against CD45 and other specific markers of immune population subsets and analyzed them by flow cytometry. The proportion of CD45+ leukocytes in this fraction was similar in the various groups of patients (Fig. 3G), as was the proportion of total lymphocytes (defined as CD45+/low side scatter) (Fig. 3H) and of various lymphocyte subsets (Figure S3B). The proportion of macrophages (defined as CD45+/CD14+ cells), including the sub-populations that express or do not express CD206, were also similar in the various groups (Fig. 3I). These data indicate that PPAT expansion is not associated with increased immune cell infiltration.

To characterize further the inflammatory state of abundant PPAT, we quantified secretion of several proinflammatory cytokines by PPAT from patients in the various groups. No significant differences were seen between the amounts of TNF-α, IL6, or MCP-1 secreted (Fig. 3 J-L), and the tissue from patients in the high PPAT group secreted slightly less IL1β than did the others (Fig. 3M). Thus, the PPAT from patients in the high PPAT group does not secrete more proinflammatory cytokines than the PPAT from the patients in the mid and low PPAT groups. Together, these data indicate that although PPAT expands by adipocyte hypertrophy, this expansion does not cause the inflammation observed in other ATs that expand by this mechanism.

Under-representation of mechano-sensing proteins in adipocytes from abundant PPAT

According to our findings described above, adipocytes are the main cell type that changes in the PPAT from patients in the high PPAT group. To investigate further the changes in the adipocytes, we isolated adipocytes from the PPAT of patients in the high PPAT and low PPAT groups and analyzed them by proteomics. Principal component analysis of the proteomics dataset separated the patients according to

bioRxiv preprint doi: https://doi.org/10.1101/2023.01.05.522843; this version posted January 6, 2023. The copyright holder for this preprint (which was not certified by peer review) is the author/funder. All rights reserved. No reuse allowed without permission.

the abundance of their PPAT (Fig. 4A). Component 1, which separated the patients according to their PPAT groups, explained 52% of the variance in the proteomic dataset (Fig. 4A). Whereas the low PPAT patients grouped closely on the scatter plot, those with high PPAT spread widely (Fig. 4A). Of the 4033 proteins identified by proteomics, statistical analysis found 352 whose abundance differed in PPAT from patients in the high and low PPAT groups: 157 were over-represented and 195 were under-represented in the samples from the high PPAT group when compared to those from the low PPAT group (Fig. 4B). Hierarchical clustering by using Ward's method on differentially represented proteins grouped the samples according to their abundance status (Fig. 4C).

To characterize further the differences between adipocytes in the PPAT of patients in the high and low PPAT groups, we used gene ontology enrichment analysis of the proteomics dataset to identify cellular components and molecular functions. We found large differences in the abundance of proteins involved in cytoskeletal organization, cell-ECM interactions and, to a lesser extent, lipid metabolism (Fig. 4D). From this analysis, the main characteristics of adipocytes from abundant PPAT can be described as having, foremost, an under-representation of proteins involved in mechano-transduction and sensing stiffness (ontology terms in bold in Fig. 4D). Among them, YAP1 (Yes-associated protein 1) is the most under-represented protein in the PPAT of patients in the high PPAT group (log2 fold-change = -5.8) when compared with the low PPAT group (Fig. 4E). YAP1 is a key mechano-transducer that senses mechanical stimuli and relays them to regulate transcription and, thus, many aspects of cell behavior (Dupont et al., 2011). ZYXIN (Ma et al., 2016) and PACSIN2 (Rausch and Hansen, 2020), proteins that participate in the nuclear translocation and activation of YAP1 upon mechanical stress, were also significantly under-represented in the most abundant PPAT, as was ROCK2, a target of YAP/TEAD transcriptional complex (Dupont et al., 2011) (Fig. 4E). We confirmed by immunofluorescence microscopy that PPAT from patients in the high PPAT group contained much less YAP1 than that from patients in the low PPAT group (Fig. 4F).

The second important characteristic of adipocytes from abundant PPAT identified by pathway enrichment analysis was under-representation of several tubulin isoforms (Fig. 4G), which was accompanied by altered microtubule organization seen by immunofluorescence microscopy (Figure 4H). Proteins involved in cytoskeletal organization, such as cortactin (CTTN), an actin nucleation factor that influences the stability of actin filaments, and members of the vinexin family (SORBS-1 and SORBS-3), which are involved in contractile force generation in response to mechanical stress (Ichikawa et al., 2017) were also under-represented (Fig. 4I).

A third notable characteristic of adipocytes from the high PPAT group was the abundance of proteins involved in lipid metabolism (Fig. 4D), which may explain, at least in part, the observed adipocyte hypertrophy. Several key proteins involved in lipolysis were under-represented in PPAT from patients

bioRxiv preprint doi: https://doi.org/10.1101/2023.01.05.522843; this version posted January 6, 2023. The copyright holder for this preprint (which was not certified by peer review) is the author/funder. All rights reserved. No reuse allowed without permission.

in the high PPAT group, including adipocyte triglyceride lipase (encoded by *PNPLA2*), hormone-sensitive lipase (encoded by *LIPE*), perilipin1 (encoded by PLIN1) and Abhydrolase domain-containing protein 5 (encoded by ABHD5) (Fig. S4A). For PNPLA2 and LIPE, a downward trend regulation at mRNA levels according to abundance status was confirmed by RT-qPCR, whereas the level of MGLL (encoding Monoacylglycerol Lipase) was unchanged (Fig. S4B). By contrast, adiponectin (encoded by ADIPOQ) and several lipid transporters that take up fatty acids like CD36 or FABP4 (Fatty Acid Binding protein 4) were over-represented and regulation of their mRNA levels according to abundance status was confirmed by RT-qPCR and similar differences were also observed for the Long-chain fatty acid transport protein 4 (encoded by SLC27A4) (Fig. S4A and S4C).

The collagen network in abundant PPAT is relatively loose

We deduce from the data described above that abundant PPAT might be subject to fewer mechanical constraints (as indicated by the under-representation of proteins involved in mechano-sensing and cytoskeletal contractile force generation) than in less abundant PPAT, which may account for its expansion without inflammation. To investigate this hypothesis, we examined the collagen networks of PPAT from patients in the high and low PPAT groups. Collagen is the most abundant ECM protein and excessive collagen deposition provides tissue rigidity. We stained the collagen fibers with picrosirius red, imaged the staining by 3D confocal microscopy and reconstructed images of the fiber network in 3D. In the reconstructions, the signal from collagen fibers was weaker in PPAT from patients in the high PPAT group than it was in the patients in the low PPAT group (as shown by the maximum intensity projection), and the collagen network was substantially less dense and had thinner fibers (Fig. 5A). These observations were verified by using Imaris software to quantify the volume and length of the collagen fibers as well as the total number of branches seen in the 3D reconstructions (Fig. 5 B–D). To confirm our findings further, we used a different approach based on quantification of hydroxyproline, a measure of the collagen content of the tissue. Consistent with the imaging analysis of the collagen fiber network, we found significantly less hydroxyproline in PPAT from patients in the high PPAT group than in patients in the low PPAT group (Fig. 5E). Together, these analyses indicate that abundant PPAT has a looser collagen network than less abundant PPAT, supporting the hypothesis that mature adipocytes in abundant PPAT are subject to fewer mechanical constraints than those in less abundant PPAT.

Abundant PPAT exhibits increased collagen degradation likely by MMP9

Our findings indicate that abundant PPAT contains less collagen organized in a looser network than in less abundant PPAT. To determine whether this reflects less collagen synthesis or more degradation of

bioRxiv preprint doi: https://doi.org/10.1101/2023.01.05.522843; this version posted January 6, 2023. The copyright holder for this preprint (which was not certified by peer review) is the author/funder. All rights reserved. No reuse allowed without permission.

the proteins, we used RT-qPCR to compare the expression of the genes encoding the major fibrillar collagens (*COL1A1* and *COL3A1*) as well as the 3 different alpha chain of the most abundant non-fibrillar collagen, collagen VI (Sun et al., 2013) (*COL6A1*, *COL6A2* and *COL6A3*) in PPAT from patients in the high and low PPAT groups. We saw no differences between them (Fig. 6A) suggesting that the smaller amount of collagen and looser network in abundant PPAT is not due to less synthesis but may be due to increased degradation.

To investigate this hypothesis, we stained PPAT samples with a fluorescent peptide (F-CHP) that binds specifically to denatured collagen strands (Hwang et al., 2017) and imaged the staining by 3D confocal microscopy. The images showed a punctate staining located alongside fibrillar structures in PPAT from patients in the high PPAT group, whereas very weak signals were seen in PPAT from patients in the low PPAT group (Fig. 6B, left panel). Quantification of the signals from F-CHP after 3D reconstruction confirmed the substantial increased in collagen degradation in PPAT from the high PPAT group when compared with the low PPAT group (Fig. 6B, right panel).

Matrix metalloproteinases are the main enzymes involved in collagen degradation. To investigate the potential involvement of various matrix metalloproteinases in the degradation of collagen in high PPAT, we quantified expression of the main metalloprotease genes expressed in AT (*MMP-2*, *MMP-9*, *MMP-11*, *MMP-14* and *BMP1*) by RT-qPCR. Significantly more *MMP9* mRNA was found in PPAT from patients in the high PPAT group than in PPAT from patients in the low PPAT group (Fig. 6C). This was confirmed by analyzing the proteomics data from isolated adipocytes (Fig. 6D), and it was reflected in elevated MMP9 activity (Fig. 6E). MMP activity is tightly regulated by the balance between expression of the genes encoding MMPs and their endogenous inhibitors the TIMPs (tissue inhibitor of metalloproteinases). Therefore, we analyzed the expression of the genes encoding various TIMP isoforms as well as those encoding the lysyl oxidases LOX and LOXL1, which cross-link ECM proteins. All these genes were expressed at similar levels in the high and low PPAT groups (Fig. S5). We conclude that the smaller amount of collagen in abundant PPAT than in less abundant PPAT and its disorganization is due to enhanced degradation that likely involves MMP9.

COL6 remodeling is associated with high endotrophin production in abundant PPAT

ECM remodeling generates bioactive fragments called matrikines that are implicated in cancer (Ricard-Blum and Salza, 2014). The matrikine endotrophin, for example, is generated by proteolytic cleavage of the C-terminal part of COL6a3 and is implicated in malignant tumor growth and progression (Bu et al., 2019; Park and Scherer, 2012). In breast cancer, endotrophin produced by AT affects both the cancer cells, by inducing epithelial to mesenchymal transition, and the tumor microenvironment, by causing fibrosis and recruiting macrophages and endothelial cells (Bu et al., 2019; Park and Scherer, 2012). These

bioRxiv preprint doi: https://doi.org/10.1101/2023.01.05.522843; this version posted January 6, 2023. The copyright holder for this preprint (which was not certified by peer review) is the author/funder. All rights reserved. No reuse allowed without permission.

features are reminiscent of the hallmarks of tumors associated with high PPAT, including dedifferentiation (as seen in Fig. 2A-B) and modifications of the microenvironment (Fig. 2D-F). Thus, we postulated that endotrophin might be involved in PCa progression in patients with abundant PPAT. To investigate this possibility, we first compared COL6 in PPAT tissue from patients in the high PPAT group with that in the low PPAT group by immunofluorescence staining and 3D confocal microscopy. The COL6 staining was weaker in the high PPAT group than in the low PPAT group, it was punctiform and the COL6 microfibrils were clearly disorganized (Fig. 7A), confirming that COL6 is degraded in abundant PPAT. To determine whether this degradation generated endotrophin, we immunostained the tissue with an antibody specific for endotrophin (Bu et al., 2019) and imaged by immunofluorescence microscopy (Fig. 7B). Much more endotrophin was seen in PPAT from patients in the high PPAT group than in that from patients in the low PPAT group (Fig. 7B), consistent with the notion that this matrikine is involved in PCa progression in patients with abundant PPAT.

To investigate the clinical relevance of our findings, we quantified endotrophin in biological fluids from patients with PCa who had been diagnosed by mpMRI (see Table S5-6 for the description of the new cohort). After quantification of endotrophin, the patients were classified into the low, mid and high PPAT groups defined above. Endotrophin plasma levels were similar in all patients regardless of their PPAT abundance status (Fig. 7C). By contrast, the endotrophin concentration in urine collected after prostate massage, that causes exfoliation of cells from the tumor into biological fluids (Fujita and Nonomura, 2018), was greater in patients in the high PPAT group than it was in patients in the low PPAT group (Fig. 7D). We conclude that patients with PCa and abundant PPAT produce more endotrophin than patients with less abundant PPAT. Together, our findings suggest a model in which the extensive collagen remodeling that occurs in abundant PPAT generates endotrophin, which increases the aggressiveness of the adjacent PCa tumors.

Discussion

Several studies have concluded that excessive fat around the prostate plays a role in PCa progression and outcome, despite differences in the methods and criteria that were used to define PPAT abundance (Nassar et al., 2018). Here, we developed a statistical definition of abundant PPAT as an excess of PPAT volume when compared to the prostate volume predicted from a large cohort of patients. We show that abundant PPAT expands by adipocyte hypertrophy but this does not cause inflammation, since changes in the ECM relieve the mechanical constraints on the expanded tissue as shown by the decrease in proteins involved in mechanical sensing and cytoskeleton organization and forces. This ECM remodeling in abundant PPAT is associated with increased expression and activity of the matrix protease MMP9 and results in generation of a matrikine, endotrophin, which, in other cancer types,

bioRxiv preprint doi: https://doi.org/10.1101/2023.01.05.522843; this version posted January 6, 2023. The copyright holder for this preprint (which was not certified by peer review) is the author/funder. All rights reserved. No reuse allowed without permission.

promotes the epithelial–mesenchymal transition and shapes a microenvironment that favors cancer progression (Funcke and Scherer, 2019; Wang and Pan, 2020). The presence of large amounts of endotrophin in the urine of patients with abundant PPAT reinforces the clinical relevance of our findings. Our main findings and the mechanism we propose are summarized in Figure 8.

To develop a definition of PPAT abundance that might be generally acceptable to the field and that might be used in clinical practice, we used mpMRI – the gold standard for imaging the prostate and surrounding tissues – to measure both prostate volume and the whole volume of PPAT rather than simply the thickness of fat or the area of the tissue at a single point. We measured these volumes by applying a slice-by-slice segmentation technique used previously in one study (Dahran et al., 2017), and used Denonvillier's fascia, the anatomical barrier between the prostate and the other part of pelvic region, as the posterior limit of the PPAT, the definition of which varied in previous studies. Using this approach, we demonstrate that the volume of the PPAT correlates with that of the prostate. As prostate size is highly variable between individuals and often increases with age (Loeb et al., 2009), some previous studies used the ratio between the PPAT volume or area and the prostate size of the individual as a way of normalizing PPAT abundance (Zhai et al., 2021; Dahran et al., 2017). We show that this approach introduces a bias towards patients with smaller prostates being identified as having abundant PPAT, consistent with the findings of a previous study (Dahran et al., 2017). To overcome this bias, we developed a linear regression model that normalizes PPAT abundance by comparing the residual value of PPAT volume to the linear relationship between PPAT and prostate volume computed from the whole cohort. Using this approach, we calculated PPAT abundance for each individual in the cohort, ranked the population according to PPAT abundance and divided it into quartiles. We observed no differences in prostate size, BMI, or age and between the patients in these quartiles, thus validating our approach.

Applying our new approach to define PPAT abundance, we find that patients with the most abundant PPAT, i.e. those in the top quartile or the high PPAT group, have the most aggressive PCa (as defined by ISUP scores and percentage of undifferentiated cells) and that this measure of PPAT abundance predicts whether a patient's ISUP score was upgraded after RP. More importantly, PPAT abundance was an independent risk factor for PCa with an ISUP score ≥ 3. As described below, PCa management suffers from the lack of strong criteria to overcome prognostic heterogeneity and to tailor the treatment strategy. Since mpMRI is now widely used prior to biopsies, the measurement of PPAT volume should be evaluated as a prognostic marker for these localized PCa in order to evaluate if these high-risk patients will benefit from additional therapies. Since we wanted to perform biological characterization of PPAT, our cohort included only patients who underwent prostatectomy and excluded patients with a low ISUP score (ISUP 1), who may choose active surveillance rather than treatment, and those with

bioRxiv preprint doi: https://doi.org/10.1101/2023.01.05.522843; this version posted January 6, 2023. The copyright holder for this preprint (which was not certified by peer review) is the author/funder. All rights reserved. No reuse allowed without permission.

highly aggressive disease (ISUP 4 or 5), who often have advanced local or distant dissemination of their tumors. A large clinical study, including unsorted patients and automation of the method, would be necessary to establish the utility of PPAT measurement in PCa risk stratification in all these different clinical situations. In addition, our definition of PPAT abundance allowed us to identify groups of PCa patients whose PPAT characteristics differ in their histology, transcriptomes and proteomes, paving the way to understand how abundant PPAT promotes PCa progression.

We find that abundant PPAT expands by adipocyte hypertrophy rather than hyperplasia. This hypertrophy may be explained by several mechanisms: the increased expression of lipid transporters involved in uptake of lipids into adipocytes and transport within the cells and the decreased expression of some proteins involved in lipolysis, favoring lipid uptake over degradation. Also, the adipocyte hypertrophy may be facilitated by loss of collagen fibrils from the ECM, which we saw in abundant PPAT, since fibrosis plays a central role in limiting the expandability of AT (Sun et al., 2013) by generating a mechanical stress on hypertrophic adipocytes. Our previous study of PPAT in obesity supports this explanation. We found that lean PPAT has a peculiar vascularization that causes a chronic state of hypoxia leading to fibrosis, this fibrosis preventing PPAT expansion in obese patients (Roumiguié et al., 2022). Thus decreasing this fibrosis is an essential step for PPAT expansion. This discovery that the abundant PPAT contains a loose meshwork of both fibrillar and non-fibrillar collagens is perhaps the most important finding from this study because it explains how the tissue expands without becoming inflamed and the mechanism whereby PPAT expansion promotes PCa aggressivity.

The expansion of PPAT we observe in PCa patients in our high PPAT group does not result in tissue inflammation or in adipocyte dysfunction. This is surprising because expansion of other ATs by hypertrophy, as in obesity, leads to increased local inflammation and changes in the secretory profile of adipocytes (Ouchi et al., 2011). We explain this finding by the loose meshwork of fibrillar and non-fibrillar collagens in high PPAT resulting from enhanced ECM degradation that decrease the expression of proteins involved in mechano-transduction and stiffness sensing. This expansion in a context of decreased mechanical constraints led to a "stress-free" expansion. This loss of mechanical constraints allows the adipocytes to enlarge without cell death, which prevents accumulation of macrophages and, subsequently, in the reduction of the inflammatory microenvironment (Sun et al., 2013; Pellegrinelli et al., 2016). Evidence from mouse models deficient in ECM or overexpressing ECM remodeling proteins, support our interpretation that the loss of mechanical constraints allows PPAT expansion without inflammation. Mice that lack COLVI and that are obese due either to a high fat diet or to *ob*/*ob* mutation have impaired ECM stability and, hence, reduced AT fibrosis resulting in adipocyte hypertrophy in the absence of inflammation (Khan et al., 2009). Similarly, in a inducible AT specific MMP14 overexpression

bioRxiv preprint doi: https://doi.org/10.1101/2023.01.05.522843; this version posted January 6, 2023. The copyright holder for this preprint (which was not certified by peer review) is the author/funder. All rights reserved. No reuse allowed without permission.

model, the overexpression of MMP14 during the early stage of high fat diet (HFD) reduced inflammation and fibrosis (Li et al., 2020). In both cases, this phenotype was linked to the decrease in ECM stiffness of AT, thereby releasing the mechanical stress to allow for its healthy expansion (Khan et al., 2009; Chun et al., 2010).

One of the main differences we saw between the ECM in the high and low PPAT groups was in COLVI, the most abundant non-fibrillar collagen in AT (Sun et al., 2013). Whereas COLVI staining revealed a typical beaded filament network (Cescon et al., 2015) in the PPAT of the low PPAT group, in the high PPAT group the staining was weak and punctiform and the filament network was disorganized. COLVI interacts with many ECM proteins, including fibronectin and collagen types I, II and IV, bridging cells to the surrounding connective tissue and organizing the three-dimensional tissue architecture (Cescon et al., 2015). Thus, the overall loss of collagen may result from initial extensive degradation of COLVI. This degradation probably involves MMP9, which we found was much more abundant in the high PPAT group than in the low PPAT group. Degradation of COLVI by MMP9 has been described previously (Veidal et al., 2011), as well as by MMP2 (Veidal et al., 2011), MMP-11 (Motrescu et al., 2008) and MMP14 (Li et al., 2020). Expression of the latter MMPs and the inhibitors TIMP 1-4 were similar in both groups, however, suggesting that MMP9 is the most important in degrading COLVI in abundant PPAT. We do not know yet what initiates ECM remodeling to allow PPAT to expand. The correlation between the volume of PPAT and the volume of the prostate suggests that steroid hormones might be involved. Consistent with this, MMP9 expression is regulated by androgens (Tang et al., 2021) and sex hormones influence the metabolism, endocrine functions and angiogenesis of certain other ATs (Karastergiou et al., 2012), so this hypothesis deserves further investigation.

We postulate that the extensive ECM remodeling we observe in abundant PPAT promotes PCa aggressivity by producing signaling molecules that act on the adjacent tumor. Enzymatic cleavage of ECM proteins, proteoglycans and glycosaminoglycans produces matrikines and matricryptins, which are active in several biological processes including cancer progression (Ricard-Blum and Salza, 2014). We investigated the role of endotrophin , a matrikine derived from proteolytic cleavage of the carboxy-terminal C5 domain of the COLVI α3 chain from the parental COLVI microfibrils during secretion (Park and Scherer, 2012; Lamandé et al., 2006), because of the substantial amounts of COLVI degradation in abundant PPAT. Also, adipocyte-derived endotrophin favors breast tumor progression and resistance to therapy in genetically engineered mice (Park and Scherer, 2012) and in xenografted human tumors (Bu et al., 2019). Endotrophin targets not only the tumor cells but also induces changes in the tumor stroma including fibrosis, angiogenesis and recruitment of immune cells (Park and Scherer, 2012; Park et al., 2013) by acting directly on several cellular components of the tumor microenvironment (Bu et al., 2019). *In vitro*, endotrophin promotes recruitment and migration of macrophages, proliferation and

bioRxiv preprint doi: https://doi.org/10.1101/2023.01.05.522843; this version posted January 6, 2023. The copyright holder for this preprint (which was not certified by peer review) is the author/funder. All rights reserved. No reuse allowed without permission.

branching of endothelial cells, and differentiation of fibroblasts into myofibroblasts (Bu et al., 2019). The tumor microenvironment in PCa patients with abundant PPAT that we report here recapitulates all the features previously shown to be promoted by endotrophin. Moreover, we found more endotrophin in the PPAT of patients in the high PPAT group than in those in the low PPAT group. We found elevated levels specifically of *MMP9* mRNA, MMP9 protein and activity in abundant PPAT. This is consistent with a report that *in vitro* MMP9 activity, along with MMP2 and MMP16, is key to produce active endotrophin (Jo et al., 2022), which might explain the high levels of this matrikine in abundant PPAT. At first sight, our findings appear to contradict those of a study that used inducible adipocyte-specific endotrophin overexpression, which found that endotrophin amplifies AT dysfunction in obesity by enhancing fibrosis and inflammation leading, ultimately, to increased insulin resistance (Sun et al., 2014). In this case, however, endotrophin was overexpressed in the context of obesity-induced fibrosis; it might be considered as a co-stimulator of this pathological condition. In abundant PPAT, by contrast, natural expression of endotrophin occurs in the context of ECM degradation.

At the moment, we have no direct evidence that endotrophin produced in the ECM of PPAT is responsible for the increase in PCa aggressiveness. Such direct evidence would require a mouse model; currently, no mouse model reproduces the abnormal expansion of PPAT. To develop a model, we would need to identify the signal that drives PPAT expansion. Also, since mouse and human prostates differ in their morphology and architecture (Oliveira et al., 2016), it is far from certain that the phenomenon we report in human would be reproduced in mice. We tried to xenograft PPAT from patients in our low PPAT and high PPAT groups close to the prostate glands of immunodeficient mice, but the tissue did not remain viable and functional for long enough to perform experiments (data not shown). Co-culture of primary PPAT explants with prostate cancer cells might be an alternative approach but previous attempts (as well as our own experiments) found rapid adipocyte dedifferentiation associated with an increase in pro-inflammatory cytokines, rendering this approach unsuitable (Gesta et al., 2003) (data not shown).

In addition to the fact that both tumors and their microenvironment in PCa patients with abundant PPAT recapitulates all the features previously shown to be promoted by endotrophin, we show that endotrophin levels are elevated in the urine of patients with abundant PPAT collected after prostate massage, thus validating the clinical relevance of our findings. Endotrophin is stable in biological fluids and serum endotrophin was previously described as a surrogate marker of disease progression in chronic fibrotic and inflammatory diseases such as diabetes, heart failure, kidney disease and liver fibrosis (Rasmussen et al., 2017; Fenton et al., 2017; Leeming et al., 2021) (for review (Williams et al., 2022). We saw no difference between the plasma levels of endotrophin in patients from high and low PPAT groups. In cancer, endotrophin acts locally and its increase in urine reflects escape from the

bioRxiv preprint doi: https://doi.org/10.1101/2023.01.05.522843; this version posted January 6, 2023. The copyright holder for this preprint (which was not certified by peer review) is the author/funder. All rights reserved. No reuse allowed without permission.

tumors and their environment. Therefore, measurement of endotrophin after prostate massage might be used to investigate the relationship between PPAT abundance/ECM remodeling and PCa progression in large cohort of patients including those undergoing treatments other than prostatectomy. Our new and robust definition of PPAT abundance can be applied to future translational studies and, potentially, to clinical practice to improve risk stratification. At current time, the use of accepted PCa risk stratification groups based on prostate-specific antigen, clinical stagging (T stage) and Gleason score assists in clinical decision making, clinical trial design and outcomes reporting. Factors from the tumor microenvironment are not considered. Since mpMRI is now widely used prior to biopsies, dedicated clinical trials should be design to assess the interest of PPAT abundance in improving current classification. In addition, our study shows that endotrophin is a good candidate biomarker and a potential pharmacological target to dampen PCa progression. Finally, knowledge of the mechanism(s) that initiate PPAT expansion might allow clinicians to identify preventive approaches to decrease PPAT abundance in order to improve the outcome of PCa patients.

bioRxiv preprint doi: https://doi.org/10.1101/2023.01.05.522843; this version posted January 6, 2023. The copyright holder for this preprint (which was not certified by peer review) is the author/funder. All rights reserved. No reuse allowed without permission.

Materials and Methods

Patients, prostate and fat measurements

Between September 2016 and July 2021, patients with localized PCa diagnosed by prostate biopsies who were opting for RP were recruited. We excluded from the study patients with metastatic PCa (as assessed by computerized tomography and/or bone scan), and patients who had received radiotherapy, hormonal or high intensity ultrasound treatment. The study was conducted in accordance with the guidelines and with the full approval of the national ethics committee (AC-2020-4031). Written informed consent was received from participants before inclusion in the study, which was conducted in accordance with the Declaration of Helsinki principles as revised in 2000.

All the patients underwent pre-operative 1.5 T mpMRI after injection with 20 mg of butyl scopolamine (Buscopan; Boehringer-Ingelheim, Paris, France). Anatomic 3D fast spin echo T2-weighted MRI, functional diffusion-weighted MRI and dynamic contrast-enhanced MRI data were acquired. After anonymization of the mpMRI data obtained from the medical records of the patients, the PPAT and prostate volume, the subcutaneous and perirectal AT area were measured by using a semi-automated segmentation technique on contiguous 3 mm T2-weighted axial slices and Olea Sphere software (Olea medical, La Ciotat, France). The subcutaneous AT area was determined by measuring the perpendicular distance between the skin and the anterior upper border of the symphysis pubis on a selected T2-weighted axial slice where it was maximum. The perirectal AT area was determined by segmenting the fat around the rectum at the level of the apex of the prostate. (Table S1). Twenty patients who underwent MRI for suspected PCa with negative results were included in this radiological study for the measure of PPAT and prostate volume (named patients no cancer). One observer, trained by a senior experienced radiologist and blind to the clinical and pathological data, carried out all segmentations and measurements. The PPAT was segmented from the level of the prostate base to the apex (see Figure 1A) (mean 14 slices per patient). The following anatomical boundaries were used to define PPAT limits on each slice: pubic symphysis at the front, obturator muscles on the lateral sides and Denonvilliers fascia at the back (as previously described (Roumiguié et al., 2022). Baseline demographic characteristics (age and BMI), serum Prostate Specific Antigen (PSA) concentration, pathological parameters of the tumor on RP pieces including the volume of the tumor, Gleason score and ISUP group (histological score reflecting the differentiation of PCa determined by a trained pathologist according the 2016 WHO classification and ISUP recommendations), percentage of undifferentiated cancer cells (defined as the percentage of the tumor with a Gleason score greater than 4), pT (pathological T) stage and extraprostatic extension were acquired from the medical records of the patients. The clinical characteristics of the cohort is presented in Table S2. The Gleason score and ISUP group was also determined on pre-operative biopsies by a trained pathologist.

bioRxiv preprint doi: https://doi.org/10.1101/2023.01.05.522843; this version posted January 6, 2023. The copyright holder for this preprint (which was not certified by peer review) is the author/funder. All rights reserved. No reuse allowed without permission.

PPAT collection and tissue processing

PPAT from patients undergoing RP were removed and the samples were anonymized. Charred samples and those weighing < 300 mg were excluded from the study. Samples were immediately put in 50 mL tubes containing 10 mL of Dulbecco's Modified Eagle's Medium (DMEM, Thermofischer scientific, Courtaboeuf, France) and were transported to the research lab within 1 h. The samples were weighed and use for several preparations. For RT-qPCR analysis, measure of MMP9 activity and dosage of hydroxyproline content, PPAT were immediately frozen in liquid nitrogen and stored at -80°C for later use. For 3D microscopy, samples were fixed with 4% paraformaldehyde solution at room temperature (RT) for 24 h. Some of the samples were also used to isolate adipocytes and the stromal vascular fraction after collagenase digestion (see below). Finally, samples were used to prepare PPAT-conditioned medium as previously described (Roumiguié et al., 2022). Briefly, 1 g of tissue was incubated overnight in 8 mL of DMEM supplemented with 1% BSA in a humidified incubator at 37°C and with 5% CO_2 and the medium was collected after filtration through a 0.2 µM filter. The conditioned media were immediately stored in small aliquots at -80°C.

Histology and immunohistochemistry

A part of the PPAT sample was sent along with the resected tumor to the Pathology Department and both tissues were embedded in paraffin. Prior staining, PPAT or tumor sections (3 µm) were deparaffinized with xylene for 5 min, dehydrated in 100% alcohol for 5 min, and then rehydrated in running tap water for 10 min. The PPATs were stained with HE as previously described (Roumiguié et al., 2022). For Masson Trichrome staining (MAST), the tumor sections were first stained in Mayer's hemalum solution for 20 min and washed in distilled water and in ammonia water each for 30 s. Then they were stained in Ponceau S solution for 1 min and washed in distilled water. They were differentiated in 1% phosphomolybdic solution for 5 min, transferred to aniline blue solution and stained for a further 5 min. The tissues were rinsed briefly in distilled water and differentiated in 1% acetic acid solution for 4 min, then dehydrated rapidly through alcohol and cleared in xylene. Automated classical immunohistochemical (IHC) stain was performed using the Benchmark ULTRA (Roche, Ventana Medical Systems, Arizona, USA) on formalin-fixed paraffin-embedded tumor sections (3 µm). After dewaxing, tissue slides were heat pre-treated using a Cell Conditioning Buffer 1 (pH 8) (Roche Diagnostic, Meylan, France) at 98°C. The slides were blocked for endogenous peroxidase activity and incubated with primary anti-CD31 (Clone JC70, (ready to use), Roche Diagnostics, Meylan, France) or anti-CD68 (clone PGM1, dilution 1/100, Agilent Technologies, Les Ulis, France) antibody. The target was then visualized using the OptiView DAB detection kit (Roche Diagnostic, Meylan, France). The tissue slides were counterstained using hematoxylin (Roche Diagnostic, Meylan, France) for 8 min

bioRxiv preprint doi: https://doi.org/10.1101/2023.01.05.522843; this version posted January 6, 2023. The copyright holder for this preprint (which was not certified by peer review) is the author/funder. All rights reserved. No reuse allowed without permission.

followed by post-coloration using Bluing reagent for 4 min at RT (Roche Diagnostic, Meylan, France). The slides were then dehydrated (ethanol and xylene) and mounted using xylene-based mounting. Tumor staining (i.e. MAST, CD31 and CD68) was quantified on 20 images at 20x magnification taken randomly for each tumor using ImageJ (v1.56.j). Color deconvolution was applied on RGB images to extract MAST or DAB specific signals which were quantified and normalized to the tissue area determined from source images. The mean diameter of adipocytes was determined using Adiposoft software a plugin of Image J (v1.56.j) as previously described (Roumiguié et al., 2022).

Isolation of AT stromal vascular fraction (SVF) and mature adipocytes

Digestion of fresh PPAT was performed as previously described (Roumiguié et al., 2022). Briefly, PPAT were digested with 250 U/ml type I collagenase (Sigma-Aldrich, Saint-Quentin-Fallavier, France) in PBS containing 2 % BSA for 30 min at 37°C under constant shaking. The samples were filtered with a 250 µm cell strainers and the cell suspensions were then gently centrifuged for 1 min at 20 g at RT to pack adipocytes on the top layer. Floating adipocytes were collected and rinsed with KRB buffer supplemented with 1mM Hepes and 0.5% FFA free-BSA (all obtained from Sigma-Aldrich, Saint-Quentin-Fallavier, France) to obtain pure adipocyte cell suspensions that were used for proteomic analysis (see below). After removal of adipocytes, the remaining cell suspension was centrifuged at 300 g for 10 min to pellet SVF cells. Erythrocytes were lysed by incubation at RT in erythrocyte lysis buffer (155 mM NH_4Cl, 5.7 mM K2HPO4, 0.1 mM EDTA, pH 7.3) for 10 min followed by successive filtration through 100, 70, and 40 µm strainers. The viable recovered cells were washed 2 times in PBS, counted and analyzed by flow cytometry.

Flow cytometry analysis

Flow cytometry was performed as previously described with minor modifications (Estève et al., 2019). Briefly, 100 000 stromal vascular cells were incubated for 30 min at 4 °C in PBS supplemented with 0.5% BSA and 2 mM EDTA containing fluorescently labeled antibodies. Brilliant Violet 510™ anti-human CD45 (clone HI30, dilution 1/20, Biolegend, Amsterdam, The Netherlands), APC anti-human CD206 (clone 19.2, dilution 1/10, BD Biosciences, Le Pont de Claix, France) and PE-Vio® 770 anti-human CD14 (clone TÜK4, dilution 1/50, Miltenyi Biotec, Paris, France) antibodies were used for macrophages phenotyping. PerCP anti-human CD34 (Clone 8G12, dilution 1/20, BD Biosciences, Le Pont de Claix, France), BV450 anti-human CD31 (Clone WM59, dilution 1/20, BD Biosciences, Le Pont de Claix, France), PE anti-human MSCA1 (Clone W8B2, dilution 1/10, Miltenyi Biotec, Paris, France), APC anti-human CD271 (Clone ME20.4-1.H4, dilution 1/10, Miltenyi Biotec, Paris, France) and Brilliant Violet 510™ anti-human CD45 (clone HI30, dilution 1/20, Biolegend, Amsterdam, The Netherlands) antibodies

bioRxiv preprint doi: https://doi.org/10.1101/2023.01.05.522843; this version posted January 6, 2023. The copyright holder for this preprint (which was not certified by peer review) is the author/funder. All rights reserved. No reuse allowed without permission.

were used for progenitor cell subset phenotyping. Brilliant Violet 510™ anti-human CD45 (clone HI30, dilution 1/20, Biolegend, Amsterdam, the Netherlands), Brilliant Violet 450 anti-human CD3 (Clone UCHT1, dilution 1/20, BD Biosciences, Le Pont de Claix, France), FITC anti-human CD4 (Clone RPA-T4, dilution 1/20, BD Biosciences, Le Pont de Claix, France), PerCP anti-human CD8 (Clone SK1, dilution 1/10, BD Biosciences, Le Pont de Claix, France) and APC anti-human CD25 (Clone 2A3, dilution 1/10, BD Biosciences, Le Pont de Claix, France) antibodies were used for lymphocyte phenotyping. As control, a panel of appropriate isotype antibodies was used. The labeled cells were washed with PBS and analyzed in a FACS Canto™ II flow cytometer using Diva Pro software (BD Biosciences, Le Pont de Claix, France). Cell debris, dead cells and doublets were excluded based on scatter signals. Compensation was established using compensation particles set (BD Biosciences, Le Pont de Claix, France) and single staining and flow cytometer calibration was performed with rainbow calibration particles (BD Biosciences, Le Pont de Claix, France).

ELISA assays

As previously described (Roumiguié et al., 2022), a panel of secreted adipokines were quantified in PPAT-CM with an ELISA kit (LXSAHM-08; R&D Systems, Noyal Châtillon sur Seiche, France) and a mixture of antibodies against Adiponectin/Acrp30, IL-6, IL-1β, Leptin, MCP1 and TNFα, according to the protocol provided by the manufacturer. Endotrophin was quantified in plasma and urine collected after prostate massage using homemade ELISA as previously described (Bu et al., 2019).

RNA extraction and RT-qPCR

For RNA extraction, 100 mg of frozen tissue was mixed with 500 µl QIAzol™ lysis reagent (Qiagen, Courtaboeuf, France) and homogenized with a Precellys ® tissue homogenizer (2 cycles of 45 seconds at 7500 rpm at 4°C) using the Cryolys cooling system. The tissue homogenates were centrifuged for 1 min at 5000 g at RT. The lipid-containing surface layer was then removed and 350µl of chloroform was added. The organic and aqueous phases were separated by centrifugation (10 min at 5000 g at RT). The upper phase, containing RNA, was recovered and mixed with ethanol for RNA extraction using the Qiagen RNeasy mini kit as described by the manufacturer (Qiagen, Courtaboeuf, France). The RNA concentration was determined with a Nanodrop 2000 spectrophotometer at a wavelength of 260nm. cDNA were reverse transcribed from 250 ng of purified RNA by using the RevertAid H Minus First Strand cDNA synthesis kit (Thermo Fisher Scientific, Illkirch-Graffenstaden, France) with hexamer random primers according to the supplier's recommendations. Gene expression was quantified by RT-qPCR on 6.25 ng of cDNA with TaqMan primers (the primers used are listed in Table S7), Thermo Fisher Scientific, Illkirch-Graffenstaden, France) and Fast Advanced TaqMan Master Mix (Thermo Fisher

bioRxiv preprint doi: https://doi.org/10.1101/2023.01.05.522843; this version posted January 6, 2023. The copyright holder for this preprint (which was not certified by peer review) is the author/funder. All rights reserved. No reuse allowed without permission.

Scientific, Illkirch-Graffenstaden, France) in a final volume of 20 µl with a CFX96real time PCR system (Bio-Rad). Results were normalized to the amount of 18S rRNA.

Sample preparation for proteomic analysis

Isolated adipocytes obtained as described above were washed in PBS three times and proteins were extracted from 500 µl of adipocyte with 500 µl 1X RIPA buffer (Sigma-Aldrich) supplemented with complete antiprotease tablet (Roche) with a precellys tissue homogenizer and Ceramic beads (CK14) with 2 cycles of 45 s at 7500rpm at 4°C. The samples were then centrifuged 10 min at 10 000 g at RT to separate and aggregate the lipids at the top layer from which they were removed. The extract was recovered without the top layer containing the lipids and centrifuged again 10 min at 10 000 g at 4°C. Protein concentration was determined using DC protein assay kit (Biorad, Biorad, Marnes-la-Coquette, France) following manufacturer instructions. 40µg of proteins was digested for proteomic characterization by mass spectrometry using the S-Trap™ micro spin column (ProtiFi, NY USA).

LC-MS/MS analysis.

Tryptic peptides were resuspended in 40 µl of 2% acetonitrile and 0.05% trifluoroacetic acid and analyzed by nano-liquid chromatography using an UltiMate 3000 system (NCS-3500RS Nano/Cap System; Thermo Fisher Scientific) coupled to an Orbitrap Q Exactive HF-X mass spectrometer (Thermo Fisher Scientific). Peptides were separated on an Acclaim PepMap C18 column (id 75 µm, length 50 cm, particle size 2 µm, Thermo Fisher Scientific) using a 10%-45% gradient of solvent B (80% acetonitrile, 0.2% formic acid), over 120 min (solvent A: 5% acetonitrile, 0.2% formic acid). The mass spectrometer was operated in data-dependent acquisition mode with the Xcalibur software.

Bioinformatic MS data analysis: Acquired MS and MS/MS data were searched with Mascot (version 2.6.1, http://matrixscience.com) against the Human UniProtKB database (Swiss-Prot/TrEmbl, 556,568 entries). Cysteine carbamidomethylation was set as a fixed modification. Methionine oxidation and acetylation of protein N-terminus were set as variable modification. Up to two missed trypsin/P cleavages were allowed. Mass tolerances in MS and MS/MS were set to 10 ppm and 0.8 Da, respectively.

Proline software (version 1.6, http://proline.profiproteomics.fr/) was used for the validation of identifications and the label-free quantification of identified proteins (Bouyssié et al., 2020). Mascot identification results were imported into Proline. Search results were validated through a false-discovery rate (FDR) set to 1% at protein and peptide-sequence match level. Proteins with a p-value < 0.05 and a ratio of average normalized area < 0.5 and > 2 were considered significant. Volcano plots were drawn to visualize significant protein abundance variations between two conditions control and assay.

bioRxiv preprint doi: https://doi.org/10.1101/2023.01.05.522843; this version posted January 6, 2023. The copyright holder for this preprint (which was not certified by peer review) is the author/funder. All rights reserved. No reuse allowed without permission.

They represent log10 (p-value) according to the log2 ratio. Label free quantification intensities were normalized between samples with the function "NormalizeBetweenArrays" from limma package (v3.40.6) in R (v3.6). Differential analysis was computed with limma package from Bioconductor. Principal component analysis was performed with R (v3.6) and FactoMineR package (v2.4). Go term enrichment analysis was performed with Molecular signature database on differentially represented proteins (V7.4 MSigDB). The mass spectrometry proteomics data have been deposited to the ProteomeXchange Consortium via the PRIDE partner repository with the dataset identifier PXD038514. Reviewer account details: Username: reviewer_pxd038514@ebi.ac.uk; Password: 5QSTgkLK.

3D confocal microscopy and quantification

For immunofluorescence staining, PPAT (250mg) were saturated and permeabilized with PBS supplemented with 3 % BSA and 0.2 % Triton X100 (Sigma-Aldrich, Saint-Quentin-Fallavier, France) for 1 h. Tissues were then incubated overnight at 4°C with the following primary antibodies diluted in PBS 3% BSA 0.2% Triton X100: anti-β-Tubulin (clone 2A1A9, dilution 1/200, Abcam, Cambridge, UK), anti-YAP1 (clone D8H1X, dilution 1/200, Cell Signaling Technology, Leiden, The Netherlands), Anti-Pan Collagen VI (clone 3C4, dilution 1/200, Millipore, Guyancourt, France) and serum anti-human ETP (Bu et al., 2019) (dilution 1/100) antibodies. Tissues were washed 5 times with PBS - 0.05% Tween for 10 min. Then, tissues were incubated with secondary antibodies coupled with fluorescent dye (dilution 1/800, Biotium, Fremont, CA, USA) according to the species in which the primary antibodies were produced for 3h at RT and with or without rhodamine-phalloidin (dilution 1/200, Thermofisher, Waltham, MA, USA) diluted in PBS, 3% BSA and 0.2% Triton X100. Tissues were washed 5 times with PBS 0.05% Tween for 10 min. Nuclei were stained with Hoechst 33342 (dilution 1/1000, Invitrogen, Villebon sur Yvette, France) for 30 min and after 3 washes in PBS Z stack images were acquired using LSM710 confocal microscope and 40X objective. For Fluorescent Collagen Hydridizing Peptides (F-CHP, Cat@FLU-300, Clinisciences, Nanterre,France), fixed AT were incubated with 20µM of F-CHP overnight at 4° C. Tissue were rinsed with PBS 5 times for 5-10 min. Z stack images were acquired using LSM710 confocal microscope and 40X objective. Staining were quantified with Imaris software (v9.2). Briefly, after segmentation and thresholding of the staining of interest, volumes were rendered with the surface module of Imaris. Extracted statistics were normalized to the volume of the tissue determined with the autofluorescence of the tissue.

For Picrosirius Red, fixed AT were incubated for 3 h in Picrosirius Red solution (1 g/L Sirius red in 1.3% picric acid). After two washes in acidified water followed by fixation and dehydration steps in 100% ethanol, images were acquired with a confocal microscope (LSM710, Zeiss International, Oberkochen, Germany) equipped with a 40 oil-immersion inverted objective with a numerical aperture of 1.3. The samples were excited at 560 nm, and fluorescence emission was collected above 580 nm. Pinhole was

bioRxiv preprint doi: https://doi.org/10.1101/2023.01.05.522843; this version posted January 6, 2023. The copyright holder for this preprint (which was not certified by peer review) is the author/funder. All rights reserved. No reuse allowed without permission.

setup at 0.7 Airy (ZEN imaging software; Zeiss International) to increase resolution. Three-dimensional reconstructions and analyses of collagen fiber organization were performed with Imaris software and the filament tracer module. The data generated were normalized to the tissue volume obtained after tissue surface reconstruction with Imaris (v9.6) (Bitplane, Gometz la Ville, France).

Hydroxyproline quantification

Fragments of PPAT of about 100 mg were weighed precisely, placed in 500 µl deionized water in a Precellys® 2mL Soft Tissue homogenizing Ceramic beads Kit (CK14) (Ozyme, Saint-Cyr-l'École, France) and extracted by using the Precellys® tissue homogenizer with 2 cycles of 45 seconds at 7500 rpm at RT. Samples were then centrifuged for 10 min at 5000 g at RT to remove lipids floating on the top layer by pipetting. Lipid-free supernatants were vortex mixed, 150 µl were mixed with an equal volume of 10 M NaOH and heated at 105°C for 1 hour to fully digest collagens. The reaction was stopped by adding 150 µl of 10M HCl. Hydroxyproline was quantified in duplicate by using the Hydroxyproline Assay Kit (Perchlorate-Free; Milpitas, CA, USA) as recommended by the supplier and normalized to the precise tissue weight initially digested.

MMP9 activity

For protein extraction, 100-250 mg of frozen tissues were incubated with 400 µl of RIPA lysis buffer (Sigma-Aldrich, Saint-Quentin-Fallavier, France). Proteins were extracted using the Precellys ® tissue homogenizer and Soft Tissue homogenizing Ceramic beads (CK14) with 2 cycles of 45 seconds at 7500 rpm at RT. The samples were then centrifuged 10 min at 5000 g at RT to separate and aggregate the lipids on the top layer. The lipid-free phase was recovered, sonicated and centrifuged again 10 min at 10 000 g at 4°C. Protein concentration was quantified with DC protein assays (Bio Rad, Marnes-la-Coquette, France). Concentration of active MMP9 on 200µg of total proteins lysate was quantified by using a Human Active MMP-9 Fluorokine E assay kit (F9M00; R&D Systems, Noyal Châtillon sur Seiche, France) according to the protocol provided by the manufacturer. Fluorescence was quantified using FLX800 fluorimeter with an excitation wavelength set to 340nm and an emission wavelength set to 405nm.

Statistics

Univariate statistical analysis of clinical data was performed using ANOVA for continuous variables or using Chi square test for qualitative variables with Prism (v5.04). Linear regression was computed with Prism v5.04 and residuals were calculated according to the fitted linear model. Multivariate analysis was performed by multiple logistic regression using the glm function from R (v3.6) to predict patients having an ISUP score above or equal to 3. For experimental data, statistical analysis was performed

bioRxiv preprint doi: https://doi.org/10.1101/2023.01.05.522843; this version posted January 6, 2023. The copyright holder for this preprint (which was not certified by peer review) is the author/funder. All rights reserved. No reuse allowed without permission.

using Student T test after testing normality distribution using Kolgomorov-Smirnov test for comparison between two groups or with ANOVA followed by test for linear trends between 3 groups. Statistical differences were considered as significant if the p-value was below 0.05.

bioRxiv preprint doi: https://doi.org/10.1101/2023.01.05.522843; this version posted January 6, 2023. The copyright holder for this preprint (which was not certified by peer review) is the author/funder. All rights reserved. No reuse allowed without permission.

Acknowledgements

This work benefited from the Toulouse Réseau Imagerie (TRI)-RIO Optical Imaging Platform at the Institute of Pharmacology and Structural Biology (Genotoul, Toulouse, France). We acknowledge Life Science Editors for professional scientific editing during the preparation of the manuscript.

This study was supported by the Ligue Nationale Contre le Cancer (Équipe Labélisée), the French National Cancer Institute (INCA PL-BIO 2016-176 to AB, BM, PV, and CM), by the Fondation Toulouse Cancer Santé (to AB, BM, OBS, PV and CM) and by the Fondation ARC (Association de Recherche contre le Cancer) Programmes Labelisés 2016 (to AB, PV and CM). The work was also funded in part by the French Ministry of Research with the Investissement d'Avenir Infrastructures Nationales en Biologie et Santé program (ProFI, Proteomics French Infrastructure project, ANR-10-INBS-08) (to OBS). DE received a post-doctoral fellowship from the Fondation pour La Recherche Médicale (SPF201809007124).

bioRxiv preprint doi: https://doi.org/10.1101/2023.01.05.522843; this version posted January 6, 2023. The copyright holder for this preprint (which was not certified by peer review) is the author/funder. All rights reserved. No reuse allowed without permission.

References

Bouyssié, D., A.-M. Hesse, E. Mouton-Barbosa, M. Rompais, C. Macron, C. Carapito, A. Gonzalez de Peredo, Y. Couté, V. Dupierris, A. Burel, J.-P. Menetrey, A. Kalaitzakis, J. Poisat, A. Romdhani, O. Burlet-Schiltz, S. Cianférani, J. Garin, and C. Bruley. 2020. Proline: an efficient and user-friendly software suite for large-scale proteomics. *Bioinformatics*. 36:3148–3155. doi:10.1093/bioinformatics/btaa118.

Bu, D., C. Crewe, C.M. Kusminski, R. Gordillo, A.L. Ghaben, M. Kim, J. Park, H. Deng, W. Xiong, X.Z. Liu, P.E. Lønning, N. Halberg, A. Rios, Y. Chang, A. Gonzalez, N. Zhang, Z. An, and P.E. Scherer. 2019. Human endotrophin as a driver of malignant tumor growth. *JCI Insight*. 4. doi:10.1172/jci.insight.125094.

Cao, Y., and J. Ma. 2011. Body mass index, prostate cancer-specific mortality, and biochemical recurrence: A systematic review and meta-analysis. *Cancer Prevention Research*. 4:486–501. doi:10.1158/1940-6207.CAPR-10-0229.

Cescon, M., F. Gattazzo, P. Chen, and P. Bonaldo. 2015. Collagen VI at a glance. *Journal of Cell Science*. 128:3525–3531. doi:10.1242/jcs.169748.

Chun, T.H., M. Inoue, H. Morisaki, I. Yamanaka, Y. Miyamoto, T. Okamura, K. Sato-Kusubata, and S.J. Weiss. 2010. Genetic link between obesity and MMP14-dependent adipogenic collagen turnover. *Diabetes*. 59:2484–2494. doi:10.2337/db10-0073.

Costello, A.J. 2020. Considering the role of radical prostatectomy in 21st century prostate cancer care. *Nature Reviews Urology*. 17:177–188. doi:10.1038/s41585-020-0287-y.

Dahran, N., M. Szewczyk-Bieda, S. Vinnicombe, S. Fleming, and G. Nabi. 2019. Periprostatic fat adipokine expression is correlated with prostate cancer aggressiveness in men undergoing radical prostatectomy for clinically localized disease. *BJU International*. 123:985–994. doi:10.1111/bju.14469.

Dahran, N., M. Szewczyk-Bieda, C. Wei, S. Vinnicombe, and G. Nabi. 2017. Normalized periprostatic fat MRI measurements can predict prostate cancer aggressiveness in men undergoing radical prostatectomy for clinically localised disease article. *Scientific Reports*. 7. doi:10.1038/s41598-017-04951-8.

Dupont, S., L. Morsut, M. Aragona, E. Enzo, S. Giulitti, M. Cordenonsi, F. Zanconato, J. Le Digabel, M. Forcato, S. Bicciato, N. Elvassore, and S. Piccolo. 2011. Role of YAP/TAZ in mechanotransduction. *Nature*. 474:179–184. doi:10.1038/nature10137.

Estève, D., N. Boulet, C. Belles, A. Zakaroff-Girard, P. Decaunes, A. Briot, Y. Veeranagouda, M. Didier, A. Remaury, J.C. Guillemot, S. Ledoux, C. Dani, A. Bouloumié, and J. Galitzky. 2019. Lobular architecture of human adipose tissue defines the niche and fate of progenitor cells. *Nature Communications*. 10. doi:10.1038/s41467-019-09992-3.

Estève, D., M. Roumiguié, C. Manceau, D. Milhas, and C. Muller. 2020. Periprostatic adipose tissue: A heavy player in prostate cancer progression. *Current Opinion in Endocrine and Metabolic Research*. 10:29–35. doi:10.1016/j.coemr.2020.02.007.

Fenton, A., M.D. Jesky, C.J. Ferro, J. Sørensen, M.A. Karsdal, P. Cockwell, and F. Genovese. 2017. Serum endotrophin, a type VI collagen cleavage product, is associated with increased mortality in chronic kidney disease. *PLoS ONE*. 12. doi:10.1371/journal.pone.0175200.

Frühbeck, G., V. Catalán, A. Rodríguez, B. Ramírez, S. Becerril, J. Salvador, I. Colina, and J. Gómez-Ambrosi. 2019. Adiponectin-leptin ratio is a functional biomarker of adipose tissue inflammation. *Nutrients*. 11. doi:10.3390/nu11020454.

Fujita, K., and N. Nonomura. 2018. Urinary biomarkers of prostate cancer. *International Journal of Urology*. 25:770–779. doi:10.1111/iju.13734.

Funcke, J.B., and P.E. Scherer. 2019. Beyond adiponectin and leptin: Adipose tissue-derived mediators of inter-organ communication. *Journal of Lipid Research*. 60:1648–1697. doi:10.1194/jlr.R094060.

Gesta, S., K. Lolmède, D. Daviaud, M. Berlan, A. Bouloumié, M. Lafontan, P. Valet, and J.S. Saulnier-Blache. 2003. Culture of Human Adipose Tissue Explants Leads to Profound Alteration of Adipocyte Gene Expression. *Horm Metab Res*. 35:158–163. doi:10.1055/s-2003-39070.

bioRxiv preprint doi: https://doi.org/10.1101/2023.01.05.522843; this version posted January 6, 2023. The copyright holder for this preprint (which was not certified by peer review) is the author/funder. All rights reserved. No reuse allowed without permission.

Gregg, J.R., D.S. Surasi, A. Childs, N. Moll, J.F. Ward, J. Kim, C.R. Daniel, C. Logothetis, T. Bathala, and J.W. Davis. 2021. The Association of Periprostatic Fat and Grade Group Progression in Men with Localized Prostate Cancer on Active Surveillance. *The Journal of urology*. 205:122–128. doi:10.1097/JU.0000000000001321.

Gucalp, A., N.M. Iyengar, X.K. Zhou, D.D. Giri, D.J. Falcone, H. Wang, S. Williams, M.D. Krasne, I. Yaghnam, B. Kunzel, P.G. Morris, L.W. Jones, M. Pollak, V.P. Laudone, C.A. Hudis, H.I. Scher, P.T. Scardino, J.A. Eastham, and A.J. Dannenberg. 2017. Periprostatic adipose inflammation is associated with high-grade prostate cancer. *Prostate Cancer and Prostatic Diseases*. 20:418–423. doi:10.1038/pcan.2017.31.

Harrison, S., K. Tilling, E.L. Turner, R.M. Martin, R. Lennon, J.A. Lane, J.L. Donovan, F.C. Hamdy, D.E. Neal, J.L.H.R. Bosch, and H.E. Jones. 2020. Systematic review and meta-analysis of the associations between body mass index, prostate cancer, advanced prostate cancer, and prostate-specific antigen. *Cancer Causes and Control*. 31:431–449. doi:10.1007/s10552-020-01291-3.

Huang, H., S. Chen, W. Li, P. Bai, X. Wu, and J. Xing. 2019. Periprostatic Fat Thickness on MRI is an Independent Predictor of Time to Castration-resistant Prostate Cancer in Chinese Patients With Newly Diagnosed Prostate Cancer Treated With Androgen Deprivation Therapy. *Clinical Genitourinary Cancer*. 17:e1036–e1047. doi:10.1016/j.clgc.2019.06.001.

Hwang, J., Y. Huang, T.J. Burwell, N.C. Peterson, J. Connor, S.J. Weiss, S.M. Yu, and Y. Li. 2017. In Situ Imaging of Tissue Remodeling with Collagen Hybridizing Peptides. *ACS Nano*. 11:9825–9835. doi:10.1021/acsnano.7b03150.

Ichikawa, T., M. Kita, T.S. Matsui, A.I. Nagasato, T. Araki, S.H. Chiang, T. Sezaki, Y. Kimura, K. Ueda, S. Deguchi, A.R. Saltiel, and N. Kioka. 2017. Vinexin family (SORBS) proteins play different roles in stiffnesssensing and contractile force generation. *Journal of Cell Science*. 130:3517–3531. doi:10.1242/jcs.200691.

Jo, W., M. Kim, J. Oh, C.-S. Kim, C. Park, S. Yoon, C. Lee, S. Kim, D. Nam, and J. Park. 2022. MicroRNA-29 Ameliorates Fibro-Inflammation and Insulin Resistance in HIF1α-Deficient Obese Adipose Tissue by Inhibiting Endotrophin Generation. *Diabetes*. 71:1746–1762. doi:10.2337/db21-0801.

Kapoor, J., B. Namdarian, J. Pedersen, C. Hovens, D. Moon, J. Peters, A.J. Costello, P. Ruljancich, and N.M. Corcoran. 2013. Extraprostatic extension into periprostatic fat is a more important determinant of prostate cancer recurrence than an invasive phenotype. *Journal of Urology*. 190:2061–2067. doi:10.1016/j.juro.2013.06.050.

Karastergiou, K., S.R. Smith, A.S. Greenberg, and S.K. Fried. 2012. Sex differences in human adipose tissues - The biology of pear shape. *Biology of Sex Differences*. 3. doi:10.1186/2042-6410-3-13.

Khan, T., E.S. Muise, P. Iyengar, Z. V. Wang, M. Chandalia, N. Abate, B.B. Zhang, P. Bonaldo, S. Chua, and P.E. Scherer. 2009. Metabolic Dysregulation and Adipose Tissue Fibrosis: Role of Collagen VI. *Molecular and Cellular Biology*. 29:1575–1591. doi:10.1128/mcb.01300-08.

Lamandé, S.R., M. Mörgelin, N.E. Adams, C. Selan, and J.M. Allen. 2006. The C5 domain of the collagen VI α3(VI) chain is critical for extracellular microfibril formation and is present in the extracellular matrix of cultured cells. *Journal of Biological Chemistry*. 281:16607–16614. doi:10.1074/jbc.M510192200.

Laurent, V., A. Guérard, C. Mazerolles, S. Le Gonidec, A. Toulet, L. Nieto, F. Zaidi, B. Majed, D. Garandeau, Y. Socrier, M. Golzio, T. Cadoudal, K. Chaoui, C. Dray, B. Monsarrat, O. Schiltz, Y.Y. Wang, B. Couderc, P. Valet, B. Malavaud, and C. Muller. 2016. Periprostatic adipocytes act as a driving force for prostate cancer progression in obesity. *Nature Communications*. 7. doi:10.1038/ncomms10230.

Laurent, V., A. Toulet, C. Attané, D. Milhas, S. Dauvillier, F. Zaidi, E. Clement, M. Cinato, S. Le Gonidec, A. Guérard, C. Lehuédé, D. Garandeau, L. Nieto, E. Renaud-Gabardos, A.C. Prats, P. Valet, B. Malavaud, and C. Muller. 2019. Periprostatic adipose tissue favors prostate cancer cell invasion in an obesity-dependent manner: Role of oxidative stress. *Molecular Cancer Research*. 17:821–835. doi:10.1158/1541-7786.MCR-18-0748.

bioRxiv preprint doi: https://doi.org/10.1101/2023.01.05.522843; this version posted January 6, 2023. The copyright holder for this preprint (which was not certified by peer review) is the author/funder. All rights reserved. No reuse allowed without permission.

Leeming, D.J., S.H. Nielsen, R. Vongsuvanh, P. Uchila, M.J. Nielsen, A.L. Reese-Petersen, D. van der Poorten, M. Eslam, D. Schuppan, M.A. Karsdal, and J. George. 2021. Endotrophin, a pro-peptide of Type VI collagen, is a biomarker of survival in cirrhotic patients with hepatocellular carcinoma. *Hepatic Oncology*. 8. doi:10.2217/hep-2020-0030.

Li, X., Y. Zhao, C. Chen, L. Yang, H. Lee, Z. Wang, N. Zhang, M.G. Kolonin, Z. An, X. Ge, P.E. Scherer, and K. Sun. 2020. Critical Role of Matrix Metalloproteinase 14 in Adipose Tissue Remodeling during Obesity. *Molecular and Cellular Biology*. 40. doi:10.1128/MCB.00564-19.

Loeb, S., A. Kettermann, H.B. Carter, L. Ferrucci, E.J. Metter, and P.C. Walsh. 2009. Prostate Volume Changes Over Time: Results From the Baltimore Longitudinal Study of Aging. *Journal of Urology*. 182:1458–1462. doi:10.1016/j.juro.2009.06.047.

Ma, B., H. Cheng, R. Gao, C. Mu, L. Chen, S. Wu, Q. Chen, and Y. Zhu. 2016. Zyxin-Siah2-Lats2 axis mediates cooperation between Hippo and TGF-β signalling pathways. *Nature Communications*. 7. doi:10.1038/ncomms11123.

Motrescu, E.R., S. Blaise, N. Etique, N. Messaddeq, M.P. Chenard, I. Stoll, C. Tomasetto, and M.C. Rio. 2008. Matrix metalloproteinase-11/stromelysin-3 exhibits collagenolytic function against collagen VI under normal and malignant conditions. *Oncogene*. 27:6347–6355. doi:10.1038/onc.2008.218.

Nassar, Z.D., A.T. Aref, D. Miladinovic, C.Y. Mah, G.V. Raj, A.J. Hoy, and L.M. Butler. 2018. Peri-prostatic adipose tissue: the metabolic microenvironment of prostate cancer. *BJU International*. 121:9–21. doi:10.1111/bju.14173.

Oliveira, D.S.M., S. Dzinic, A.I. Bonfil, A.D. Saliganan, S. Sheng, and R.D. Bonfil. 2016. The mouse prostate: A basic anatomical and histological guideline. *Bosnian Journal of Basic Medical Sciences*. 16:8–13. doi:10.17305/bjbms.2016.917.

Ouchi, N., J.L. Parker, J.J. Lugus, and K. Walsh. 2011. Adipokines in inflammation and metabolic disease. *Nature Reviews Immunology*. 11:85–97. doi:10.1038/nri2921.

Park, J., T.S. Morley, and P.E. Scherer. 2013. Inhibition of endotrophin, a cleavage product of collagen VI, confers cisplatin sensitivity to tumours. *EMBO Molecular Medicine*. 5:935–948. doi:10.1002/emmm.201202006.

Park, J., and P.E. Scherer. 2012. Adipocyte-derived endotrophin promotes malignant tumor progression. *Journal of Clinical Investigation*. 122:4243–4256. doi:10.1172/JCI63930.

Pellegrinelli, V., S. Carobbio, and A. Vidal-Puig. 2016. Adipose tissue plasticity: how fat depots respond differently to pathophysiological cues. *Diabetologia*. 59:1075–1088. doi:10.1007/s00125-016-3933-4.

Pernar, C.H., E.M. Ebot, K.M. Wilson, and L.A. Mucci. 2018. The epidemiology of prostate cancer. *Cold Spring Harbor Perspectives in Medicine*. 8. doi:10.1101/CSHPERSPECT.A030361.

Rasmussen, D.G.K., A. Fenton, M. Jesky, C. Ferro, P. Boor, M. Tepel, M.A. Karsdal, F. Genovese, and P. Cockwell. 2017. Urinary endotrophin predicts disease progression in patients with chronic kidney disease. *Scientific Reports*. 7. doi:10.1038/s41598-017-17470-3.

Rausch, V., and C.G. Hansen. 2020. The Hippo Pathway, YAP/TAZ, and the Plasma Membrane. *Trends in Cell Biology*. 30:32–48. doi:10.1016/j.tcb.2019.10.005.

Ricard-Blum, S., and R. Salza. 2014. Matricryptins and matrikines: Biologically active fragments of the extracellular matrix. *Experimental Dermatology*. 23:457–463. doi:10.1111/exd.12435.

Van Roermund, J.G.H., K.A. Hinnen, C.J. Tolman, G.H. Bol, J.A. Witjes, J.L.H.R. Bosch, L.A. Kiemeney, and M. Van Vulpen. 2011. Periprostatic fat correlates with tumour aggressiveness in prostate cancer patients. *BJU International*. 107:1775–1779. doi:10.1111/j.1464-410X.2010.09811.x.

Roumiguié, M., D. Estève, C. Manceau, A. Toulet, J. Gilleron, C. Belles, Y. Jia, C. Houël, S. Pericart, S. LeGonidec, P. Valet, M. Cormont, J.-F. Tanti, B. Malavaud, A. Bouloumié, D. Milhas, and C. Muller. 2022. Periprostatic adipose tissue displays a chronic hypoxic state that limits its expandability. *The American Journal of Pathology*. doi:10.1016/j.ajpath.2022.03.008.

bioRxiv preprint doi: https://doi.org/10.1101/2023.01.05.522843; this version posted January 6, 2023. The copyright holder for this preprint (which was not certified by peer review) is the author/funder. All rights reserved. No reuse allowed without permission.

Salji, M., J. Hendry, A. Patel, I. Ahmad, C. Nixon, and H.Y. Leung. 2018. Peri-prostatic Fat Volume Measurement as a Predictive Tool for Castration Resistance in Advanced Prostate Cancer. *European Urology Focus*. 4:858–866. doi:10.1016/j.euf.2017.01.019.

Sasaki, T., Y. Sugino, M. Kato, K. Nishikawa, and H. Kanda. 2020. Pre-treatment ratio of periprostatic to subcutaneous fat thickness on MRI is an independent survival predictor in hormone-naïve men with advanced prostate cancer. *International Journal of Clinical Oncology*. 25:370–376. doi:10.1007/s10147-019-01559-y.

Shiao, S.L., G.C.Y. Chu, and L.W.K. Chung. 2016. Regulation of prostate cancer progression by the tumor microenvironment. *Cancer Letters*. 380:340–348. doi:10.1016/j.canlet.2015.12.022.

Sun, K., J. Park, O.T. Gupta, W.L. Holland, P. Auerbach, N. Zhang, R. Goncalves Marangoni, S.M. Nicoloro, M.P. Czech, J. Varga, T. Ploug, Z. An, and P.E. Scherer. 2014. Endotrophin triggers adipose tissue fibrosis and metabolic dysfunction. *Nature communications*. 5:3485. doi:10.1038/ncomms4485.

Sun, K., J. Tordjman, K. Clément, and P.E. Scherer. 2013. Fibrosis and adipose tissue dysfunction. *Cell Metabolism*. 18:470–477. doi:10.1016/j.cmet.2013.06.016.

Tan, W.P., C. Lin, M. Chen, and L.A. Deane. 2016. Periprostatic Fat: A Risk Factor for Prostate Cancer? *Urology*. 98:107–112. doi:10.1016/j.urology.2016.07.042.

Tang, Q., B. Cheng, R. Dai, and R. Wang. 2021. The Role of Androgen Receptor in Cross Talk Between Stromal Cells and Prostate Cancer Epithelial Cells. *Frontiers in Cell and Developmental Biology*. 9. doi:10.3389/fcell.2021.729498.

Veidal, S.S., M.A. Karsdal, E. Vassiliadis, A. Nawrocki, M.R. Larsen, Q.H.T. Nguyen, P. Hägglund, Y. Luo, Q. Zheng, B. Vainer, and D.J. Leeming. 2011. MMP mediated degradation of type VI collagen is highly associated with liver Fibrosis - Identification and validation of a novel biochemical marker assay. *PLoS ONE*. 6. doi:10.1371/journal.pone.0024753.

Wang, J., and W. Pan. 2020. The biological role of the collagen alpha-3 (Vi) chain and its cleaved c5 domain fragment endotrophin in cancer. *OncoTargets and Therapy*. 13:5779–5793. doi:10.2147/OTT.S256654.

Williams, L., T. Layton, N. Yang, M. Feldmann, and J. Nanchahal. 2022. Collagen VI as a driver and disease biomarker in human fibrosis. *FEBS Journal*. 289:3603–3629. doi:10.1111/febs.16039.

Woo, S., J.Y. eon Cho, S.Y. oun Kim, and S.H. yup Kim. 2015. Periprostatic fat thickness on MRI: correlation with Gleason score in prostate cancer. *AJR. American journal of roentgenology*. 204:W43–W7. doi:10.2214/AJR.14.12689.

Zhai, L., Y. Fan, S. Sun, H. Wang, Y. Meng, S. Hu, X. Wang, W. Yu, and J. Jin. 2018. PI-RADS v2 and periprostatic fat measured on multiparametric magnetic resonance imaging can predict upgrading in radical prostatectomy pathology amongst patients with biopsy Gleason score 3 + 3 prostate cancer. *Scandinavian Journal of Urology*. 52:333–339. doi:10.1080/21681805.2018.1545799.

Zhai, T.S., L.T. Hu, W.G. Ma, X. Chen, M. Luo, L. Jin, Z. Zhou, X. Liu, Y. Kang, Y.X. Kang, J.X. Zhang, H. Liu, J.Y. Lu, X.D. Yao, and L. Ye. 2021. Peri-prostatic adipose tissue measurements using MRI predict prostate cancer aggressiveness in men undergoing radical prostatectomy. *Journal of Endocrinological Investigation*. 44:287–296. doi:10.1007/s40618-020-01294-6.

Zhang, Q., L. Sun, J. Qi, Z. Yang, T. Huang, and R. Huo. 2014. Periprostatic adiposity measured on magnetic resonance imaging correlates with prostate cancer aggressiveness. *Urol J*. 11:1793–1799.

Zhao, S., C.M. Kusminski, and P.E. Scherer. 2021. Adiponectin, Leptin and Cardiovascular Disorders. *Circulation Research*. 136–149. doi:10.1161/CIRCRESAHA.120.314458.

Zwick, R.K., C.F. Guerrero-juarez, V. Horsley, V. Maksim, N. Haven, C. Biology, B. Gross, S. Cell, and N. Haven. 2019. Anatomical, physiological and functional diversity of adipose tissue. *Cell Metabolism*. 27:68–83. doi:10.1016/j.cmet.2017.12.002.Anatomical.

bioRxiv preprint doi: https://doi.org/10.1101/2023.01.05.522843; this version posted January 6, 2023. The copyright holder for this preprint (which was not certified by peer review) is the author/funder. All rights reserved. No reuse allowed without permission.

Figure legends

Figure 1: A new statistical approach to defining abundant PPAT relative to prostate volume

A) Left panel: Representative 3D projection and reconstruction of axial sections from T2-weighted mpMRI signals and regions of interest delineating the prostate (pink) and the PPAT (green); Right panel: single axial MRI sections from the base, middle, and apex of the prostate. The localization of PPAT, prostate (P) and the anatomical limits of PPAT are shown on single axial MRI section (B, Bladder; OM, Obturator Muscle; P, Prostate; PPAT, Periprostatic Adipose Tissue; PS, Pubic Symphysis; R, Rectum; SV, Seminal Vesicles; orange dotted lines indicate Denonvillier's fascia). Segmented area represents the region of interest delineating the prostate (pink) and the PPAT (green) for each single MRI section presented. **B)** Correlation between prostate weight recorded after prostatectomy and prostate volume measured on mpMRI (n=351). Linear regression was used to draw the slope of best fit and linear correlation coefficient (r^2) and P-value are indicated (p). **C)** Lack of correlation between prostate volume and the BMI of the patient (n=371); patients without PCa are indicated in red. **D)** Correlation between PPAT and prostate volume (n=371); patients without PCa are indicated in red. Linear regression was used to draw the slope of best fit and linear correlation coefficient (r^2) and P-value are indicated (p). **E)** Scatter plot of patients ranked according to PPAT abundance showing patients with low, mid and high PPAT abundance. PPAT abundance was calculated from the residual value for each patient with respect to the linear regression model in part D (n=371); patients without PCa are indicated in red. **F)** PPAT volume measured on MRI according to the abundance quartile (n=86-87 per quartile). **G)** Prostate volume of the patients in each abundance quartile (n=86-87 per quartile). **H)** BMI of the patients in each abundance quartile (n=86-87 per quartile). **I)** Distribution of patients' age in each abundance quartile (n=86-87 per quartile). Individual patient's data are indicated by dots, bars indicate means ± SEM. Statistical differences between groups were evaluated by ANOVA followed by a post-test for linear trend (*** $p < 0.001$).

Figure 2: Abundant PPAT is associated with aggressive PCa

A) Percentage of patients in the low, mid and high PPAT groups who have ISUP scores < 3 and ≥ 3. **B)** Raincloud plot of the percentage of undifferentiated cancer cells observed in prostate tumor slices from patients in the low, mid and high PPAT groups (Low, n= 88; Mid, n=176; High, n=87). **C)** Percentage of patients in the low, mid and high PPAT groups whose ISUP score was upgraded or not upgraded upon analysis of the tumors after prostatectomy. **D)** Multivariate analysis using logistic regression modelling of the effect of the indicated variables on the relative risk (odds ratio) that the PCa has an ISUP score ≥ 3 (Abundance, low, mid and high PPAT groups; Prostate, prostate volume (cm^3); Age (years); PSA, plasma PSA concentration (ng/ml); Gleason_bio, Gleason score on biopsy). **E-G)** Representative images

bioRxiv preprint doi: https://doi.org/10.1101/2023.01.05.522843; this version posted January 6, 2023. The copyright holder for this preprint (which was not certified by peer review) is the author/funder. All rights reserved. No reuse allowed without permission.

of prostate tumor slices from a patient in the 1st quartile of PPAT abundance (Low PPAT) and a patient in the 4th quartile (High PPAT) (left) after Masson's trichrome staining (E), immuno-staining for CD31 (F) and immuno-staining for CD68 (G). Immuno-stained tumor sections were counterstained with hematoxylin. Scale bars, 100µm. Quantification of the staining (right). Significant differences between groups were evaluated by Chi-square test for qualitative variables (A and C), by using ANOVA with post-test for linear trend (**p< 0.01; B) or Student's t test for quantitative variables (*p<0.05; ** p<0.01; E, F and G). Odds ratio were determined by using the multivariate logistic regression model (D).

Figure 3: PPAT expands by adipocyte hypertrophy with no associated inflammation

A) Representative images of PPAT sections stained with hematoxylin and eosin (H&E) and used to quantify adipocyte diameter in PPAT from patients in the low and high groups. The corresponding quantification mask is shown. Scale bars, 250µm. **B)** The size distribution (left panel) and mean diameters (right panel) of adipocytes in PPAT from patients in the low (n=12) and high (n=14) groups. **C)** Percentage of progenitor cells (CD45-/CD34+/CD31-) in the stroma-vascular fraction (SVF) of PPAT from patients in the low (n=8), mid (n=16) and high (n=11) groups, as quantified by flow cytometry quartile). **D-F)** Quantification of the concentration of adiponectin **(**D) and leptin (E) in the conditioned medium of PPAT from patients in the low (n=9), mid (n=9) and high (n=11) groups, and the adiponectin to leptin ratio (F). **G)** Percentage of cells in the SVF of PPAT from patients in the low (n=8), mid (n=15) and high (n=11) groups that are CD45+ leukocytes. **H**) Percentage of cells as in (G) that are low FSC/low SSC/CD45+/CD3+ T cells in the low (n=8), mid (n=15) and high (n=11) groups. **(I)** Percentage of cells as in (G) that are CD45+/CD14+ macrophages (all macrophages), CD45+/CD14+/CD206- recruited macrophages (CD206-), or CD45+/CD14+/CD206+ resident macrophages (CD206+) in the low (n=8), mid (n=15) and high (n=11) groups. All percentages in G-I were quantified by flow cytometry. **J-M)** Quantification of the concentrations of TNFα **(J)**, IL6 **(K)**, MCP1 **(L)** and IL1β **(M)** in the conditioned medium of PPAT from patients in the low, mid and high groups (n=8-10). Bars indicate means +/- SEM. Two-way ANOVA followed by Bonferroni post-test was used to analyze adipocyte diameter. Other statistical differences were evaluated by ANOVA with post-test for linear trend (*p<0.05; ** p<0.01).

Figure 4: Under-representation of mechano-sensing proteins in adipocytes from abundant PPAT

A) Principal component analysis of the proteomics datasets from adipocytes isolated from the PPAT of individual patients (each indicated by a dot and a label) in the low and high groups (n= 6-7 per group). The ellipses indicate grouping according to PPAT abundance. **B)** Volcano plot representing the log2 fold-change of the relative protein representation in the proteomics dataset and the -log10 of the p-value calculated by using limma differential expression analysis (n=6-7 per group), showing under-

bioRxiv preprint doi: https://doi.org/10.1101/2023.01.05.522843; this version posted January 6, 2023. The copyright holder for this preprint (which was not certified by peer review) is the author/funder. All rights reserved. No reuse allowed without permission.

represented (pink) and over-represented (green) proteins. **C**) Hierarchical clustering of differentially under-represented (pink) and over-represented (green) proteins in the PPAT of patients in the low (grey) and high (black) quartiles. **D)** Cellular components and biological functions of the over-represented (black) and under-represented (grey) proteins in the PPAT of patients in the high quartile, as determined by gene ontology enrichment terms. The -log10 of the q-Value are represented in x axis and the percentage of proteins that were differentially expressed in the pathways are mentioned in red on the side of each bar plot. **E)** Quantification of the indicated proteins in the PPAT of patients in the low and high quartile (n=6-7 per group) by mass spectrometry. **F)** Whole PPAT from patients in the low and high groups were stained with anti-YAP1 antibody and phalloidin (to stain actin and facilitate cell visualization) and DAPI (to stain DNA)**.** Representative maximum intensity projection of images obtained by 3D confocal microscopy are shown. Scale bars, 50 μm**. G)** Quantification of the indicated isoforms of tubulin, as in E (n=6-7 per group). **H)** Whole PPAT from patients in the low and high groups were stained with anti-ß-tubulin antibody and DAPI, as in F. **I)** Quantification of the indicated proteins, as in E (n=6-7 per group). Bars indicate means ± SEM. Statistical differences were calculated by using Student's T test. *p < 0.05; ** p< 0.01; *** p<0.001.

Figure 5: The collagen network in abundant PPAT is relatively loose

A) Whole PPAT from representative patients in the low and high groups were stained with picrosirius red to show collagen fibers, imaged in 3D by confocal microscopy (top), reconstructed in 3D (middle), and the reconstructed collagen fiber images were isolated and color-coded according to their diameter (bottom). Scale bars, 50 μm. **B-D)** Various morphometric parameters were quantified in 3D images of PPAT from patients in the low and high groups after collagen fiber reconstruction (n=9-16): total collagen volume (B), length of collagen fibers (C), and number of branches per collagen fiber (D). **E)** Quantification of hydroxyproline concentration in PPAT from patients in the low (n=18) and high groups (n=11). Bars indicate means ± SEM. Statistical differences were calculated by using Student's T test. *p < 0.05; ** p< 0.01.

Figure 6: Abundant PPAT exhibits increased collagen degradation likely by MMP9

A) Relative expression of genes encoding the indicated collagen isoforms in whole PPAT from patients in the low (n=13) and high qroups (n=11). **B)** Representative confocal images of PPAT stained with fluorescent collagen-hybridizing peptide (F-CHP). The maximum intensity projection of Z-stacked images (left panel) at low magnification and at higher magnification image (Zoom). The areas corresponding to the Zoom images are indicated by the orange dotted lines. Scale bars, 50 μm. F-CHP staining in 3D images was quantified (right panel; n=6-7). **C)** Relative expression of genes encoding the

bioRxiv preprint doi: https://doi.org/10.1101/2023.01.05.522843; this version posted January 6, 2023. The copyright holder for this preprint (which was not certified by peer review) is the author/funder. All rights reserved. No reuse allowed without permission.

indicated metalloproteinase (MMP) isoforms in PPAT from patients in the low (n=11) and high (n=10) quartiles. **D)** Relative MMP9 protein expression quantified in isolated mature adipocytes by mass spectrometry (n=6-7 per quartile). **E)** MMP9 enzyme activity in protein extracts of PPAT from patients in the low (n=13) and high quartiles (n=12). Bars indicate means ± SEM. Statistical differences were calculated by using Student's T test. *p < 0.05; *** p< 0.001.

Figure 7: COL6 remodeling is associated with high endotrophin production in abundant PPAT

A) Representative confocal images of PPAT from three patients in the low quartile (#1-3) and high quartile (#4-6) stained with an anti-collagen VI antibody that recognizes all collagen VI forms (pan collagen VI). Maximum intensity projections of Z-stacked images at low magnification are shown (left panels) and at higher magnification (Zoom). The areas corresponding to the Zoom images are indicated by the orange dotted lines. Scale bars, 50µm. **B)** Representative confocal immunofluorescence microscopy images of PPAT stained with anti-Pan collagen VI (pink) and anti-endotrophin (green) antibodies. 3D views of Z-stacked images (left). Scale bars, 50µm. Endotrophin staining was quantified on 3D images (right panel; n=8-9). **C)** ETP concentration in plasma from patients with PCa, as quantified by ELISA (Low, n= 20; Mid, n=42; High, n=20). **(D)** ETP concentration in urine from patients with PCa collected after prostate massage, as quantified by ELISA (Low, n= 17; Mid, n=32; High, n=13). Bars indicate means ± SEM. Statistical differences were calculated by using Student's T test (*p < 0.05 for B) and ANOVA with post-test for linear trend (**p<0.01 for C and D).

Figure 8: Collagen remodeling leads to inflammation-free expansion of periprostatic adipose tissue and promotes prostate cancer progression

As shown before (Roumiguié et al., 2022), PPAT exhibit a peculiar vascularization leading to chronic hypoxia and fibrosis that limits its expansion in obese individuals. To expand, collagen degradation occurs in high PPAT that exhibit hypertrophic adipocytes due to the increased expression of lipid transporters and the decreased expression of proteins involved in lipolysis, favoring lipid uptake over degradation. The decrease in ECM stiffness release the mechanical stress on adipocytes and allows the healthy expansion of high PPAT. The degradation of ECM and particularly COL VI, likely by MMP-9, contributes to the release of a matrikine, endotrophin. Endotrophin increases the aggressiveness of the adjacent PCa tumors by promoting cancer cell dedifferentiation and changes in the tumor microenvironment (increase in fibrosis, angiogenesis and macrophage infiltration). High levels of endotrophin are found in the urine of patients with abundant PPAT.

bioRxiv preprint doi: https://doi.org/10.1101/2023.01.05.522843; this version posted January 6, 2023. The copyright holder for this preprint (which was not certified by peer review) is the author/funder. All rights reserved. No reuse allowed without permission.

Legend of Supplementary Figures

Fig. S1: Subcutaneous and perirectal AT areas are correlated with BMI

Linear regression between the subcutaneous (**A,** n= 195**)** and perirectal (**B,** n=256**)** adipose tissue area measured on pre-operative mpMRI and the BMI of the patients. Linear regression was used to draw the slope of best fit and linear correlation coefficient (r^2) and P-value are indicated (p).

Fig. S2: NPFV is not an appropriate measure of PPAT abundance

A) Scatter plot of PCa patients ranked according to normalized periprostatic fat volume (NPFV) compared to PPAT abundance calculated by our model in Figure 1D (left panel), and the percentage of patients that were classified in different abundance quartiles depending on the method used to define abundance (right panel). Quartiles were defined according to NPFV ratio as low ratio (1^{st} quartile) mid ratio (2^{nd} and 3^{rd} quartiles) or high ratio (4^{th} quartile). **B-C)** Scatter plots of PPAT volume (B) and prostate volume (C) in individual patients in each quartile. Bars indicate means ± SEM. Differences between groups were determined by using ANOVA followed by Tuckey post-test. * $p< 0.05$; ** $p<0.01$; ***$p<0.001$. **D)** Multivariate analysis using logistic regression modelling of the effect of the indicated variables on the relative risk (odds ratio) that the PCa has an ISUP score ≥ 3 **(**Abundance, low, mid and high PPAT groups; Prostate, prostate volume (cm^3); Age (years); PSA, plasma PSA concentration (ng/ml); Gleason_bio, Gleason score on biopsy).

Fig. S3: Adipose progenitor cell and lymphocytes subsets are not modified according to PPAT abundance

A) Percentage of progenitor cell subsets (MSCA1+, MSCA1-/ CD271+ (CD271+) and MSCA1-/CD271- (-/-) in the stromal stromavascular fraction (SVF) of PPAT from patients in the low, mid and high groups, as quantified by flow cytometry. **B)** Percentage of lymphocytes subsets (CD4+: Cytotoxic T cell, CD8+: Helper T cell, CD4+/CD25+ Regulator T cell, CD19+: B lymphocytes) gated on the total lymphocytes (Low FSC/Low SSC/CD45+/CD3+) in the stromal vascular fraction (SVF) of PPAT from patients in the low, mid and high groups, as quantified by flow cytometry. Bars indicate means ± SEM. No statistical differences were observed by using Student's T test.

Fig. S4: Proteins involved in lipolysis and lipid uptake are under-represented and over-represented in abundant PPAT

A) Volcano plot representing the log2 fold-change of the relative protein representation in the proteomics dataset and the -log10 of the p-Value calculated by using limma differential expression analysis (n=6-7 /group), showing under-represented (red) and over-represented (green) proteins.

bioRxiv preprint doi: https://doi.org/10.1101/2023.01.05.522843; this version posted January 6, 2023. The copyright holder for this preprint (which was not certified by peer review) is the author/funder. All rights reserved. No reuse allowed without permission.

Proteins of interest are indicated by name of their genes. **B**) Scatter plot of the relative expression of *PNPLA2*, *LIPE* and *MGLL*, which encode lipolysis effectors determined by RT- qPCR, according to PPAT abundance determined by our model defined in Figure 1D (n=18). **C)** Scatter plots of the relative gene expression of *CD36*, *FABP4* and *SLC27A4*, which encode lipid transporters determined by RT-qPCR, according to PPAT abundance determined by our model defined in Fig. 1D (n=18).

Fig. S5: Absence of modifications of LOX or TIMP isoforms expression in low versus abundant PPAT. Relative expression of several genes encoding lysyl oxidase (LOX) or tissue inhibitor of metalloproteinase (TIMP) isoforms in PPAT from patients in the low and high quartiles (n=11 per quartile). Bars indicate means ± SEM. No statistical differences were observed by using Student's T test.

bioRxiv preprint doi: https://doi.org/10.1101/2023.01.05.522843; this version posted January 6, 2023. The copyright holder for this preprint (which was not certified by peer review) is the author/funder. All rights reserved. No reuse allowed without permission.

Table S1: Anthropometrical characteristics of the PCa patients

Characteristic	**N = 351**[1]
Age (years)	65 (60, 69)
BMI (kg/m²)	25.48 (24.21, 27.76)
Missing	19
PPAT volume (cm³)	43 (34, 53)
Subcutaneous AT area (cm²)	35 (28, 44)
Missing	156
Prostate volume (cm³)	44 (35, 60)
Perirectal AT area (cm²)	25.9 (22.4, 30.3)
Missing	96

[1]Data are presented as the median value with inter-quartile range (IQR) in brackets. BMI, Body mass index

bioRxiv preprint doi: https://doi.org/10.1101/2023.01.05.522843; this version posted January 6, 2023. The copyright holder for this preprint (which was not certified by peer review) is the author/funder. All rights reserved. No reuse allowed without permission.

Table S2 : Clinical and pathological characteristics of the PCa patients

Characteristic	**N = 351**[1]
PSA (ng/ml)	7.0 (5.5, 10.0)
Missing	4
Tumor Volume (cm^3)	5.8 (3.2, 9.8)
Undifferentiated cancer cells (%)	40 (20, 65)
Missing	2
ISUP	
1	14 (4.0%)
2	193 (55%)
3	123 (35%)
4	20 (5.7%)
5	1 (0.3%)
pT	
2a	10 (2.8%)
2b	22 (6.3%)
2c	148 (42%)
3a	127 (36%)
3b	44 (13%)
Extra-prostatic extension	156 (44%)
Adjuvant treatment	
No	298 (85%)
Chemotherapy	27 (7.7%)
Hormonotherapy	2 (0.6%)
Radiotherapy	24 (6.8%)
Biochemical recurrence	38 (11%)
Missing	2

[1]Data are presented as the median value with inter-quartile range (IQR) in brackets or as percentage (%) in brackets
PSA, prostate specific antigen

bioRxiv preprint doi: https://doi.org/10.1101/2023.01.05.522843; this version posted January 6, 2023. The copyright holder for this preprint (which was not certified by peer review) is the author/funder. All rights reserved. No reuse allowed without permission.

Table S3 : Clinical and pathological characteristics of the PCa patients according to PPAT abundance

Characteristic[1]	Low, N = 88	Mid, N = 176	High, N = 87	p-value
PSA (ng/ml), Median (IQR)	7.0 (5.1, 9.6)	7.0 (5.2, 9.0)	8.0 (6.1, 11.1)	0.0179[2]
(Missing)	1	3	0	
Tumor Volume (cm^3), Median (IQR)	5.1 (2.8, 9.5)	6.2 (3.3, 9.9)	6.0 (3.0, 9.9)	0.4400[2]
Gleason score on biopsies ≥ 3, n (%)	21 (24)	55 (31)	30 (34)	0.2790[3]
Missing	0	1	0	
Undifferentiated cancer cells (%), Median (IQR)	28 (10, 60)	40 (20, 70)	55 (22, 72)	0.0008[2]
(Missing)	0	2	0	
ISUP ≥ 3, n (%)	26 (30)	73 (41)	45 (52)	0.0115[3]
Upgrading, n (%)	10 (15)	30 (25)	22 (39)	0.0104[3]
Missing	21	56	30	
pT n (%)				0.2413[3]
2a or 2b	6 (6.8)	17 (9.7)	9 (10)	
2c	42 (48)	67 (38)	39 (45)	
3a	35 (40)	66 (38)	26 (30)	
3b	5 (5.7)	26 (15)	13 (15)	
Extra-prostatic extension	39 (44)	81 (46)	36 (41)	0.7752[3]

[1]Data are presented either as the median value with inter-quartile range (IQR) in brackets or percentage (%) in brackets. PSA, prostate specific antigen

Kruskal-Wallis rank sum test

[3] Pearson's Chi-squared test

bioRxiv preprint doi: https://doi.org/10.1101/2023.01.05.522843; this version posted January 6, 2023. The copyright holder for this preprint (which was not certified by peer review) is the author/funder. All rights reserved. No reuse allowed without permission.

Table S4: Clinical and pathological characteristics of the PCa patients according to NPFV

Characteristic[1]	**Low**, N = 88	**Mid**, N = 87	**High**, N = 87	**p-value**
PSA (ng/ml), Median (IQR)	7.0 (5.8, 9.8)	7.2 (5.4, 9.8)	7.0 (5.5, 9.8)	0.6948[2]
Missing	0	4	0	
Tumor Volume (cm³), Median (IQR)	6.8 (3.7, 10.6)	5.6 (3.2, 9.4)	5.8 (2.8, 9.0)	0.2857[2]
Gleason score on biopsy≥3, n (%)	24 (27)	53 (30)	29 (33)	0.6835[3]
Missing	0	1	0	
Undifferentiated cancer cells (%), Median (IQR)	38 (19, 60)	35 (16, 70)	40 (20, 68)	0.5589[2]
Missing	0	2	0	
ISUP ≥ 3, n (%)	32 (36)	73 (41)	39 (45)	0.515[3]
Upgrading, n (%)	14 (22)	34 (28)	14 (24)	0.6503[3]
Missing	24	54	29	
pT, n (%)				0.6643[3]
2a or 2b	8 (9.1)	16 (9.1)	8 (9.2)	
2c	39 (44)	74 (42)	35 (40)	
3a	33 (38)	66 (38)	28 (32)	
3b	8 (9.1)	20 (11)	16 (18)	
Extraprostatic extension, n (%)	36 (41)	80 (45)	40 (46)	0.74053

[1]Data are presented as the median value with inter-quartile range (IQR) in brackets or as number of values and percentage (%) in brackets. PSA, prostate specific antigen
[2] Kruskal-Wallis rank sum test
[3] Pearson's Chi-squared test

bioRxiv preprint doi: https://doi.org/10.1101/2023.01.05.522843; this version posted January 6, 2023. The copyright holder for this preprint (which was not certified by peer review) is the author/funder. All rights reserved. No reuse allowed without permission.

Table S5: Anthropometrical characteristics of the patients in the cohort used for endotrophin quantification in biological fluids

Characteristic	**N = 78**[1]
Age (years)	66.0 (61.8, 69.0)
Missing	6
BMI (kg/m²)	25.68 (24.32, 27.15)
Missing	12
PPAT Volume (cm³)	41 (33, 52)
Prostate Volume (cm²)	48 (38, 62)
PPAT Abundance (Group)	
Low	20 (26%)
Mid	37 (47%)
High	21 (27%)
[1]	

[1]Data are presented as the median value with inter-quartile range (IQR) in brackets. BMI, Body mass index

bioRxiv preprint doi: https://doi.org/10.1101/2023.01.05.522843; this version posted January 6, 2023. The copyright holder for this preprint (which was not certified by peer review) is the author/funder. All rights reserved. No reuse allowed without permission.

Table S6: Clinical and pathological characteristics of the patients in the cohort used for endotrophin quantification in biological fluid

Characteristic	**N = 78**[1]
PSA (ng/ml)	6.0 (4.0, 10.0)
Missing	1
Tumor Volume (cm^2)	3 (2, 6)
Missing	37
Undifferentiated cancer	30 (10, 65)
Missing	6
ISUP	
0	1 (1.3%)
1	25 (32%)
2	31 (40%)
3	13 (17%)
4	4 (5.2%)
5	3 (3.9%)
Missing	1
pT	
pT2a or 2b	4 (5.3%)
pT2c	48 (64%)
pT3a	16 (21%)
pT3c	7 (9.3%)
Missing	3

[1]Data are presented as the median value with inter-quartile range (IQR) in brackets or as percentage (%) in brackets
PSA, prostate specific antigen

bioRxiv preprint doi: https://doi.org/10.1101/2023.01.05.522843; this version posted January 6, 2023. The copyright holder for this preprint (which was not certified by peer review) is the author/funder. All rights reserved. No reuse allowed without permission.

Table S7: List of primers used for RT-qPCR

Gene name	Reference
18S	Hs99999901_s1
CD36	Hs00354519_m1
FABP4	Hs01086177_m1
LIPE	Hs00943410_m1
MGLL	Hs00996004_m1
PNPLA2	Hs00386101_m1
SLC27A4	Hs00192700_m1
COL1A1	Hs00164004_m1
COL3A1	Hs00943809_m1
COL6A1	Hs01095585_m1
COL6A2	Hs00365167_m1
COL6A3	Hs00915125_m1
MMP14	Hs00237119_m1
MMP11	Hs00968295_m1
MMP2	Hs01548727_m1
MMP9	Hs00957562_m1
BMP1	HS00241807_m1
LOX	Hs00942483_m1
LOXL1	Hs00935937_m1
TIMP1	Hs99999139_m1
TIMP2	Hs00234278_m1
TIMP3	Hs00165949_m1
TIMP4	Hs00162784_m1

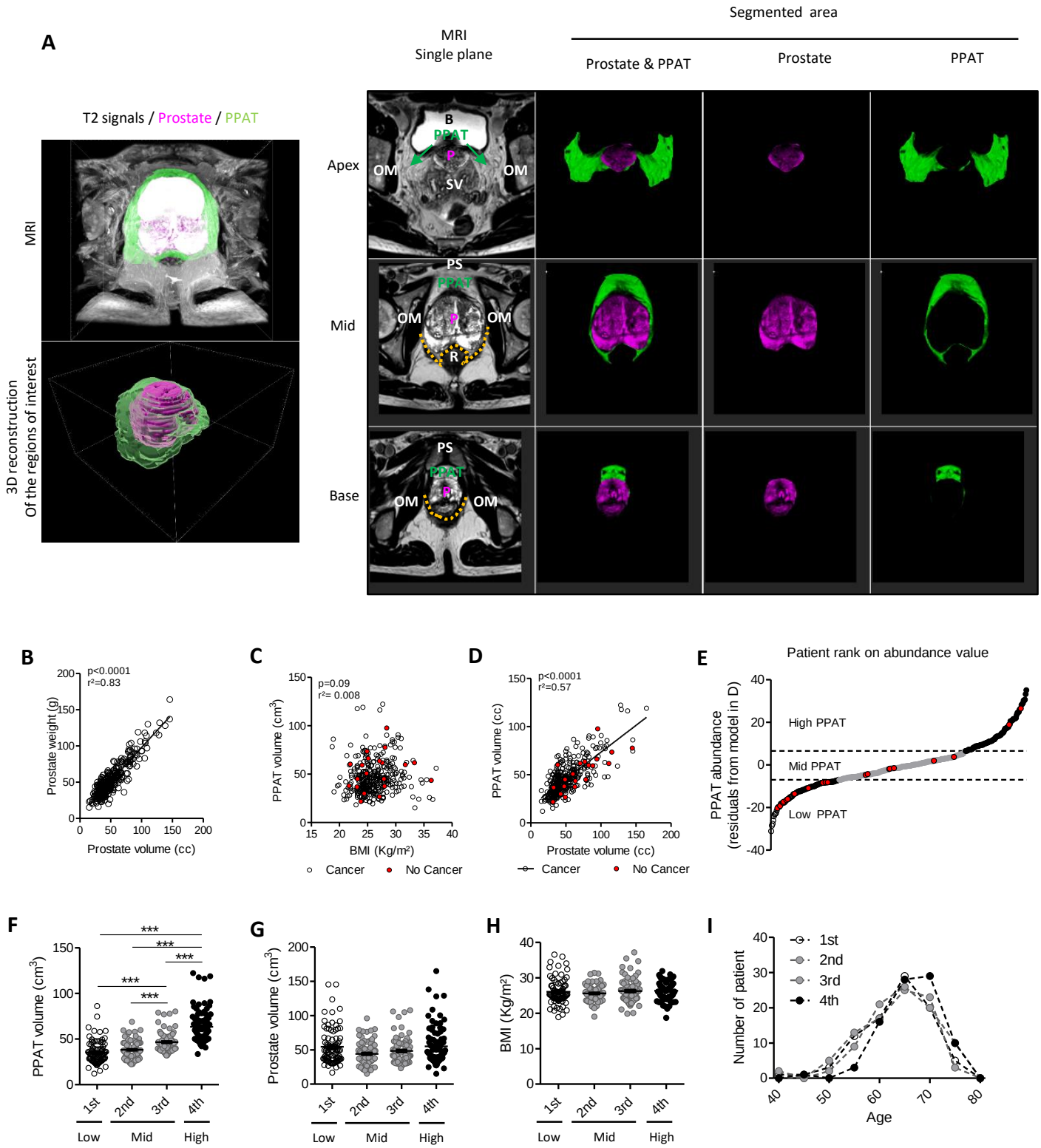


Figure 1. A new statistical approach to defining abundant PPAT relative to prostate volume

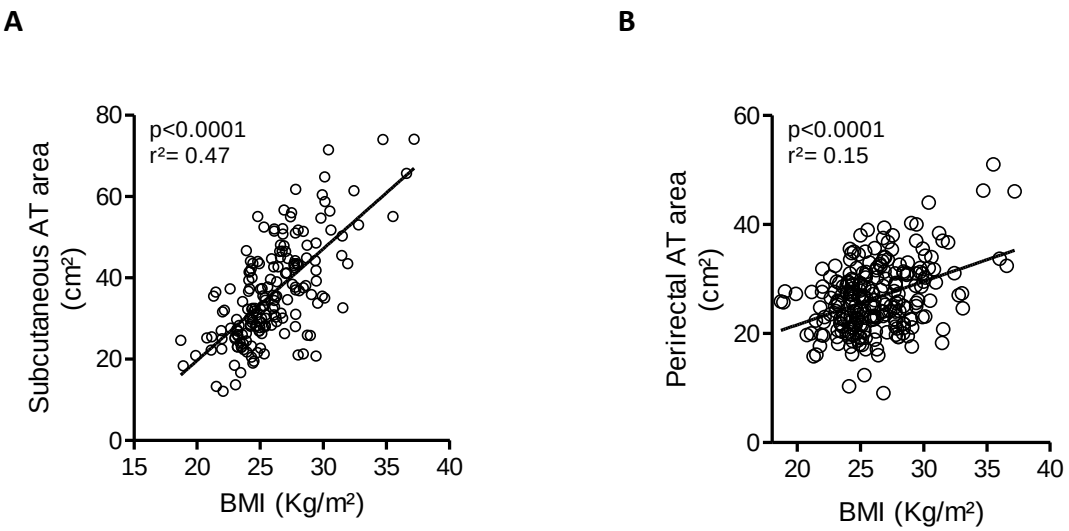
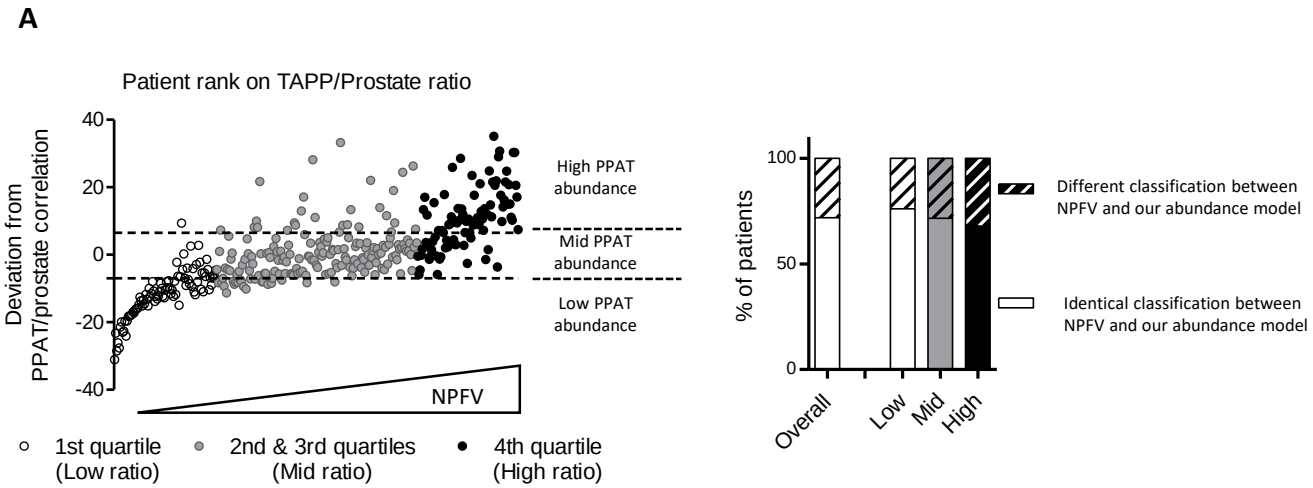
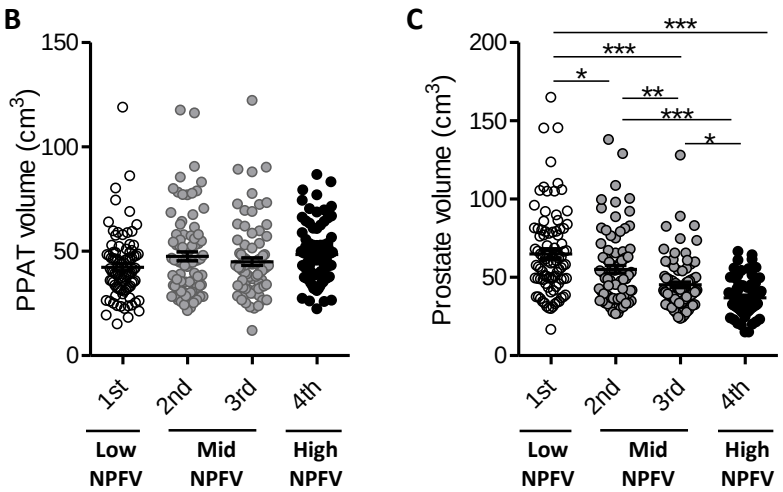


Figure S1. Subcutaneous and perirectal AT areas are correlated with BMI

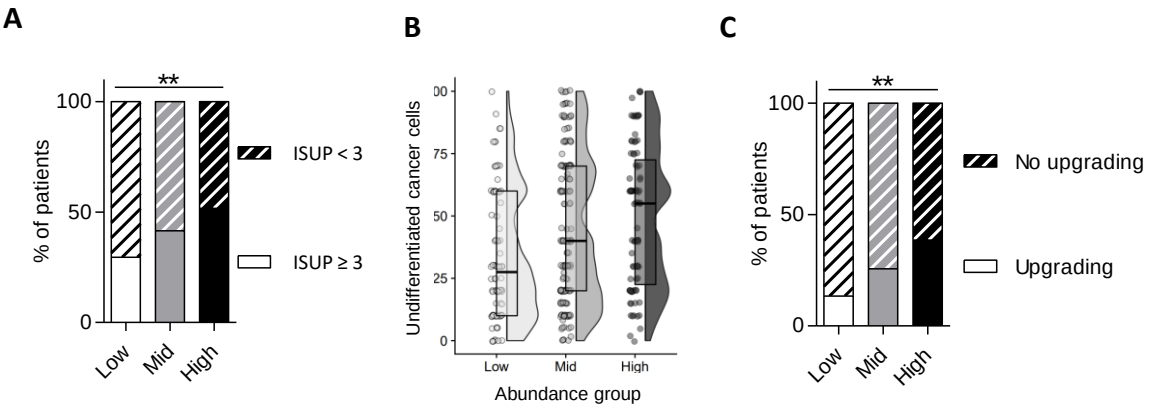




D

Predictor (ISUP ≥ 3)		N	Odds ratio	p
NPFV	Low	88	Reference	
	Mid	172	1.26 (0.67, 2.43)	0.477
	High	87	1.27 (0.58, 2.83)	0.550
Prostate		347	1.00 (0.98, 1.01)	0.599
Age		347	1.01 (0.97, 1.05)	0.762
PSA		347	1.08 (1.02, 1.14)	0.009
Gleason_bio	1	73	Reference	
	2	170	2.21 (1.10, 4.79)	0.033
	3	71	13.74 (6.10, 33.27)	<0.001
	4	33	23.66 (7.84, 84.55)	<0.001

Fig. S2. NPFV is not an appropriate measure of PPAT abundance



D

Predictor (ISUP ≥3)		N	Odds ratio	Odds ratio (CI)	p
Abundance	Low	87		Reference	
	Mid	173		1.71 (0.90, 3.32)	0.10
	High	87		2.43 (1.18, 5.11)	0.02
Prostate		347		1.00 (0.98, 1.01)	0.50
Age		347		1.00 (0.96, 1.04)	0.92
PSA		347		1.08 (1.02, 1.14)	0.01
Gleason_bio	1	73		Reference	
	2	170		2.36 (1.16, 5.15)	0.02
	3	71		14.33 (6.31, 35.01)	<0.001
	4	33		26.39 (8.62, 95.72)	<0.001

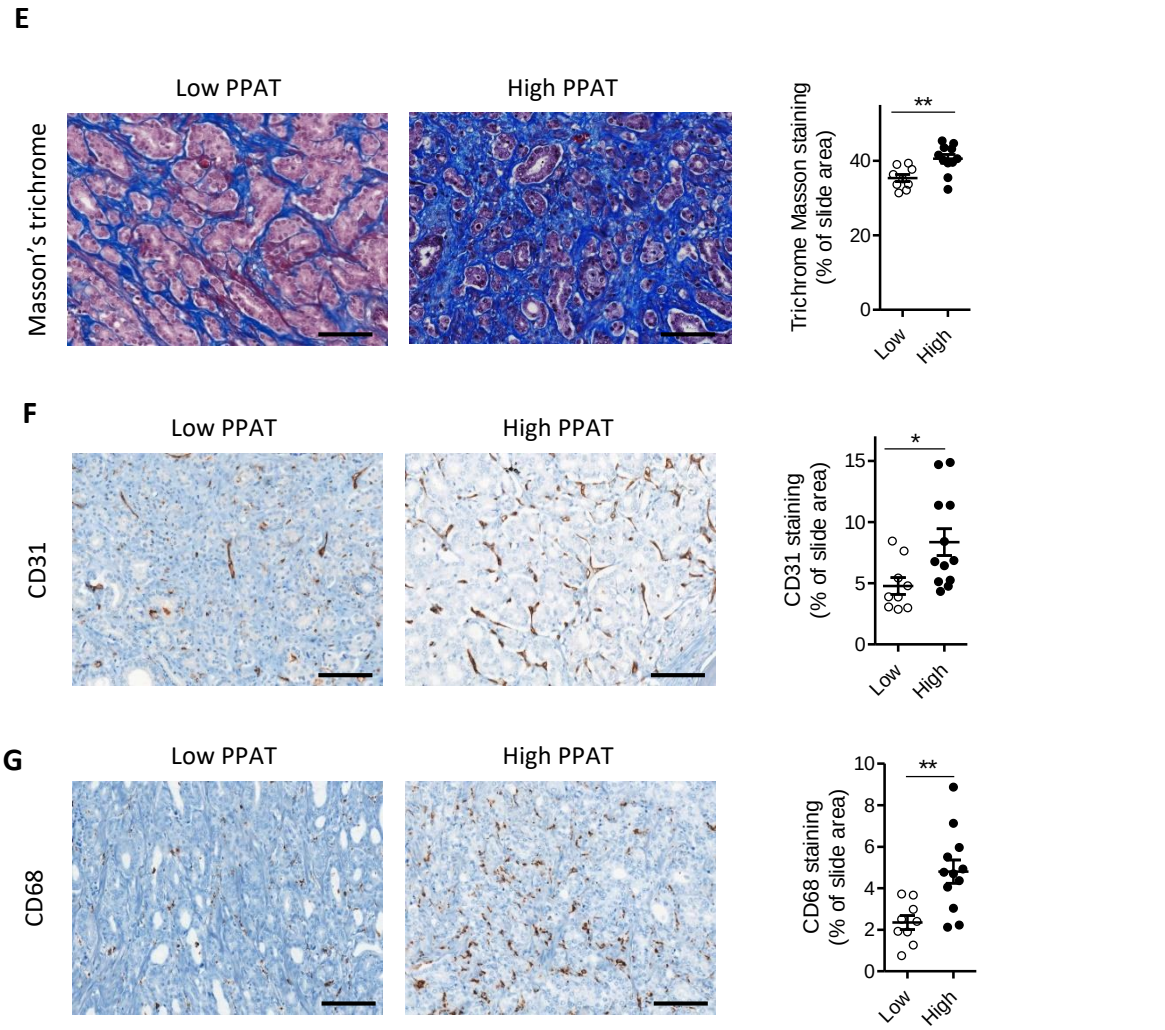


Figure 2. Abundant PPAT is associated with aggressive tumors

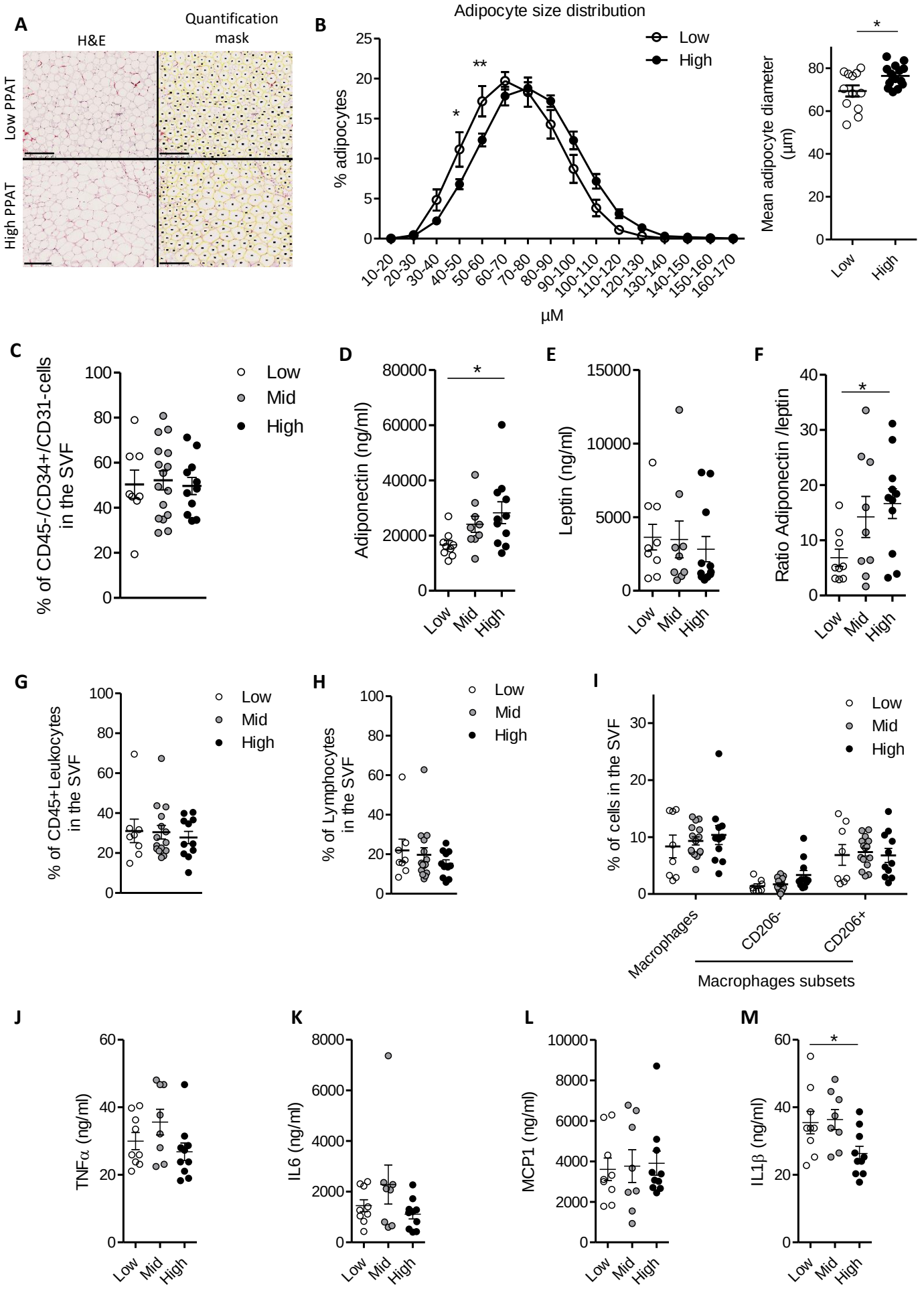


Figure 3: PPAT expands by adipocyte hypertrophy with no associated inflammation

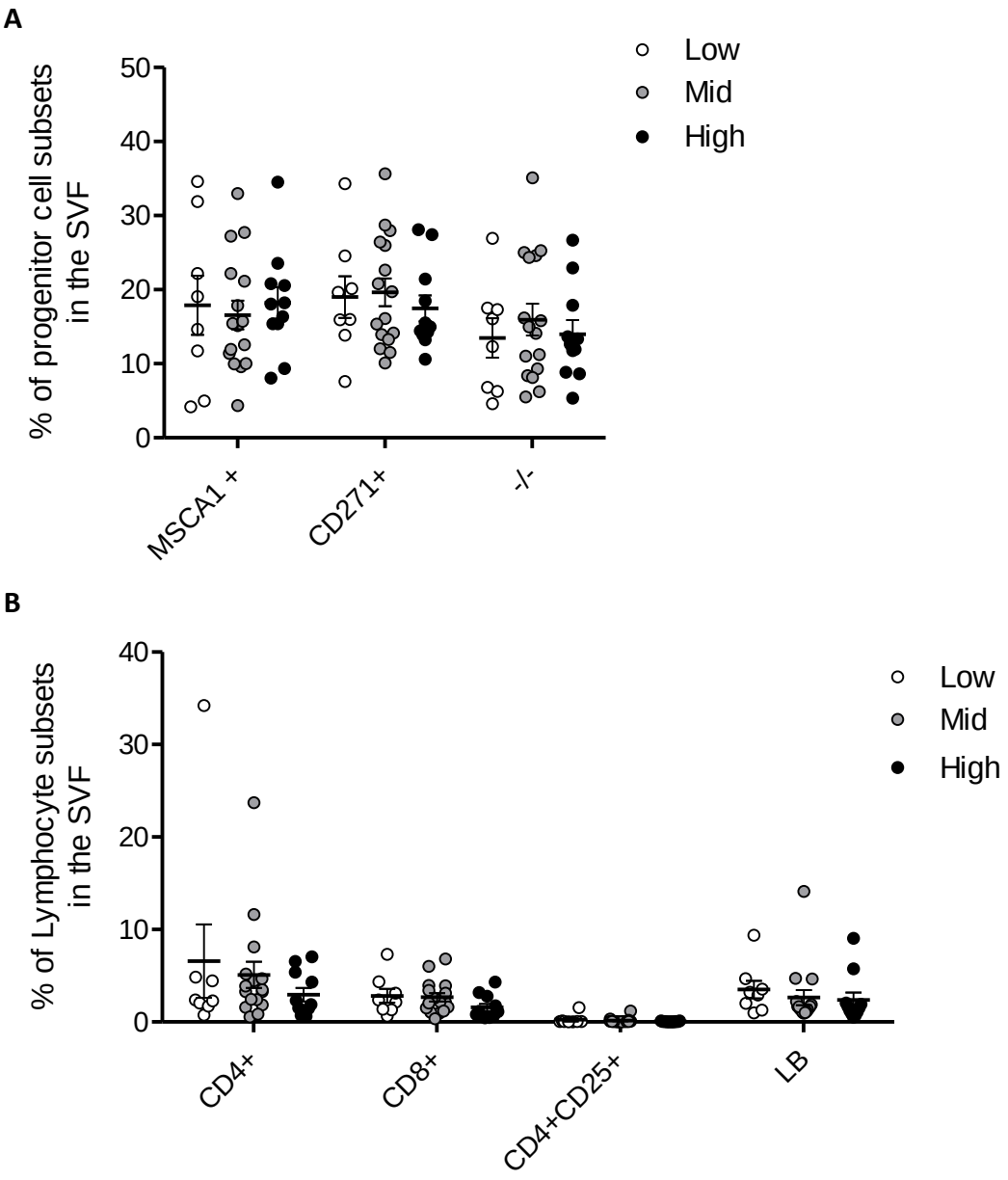


Figure S3. Adipose progenitor cell and lymphocytes subsets are not modified according to PPAT abundance

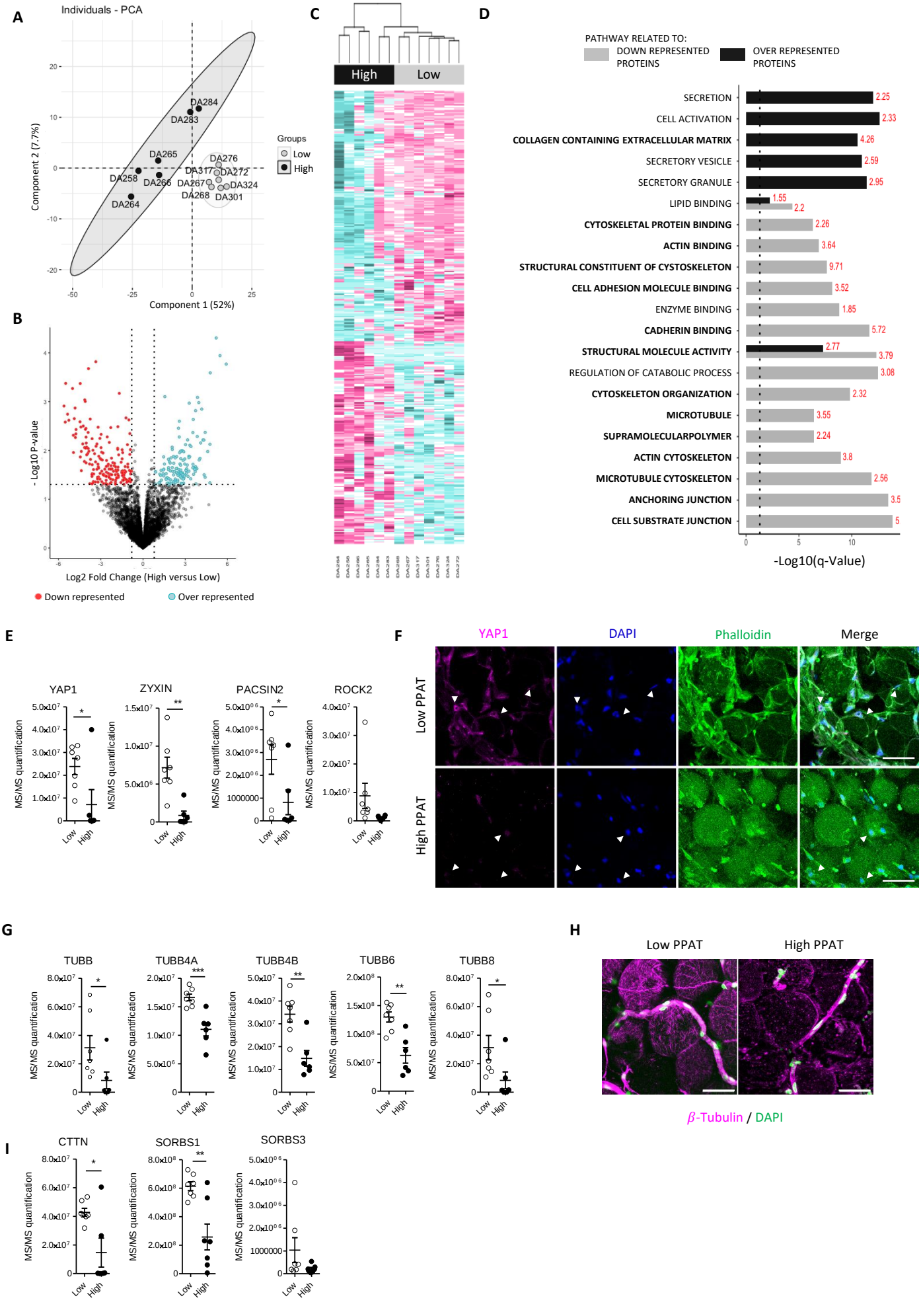


Figure 4: Under-representation of mechano-sensing proteins in abundant PPAT

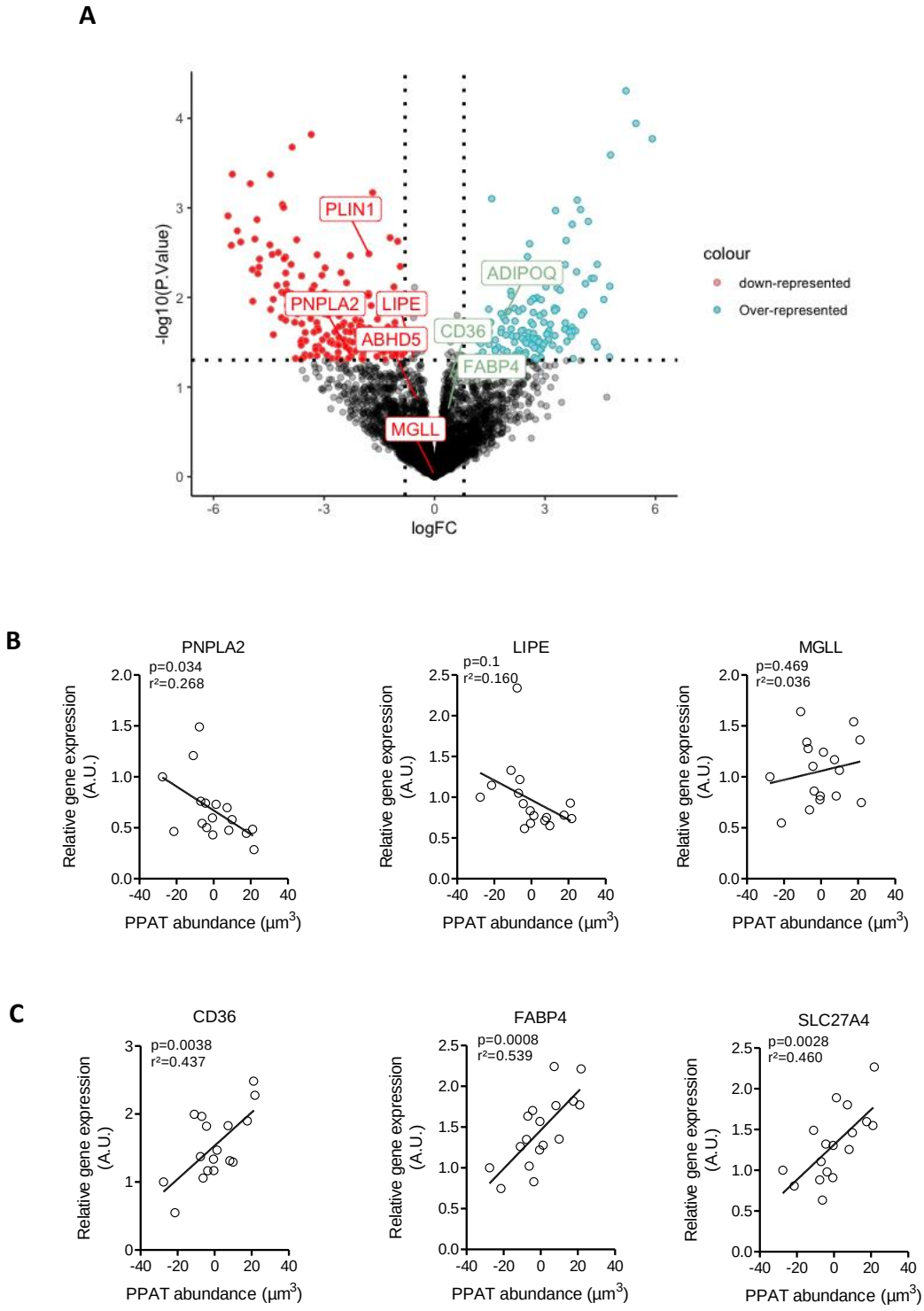


Figure S4. Proteins involved in lipolysis and lipid uptake are under-represented and over-represented in abundant PPAT

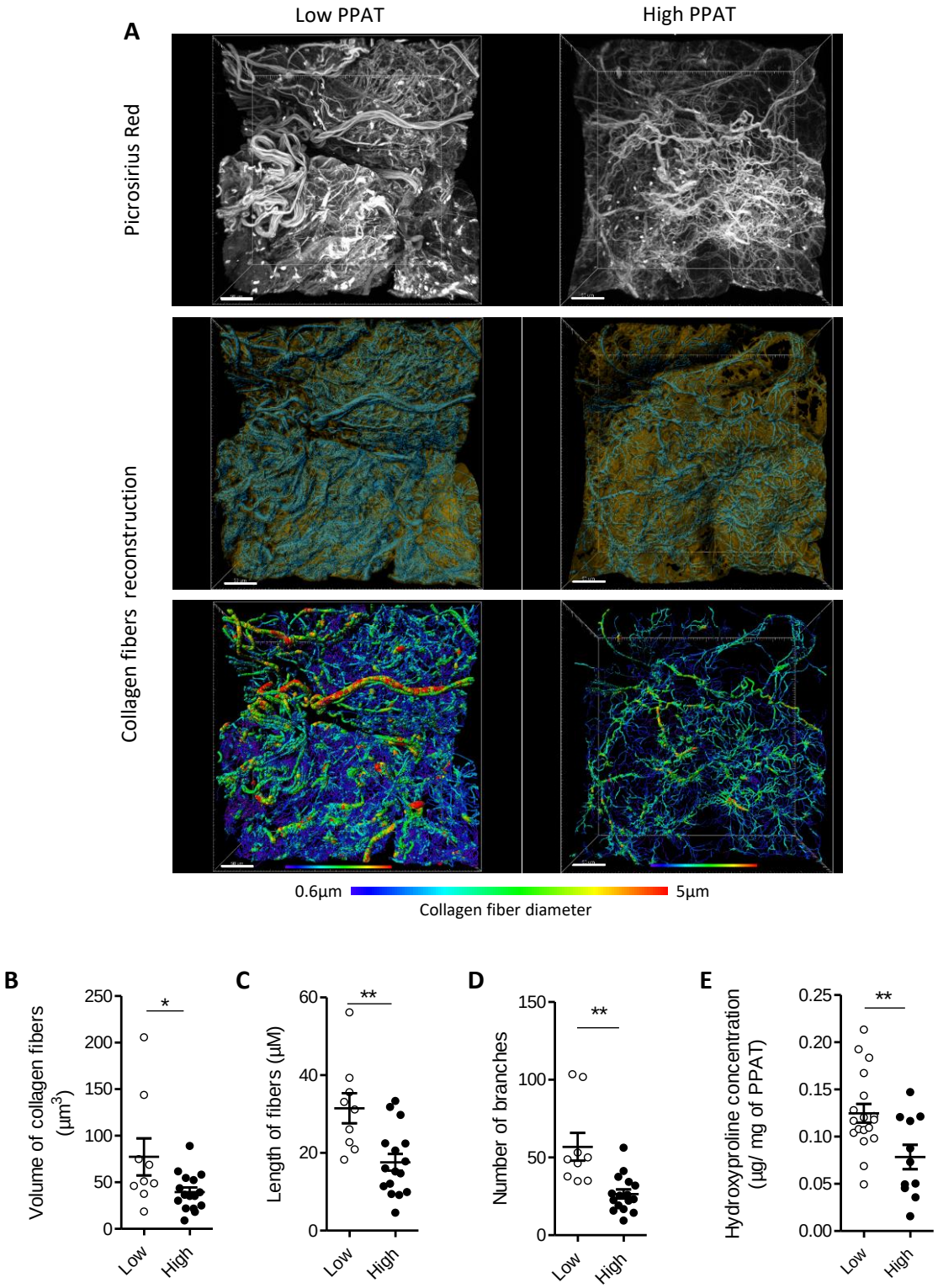


Figure 5: The collagen network in abundant PPAT is relatively loose

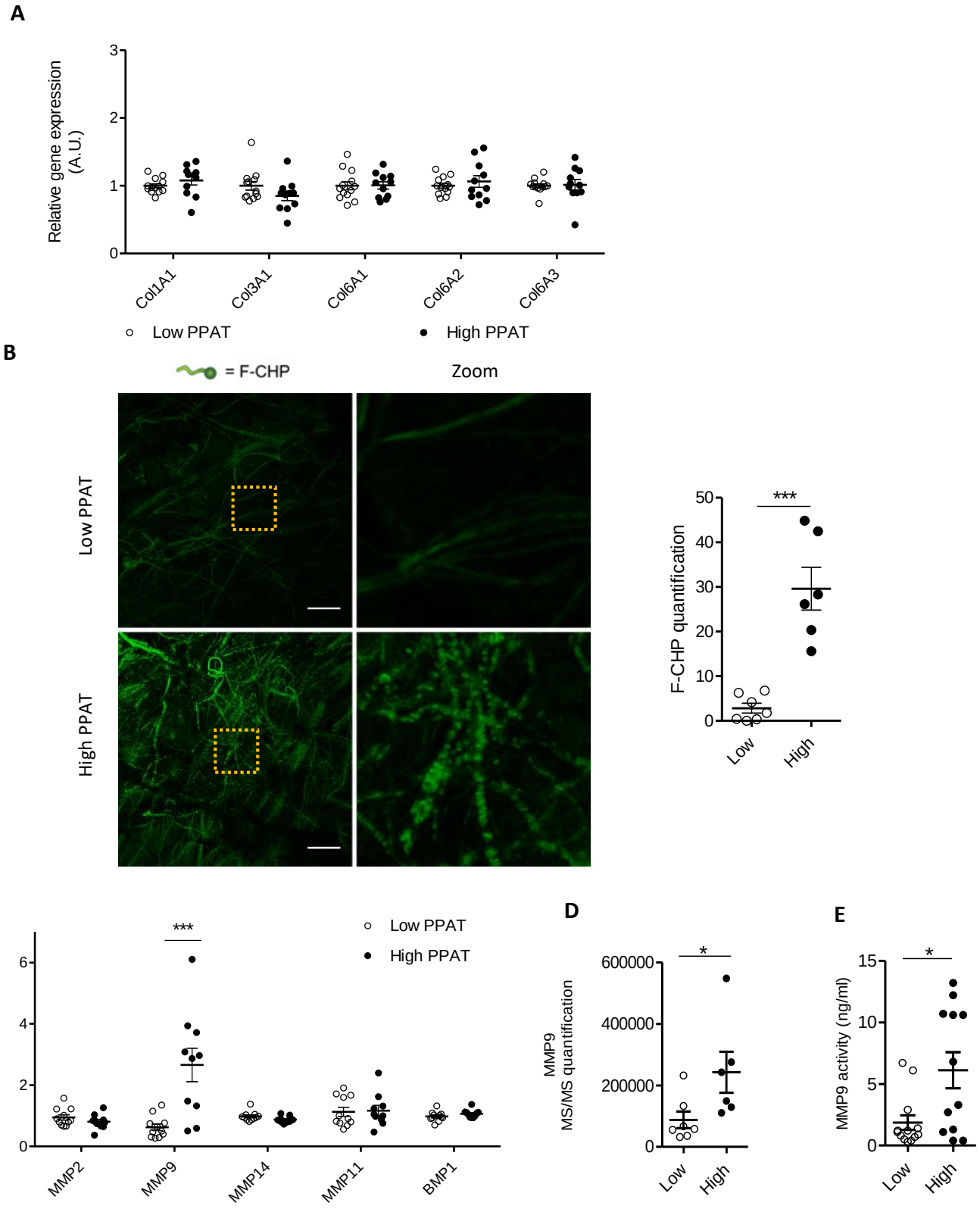


Figure 6: Abundant PPAT exhibits increased collagen degradation likely by MMP9

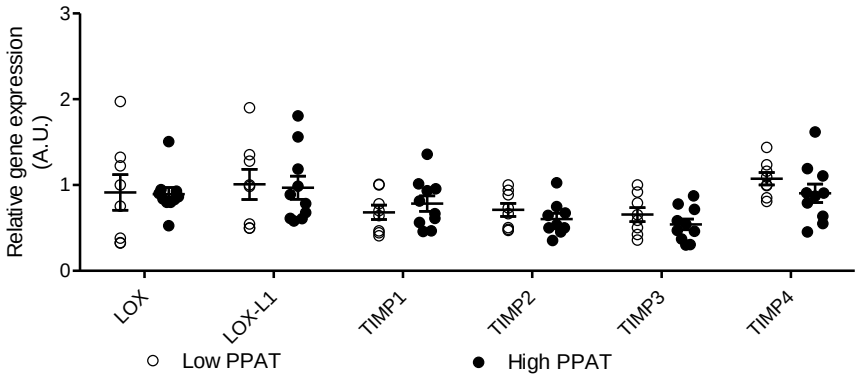
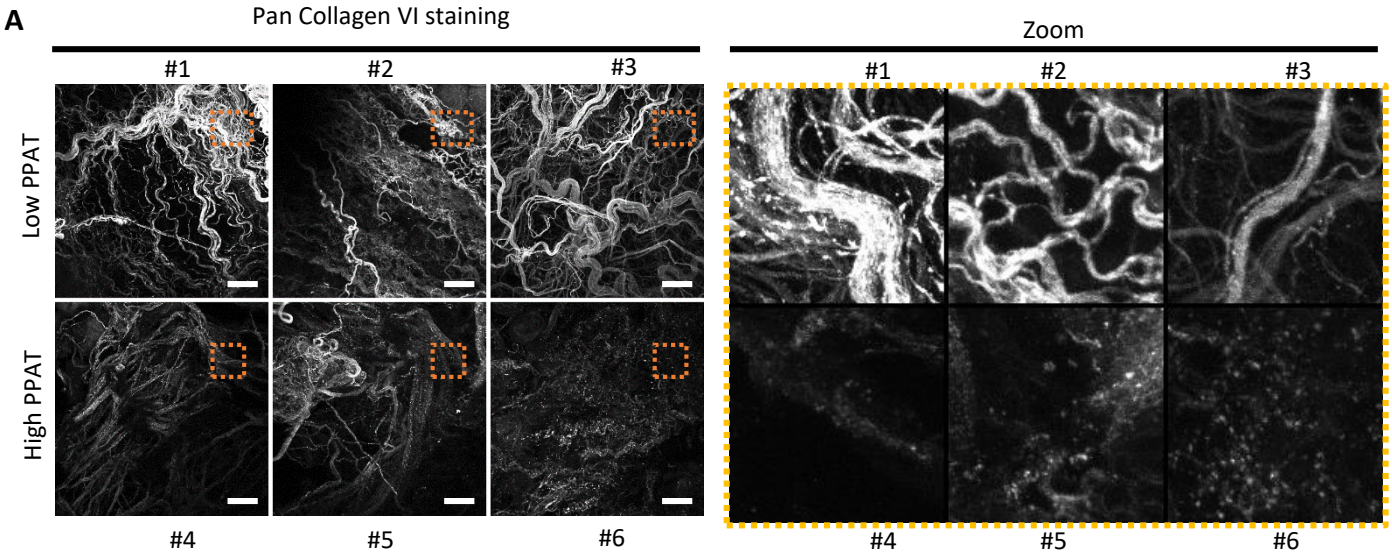
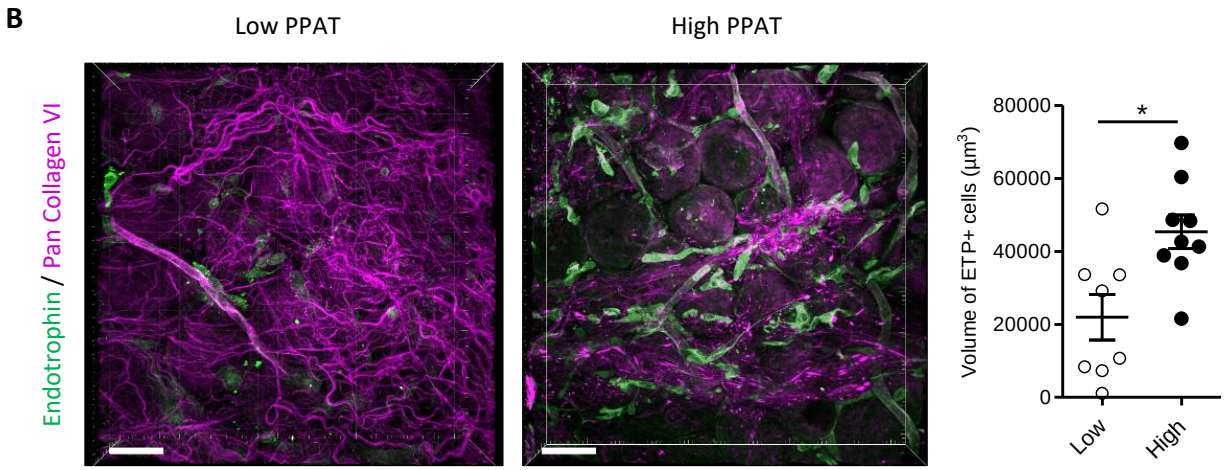
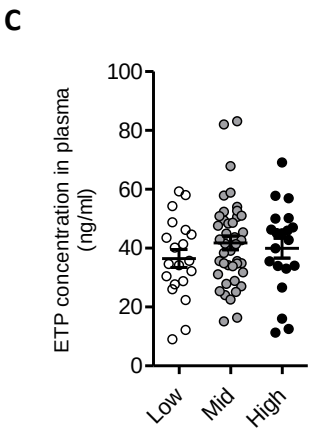


Figure S5. Absence of modifications of LOX or TIMP isoforms expression in low versus abundant PPAT.







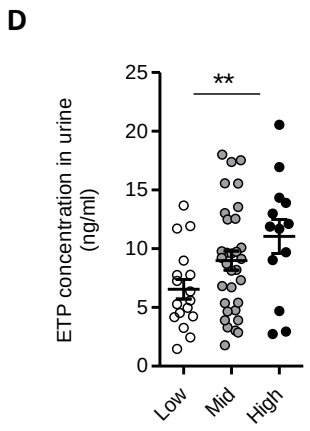


Figure 7: COL6 remodeling is associated with high endotrophin production in abundant PPAT

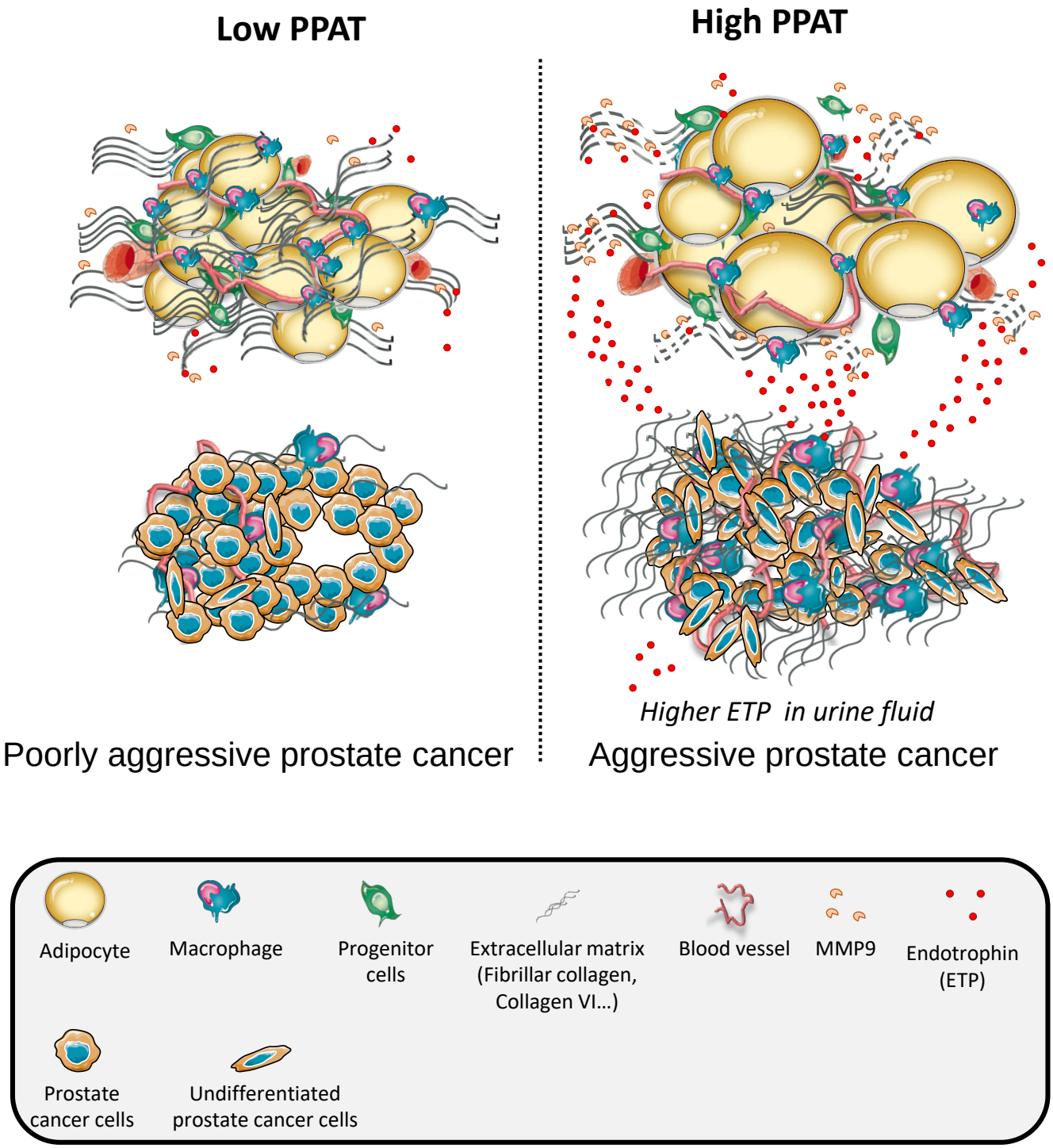


Figure 8: Collagen remodeling leads to inflammation-free expansion of periprostatic adipose tissue and promotes prostate cancer progression

3. Role of androgen metabolites from the periprostatic adipose tissue in the development of castration resistance of prostate cancer

PCa is a hormone dependent cancer, androgens being essential to its development and progression. The testis produce testosterone which is converted into its active form 5α-dihydrotestosterone (5α-DHT) by the prostate to activate the androgen receptor (AR) signaling[97]. Androgen deprivation therapy is the first-line treatment of locally advanced PCa and consists in inhibiting the production of testosterone by the testis[114,115,118]. However, the disease will progress into castration resistant PCa (CRPC) after a few years[603]. One major mechanism of resistance is based on androgen synthesis at the tumour level through alternative pathways and increased expression of enzymes involved in steroidogenesis. As seen in the introduction of the manuscript, emerging evidence in the literature have demonstrated that the tumour environment could also contribute to CRPC occurrence that is defined by the androgen-dependent growth of the tumors despite the efficient inhibition of the production of androgens by the testis[180,181]. Pernigoni et al, showed that commensal gut microbiota favours PCa tumour growth and progression to CRPC by producing androgens from androgen precursors[180]. Cui et al, recently found that cancer associated fibroblasts (CAFs) promote intratumoural production of androgens from extragonadal sources through the increase in expression of steroidogenic enzymes[181]. Among PCa microenvironment, periprostatic adipose tissue (PPAT) is a white adipose tissue (AT) that surrounds the prostate gland. My team and others have demonstrated that PPAT is a key player in PCa progression through its ability to secrete soluble factors such as chemokines, proinflammatory cytokines and lipid metabolites[419]. It is tempting to speculate that PPAT could also contribute to the occurrence of CPRC. As depicted in the review presented in the introduction, AT is described as a reservoir of sex steroids capable of locally synthesizing steroid precursors *de novo* from cholesterol and/or converting steroids captured from the bloodstream through the expression of biosynthesis (CYP11A, CYP17A) and conversion (3βHSD, 17βHSD, SRD5A) enzymes enabling the production of androgens such as DHEA, androstenedione, testosterone and 5α-DHT[604]. Moreover, we performed an extensive structural and functional characterization of PPAT compared to a control tissue, the abdominopelvic adipose tissue (APAT). Among the obtained results, we have shown that PPAT displays an increased androgenic signaling using transcriptomic approaches (Article presented in Result's part 1). All these indirect arguments suggest that PPAT might possess a specific steroid metabolism that could be involved in regulating both physiological and pathophysiological processes in the prostate. Accordingly, **the aim of my PhD project was to determine if PPAT**

has a specific steroid metabolism that could favor CRPC which to our knowledge has never been tested (Fig. 1). My first aim was to characterize the androgen metabolism in PPAT (compared to a control tissue, APAT) and my second aim was to evaluate the effect of PPAT in PCa models *in vitro* on survival and proliferation.

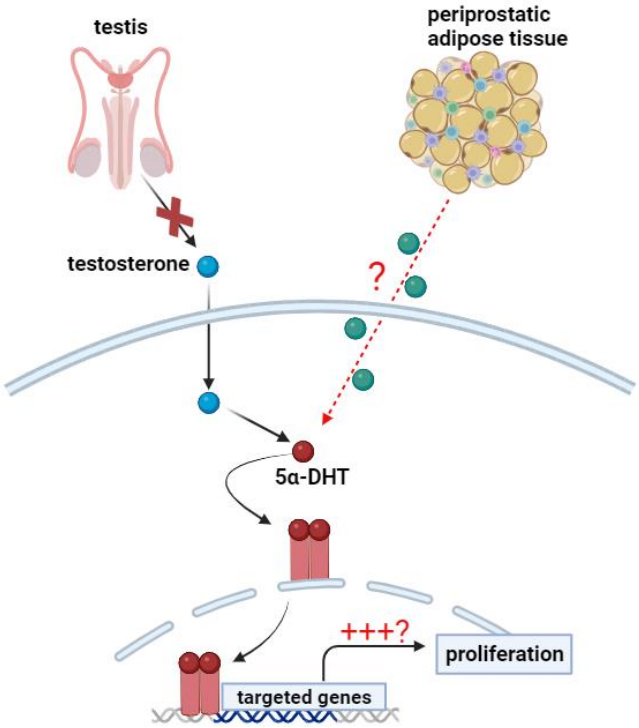


Figure 1. Androgens from periprostatic adipose tissue (PPAT) may promote hormone-sensitive PCa proliferation in CRPC in which testosterone production from testis has been inhibited.

Experimental results and discussion

PPAT contains higher levels of androgen metabolites involved in alternate route for 5α-DHT synthesis.

Preliminary experiments were performed to evaluate the quantity of AT needed to dose steroid hormones from PPAT and paired APAT. These preliminary experiments allow us to determine that 200-400 mg of PPAT was sufficient to extract quantifiable amount of sex steroid from PPAT and paired APAT.

As described in the introduction part of my manuscript, androgen synthesis starts from cholesterol via progestogens (see **Fig. 2** for a schematic representation of the sex steroid biosynthesis pathway).

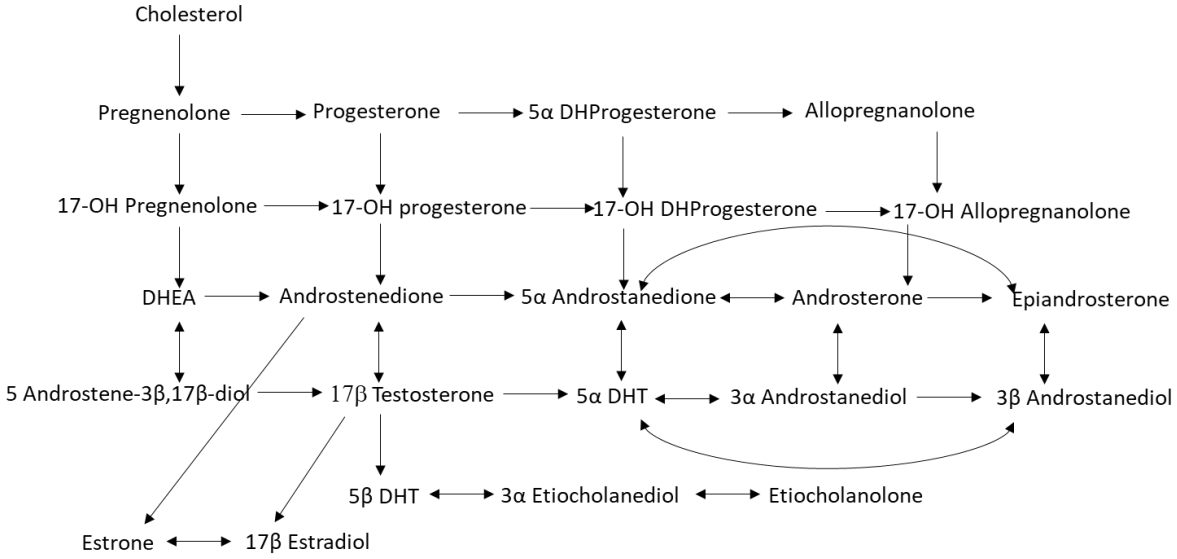


Figure 2. Sex steroid biosynthesis pathways from cholesterol. Abbreviations used: 5α DHT: 5α dihydrotestosterone; 5β DHT: 5β dihydrotestosterone; 17-OH DHprogesterone: 17-OH dihydroprogesterone; DHEA: dehydroepiandrosterone. The single arrows represent the conversion from one metabolite to another metabolite. The double arrows represent the interconversion between two metabolites.

Our results obtained from whole PPAT and paired APAT (n=11 patients) showed that all progestogens (except 17-OH dihydroprogesterone), which can be converted directly from cholesterol, were detected in PPAT and APAT (**Table 1 and Fig. 2**). Nine androgens were detected in both ATs, with DHEA as the most abundant, followed by androstenedione, 17β testosterone and androsterone (**Table 1**).

Compound	APAT (ng/g lipids)	PPAT (ng/g lipids)	*p* values	Percent of total steroids in APAT	Percent of total steroids in PPAT
Pregnenolone	16.84 ±12.69	18.2 ±13.6	NS	23.5%	21.9%
Progesterone	2.63 ±4.25	3.2 ±5.0	NS	3.67%	3.85%
5α dihydroprogesterone	0.44 ±0.54	0.4 ±0.5	NS	0.61%	0.48%
Allopregnanolone	4.32 ±8.84	6.7 ±8.2	NS	6.03%	8.06%
17-OH pregnenolone	7.15 ±3.69	9.0 ±6.4	0.085	9.98%	10.83%
17-OH progesterone	2.88 ±2.91	3.5 ±3.65	NS	4.02%	4.21%
17-OH allopregnanolone	0.20 ±0.09	0.16 ±0.06	NS	0.28%	0.19%
DHEA	20.40 ±7.97	22.99 ±9.46	NS	28.47%	27.66%
Androstenedione	6.06 ±1.77	6.38 ±2.20	NS	8.46%	7.68%
5α androstanedione	0.34 ±0.10	0.62 ±0.11	<0.01	0.47%	0.75%
Androsterone	3.40 ±1.14	2.91 ±0.92	NS	4.74%	3.5%
5 androstene3β,17β-diol	0.29 ±0.38	0.54 ±0.59	NS	0.4%	0.65%
17β Testosterone	5.18 ±1.61	5.23 ±1.53	NS	7.23%	6.29%
5α DHT	0.32 ±0.20	0.33 ±0.28	NS	0.45%	0.4%
Epiandrosterone	0.43 ±0.12	0.78 ±0.17	<0.01	0.6%	0.94%
Etiocholanolone	0.49 ±0.18	1.66 ±0.71	<0.01	0.68%	2%
Estrone	0.24 ±0.05	0.42 ±0.10	<0.05	0.33%	0.51%
17β estradiol	0.04 ±0.02	0.09 ±0.16	NS	0.06%	0.11%
3β androstanediol	ND	ND			
5β DHT	ND	ND			
3α etiocholanediol	ND	ND			
Total	71.65	83.11		100%	100%

Table 1. Difference in sex steroids concentrations between whole APAT and whole paired PPAT. Dosage by GC-APCI-MS (n=11 for APAT/PPAT, n=8 for androsterone). Mean ± SEM are indicated. Statistical differences were calculated by using Student's T test. NS: not significant; ND: not detected. For comparative reasons concentrations were also calculated for values between LOD (limit of detection) and LOQ (limit of quantification) and under LOD for the metabolites which were only detected in either PPAT or APAT. DHT: 5α-dihydrotestosterone; DHEA: dehydroepiandrosterone. Quantification of androsterone was not reliable in 4 samples.

Interestingly, as shown in **Fig. 3** and **Table 1**, our results highlight that PPAT contains, at higher levels than APAT, several steroid species such as 5α androstanedione and epiandrosterone involved in alternate routes for 5α-DHT synthesis in favor of our main hypothesis as discussed in the introduction of my manuscript. In fact, 5α androstanedione has been shown to be implicated in CRPC by generating 5α-DHT independently of testosterone[605]. Moreover, production of 5α-DHT from degradation of metabolites like epiandrosterone could be a mechanism of intratumoural production of active androgens from inactive androgens in CRPC[606]. As 3β-androstanediol was not detected in PPAT, this result suggests that epiandrosterone is probably synthesized from androsterone or 5α androstanedione (see **Fig. 2**). Also, PPAT contained higher content than APAT of etiocholanolone, one of the degradation metabolites of 17β testosterone (**Table 1** and **Fig. 3**). This metabolite is a neurosteroid with pro-inflammatory and anticonvulsant properties[607,608]. Intermediate metabolites, including 5β-DHT and 3α etiocholanediol, were not detected in PPAT nor APAT suggesting that part of testosterone is degraded into etiocholanolone (**Table 1**). Anti-proliferative effects of

etiocholanolone and epiandrosterone have been shown in cellular models of colorectal cancer, but the molecular mechanisms involved have not been elucidated[609]. These two metabolites could have different effects on the viability and proliferation of PCa cells, which would be interesting to evaluate.

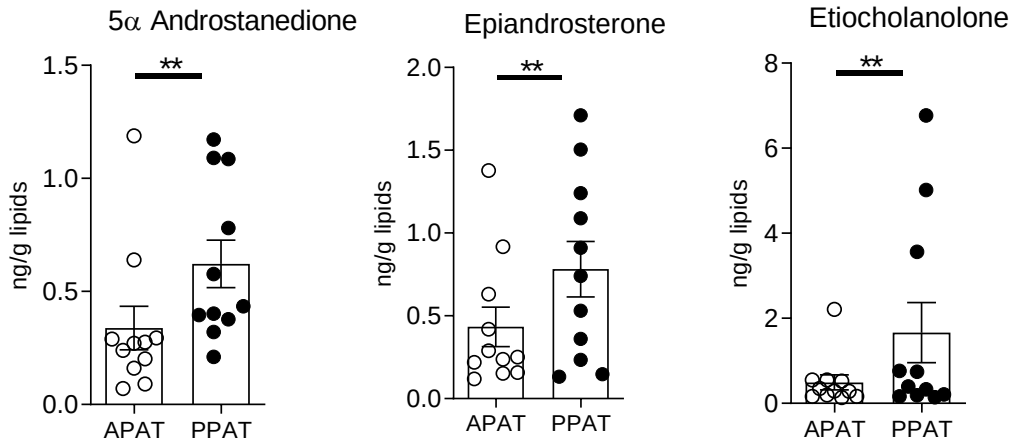
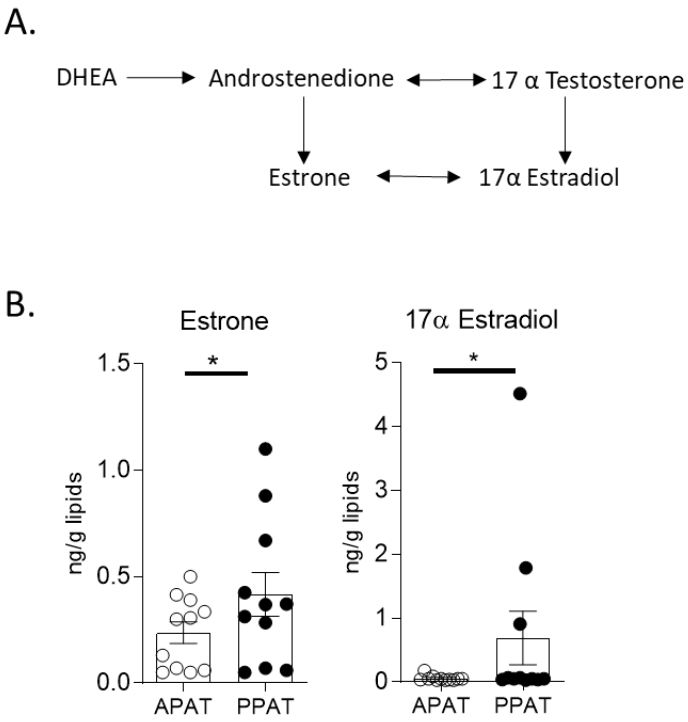


Figure 3. PPAT contains higher levels of androgen metabolites involved in the alternate route for 5α-DHT synthesis. Cconcentrations of 5α-androstanedione, epiandrosterone and etiocholanolone in whole APAT and paired whole PPAT measured by GC-APCI-MS (n=11). Statistical differences were calculated by using Student's T test, **p<0.01.

Among estrogens species, the active metabolite estrone and the less active one 17α estradiol[610] (synthesized from 17α testosterone, **Supplementary Fig. 1A**) were more abundant in PPAT compared to APAT (**Table 1** and **Supplementary Fig. 1B**). Literature has shown that estrogen participated in CRPC progression and promoted tumor metastasis via estrogen receptor[611]. Estrogen can interact with androgen receptor (AR) signaling, which is crucial for PCa growth. Moreover, estrogen-AR cross talk can enhance AR-mediated gene expression and promote the growth and survival of PCa cells, even in the presence of low androgen levels [612].



Supplementary Figure 1. PPAT contains higher levels of estrogens metabolites compared to APAT. A. 17α estradiol biosynthesis pathways from DHEA. **B.** Concentrations of estrone, 17α estradiol in whole PPAT and paired whole APAT measured by GC-APCI-MS (n=11). Statistical differences were calculated by using Student's T test, *p<0.05.

Steroid enzyme mRNA expression in whole AT partially explain the higher accumulation of 5α-androstanedione, epiandrosterone and etiocholanolone in PPAT than in APAT.

To complete these results, we then evaluated the gene expression of the key enzymes involved in the sex steroid metabolism (**Fig. 4**) in whole PPAT and paired APAT through RT-qPCR.

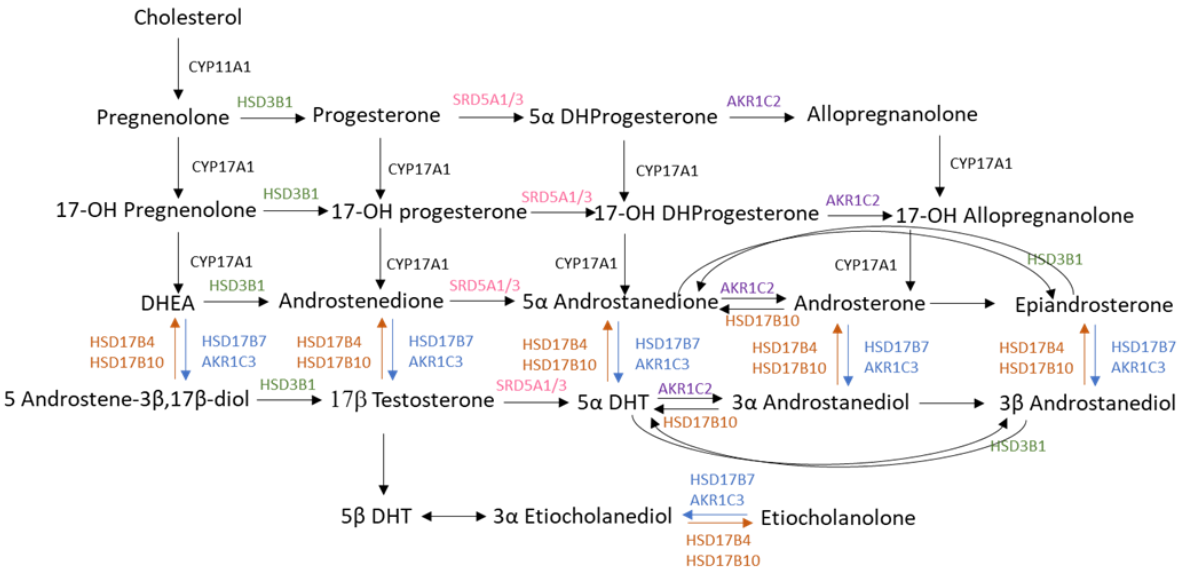


Figure 4: Biosynthesis pathways of sex steroids from cholesterol with involved steroidogenic enzymes. Gene name of enzymes are indicated. 3β Hydroxysteroid dehydrogenase (HSD) type 1 encoded by HSD3B1 is indicated

in green; 17β HSD type 4 and 10 encoded by HSD17B4 and HSD17B10 are indicated in orange; 17β HSD type 5 and 7 encoded by AKR1C3 and HSD17B7 are indicated in blue; 5α reductase type 1 and 3 encoded by SRD5A1 and SRD5A3 are indicated in pink; 3α HSD type 3 encoded by AKR1C2 is indicated in purple. Cytochrome P450 side-chain cleavage encoded by CYP11A1 and cytochrome P450 17α-hydroxylase/17, 20-lyase encoded by CYP17A1 are indicated in black.

The enzyme encoded by CYP11A1 which is responsible for the conversion of cholesterol into pregnenolone was more expressed in PPAT compared to APAT but CYP17A1 mRNA was not detected in both AT suggesting that while PPAT is able to perform the first reaction of *de novo* synthesis of steroids from cholesterol, it is not able to further convert pregnenolone into progestogens and DHEA (**Fig. 4 and 5**). Thus, we can speculate that progestogens detected in APAT and PPAT could come from the circulation as described for others AT[479]. The detection of 3β HSD (HSD3B1), 17β HSD (HSD17B4, B7 and B10) and 5α reductases mRNA (SRD5A1/3) showed the ability of PPAT to convert DHEA into downstream active androgens (**Fig. 5**). Interestingly, lower expression of AKR1C2 and AKR1C3 mRNA in PPAT compared to APAT could explain the accumulation of 5α-androstanedione, epiandrosterone and etiocholanolone (**Fig. 4 and 5**). However, the fact that we found higher expression of HSD17B7, which has the same function than AKR1C3, and lower expression of SRD5A3 in PPAT than in APAT are not at first sight in accordance with the results of the dosage of the androgen metabolites (**Fig. 4 and 5**). Although AKR1C3 and HSD17B7 play the same role in several enzymatic reactions, it should be noticed that in our samples, the relative mRNA expression of HSD17B7 is clearly lower than the one of AKR1C3 (**Fig. 5**). Furthermore, these enzymes have their own substrate preference. HSD17B7 enzyme may be less important for 5α androstanedione conversion than AKR1C3 since it has been shown to be predominantly involved in the conversion between estrone and estradiol[613]. Finally, it has been reported that AKR1C3 enzymes has more affinity for androstenedione than 5α-DHT but the study did not investigate the affinity for 5α androstanedione[505]. SRD5A3 mRNA level was found higher than other isoforms not only in our study but also in subcutaneous and omental AT of men[528]. However, the role of SRD5A3 in the conversion between androstenedione and 5α androstanedione has not been fully described[150]. However, these results need to be confirmed at protein levels by Western blot to validate the regulation of the expression of these enzymes in PPAT versus APAT. Furthermore, as we will see below, AT are composed of adipocytes and the so-called SVF, we therefore repeated these experiments in isolated adipocytes.

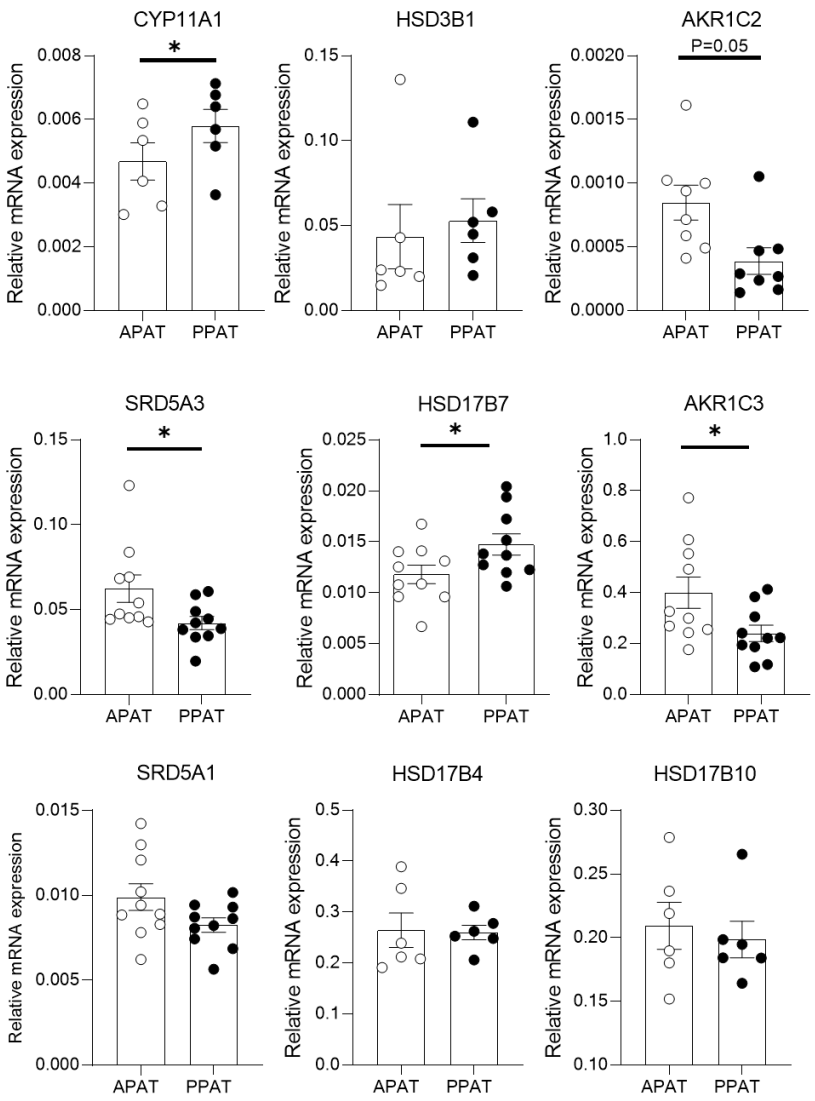


Figure 5. Steroid enzyme mRNA expression in whole AT partially explain the higher accumulation of 5α androstanedione, epiandrosterone and etiocholanolone in PPAT versus APAT. Sex steroids enzyme relative mRNA expression in whole adipose tissue from PPAT and APAT analysed by RT-qPCR (n=6-10). Statistical differences were calculated by using Student's T test, *p<0.05.

Adipocytes are the main source of androgen metabolites in PPAT. We then set up the experiments to dose the steroid hormones in isolated adipocytes and stroma vascular fraction (SVF) from PPAT. As explained in the Material and method section, PPAT were digested by collagenase. After digestion the cell suspension is filtered and floating adipocytes are collected and washed several times. The cells present in the pellet are called SVF (stroma vascular fraction) and include adipose progenitor cells, fibroblasts, mural, endothelial and immune cells[614]. Preliminary experiments performed with the LABERCA laboratory, using increasing amounts of cells from the SVF fraction (from 0.42 million to 0.7 million) and different protocols to detect molecules at low concentrations, showed that the steroid metabolites were undetectable in this cellular fraction (data not shown). The quality controls put in place to ensure

sample preparation and data quality assess the validity of these results. Thus, we can deduct from these results than if androgen metabolites are synthetized by cells of the SVF fraction, their amount is very low within the AT. This hypothesis is reinforced by the results obtained with adipocytes.

In fact, these metabolites (7 progestogens, 9 androgens and estrone) were detected in isolated adipocytes (**Table 2** and **Fig. 6**) but as shown in **Table 2** the content of most sex steroids was significantly higher in whole PPAT compared to isolated adipocytes. One hypothesis to explain these results is that the secreted steroid metabolites by adipocytes are stored (as many soluble factors) in the extra-cellular matrix (ECM) and could be lost during the extraction procedure that include digestion of the ECM to isolate adipocytes. Some metabolites such as allopregnanolone, androsterone, 5α androstanedione and 5α-DHT were detected at similar levels between PPAT and adipocytes (**Table 2**). These could suggest that these metabolites are only synthesized by adipocytes where they are stored after their synthesis with slow release in the extra-cellular content. Concerning our metabolites of interest, it is interesting to note that 5α androstanedione concentration was slightly higher in isolated adipocytes than in whole PPAT although the differences were not significant (**Table 2** and **Fig. 6**) whereas the content of epiandrosterone and etiocholanolone was significantly decreased in adipocytes compared to whole PPAT (**Table 2** and **Fig. 6**). Concerning androgens, our results are in accordance with the literature although the data are relatively sparse. For example, it has been shown that adipocytes are the main source for 17β HSD and AKR1C enzymes which are involved in the synthesis of 5α-DHT whereas no 5α reduction of testosterone into DHT was detected in SVF cells such as preadipocytes[615]. By contrast, in studies conducted in women AT, aromatase activity that is involved in the conversion of androgens into estrogens was shown to be at least 10-fold higher in SVF than in adipocytes; with both progenitor cells and endothelial cells involved in this change[616,617]. In conclusion of this part, our results show that within PPAT, isolated adipocytes are the main source of androgens especially the main metabolites involved in the alternate pathway of active androgen synthesis,

Compound	AT (ng/g lipids)	Adipocytes (ng/g lipids)	*p* values
Pregnenolone	16.40±2.30	12.57±1.63	<0.05
Progesterone	1.21±0.10	0.92±0.09	<0.0001
5α dihydro-progesterone	0.47±0.12	ND	
Allopregnanolone	2.53±0.83	2.53±0.81	NS
17 OH Pregnenolone	4.94±1.69	1.43±0.38	<0.001
17OH Progesterone	5.27±0.86	1.27±0.28	<0.001
17OH Allopregnanolone	0.15±0.034	0.04±0.003	<0.01
Dehydroepiandrosterone	21.37±3.64	10.83±2.14	<0.001
Androstenedione	5.89±0.51	3.75±0.38	<0.0001
5α Androstanedione	0.30±0.06	0.42±0.06	NS
Androsterone	3.24±0.63	2.28±0.24	NS
5 Androstene3β,17β-diol	1.43±0.38 N=4	ND	
17β Testosterone	4.30±0.52	1.99±0.31	<0.0001
5α DHT	0.51±0.10	0.37±0.03	NS
Epiandrosterone	0.65±0.15	0.29±0.09	<0.01
Etiocholanolone	0.34±0.06	0.20±0.03	<0.05
Estrone	0.45±0.11	0.27±0.06	<0.01
17β Estradiol	ND	ND	
3β Androstanediol	ND	ND	
5β DHT	ND	ND	
3α Etiocholanediol	ND	ND	

Table 2. Difference in sex steroids concentrations between whole PPAT and paired isolated adipocytes. Dosage by GC-APCI-MS (n=10, n=4 for 5 Androstene3β, 17β-diol). ND: Not detected in any sample. Statistical differences were calculated by using Student's T test, *p<0.05, **p<0.01, ***p<0.001, ****p<0.0001. NS: Not significant

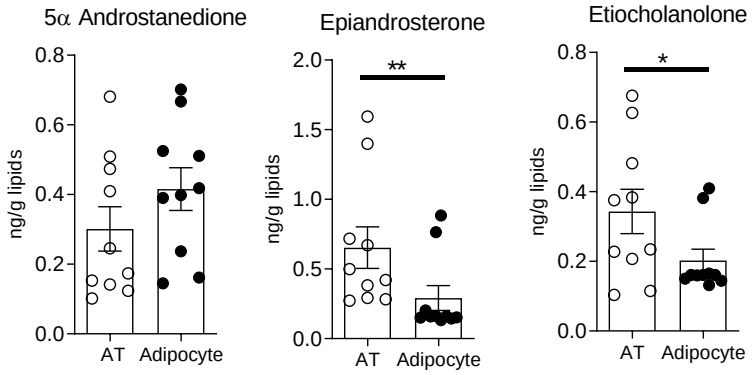


Figure 6. Adipocytes are the main source of 5α androstanedione in PPAT. Concentrations of 5α-androstanedione, epiandrosterone and etiocholanolone in whole PPAT and paired isolated adipocytes measured by GC-APCI-MS (n=10). Statistical differences were calculated by using Student's T test, *p<0.05, **p<0.01.

Steroid enzyme gene expression in adipocytes favor the accumulation of 5α androstanedione, epiandrosterone and etiocholanolone in PPAT compared to APAT.

As previously, we then evaluated the gene expression of the key enzymes involved in the sex steroid metabolism in isolated adipocytes from PPAT compared to isolated adipocytes from paired APAT using RT-qPCR. Significant lower expression of AKR1C3 mRNA and significant

higher expression of HSD17B10 mRNA in isolated adipocytes from PPAT compared those isolated from APAT could explain the accumulation of 5α androstanedione, epiandrosterone and etiocholanolone (Fig. 7). Differently than in whole PPAT, we observed lower expression of SRD5A1 mRNA in PPAT adipocytes compared to APAT adipocytes whereas SRD5A3, AKR1C2, HSD17B7 and HSD17B4 and HSD3B1 mRNA expression were not different between the two ATs (**Fig. 7**). Thus, in isolated adipocytes, the profile of steroidogenic enzyme expression better explains the accumulation of 5α androstanedione, epiandrosterone and etiocholanolone than in whole AT, confirming that adipocytes are the main sources for androgens in PPAT.

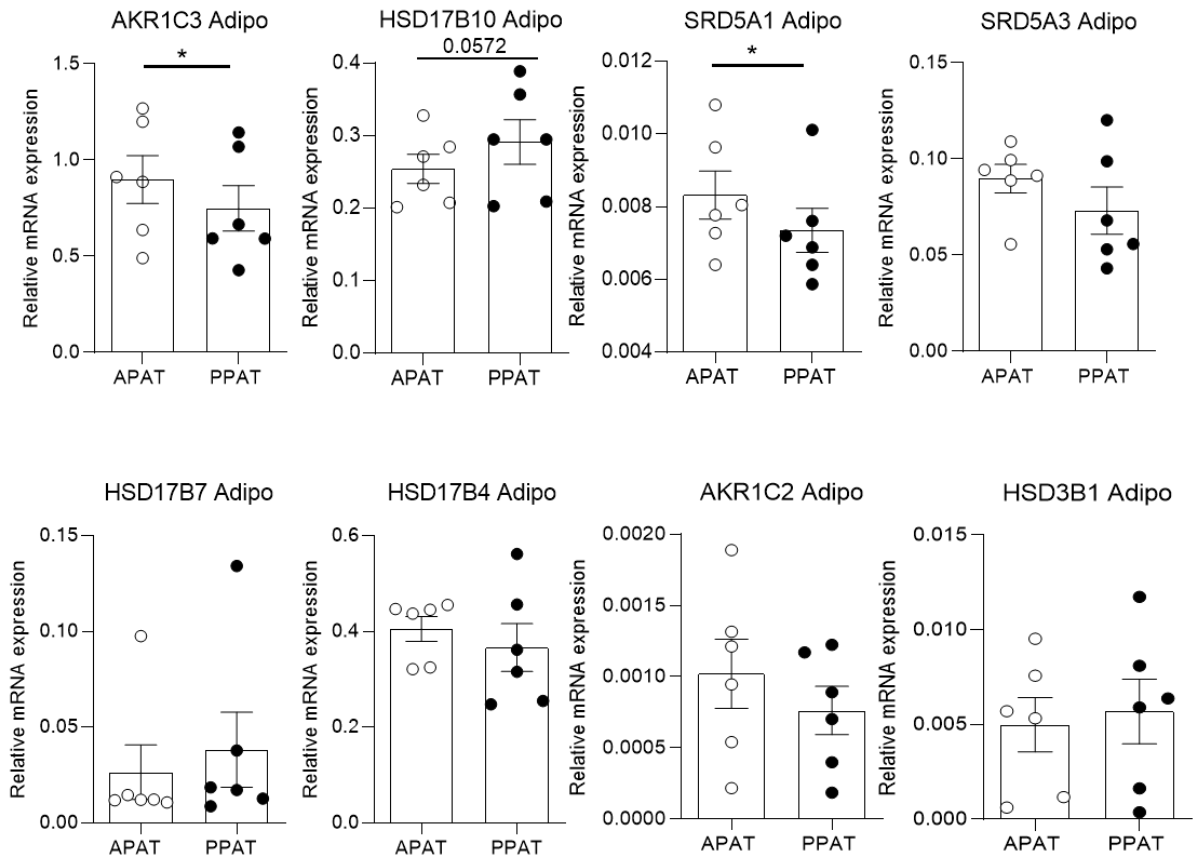


Figure 7. Steroid enzyme gene expression in adipocytes favor the accumulation of 5α androstanedione, epiandrosterone and etiocholanolone in PPAT compared to APAT. Relative mRNA expression of steroidogenic enzyme in isolated adipocyte from PPAT and paired APAT evaluate by RT-qPCR (n=6). Statistical differences were calculated by using Student's T test, *p<0.05.

In conclusion, our results showed that sex steroids including androgens, estrogens and progestogens are detectable in both PPAT and APAT. Among these species, 2 androgen precursors including 5α androstanedione and epiandrosterone and one inactive androgen etiocholonolone are higher present in PPAT than APAT. We showed that adipocytes are the main site of sex steroid storage by comparing their concentration in paired PPAT and isolated

PPAT adipocytes. Interestingly, we found lower AKR1C3 mRNA expression in both PPAT and adipocytes, lower AKR1C2 mRNA expression in PPAT and higher HSD17B10 mRNA expression in isolated adipocytes, which could explain the accumulation of 5α androstanedione, epiandrosterone and etiocholanolone.

Prostate cancer cell lines express the steroidogenic enzymes involved in the alternate pathway of 5α-DHT synthesis described in CRPC.

The next aim of my project was to study the impact of androgens secreted by PPAT and APAT on PCa cell lines behavior. We used androgen dependent (LNCaP), androgen sensitive (22RV1) and androgen independent (PC3 and DU-145) PCa cell lines[37] to study the impact of androgens secreted by PPAT on cell survival and proliferation. These cell lines were obtained from bone (22RV1 and PC3), brain (DU145) or lymph node (LNCaP) metastasis and are considered as CRPC models[147]. We first investigated the levels of the mRNA expression of the steroidogenic enzymes involved in the alternate pathways of 5α-DHT synthesis previously described in CRPC[164] by RT-qPCR in the four PCa cells lines cultivated in normal FBS contained medium. A schematic representation of the metabolites and enzymes involved is presented in **Figure 8**.

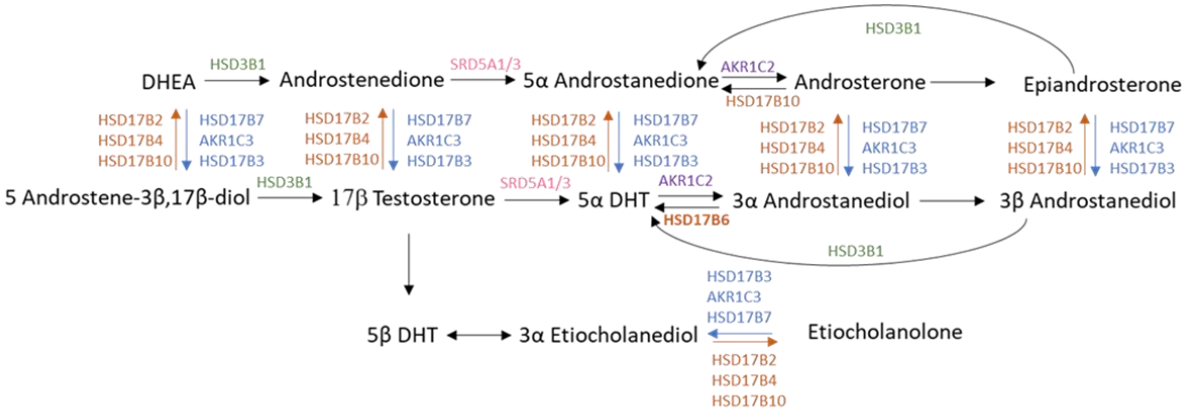


Figure 8. Simplified pathways of steroidogenesis involved in androgen biosynthesis in prostate cancer. Gene name of enzymes are indicated. 3β Hydroxysteroid dehydrogenase (HSD) type 1 encoded by HSD3B1 is indicated in green; 17β HSD type 2, 4 and 10 encoded by HSD17B4, HSD17B2 and HSD17B10 are indicated in orange; 17β HSD type 3, 5 and 7 encoded by HSD17B3, AKR1C3 and HSD17B7 are indicated in blue; 5α reductase type 1 and 3 encoded by SRD5A1 and SRD5A3 are indicated in pink; 3α HSD type 3 encoded by AKR1C2 is indicated in purple.

Our preliminary results indicated that, as expected, the androgen dependent and sensitive cell lines LNCaP and 22RV1 expressed AR, but not the androgen independent cell lines PC3 and DU145 (**Fig. 9**). The expression of HSD3B1, the first enzyme that convert DHEA into downstream androgens and epiandrosterone into 5α androstanedione (**Fig. 8**) was expressed at low level by both the androgen dependent cell line LNCaP and the androgen-sensitive cell line 22RV1. In androgen independent cell lines, HSD3B1 mRNA were difficult to detect in PC3

(only detected in one experiment among three) and not expressed in DU145 (**Fig. 9**). All four cell lines expressed SRD5A1 and SRD5A3 (**Fig. 9**) showing their ability to convert androstenedione into 5α androstanedione or testosterone into 5α-DHT (**Fig. 8**). In accordance with the literature, we found that they did not express SRD5A2 which has been shown to be mainly expressed in normal prostate[618]. In CRPC, decreased expression of SRD5A2 is associated with a shift toward increased expression of SRD5A1 which displays more affinity for androstenedione than testosterone favoring the "5α androstanedione pathway"[130]. We then investigated the expression of the reductive enzymes involved in the alternate pathway (5α androstanedione conversion to the active androgen 5α-DHT): HSD17B7, AKR1C3 and HSD17B3 (**Fig. 8**). All cell lines expressed HSD17B7 whereas AKR1C3 was expressed by all cell lines except LNCaP with a higher level in 22RV1 (**Fig. 9**). In accordance with the literature[167,619]. HSD17B3, which display the same function than HSD17B7 and AKR1C3, was expressed in all cell lines and at higher levels in PC3 (**Fig. 9**). Finally, among the oxidative enzymes that catalyze the opposing reaction (5α-DHT back conversion into 5α androstanedione), in accordance with the literature**,** HSD17B2 was expressed at high levels in PC3 and not in the other models[620]. HSD17B4 and HSD17B10 were expressed in all cell lines but HSD17B10 was expressed at lower level in the androgen independent cell lines DU145 (**Fig. 9**) confirming the literature[621]. Altogether, these results suggest that all the PCa cell lines could be able to synthetize androgens independently of their AR status. They also suggest the ability of the androgen dependent cell lines LNCaP to synthesize 5α-DHT from 5α androstanedione or epiandrosteronene, the two metabolites found increased in PPAT. Again, as stated before it would be important to confirm these results at protein level by Western blot.

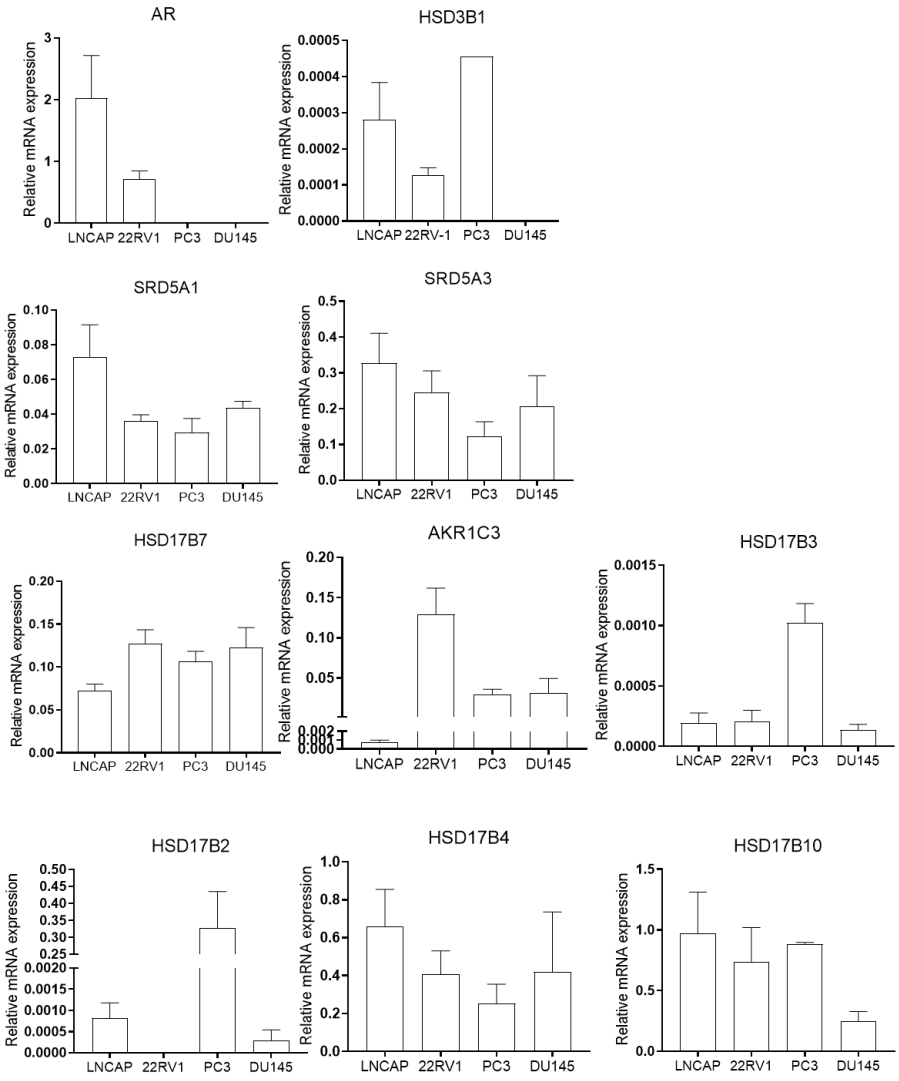


Figure 9. Androgen dependent and independent PCa cells express steroidogenic enzymes involved in the alternate pathway of 5α-DHT synthesis described in CRPC. Relative mRNA expression of the indicated genes encoding the enzymes involved in sex steroid metabolism in PCa cell lines (n=3). Results were normalized to the amount of 18S rRNA). Bars indicate means ± SEM.

Setting up the experimental conditions to evaluate the effect of androgens secreted by PPAT on PCa cell lines proliferation and survival.

To evaluate the effect of androgens present in PPAT-conditioned medium on PCa cell lines proliferation and survival it is mandatory to use serum that does not contain androgens ("charcoal-stripped serum", CFBS). First, to demonstrate that the growth of LNCaP was dependent of androgens, these cells were incubated for 48 hours in the presence of androgen-

depleted serum containing medium and then various concentrations of 5α-DHT from 0.1 to 50 nM were added. Cell viability was then evaluated by MTT after 3 days.

Our results indicated that 5α-DHT could promote LNCaP cell survival in 5% CFBS containing medium in a dose dependent manner from 0.1 nM to 10 nM, the maximum of the effect being obtained at 10mM in accordance with the literature[622] (**Fig. 10A**). To demonstrate that LNCaP were able to use 5α androstanedione as a precursor of active androgen to proliferate, as previously, we incubated the cells for 48 hours in the presence of 5% CFBS containing medium and then treated them with various concentrations of purified 5α androstanedione. Cell growth was analyzed measuring cell confluence by real time imaging (Incucyte) after 3 days. In accordance with the literature[623], our results showed that 5α androstanedione could promote LNCaP cell proliferation in a dose -dependent manner between 1 and 100 nM whereas higher concentrations did not modify cell growth (**Fig. 10B**). We also evaluated the effect of purified etiocholanolone on LNCaP cell growth and our preliminary result showed a decreased cell viability in 5%FBS containing medium.

These results indicate that LNCaP cultivated in 5% CFBS containing medium represent an appropriate model to study the effect of androgens secreted by PPAT on cell proliferation.

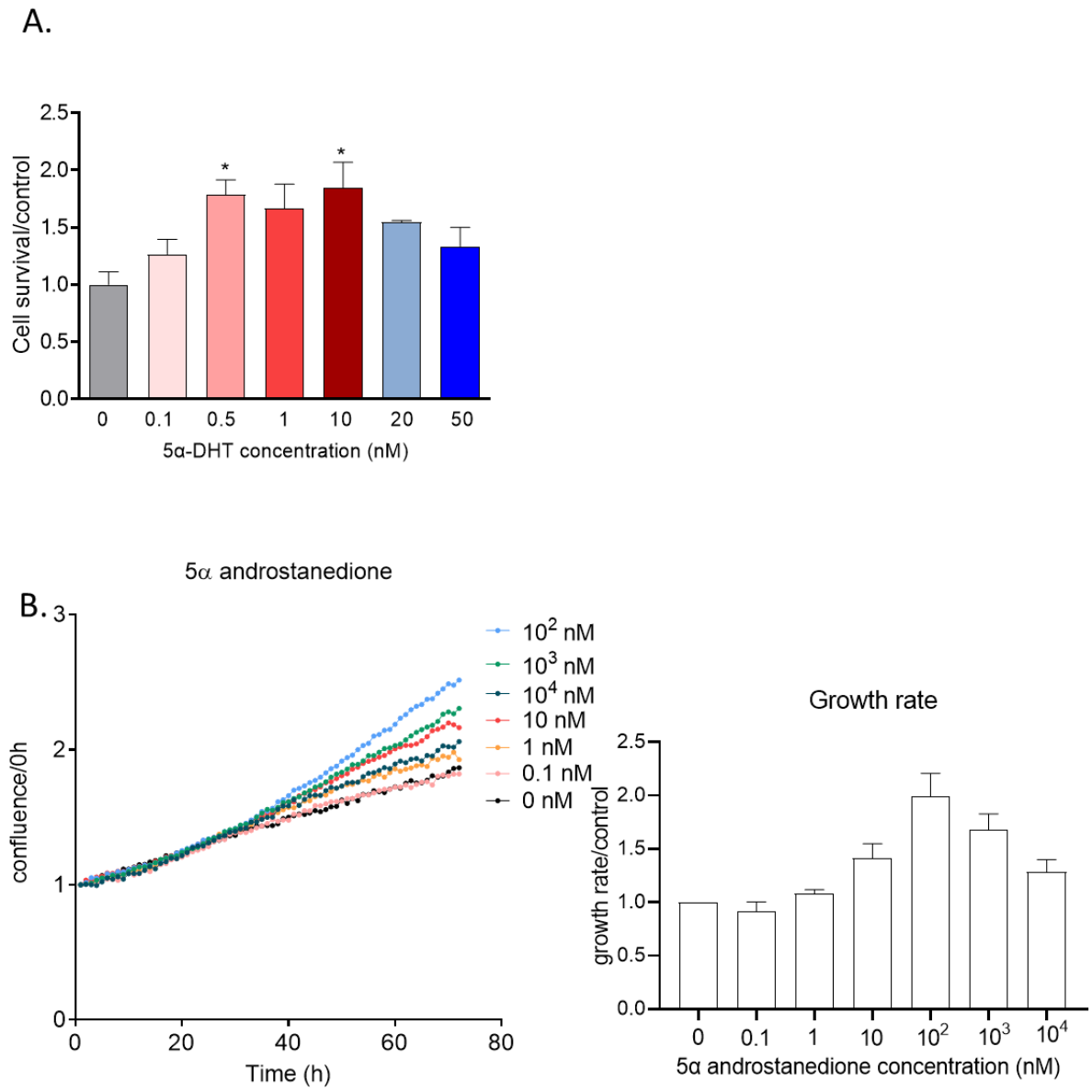


Figure 10. 5α-DHT and 5α androstanedione promote LNCaP cell survival and proliferation in androgen depleted medium. A) Cell viability analysed by MTT in LNCaP incubated for 2 days in the presence of 5% charcoal stripped FBS (CFBS) containing medium and then treated or not with different concentration of 5α-DHT for 3 days (n=3). **B)** Cell confluence analysed by Incucyte in LNCaP incubated for 2 days in the presence of 5% CFBS containing medium and then treated or not with different concentration of purified 5α androstanedione for 3 days (n=3). Results were normalized by control (untreated cells). Bars indicate means ± SEM. Statistical differences were calculated by using Anova test, *p<0.05.

As previously published by the team[445], we usually use 1% of BSA to prepare PPAT-CM to ensure efficient delivery and stability of molecules such as fatty acids, hormones and peptides into cultured cells. Experiments were performed to evaluate the importance of BSA concentrations in the effect of PPAT on LNCaP growth and survival, since we observed in preliminary experiments that BSA concentration could affect LNCaP survival (data not shown).

As shown in **Fig. 11**, in the presence of CFBS serum, PPAT-CM promote LNCaP survival and growth at similar levels than 10mM DHT when PPAT-CM was prepared in 0.25 and 0.5 % BSA. This effect was no longer observed at higher BSA concentrations (1%) BSA or when BSA was omitted during the PPAT-CM preparation (0% BSA) (**Fig. 11**). For further experiments, we decided to use PPAT-CM prepared in 0. 25%BSA. **In addition, these first set of experiments demonstrate for the first time that PPAT-CM is able to sustain the survival and growth of LNCaP in the absence of androgens.**

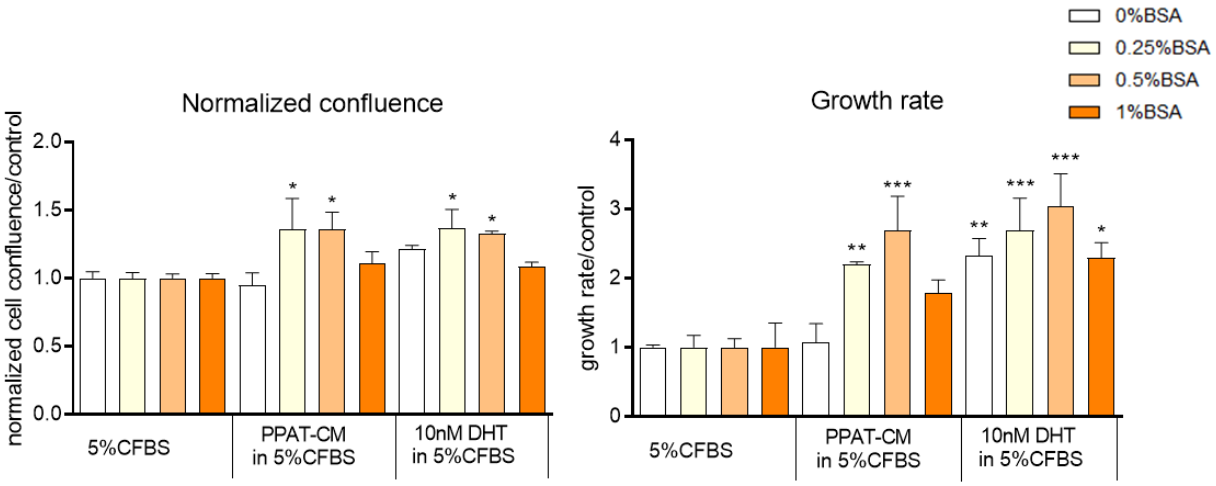


Figure 11. PPAT conditioned medium prepared in 0.25% and 0.5% BSA exhibit higher pro-proliferative effect than other BSA concentration in LNCaP cultivated in androgen depleted medium. Cell confluence analysed by Incucyte (left panel) and cell growth rate analysed by Incucyte (right panel) in LNCaP incubated for 2 days in the presence of 5% CFBS containing medium and then treated or not with PPAT conditioned medium (PPAT-CM) prepared in 5% CFBS and different BSA concentrations for 3 days (n=3-5). Normalized confluence represents the final confluence after 3 days divided by initial confluence. Results were normalized by control (untreated cells). Bars indicate means ± SEM. Statistical differences were calculated by using Anova test, *p<0.05 **p<0.01, ***p<0.001.

Effect of PPAT and APAT-CM on the proliferation of androgen-dependant, sensitive and independent cell lines

We first evaluated the effect of PPAT and APAT-CM on the proliferation of the LNCaP cells using two different approaches: the growth rate as determined by live imaging experiment (Incucyte) and BrdU incorporation (as a reflection of the number of cells in S phase). As expected from **Fig. 11**, we found that in the presence of CFBS containing medium, PPAT-CM but also APAT-CM was able to support LNCaP proliferation as determined by live imaging and BrdU incorporation (**Fig. 12A**). Very interestingly, no effect was observed when the experiments were performed in FBS containing medium (**Fig. 12B**) showing that the effect of PPAT and APAT-CM on LNCAP is strictly dependent on androgens. Although PPAT contained higher concentration of 5α androstanedione and epiandrostreone than APAT, we

have shown that other androgen precursors as well as 5α -DHT are secreted by APAT (**Table 1**) that promote LNCaP cell growth. However, using CM from distant AT could artificially force this crosstalk to occur. In fact, *in vivo*, the vasculature that services the prostate crosses PPAT, thereby facilitating local tissue crosstalk, at the anterior surface of the prostate, where there is direct contact with PPAT[419].

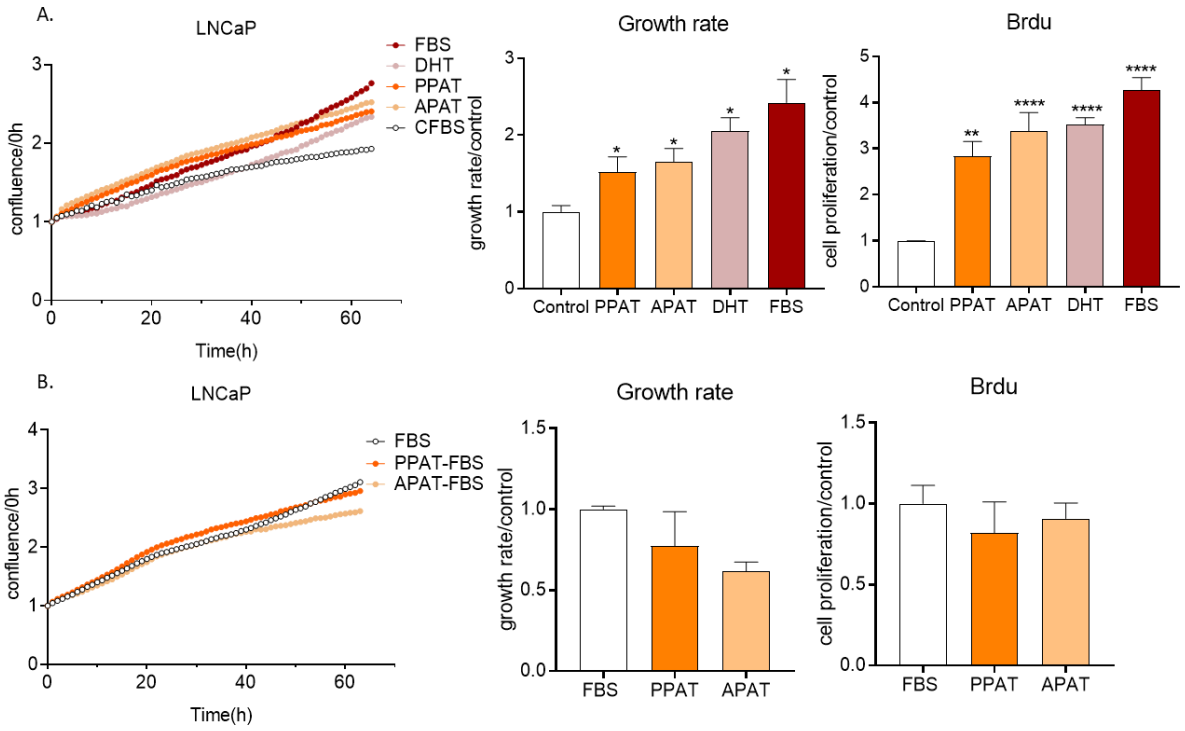


Figure 12. PPAT and APAT secretions promote proliferation of androgen-dependent cell line LNCaP in androgen depleted medium but not in androgen containing medium. A) Cell growth analysis by Incucyte (left and middle panel) and cell proliferation analysed by BrdU incorporation (right panel) in LNCaP incubated for 2 days in the presence of 5% CFBS containing medium and then treated or not with PPAT-CM, APAT-CM, 10nM 5α-DHT or FBS containing medium (FBS) for 3 days (n=3-7). **B)** Cell growth analysis by Incucyte (left and middle panel) and cell proliferation analysed by BrdU incorporation (right panel) in LNCaP treated or not with PPAT-CM, APAT-CM in FBS containing medium (FBS) for 3 days (n=3-5). Representative growth curve are shown. Growth rate were calculated within exponential growth phase. All results were normalized by control (untreated cells). Bars indicate means ± SEM. Statistical differences were calculated by using Anova test, *p< 0.05, **p<0.01, ****p<0.0001.

Preliminary experiments performed with the androgen sensitive cell line 22RV-1 show that 5α-DHT treatment as well as PPAT and APAT-CM promoted the growth of these cells (**Fig. 13A**). As expected, the androgen-independent cell lines PC3 and DU145 were not sensitive to 5α-DHT treatment and PPAT-CM and APAT-CM promoted PC3 but not DU145 proliferation in the presence of CFBS containing medium (**Fig. 13B** and **13C**). These results indicate other growth factors (like the pro-inflammatory cytokines IL-6) or adipokines (such as leptin) secreted by PPAT may support the proliferation of androgen-independent cell line PC3[419] whereas DU145 cell line does not respond to PPAT-CM contained growth factors.

In opposition to our study, previous studies reported the pro-proliferative effect of PPAT-CM in androgen-independent cell line PC3 and DU145 but not in androgen-dependent cell line LNCaP[624,625]. In these studies, they cultivated PCa cells in FBS free medium whereas we used CFBS containing medium, which is necessary to reveal the growth of androgen dependent cells. **To conclude, our results demonstrate for the first time the ability of PPAT-CM to sustain the growth of PCa cells in an androgen-dependant manner.**

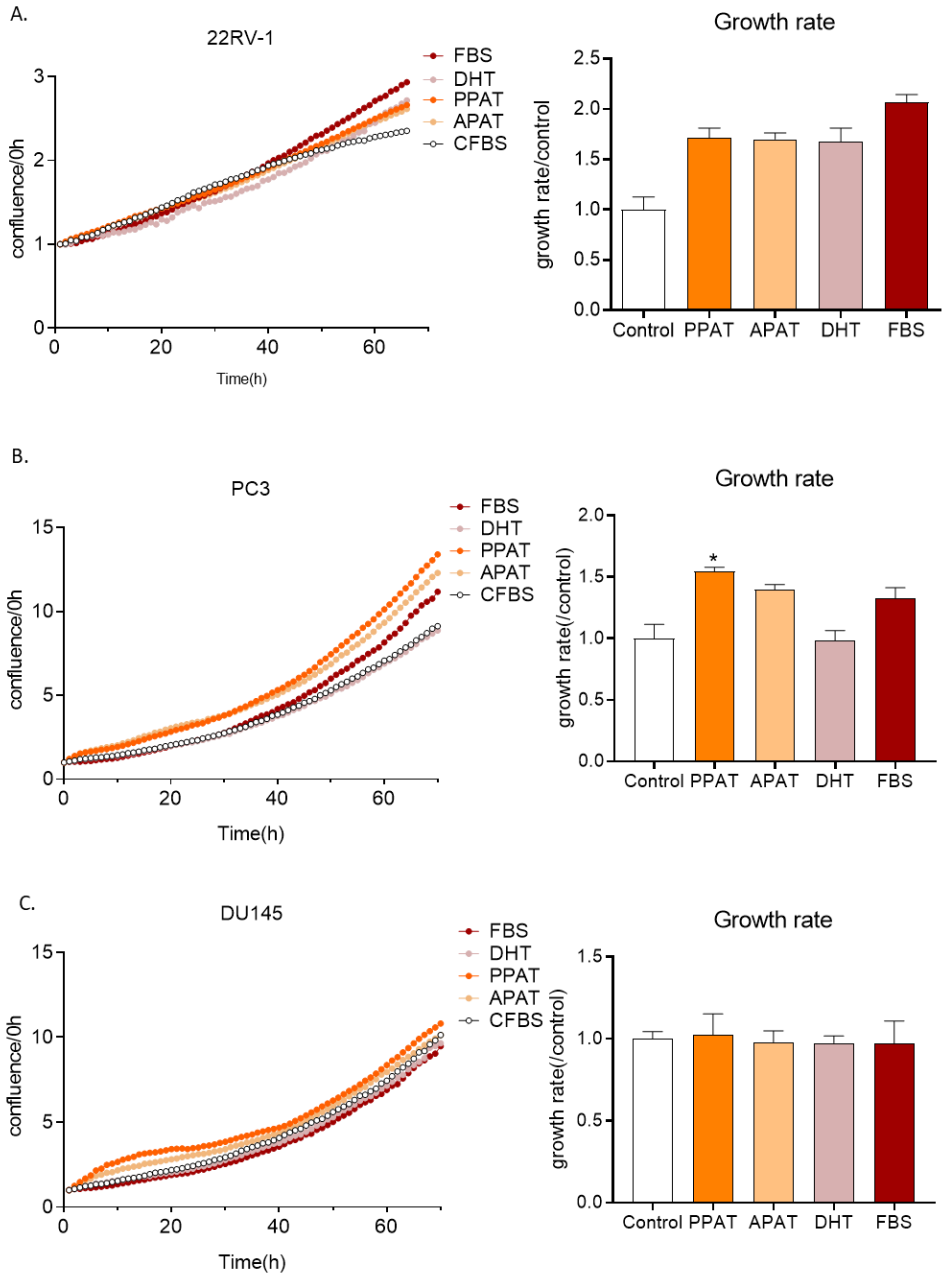


Figure 13. APAT and PPAT secretions promote proliferation of androgen independent cell line PC3 in androgen depleted medium. Cell growth analysis by Incucyte in 22RV1 **(A),** PC3 **(B)** and DU145 **(C)** incubated for 2 days in the presence of 5% CFBS containing medium and then treated or not with PPAT-CM, APAT-CM, 10nM 5α-DHT or FBS containing medium (FBS) for 3 days (n=3-5). Representative growth curves are shown and growth rate were calculated within exponential growth phase. All results were normalized by control (untreated cells). Bars indicate means ± SEM. Statistical differences were calculated by using Anova test, *p<0.05.

Androgen depletion induced up-regulation of AKR1C3 is reverse by PPAT-CM treatment.
We then investigated if in the absence of androgens, PPAT-CM could regulate the steroidogenic enzyme expression in LNCaP in order to further confirm that it contains steroid metabolites with a functional impact on tumor cells. In fact, it has been previously demonstrated that steroidogenic enzymes expression was increased in androgen-dependent cell line DuCaP cultivated in CFBS containing medium for 12 days to favor intra-tumoural hormone synthesis[178]. In CRPC (where the testicular source of androgens is totally inhibited), it has been described an upregulation of AKR1C3 and HSD17B3 and a downregulation of HSD17B2 and HSD17B4[130]. The flux (androstenedione→5α-androstanedione→5α-DHT) has been shown to be more rapid and predominated than the flux (androstenedione→testosterone→5α-DHT) in CRPC[147]. As expected from these results, we observed that growing LNCaP cells in androgen-depleted medium led to overexpression of AKR1C3 (**Fig. 14)** involved in the 5α androstanedione→5α-DHT transformation (**Fig. 8**). By contrast, the levels of HSD17B7 displaying the same function than AKR1C3 and SRD5A1/3 catalyzing the synthesis of 5α androstanedione and 5α-DHT from respectively androstenedione and testosterone and HSD3B1 involved in androgen synthesis from DHEA or epiandrosterone (**Fig. 8)** were unchanged compared to FBS containing medium (**Fig. 14**). Concerning the enzyme catalyzing the opposing reaction (5α-DHT back conversion into 5α-androstanedione) (**Fig. 8)**, HSD17B4 expression tended to decrease in androgen-depleted medium whereas HSD17B2 and HSD17B10 expression were unchanged compared to FBS containing medium (**Fig. 14**). Very interestingly, PPAT-CM reversed the changes in AKR1C3 and HSD17B4 expression showing indirectly that androgen metabolites are present in this medium that render the increase in intra-tumour synthesis unnecessary (**Fig. 14**). HSD17B2 expression exhibited an increases trend in PPAT-CM compared to androgen-depleted medium. It has been described that AKR1C3 expression is repressed by the activation of androgen signaling pathway in a negative feedback mechanism[130]. **The regulation of AKR1C3 and HSD17B4 expression by PPAT-CM suggest that PPAT could provide androgen substrate such as 5α androstanedione for alternate androgen synthesis in LNCaP.**

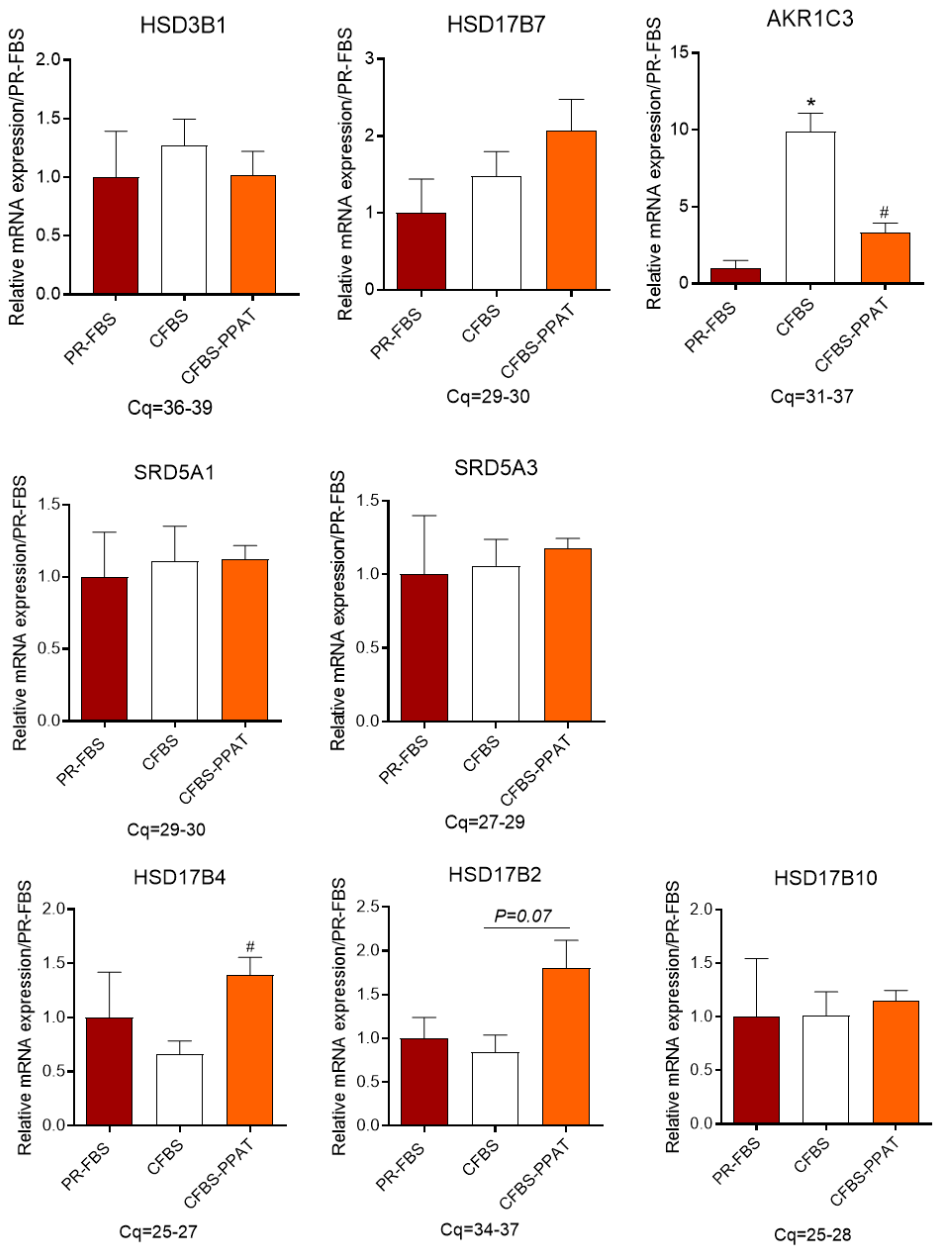


Figure 14. Androgen depletion induced up-regulation of AKR1C3 and down-regulation of HSD17B4 is reverse by PPAT-CM treatment in LNCaP. Relative mRNA expression of indicated genes encoding the enzymes involved in steroid metabolism in LNCaP cultivated in FBS or CFBS containing medium or treated with PPAT-CM (PPAT) for 3 days (n=3 for CFBS and PR-FBS; n=5 for PPAT-CM). Bars indicate means ± SEM. Statistical differences were calculated by using Anova test, *$p<0.05$ represents the comparasion between PR-FBS and CFBS; #$p<0.05$ represents the comparasion between CFBS and PPAT-CM.

PPAT pro-proliferative effect is inhibited by antiandrogen Bicalutamide. To investigate whether the pro-proliferative effect of PPAT-CM observed in LNCaP in the absence of androgen is indeed an AR-mediated response, experiments were performed in the presence or absence of AR antagonist bicalutamide in PPAT-CM in the presence of CFBS containing medium (**Fig. 15**). We investigated LNCaP cell growth by live imaging (left and middle panel) and viability by MTT (right panel). As shown in **Fig. 15A**, Bicalutamide blocked

PPAT-CM induced LNCaP cell proliferation and cell viability in a dose dependent manner. In parallel we have verified that these doses of bicalutamide have no effects on the survival of LNCaP in CFBS containing medium (**Fig. 15B**). **Thus, our result supports the fact that PPAT-CM contributes to the activation of AR in order to support LNCaP proliferation and survival.**

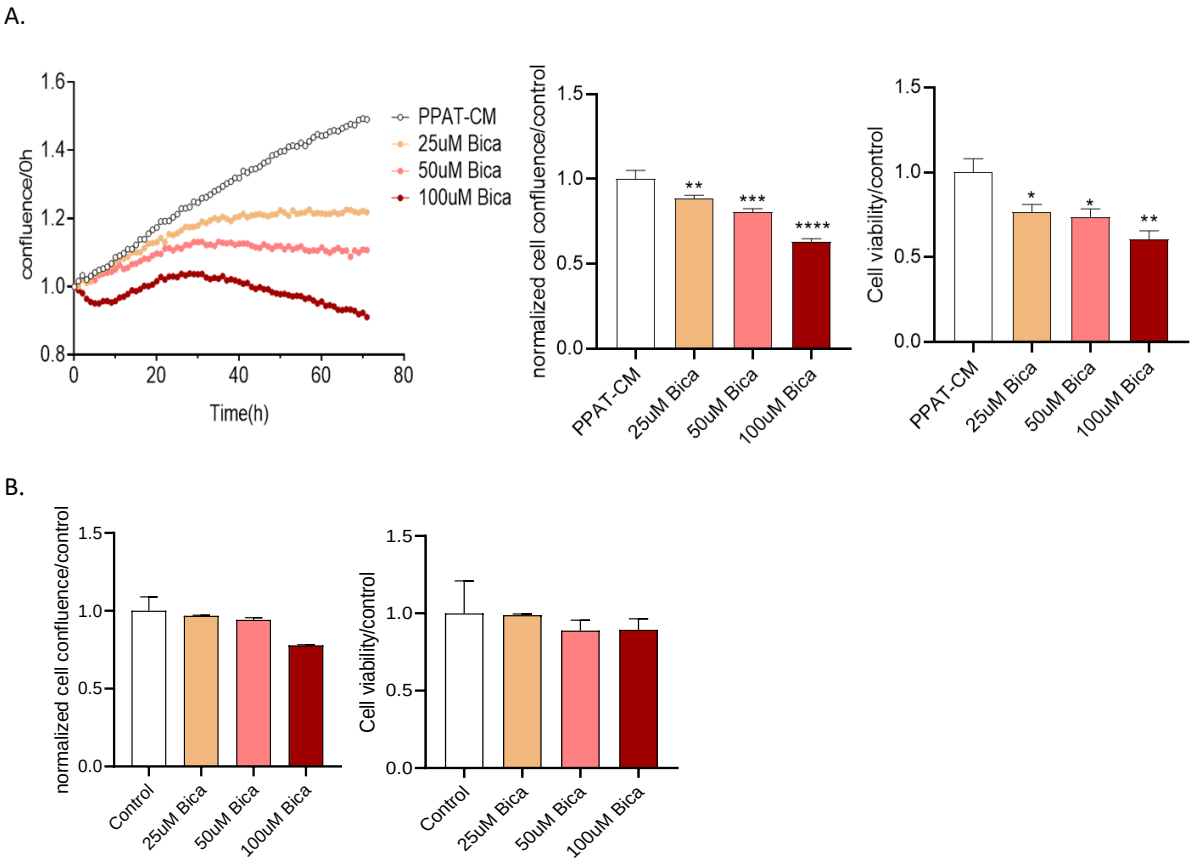


Figure 15. The antiandrogen bicalutamide inhibits PPAT-CM induced cell growth (A) and its influence on the the survival of LNCaP in CFBS containing medium (B). Cell growth analysis by Incucyte (left and middle panel of A, left panel of B) and cell viability analysed by MTT (right panel of A and B). LNCaP cultivated in CFBS were pre-treated with PPAT-CM (A) or kept in CFBS (B) for 3 days, then medium was updated with or without different concentration of bicalutamide prepared in PPAT-CM (A) or kept in CFBS (B) for another 3 days (n=3). Representative growth curve is shown. Normalized confluence represents the final confluence after 6 days divided by initial confluence. Results were normalized by control (PPAT-CM or CFBS group). Bars indicate means ± SEM. Statistical differences were calculated by using Anova test, *p<0.05, **p<0.01, ***p<0.001, ****p<0.0001.

PPAT secretions upregulate AR responsive gene in LNCaP in androgen-depleted medium

To further confirm if the pro-proliferative effect of PPAT-CM in LNCaP was due to the activation of AR signaling pathway, we evaluated, by RT-qPCR, the relative gene expression of AR-targeted genes in LNCaP cultivated in FBS or CFBS containing medium or treated with

either PPAT-CM (PPAT) or DHT prepared in CFBS containing medium for 3 days. Our results showed that AR-targeted genes such as KLK3 and FKBP5 encoding respectively for PSA (Prostate specific antigen) and FKBP Prolyl Isomerase 5 were increased in LNCaP cultivated in PPAT-CM as well as in DHT and FBS containing medium compared to CFBS contained medium (**Fig. 16**). These results directly showed that PPAT-CM could activate AR signaling pathway.

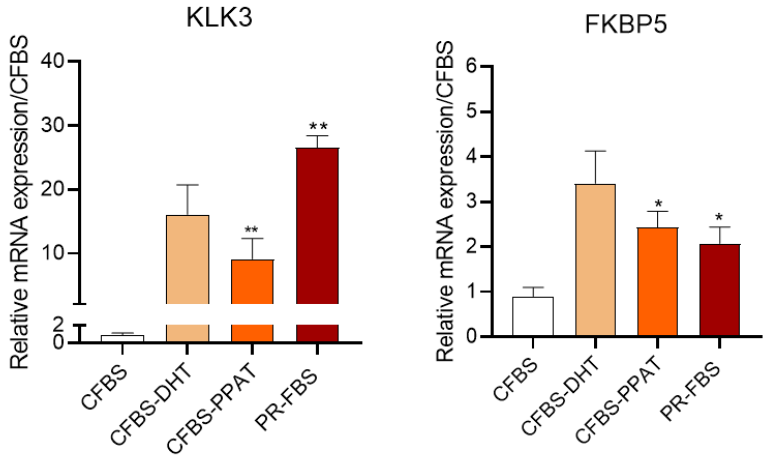


Figure 16. PPAT-CM increased AR responsive gene expression in LNCaP. Relative mRNA expression of AR-responsive genes in LNCaP cultivated in FBS or CFBS containing medium or treated with either PPAT-CM (PPAT) or DHT for 3 days (n=3 for CFBS and PR-FBS; n=2 for DHT; n=5 for PPAT-CM). Bars indicate means ± SEM. Statistical differences were calculated by using Anova test, *p<0.05, **p<0.01

CONCLUSION

In conclusion, we have demonstrated here for the first time that PPAT is able to accumulate steroid metabolites such as 5α androstanedione and epiandrosterone, involved in the alternate routes for 5α-DHT synthesis in CPRC. Within PPAT, mature adipocytes appear to be the main source of androgen metabolites. Regulation of expression of enzymes involved in steroidogenesis could explain the higher content of 5α androstanedione and epiandrosterone in PPAT compared to another proximal adipose depot APAT; although these results need to be confirmed at protein levels. Although we did not directly demonstrated the secretion of steroid by PPAT, our study bring several experimental arguments in favor of a functional effect of the steroids metabolites contained in PPAT on PCa cells : i) PPAT-CM can support cell growth and proliferation of an androgen-dependent cell line LNCaP cultivated in androgen-deprived medium but not in androgen containing medium ii) the regulation of steroidogenic enzymes expression in the absence of androgens is reversed by PPAT-CM iii) the pro-proliferative effect

of PPAT-CM is inhibited by an AR antagonist, bicalutamide, and iv) PPAT-CM upregulates AR targeted gene expression in LNCaP. Additional approaches would be developed (inhibition of specific enzymes involved in steroidogenesis in tumor cells, development of a coculture model with isolated adipocytes) that are described in the final discussion and perspectives part of my manuscript. These new results demonstrated that PPAT is a new source of androgens for CRPC and also paved the way to explain why changes in PPAT (as seen in obesity or during PPAT accumulation independently of BMI) leads to more aggressive PCa that exhibit resistance to androgen deprivation therapy and could allow to propose new risk stratifications and/or identify new therapeutic targets.

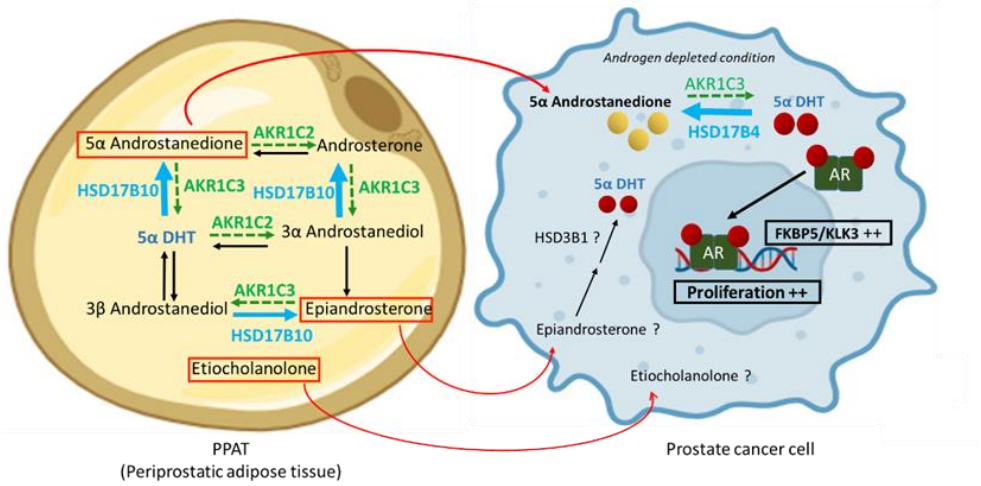


Figure 17. **PPAT: a new source of androgens for CRPC.** PPAT (mainly adipocytes) is able to accumulate steroid metabolites such as 5α androstanedione and epiandrosterone, involved in the alternate routes for 5α-DHT synthesis in CPRC (and also etiocholanolone) compared to another proximal adipose depot APAT. The regulation of expression of steroidogenic enzymes (decrease of AKR1C3/C2 and increase of HSD17B10 expression) could explain the higher content of 5α androstanedione, epiandrosterone and etiocholanolone in PPAT. Secretions from PPAT can activated AR responsive gene such as FKBP5 and KLK3 and support the proliferation of an androgen-dependent cell line LNCaP cultivated in androgen-deprived medium. The regulation of steroidogenic enzymes in LNCaP in the absence of androgens is reversed by PPAT (down-regulation of AKR1C3 and up-regulation of HSD17B4) showing that 5α androstanedione involved in these enzymes' regulation may contribute to PPAT pro-proliferative effect. The role of epiandrosterone and etiocholanolone in this crosstalk still needs to be elucidated.

GENERAL DISCUSSION/PERSPECTIVES

GENERAL DISCUSSION AND PERSPECTIVES

PCa is initially driven by active androgens which stimulate the growth of cancer cells via the AR pathway. The primary treatment for PCa is androgen deprivation therapy (ADT). However, the tumor adapts to low androgen levels and finds mechanisms to thrive despite androgen depletion, becoming CRPC and bringing new challenges to the treatment. It is vital to understand the mechanisms for the development of CRPC. Emerging evidence suggests that the tumor microenvironment can cooperate with the tumor to sustain CRPC by providing steroid metabolites able to reactivate the AR signaling as described in the introduction.

The main hypothesis of our work was that PPAT can be a source of steroid metabolites. First, PPAT's proximity to PCa and vascularization of the prostate crossing PPAT favor molecular exchanges between PPAT and cancer cells[419]. Second, as others AT, PPAT is an endocrine tissue secreting a large number of soluble molecules that play an important role in PCa development including metastasis, invasion and proliferation as described in the introduction of this manuscript. However, the role of sex steroid in this crosstalk was clearly missing although we speculated that like others AT, PPAT was a source of steroid metabolites. Furthermore, our preliminary data showed an overexpression of genes involved in the androgen and estrogen signaling pathways in PPAT compare to APAT (Article presented in Result's part 1). Third, we have shown that PPAT volume correlates with the volume of the prostate, suggesting that the development of these two tissues may be dependent on common signals involving steroids (Article presented in Result's part 2). Fourth, 5α reductase inhibitors decreased the volume of PPAT, suggesting that its development is androgen dependent[456]. These facts trigger our interest in sex steroid especially androgens in PPAT and we decide to investigate androgen metabolism profile and metabolic capacity in PPAT and whether these androgens from PPAT could affect PCa development.

The first part of our results demonstrated that PPAT (and within PPAT mainly adipocytes) contained androgens, estrogens and progestogens. Furthermore, 5α androstanedione and epiandrosterone, two precursors involved in CRPC development, were more abundant in PPAT compared to a control AT (APAT).

Our study showed that adipocytes isolated from PPAT exhibit a similar sex steroid dosage profile with paired APAT whereas we were not able to detect sex steroids in SVF as tested with varied protocols and cell numbers. Thus, these results lead us to propose that within PPAT the

adipocytes are the main site for androgen synthesis and storage. Indeed, according to our knowledge, sex steroid dosages in SVF have never been performed in any study. Moreover, 5α reduction of testosterone into 5α-DHT was not detected in SVF cells such as preadipocytes[615]. We also found that SVF displayed significantly higher aromatase mRNA expression than adipocytes, as indicated by our observations in both PPAT and APAT (data not included), as well as in other AT[616,617]. All these results which showed that in opposition to androgens, SVF plays a more important role in estrogen regulation in AT.

Our previous work has shown that PPAT exhibited a specific vascularization and increased VEGF expression in response to chronic hypoxia. Estrogen responsive genes were upregulated in PPAT compared to APAT (Article presented in the Result's part 2). Estradiol and estrogen receptor α are known to upregulate VEGF expression in AT[626]. Interestingly, we found that estrone, a precursor for estradiol, was more present in PPAT and estrogen receptor α relative mRNA level was higher in PPAT than APAT (data not shown), which could explain the upregulation of VEGF expression.

Moreover, by evaluating the sex steroid enzyme metabolism by RT-qPCR, we found lower AKR1C3 and AKR1C2 mRNA expression in both PPAT and adipocytes and higher HSD17B10 mRNA expression in isolated adipocytes from PPAT compared to APAT, which could explain the accumulation of the two androgens precursor 5α androstenedione and epiandrosterone and also one inactive androgen etiocholanolone.

Our preliminary results indicated an anti-proliferative effects of etiocholanolone in LNCaP cells cultivated in 5%FBS containing medium (data not shown) as already described in cellular models of colorectal cancer[609]. Although these results need to be confirmed in LNCaP cells cultivated in androgen depleted medium, it suggests that the accumulation of etiocholanolone may not explain the role of PPAT in CRPC.

As described in the introduction part of this manuscript, alternative 5α-androstanedione pathway bypassing testosterone has been shown to be the preferred pathway in CRPC[40,159] and production of 5α-DHT from epiandrosterone was found to one of the mechanisms of intratumoural active androgen production from inactive androgens in CRPC[606]. Based on these studies, we hypothesis 5α androstanedione and epiandrosterone, two androgens precursors from PPAT could play a role in promoting CRPC cell line growth. Thus, to reinforce our hypothesis, the sex steroid secretion profile in PPAT-CM is currently being evaluated by the LABERCA laboratory in Nantes. We hope to have a clear view about the androgen species quantitatively

and qualitatively. It is deserved to notice that other metabolites such as DHEA could also be important in promoting PCa cell growth due to its highest concentration in PPAT[627,628].

The second part of our results showed that PPAT-CM promotes androgen dependent cell line LNCaP growth and upregulates AR responsive gene expression in androgen-deprived medium and this effect is inhibited by AR antagonist suggesting that androgens secreted from PPAT could activate AR signaling pathway.

To confirm that PPAT-CM promote cell proliferation through AR activation, we wanted to use LNCaP cells invalidated for AR by CrispCas9 strategy (AR-KO LNCaP) that was provided to us by Pr. Dean Tang (Roswell Park Comprehensive Cancer Center in New York)[629]. Unfortunately, we found that these cells still proliferated in androgen deprived medium and still expressed AR at mRNA and protein levels (data not shown). These results highlight the profound androgen dependency of LNCaP cells. We are planning to investigate the pro-proliferative effect of PPAT-CM on LNCaP in which AR will be silenced transiently by RNA interference approaches.

However, we cannot formerly exclude that the observed effects could be independent of direct AR activation by androgens. As the AR activation could bypass androgen as described in the introduction (Chapter 7.2), we can speculate that other growth factors secreted from PPAT, such as IL6 or TNFα, may activate AR signaling pathway in a cooperative way or even independently of active androgens from PPAT. Also, our team previously showed that FFA liberated from PPAT are used by PCa cells to increase their oxidative stress and then promote invasiveness[445]. Thus, we can speculate that these FFA from PPAT could be incorporated into cholesterol esters in the form of lipid droplets and then be involved in the activation of PI3K/AKT pathway to regulated AR signaling pathway in LNCaP as it has been shown that the esterified cholesterol accumulation in LDs is associated with high-grade PCa and metastases by activation of PI3K/AKT pathway in PC3[439].

New models

PPAT adipocytes represent a major site for androgen synthesis as seen in the first part of our results. In this context, to validate the functional results obtained with PPAT-CM on PCa growth, 3D co-culture adipocytes with PCa cells will be a more interesting model to mimic the communication between PPAT and PCa *in vivo*. It is therefore important to set up a 3D culture model of adipocytes, isolated from PPAT that preserves the functional and morphological integrity of the adipocytes. In fact, our preliminary results showed that PPAT adipocytes

cultured under a membrane (MAAC) exhibited well-preserved morphology, viability, and adiponectin secretion overtime compared with another well-established 3D model which was firstly used to culture with mammary adipocyte[630,631]. Moreover, PPAT adipocytes under MAAC co-cultured with LNCaP cells in androgens depleted medium induced an increase in LNCaP cell viability. These results are encouraging but need to be confirmed. Besides, tumoroids, which are patient-derived organoids and therefore represent a more integrated and physiological model of PCa than cell lines could be used in future. We have established a collaboration with Dr. Clémentine Le Magnen (Department of Biomedicine, University of Basel), who has two androgen-dependent tumoroid models (unpublished). PPAT-CM and co-culture model will be tested with these tumoroid models.

Furthermore, we will investigate the effects of PPAT-CM and co-culture on the resistance of PCa to second line treatments (the androgen synthesis inhibitor, abiraterone and AR inhibitors bicalutamide and enzalutamide). Androgen precursors such as cholesterol, DHEA and progesterone are upregulated in enzalutamide-resistant PCa cells compared to parental cells[212]. Thus, PPAT representing a reservoir of androgen precursors could be involved in the resistance of PCa to these drugs.

Finally, the androgens found in PPAT may be particularly clinically important in a subgroup of patients with abundant PPAT. PPAT is a very specific AT whose accumulation is independent of BMI[419,455]. Our group showed that PPAT presents a state of chronic hypoxia responsible for an inflammatory state and fibrosis which opposes its expansion in obesity (article presented in Result's part 1). However, there is considerable heterogeneity in PPAT abundance between patients. Numerous clinical studies have shown that patients with the most abundant PPAT represent more aggressive PCa with more undifferentiated tumors and a more rapid onset of castration resistance[453,454]. Thus, the abundance of PPAT appears to be an important risk factor in the development of aggressive PCa. My team has shown that abundant PPAT accumulates by adipocyte hypertrophy and, unlike obesity, this hypertrophy is not accompanied by an inflammatory state of PPAT. This hypertrophy without inflammation is due to a decrease in mechanical stress on adipocytes related to a looser extracellular matrix in abundant PPAT, which allows their expansion. We have shown that a matrikin, endotrophin, could participate to the aggressiveness of PCa in patients displaying abundant PPAT (Article presented in Result's part 2).

We hypothesize androgenic precursors and their secretion could be modified quantitatively and /or qualitatively in patients with abundant PPAT which would promote the development of resistance to castration. In addition, a bidirectional dialogue between the two cell populations (adipocytes and tumor cells) could amplify this phenomenon. Thus, it will be interesting: (i) to characterize the regulation of metabolism, content and secretion of androgenic precursors in both abundant and non-abundant PPAT (ii) to determine whether androgenic steroids secreted by abundant PPAT promote PCa proliferation and castration resistance (iii) to evaluate whether a metabolic dialogue involving steroids exists between adipocytes and tumor cells.

The mechanisms contributing to the appearance of abundant PPATs are not known. It would be interesting to assess whether specific androgenic signaling is present in abundant PPAT, which would help explain their expansion. As described in the introduction, in general, androgens are known to reduce body fat by inhibiting adipogenesis and stimulating lipolysis. Thus, we expect that lower levels of androgens in abundant PPAT compared to non-abundant PPAT could explain adipocyte hypertrophy observed in abundant PPAT. But tissue specific effects should be considered and androgens may have different effects on PPAT compared to more largely studied VAT and SAT.

In conclusion, my work highlights that androgens secreted by PPAT could play an important role in the progression of CRPC. Identifying the molecular mechanisms involved in this metabolic dialogue will enable us to identify potential molecular prognostic indicators and define new targets of interest in the treatment of CRPC.

MATERIALS AND METHODS

Material and Methods

Adipose tissue collection and adipocyte isolation

Paired anterior PPAT and APAT from patients were collected from patients undergoing prostatectomies at Toulouse-CHU in accordance with the guidelines and with the full approval of the national ethics committee (AC-2020-4031). Written informed consent was received from participants before inclusion in the study, which was conducted in accordance with the declaration of Helsinki principles as revised in 2000. The quality of the samples was evaluated. Samples were immediately put in 50mL tubes containing 10mL of DMEM and carried out to the lab within 1h. First, paired PPAT and APAT (200-400 mg) were immediately frozen in liquid nitrogen and stored at -80°C and further used for qPCR analysis and steroid quantification. Second, some paired PPAT and APAT samples were used to prepare **PPAT or APAT conditioned medium** (PPAT-CM and APAT-CM respectively). 1 g of either PPAT or APAT were cut into tiny pieces as much as possible then washed twice in phenol red free (PR-) RPMI containing 1, 0.5 or 0,25 % BSA medium. Then 1 g tissue pieces were incubated at 37°C in a humidified incubator with 5% CO2 in 2mL of PR-RPMI 0.5% BSA medium for 24h. The supernatant was collected after filtration through a 200µM filter and centrifuge 5000g for 5 minutes. PPAT-CM and APAT-CM were separated into small aliquots and immediately stored at -80°C.

Isolation of adipose tissue stroma-vascular fraction (SVF)

Digestion of fresh PPAT and APAT were performed as previously described[632]. Briefly, AT were digested with type II collagenase (Sigma Aldrich) at 250U/mL in PBS 2% BSA for 40 min at 37°C with with shaking). After digestion, the cell suspension was filtered through a 200 µM strainer to remove cell debris and undigested fragments. Then cell suspension was centrifuged 20g for 1 min and separated into 2 layers adipocytes and SVF. Floating adipocytes were collected and washed with Krebs Ringer Buffer HEPES Albumin (KRBHA: KRBH supplemented with 150mM NaHCO3, 10mM HEPES, 0.5% BSA) 3 times to obtain pure isolated adipocytes. SVF suspension was centrifuged 400g 5 min to get the SVF cell pellet. Then erythrocyte lysis was performed by homogenizing SVF cell pellet with erythrocyte lysis buffer with pipette (155 mmol/L NH4Cl, 5.7 mmol/L K2HPO4, 0.1 mmol/L EDTA, pH 7.3) for 30 times followed by successive filtrations through 100, 70, and 40 -µm strainers. The viable recovered cells were washed with PBS and counted with subsequent centrifuge to get the dry pellet. Both SVF pellet and purified adipocytes were frozen at -80°C for RT-qPCR and steroid

quantification.

Cell culture

Human prostate cancer cell line PC-3, LNCaP, 22RV-1, DU145 was purchased from ATCC. Generally, 5% fetal bovine serum (FBS) (Gibco) is prior to be used other than 10% FBS to keep cells in a low-nutrient status and observe the effect of extrogenous factors better. However, DU145 cells grow better while maintaining in RPMI-1640 (Gibco, Invitrogen, Carlsbad, CA, USA) medium supplemented with 10% FBS compare to 5% FBS. The other cell lines were maintained in RPMI-1640 medium supplemented with 5% FBS at 37°C in 5% CO2 since they grow in a similar way as in 10% FBS. To prevent the effects of androgenic and estrogenic components from RPMI and FBS, all cell lines except DU145 were seeded in phenol red free (PR-) RPMI supplemented with 5% charcoal-stripped FBS (CS-FBS) for experiments. DU145 were seeded in PR-RPMI supplemented with 10% charcoal-stripped FBS (CS-FBS) for experiments.

Cell viability, cell confluence and cell proliferation test

MTT assay (cell viability test), **incucyte imaging** (cell confluence) and **BrdU incorporation** (cell proliferation) were performed separately to evaluate the effect of DHT, androstenedione and PPAT/APAT-CM on the four PCa cell lines. PCa cells (PC3/DU145: 1000 cells, LNCaP: 7000 cells, 22RV-1: 5000 cells) were seeded in PR-RPMI medium with 5% CS-FBS (10% for DU145) in 96-well plates (Corning 3599). After attachment (48h for LNCaP and 24h for the others cells), PCa cells were cultivated during 3 days in various conditions (PPAT/APAT-CM, DHT, androstanedione) in PR-RPMI with 5% CS-FBS (10% for DU145) supplemented with BSA or not (for 5α androstanedione). During 3 days, cells are imaged with IncuCyte live-cell imaging system (Sartious) every hour. Growth rate was calculated within the exponential growth curve. Cell confluence analysed after 3 days was divided by the initial confluence at day 0 to get the normalized confluence. After 3 days, cell viability was detected with the addition of 10µl of 5 mg/ml 3-(4-5-dimethylthiazol2-yl)-2.5-dyphenyltetrazolium bromide (MTT; Sigma-Aldrich, Corp.) solution into each well. Plates were incubated for 2h at 37 °C in a humidified atmosphere of 5% CO2. 100µl of SDS-HCL was added to each well to dissolve the resultant formazan crystals. The optical density (OD) of each well was measured the day after at 570nm using a µQuant microplate reader (Agilent - BioTek instruments, Les Ulis, France) and used to evaluate cell viability.

For the effects of PPAT and APAT-CM on LNCaP, BrdU labeling solution was added after 3-days treatments. An ELISA BrdU was performed as the manufacturer's protocol (Ozyme). Absorbance was measured at 450 nm using the µQuant microplate reader. Proliferation rate was reflected by the OD value.

RNA extraction and RT-qPCR

For **whole adipose tissue** RNA extraction, 200 mg of frozen tissue was mixed with 500 µL QIAzol^{TM} lysis reagent (Qiagen) and homogenized with the Precellys ® tissue homogenizer (2 cycles of 45 s at 7500 rpm at 4°C) using the Cryolys Cooling system. The tissue homogenates were centrifuged 10 min at 5000g at RT. The lipid-containing surface layer was then removed and chloroform added. The organic and aqueous phases were separated by centrifugation (10 min at 5000 g at RT). The upper aqueous phase containing RNA was recovered.

For **adipocytes**, 500µl of frozen adipocytes was mixed and homogenized with the same volume of QIAzol^{TM} lysis reagent with the subsequent centrifugation (10 min at 500 g at RT). In a similar way with adipose tissue, the lipid-containing surface layer was then removed slowly and chloroform was added into the rest part. The organic and aqueous phases separation was obtained by centrifugation (10 min at 5000g at RT) and the aqueous phases was collected.

SVF and PCa cell pellets containing at least 1 million cells were homogenized with 300µl prepared buffer RLT plus buffer (lysis buffer from kit) and then through gDNA eliminator spin column. The flow-through containing mRNA was kept for the following procedures.

The solution containing RNA recovered from adipose tissue, adipocytes, SVF and PCa cells separately was mixed with ethanol for RNA extraction using the Qiagen RNeasy mini kit as described by manufacturer. The RNA concentration was determined with a Nanodrop 2000 spectrophotometer at a wavelength of 260nm. cDNA were reverse transcribed from 250ng of purified RNA using ReverAid H Minus First Strand cDNA synthesis kit (Thermo Scientific) with hexamer random primers following provider recommendations. Gene expression were quantified using quantitative RT-qPCR on 6.25 ng of cDNA with taqman primers (AKR1C3, Hs00366267_m1; HSD17B3, Hs00970004_m1; HSD17B7, Hs00996127_m1; 18s, Hs99999901_s1; HSD17B2, Hs00157993_m1; HSD17B4, Hs01069908_m1; HSD17B10, Hs00189576_m1; AR, Hs00171172_m1; CYP17A1, Hs01124136_m1; SRD5A1, Hs00602694_mH; SRD5A3, Hs00430681_m1; AKR1C2, Hs00912742_m1; CYP11A1, Hs00167984_m1; HSD3B1 primer was synthesized: Forward, 5'-

CCTTCAACCGCCACATAGTC -3'; Reverse, 5'- CAAGGAGACCCTGAAGTCCA -3'; Reverse complement probe, TGGTTCCCTTGTGGACCGGCA, Thermo Fisher Scientific) and fast advanced taqman master mix (Thermofisher Scientific) in a final volume of 20µl with a CFX96real time PCR system (Bio-Rad). Results were normalized to 18S rRNA levels.

Steroid quantification

AT and adipocytes: Extraction of lipids from each analyzed sample was performed according to the Folch method[633]. Briefly, **adipose tissue** (200 to 400 mg) were spiked with 20µl of internal standards and homogenized in 4 mL chloroform/methanol (2:1, v/v), followed by mechanical disruption using a Precellys ® tissue homogenizer (1 cycles of 30 s at 6000 rpm at 4°C). The resulting supernatant was collected. The residual was subjected to a secondary homogenization step utilizing chloroform/methanol (2:1, v/v) and was then reprocessed through precelly grinding, leading to the acquisition of a supplementary supernatant fraction. Chloride solution (0.58%) was added into the supernatant, and the resultant mixture was then vortexed for 20 s and centrifuged at 3000 rpm during 10 min at 4 °C. The organic layer was transferred into a glass tube and evaporated to dryness (N2, 45 °C), allowing for the quantification of extracted lipid content by gravimetry.

Steroids were then extracted from the lipid fraction by adding 3 mL methanol/water (80:20, v/v), incubated at 50 °C for 10 min, vortexed for 20 s, centrifuged, and frozen at −20 °C for 30 min. Following the freezing step, separation between the methanolic phase and the solid lipid fraction was effectively achieved. The methanolic phase was evaporated to dryness (N2, 40 °C, 1h). The residue was dissolved in 0.5 mL cyclohexane/ethylacetate (50:50, v/v) and subsequently injected onto a gel permeation chromatography (GPC) column. Elution during GPC was performed using a solvent mixture of ethyl acetate/cyclohexane (50:50, v/v) at a flow rate of 1.1 mL/min. GPC fractions containing the steroid hormones and metabolites were collected between 19 and 33 min. The collected eluates underwent evaporation to dryness (N2, 40 °C) and then was reconstituted with 200µl methanol. This reconstituted solution was transferred into GC vial and subjected to a secondary evaporation step. The resulting residual was derivatized with 20µL MSTFA/TMIS/DTE (1000:5:5, v/v/ v) at 40 °C for 30 min. 1 microliters of each final extract was injected onto the GC-MS/MS systems, leading to the precise quantification of the target steroid compounds. The results were normalized by lipid content and expressed as ng/g lipid.

For **adipocytes** steroid quantification, the same protocol was used as adipose tissue without the grinding step, which is not necessary for adipocytes.

For **SVF** two protocol were tested. In the first protocol, SVF pellet containing 0.42 million cells was reconstituted with 190µL methanol and rinsed with 380 µL chloroform with subsequent transfer to precellys tube. The SVF solution was added with 20µl of internal standards and grinded with Precellys ® tissue homogenizer (1 cycles of 30 s at 6500 rpm at 4 °C). The contents of the precellys was added with 120 µL of water with the subsequent vortex for 20 s and centrifugation for 5 min at 3000 rpm. Chloroform/methanol phase was then collected and evaporated (N2, 40 °C).

In the second protocol, SVF pellet containing 0.7 million cells was reconstituted with 400µL of methanol/water (80:20, v/v) and rinsed with 50 µL of the same mixture with subsequent transfer to precellys tube. The SVF solution was added with 20µl of internal standards and grinded as described in the first protocol. The supernatant was collected and transfer to a 10kD filter system with subsequent centrifugation for 10 min at 8,000 rpm, 5°C and evaporation (N2, 40 °C).

Subsequent steps are the same for these two protocols: the resulting residual was derivatized with 20µL MSTFA/TMIS/DTE (1000:5:5, v/v/ v) at 40 °C for 30 min. 1 and 2 microliters of each final extract was injected onto the GC-MS/MS systems.

Statistical Analysis

Statistical analyses were performed with GraphPad Prism version 8.04 (GraphPad Software, San Diego, CA). Comparisons between more than 2 groups was performed using a Anova test and Student's T test was used between 2 groups. Normal distribution of the data was determined using the Kolgomorov-Smirnov test.

REFERENCES

1. Hayward, S. W. & Cunha, G. R. The prostate: development and physiology. *Radiol. Clin. North Am.* **38**, 1–14 (2000).
2. Berry, S. J., Coffey, D. S., Walsh, P. C. & Ewing, L. L. The development of human benign prostatic hyperplasia with age. *J. Urol.* **132**, 474–479 (1984).
3. *Martini, F. H., Tallitsch, R. B. & Nath, J. L. Human Anatomy. (Pearson, 2017).*
4. Aumüller, G. Morphologic and endocrine aspects of prostatic function. *The Prostate* **4**, 195–214 (1983).
5. Lilja, H. A kallikrein-like serine protease in prostatic fluid cleaves the predominant seminal vesicle protein. *J. Clin. Invest.* **76**, 1899–1903 (1985).
6. Stamey, T. A. *et al.* Prostate-specific antigen as a serum marker for adenocarcinoma of the prostate. *N. Engl. J. Med.* **317**, 909–916 (1987).
7. Schalken, J. A. & van Leenders, G. Cellular and molecular biology of the prostate: stem cell biology. *Urology* **62**, 11–20 (2003).
8. Griend, D. J. V. *et al.* The Role of CD133 in Normal Human Prostate Stem Cells and Malignant Cancer-Initiating Cells. (2011).
9. Ishii, K., Takahashi, S., Sugimura, Y. & Watanabe, M. Role of Stromal Paracrine Signals in Proliferative Diseases of the Aging Human Prostate. *J. Clin. Med.* **7**, 68 (2018).
10. Cunha, G. R. Role of mesenchymal-epithelial interactions in normal and abnormal development of the mammary gland and prostate. *Cancer* **74**, 1030–1044 (1994).
11. Olumi, A. F. *et al.* Carcinoma-associated fibroblasts direct tumor progression of initiated human prostatic epithelium. *Cancer Res.* **59**, 5002–5011 (1999).
12. Bhowmick, N. A. *et al.* TGF-beta signaling in fibroblasts modulates the oncogenic potential of adjacent epithelia. *Science* **303**, 848–851 (2004).
13. *https://www.wcrf.org/cancer-trends/prostate-cancer-statistics/*.
14. Carioli, G. *et al.* European cancer mortality predictions for the year 2020 with a focus on prostate cancer. *Ann. Oncol.* **31**, 650–658 (2020).
15. Grosclaude, P. *et al.* Le cancer de la prostate, évolution de l'incidence et de la mortalité en France entre 1980 et 2011. *Prog. En Urol.* **25**, 536–542 (2015).
16. Albertsen, P. C., Hanley, J. A., Gleason, D. F. & Barry, M. J. Competing Risk Analysis of Men Aged 55 to 74 Years at Diagnosis Managed Conservatively for Clinically Localized Prostate Cancer. **280**,.
17. *Haute Autorité de Santé - ALD n° 30 - Cancer de la prostate. Available at: https://www.has-sante.fr/portail/jcms/c_725257/fr/ald-n-30-cancer-de-la-prostate. (Accessed: July 2023)*.
18. *synthèse sur les bénéfices et les risques d'un dépistage du cancer de la prostate par dosage du PSA - Ref : ETATPROSTATE15 | Institut National Du Cancer. Available at:http://www.e-cancer.fr/Expertises-et-publications/Catalogue-des-publications/Synthese-sur-les-benefices-et-les-risques-d-un-depistage-du-cancer-de-la-prostate-par-dosage-du-PSA. (Accessed: July 2023)*.
19. Cooner, W. H. *et al.* Prostate cancer detection in a clinical urological practice by ultrasonography, digital rectal examination and prostate specific antigen. *J. Urol.* **143**, 1146–1152; discussion 1152-1154 (1990).
20. Thompson, I. M. *et al.* Assessing prostate cancer risk: results from the Prostate Cancer Prevention Trial. *J. Natl. Cancer Inst.* **98**, 529–534 (2006).
21. Salomon, L. *et al.* [Recommendations Onco-Urology 2010: Prostate cancer]. *Progres En Urol. J. Assoc. Francaise Urol. Soc. Francaise Urol.* **20 Suppl 4**, S217-251 (2010).
22. Smith, D. S., Humphrey, P. A. & Catalona, W. J. The early detection of prostate carcinoma with prostate specific antigen: The Washington University experience. *Cancer* **80**, 1852–1856 (1997).
23. Stamey, T. A. *et al.* Prostate-specific antigen as a serum marker for adenocarcinoma of the prostate. *N. Engl. J. Med.* **317**, 909–916 (1987).
24. Chang, S. L., Harshman, L. C. & Presti, J. C. Impact of Common Medications on Serum Total Prostate-Specific Antigen Levels: Analysis of the National Health and Nutrition Examination Survey. *J. Clin. Oncol.* **28**, 3951–3957 (2010).

25. Teoh, J. *et al.* The performance characteristics of prostate-specific antigen and prostate-specific antigen density in Chinese men. *Asian J. Androl.* **19**, 113 (2017).
26. Ghafoori, M., Varedi, P., Hosseini, S. J., Asgari, M. & Shakiba, M. Value of Prostate-Specific Antigen and Prostate- Specific Antigen Density in Detection of Prostate Cancer in an Iranian Population of Men. **6**, (2009).
27. *https://prostatecanceruk.org/prostate-information-and-support/prostate-tests/digital-rectal-examination-dre*.
28. Rozet, F. *et al.* [CCAFU french national guidelines 2016-2018 on prostate cancer]. *Progres En Urol. J. Assoc. Francaise Urol. Soc. Francaise Urol.* **27 Suppl 1**, S95–S143 (2016).
29. Gleason, D. F. & Mellinger, G. T. Prediction of prognosis for prostatic adenocarcinoma by combined histological grading and clinical staging. *J. Urol.* **111**, 58–64 (1974).
30. Epstein, J. I. *et al.* The 2014 International Society of Urological Pathology (ISUP) Consensus Conference on Gleason Grading of Prostatic Carcinoma: Definition of Grading Patterns and Proposal for a New Grading System. *Am. J. Surg. Pathol.* **40**, 244–252 (2016).
31. Epstein, J. I. *et al.* A Contemporary Prostate Cancer Grading System: A Validated Alternative to the Gleason Score. *Eur. Urol.* **69**, 428–435 (2016).
32. Lamy, P.-J. *et al.* Prognostic Biomarkers Used for Localised Prostate Cancer Management: A Systematic Review. *Eur. Urol. Focus* **4**, 790–803 (2018).
33. D'Amico, A. V. *et al.* Biochemical outcome after radical prostatectomy, external beam radiation therapy, or interstitial radiation therapy for clinically localized prostate cancer. *JAMA* **280**, 969–974 (1998).
34. Roumiguie, M. *et al.* Improvement of the intermediate risk prostate cancer sub-classification by integrating MRI and fusion biopsy features. *Urol. Oncol. Semin. Orig. Investig.* **38**, 386–392 (2020).
35. Zumsteg, Z. S. A New Risk Classification System for Therapeutic Decision Making with Intermediate-risk Prostate Cancer Patients Undergoing Dose-escalated External-beam Radiation Therapy. *Eur. Urol.* (2013).
36. Beauval, J. B. *et al.* Improved decision making in intermediate-risk prostate cancer: a multicenter study on pathologic and oncologic outcomes after radical prostatectomy. *World J Urol* (2017).
37. Sailer, V. *et al.* Experimental in vitro, ex vivo and in vivo models in prostate cancer research. *Nat. Rev. Urol.* **20**, 158–178 (2023).
38. van Bokhoven, A. *et al.* Molecular characterization of human prostate carcinoma cell lines. *The Prostate* **57**, 205–225 (2003).
39. Ghandi, M. *et al.* Next-generation characterization of the Cancer Cell Line Encyclopedia. *Nature* **569**, 503–508 (2019).
40. Chang, K.-H. *et al.* Dihydrotestosterone synthesis bypasses testosterone to drive castration-resistant prostate cancer. *Proc. Natl. Acad. Sci. U. S. A.* **108**, 13728–13733 (2011).
41. Gillet, J.-P., Varma, S. & Gottesman, M. M. The clinical relevance of cancer cell lines. *J. Natl. Cancer Inst.* **105**, 452–458 (2013).
42. Souza, A. G. *et al.* Comparative Assay of 2D and 3D Cell Culture Models: Proliferation, Gene Expression and Anticancer Drug Response. *Curr. Pharm. Des.* **24**, 1689–1694 (2018).
43. Sutherland, R. M. Cell and Environment Interactions in Tumor Microregions: The Multicell Spheroid Model. *Sci. New Ser.* **240**, 177–184 (1988).
44. Hagemann, J. *et al.* Spheroid-based 3D Cell Cultures Enable Personalized Therapy Testing and Drug Discovery in Head and Neck Cancer. *Anticancer Res.* **37**, 2201–2210 (2017).
45. Halfter, K. *et al.* Prospective cohort study using the breast cancer spheroid model as a predictor for response to neoadjuvant therapy – the SpheroNEO study. *BMC Cancer* **15**, 519 (2015).
46. Ingram, M. *et al.* Tissue engineered tumor models. *Biotech. Histochem. Off. Publ. Biol. Stain Comm.* **85**, 213–229 (2010).

47. Hsiao, A. Y. *et al.* Microfluidic system for formation of PC-3 prostate cancer co-culture spheroids. (2009).
48. Linxweiler, J. *et al.* Patient-derived, three-dimensional spheroid cultures provide a versatile translational model for the study of organ-confined prostate cancer. *J. Cancer Res. Clin. Oncol.* **145**, 551–559 (2019).
49. Drost, J. *et al.* Organoid culture systems for prostate epithelial and cancer tissue. *Nat. Protoc.* **11**, 347–358 (2016).
50. Pauli, C. *et al.* Personalized *In Vitro* and *In Vivo* Cancer Models to Guide Precision Medicine. *Cancer Discov.* **7**, 462–477 (2017).
51. Gao, D. *et al.* Organoid Cultures Derived from Patients with Advanced Prostate Cancer. *Cell* **159**, 176–187 (2014).
52. Servant, R. *et al.* Prostate cancer patient-derived organoids: detailed outcome from a prospective cohort of 81 clinical specimens. *J. Pathol.* **254**, 543–555 (2021).
53. Kamatar, A., Gunay, G. & Acar, H. Natural and Synthetic Biomaterials for Engineering Multicellular Tumor Spheroids. *Polymers* **12**, 2506 (2020).
54. Van Hemelryk, A. *et al.* Modeling Prostate Cancer Treatment Responses in the Organoid Era: 3D Environment Impacts Drug Testing. *Biomolecules* **11**, 1572 (2021).
55. Fong, E. L. S. *et al.* Hydrogel-Based 3D Model of Patient-Derived Prostate Xenograft Tumors Suitable for Drug Screening. *Mol. Pharm.* **11**, 2040–2050 (2014).
56. Bray, L. J. *et al.* Multi-parametric hydrogels support 3D in vitro bioengineered microenvironment models of tumour angiogenesis. *Biomaterials* **53**, 609–620 (2015).
57. Shokoohmand, A. *et al.* Microenvironment engineering of osteoblastic bone metastases reveals osteomimicry of patient-derived prostate cancer xenografts. *Biomaterials* **220**, 119402 (2019).
58. Bock, N. *et al.* Engineering osteoblastic metastases to delineate the adaptive response of androgen-deprived prostate cancer in the bone metastatic microenvironment. *Bone Res.* **7**, 13 (2019).
59. Bock, N. *et al.* In vitro engineering of a bone metastases model allows for study of the effects of antiandrogen therapies in advanced prostate cancer. *Sci. Adv.* **7**, eabg2564 (2021).
60. Pereira, B. A. *et al.* Tissue engineered human prostate microtissues reveal key role of mast cell-derived tryptase in potentiating cancer-associated fibroblast (CAF)-induced morphometric transition in vitro. *Biomaterials* **197**, 72–85 (2019).
61. Zhao, H. *et al.* Patient-derived tissue slice grafts accurately depict response of high-risk primary prostate cancer to androgen deprivation therapy. *J. Transl. Med.* **11**, 199 (2013).
62. Figiel, S. Functional Organotypic Cultures of Prostate Tissues. *Am. J. Pathol.*
63. Van De Merbel, A. F. *et al.* An ex vivo Tissue Culture Model for the Assessment of Individualized Drug Responses in Prostate and Bladder Cancer. *Front. Oncol.* **8**, 400 (2018).
64. Zhang, W. *et al.* Ex vivo treatment of prostate tumor tissue recapitulates in vivo therapy response. *The Prostate* **79**, 390–402 (2019).
65. Chakrabarty, S. *et al.* A Microfluidic Cancer-on-Chip Platform Predicts Drug Response Using Organotypic Tumor Slice Culture. *CANCER Res.*
66. Dorrigiv, D. *et al.* Microdissected Tissue vs. Tissue Slices—A Comparative Study of Tumor Explant Models Cultured On-Chip and Off-Chip. (2021).
67. Kashaninejad, N. *et al.* Organ-Tumor-on-a-Chip for Chemosensitivity Assay: A Critical Review. *Micromachines* **7**, 130 (2016).
68. Wu, X., Gong, S., Roy-Burman, P., Lee, P. & Culig, Z. Current mouse and cell models in prostate cancer research. *Endocr. Relat. Cancer* **20**, R155-170 (2013).
69. Chung, L. W. K. *et al.* Co-inoculation of tumorigenic rat prostate mesenchymal cells with non-tumorigenic epithelial cells results in the development of carcinosarcoma in syngeneic and athymic animals. *Int. J. Cancer* **43**, 1179–1187 (1989).
70. Gillet, J.-P., Varma, S. & Gottesman, M. M. The clinical relevance of cancer cell lines. *J. Natl. Cancer Inst.* **105**, 452–458 (2013).

71. Voskoglou-Nomikos, T., Pater, J. L. & Seymour, L. Clinical Predictive Value of the in Vitro Cell Line, Human Xenograft, and Mouse Allograft Preclinical Cancer Models.
72. Yin, Z. *et al.* Current research developments of patient-derived tumour xenograft models (Review). *Exp. Ther. Med.*
73. Stephenson, R. A. *et al.* Metastatic Model for Human Prostate Cancer Using Orthotopic Implantation in Nude Mice. *JNCI J. Natl. Cancer Inst.* **84**, 951–957 (1992).
74. Thalmann, G. N. *et al.* Androgen-independent cancer progression and bone metastasis in the LNCaP model of human prostate cancer. *Cancer Res.* **54**, 2577–2581 (1994).
75. Pettaway, C. A. *et al.* Selection of highly metastatic variants of different human prostatic carcinomas using orthotopic implantation in nude mice. *Clin. Cancer Res. Off. J. Am. Assoc. Cancer Res.* **2**, 1627–1636 (1996).
76. Patel, B. J. *et al.* CL1-GFP: an androgen independent metastatic tumor model for prostate cancer. *J. Urol.* **164**, 1420–1425 (2000).
77. Lange, T. *et al.* Development and Characterization of a Spontaneously Metastatic Patient-Derived Xenograft Model of Human Prostate Cancer. *Sci. Rep.* **8**, 17535 (2018).
78. Navone, N. M. *et al.* Movember GAP1 PDX project: An international collection of serially transplantable prostate cancer patient-derived xenograft (PDX) models. *The Prostate* **78**, 1262–1282 (2018).
79. Lawrence, M. G. *et al.* The future of patient-derived xenografts in prostate cancer research. *Nat. Rev. Urol.* **20**, 371–384 (2023).
80. Hurwitz, A. A., Foster, B. A., Allison, J. P., Greenberg, N. M. & Kwon, E. D. The TRAMP mouse as a model for prostate cancer. *Curr. Protoc. Immunol.* **Chapter 20**, 20.5.1-20.5.23 (2001).
81. Alajati, A. *et al.* CDCP1 overexpression drives prostate cancer progression and can be targeted in vivo. *J. Clin. Invest.* **130**, 2435–2450 (2020).
82. Rambur, A. *et al.* Drosophila Accessory Gland: A Complementary In Vivo Model to Bring New Insight to Prostate Cancer. *Cells* **10**, 2387 (2021).
83. Bernards, A. & Hariharan, I. K. Of flies and men--studying human disease in Drosophila. *Curr. Opin. Genet. Dev.* **11**, 274–278 (2001).
84. Bier, E. Drosophila, the golden bug, emerges as a tool for human genetics. *Nat. Rev. Genet.* **6**, 9–23 (2005).
85. Rambur, A. *et al.* Sequential Ras/MAPK and PI3K/AKT/mTOR pathways recruitment drives basal extrusion in the prostate-like gland of Drosophila. *Nat. Commun.* **11**, 2300 (2020).
86. de Celis, J. F. & García-Bellido, A. Roles of the Notch gene in Drosophila wing morphogenesis. *Mech. Dev.* **46**, 109–122 (1994).
87. Imberg-Kazdan, K. *et al.* A genome-wide RNA interference screen identifies new regulators of androgen receptor function in prostate cancer cells. *Genome Res.* **23**, 581–591 (2013).
88. Bill-Axelson, A. *et al.* Radical prostatectomy or watchful waiting in early prostate cancer. *N. Engl. J. Med.* **370**, 932–942 (2014).
89. Haglind, E. *et al.* Urinary Incontinence and Erectile Dysfunction After Robotic Versus Open Radical Prostatectomy: A Prospective, Controlled, Nonrandomised Trial. *Eur. Urol.* **68**, 216–225 (2015).
90. Wallis, C. J. D. *et al.* Second malignancies after radiotherapy for prostate cancer: systematic review and meta-analysis. *BMJ* **352**, i851 (2016).
91. Hennequin, C. *et al.* [Prostate brachytherapy: indications and outcomes]. *Progres En Urol. J. Assoc. Francaise Urol. Soc. Francaise Urol.* **23**, 378–385 (2013).
92. Warmuth, M., Johansson, T. & Mad, P. Systematic review of the efficacy and safety of high-intensity focussed ultrasound for the primary and salvage treatment of prostate cancer. *Eur. Urol.* **58**, 803–815 (2010).
93. Ganzer, R. *et al.* Fourteen-year oncological and functional outcomes of high-intensity focused ultrasound in localized prostate cancer. *BJU Int.* **112**, 322–329 (2013).

94. Crouzet, S. *et al.* Whole-gland ablation of localized prostate cancer with high-intensity focused ultrasound: oncologic outcomes and morbidity in 1002 patients. *Eur. Urol.* **65**, 907–914 (2014).
95. Kantoff, P. W. *et al.* Sipuleucel-T immunotherapy for castration-resistant prostate cancer. *N. Engl. J. Med.* **363**, 411–422 (2010).
96. Cunha, G. R. Role of mesenchymal-epithelial interactions in normal and abnormal development of the mammary gland and prostate. *Cancer* **74**, 1030–1044 (1994).
97. Cunha, G. R. *et al.* The endocrinology and developmental biology of the prostate. *Endocr. Rev.* **8**, 338–362 (1987).
98. Hiller-Sturmhöfel, S. & Bartke, A. The endocrine system: an overview. *Alcohol Health Res. World* **22**, 153–164 (1998).
99. Aragon-Ching, J. B., Williams, K. M. & Gulley, J. L. Impact of androgen-deprivation therapy on the immune system: implications for combination therapy of prostate cancer. *Front. Biosci. J. Virtual Libr.* **12**, 4957–4971 (2007).
100. Claessens, F. *et al.* Diverse roles of androgen receptor (AR) domains in AR-mediated signaling. *Nucl. Recept. Signal.* **6**, e008 (2008).
101. Davey, R. A. & Grossmann, M. Androgen Receptor Structure, Function and Biology: From Bench to Bedside. *Clin. Biochem. Rev.* **37**, 3–15 (2016).
102. Kaarbø, M., Klokk, T. I. & Saatcioglu, F. Androgen signaling and its interactions with other signaling pathways in prostate cancer. *BioEssays News Rev. Mol. Cell. Dev. Biol.* **29**, 1227–1238 (2007).
103. Jin, H.-J., Kim, J. & Yu, J. Androgen receptor genomic regulation. *Transl. Androl. Urol.* **2**, 157–177 (2013).
104. Itkonen, H. & Mills, I. G. Chromatin binding by the androgen receptor in prostate cancer. *Mol. Cell. Endocrinol.* **360**, 44–51 (2012).
105. Mills, I. G. Maintaining and reprogramming genomic androgen receptor activity in prostate cancer. *Nat. Rev. Cancer* **14**, 187–198 (2014).
106. Yang, X. *et al.* Complex regulation of human androgen receptor expression by Wnt signaling in prostate cancer cells. *Oncogene* **25**, 3436–3444 (2006).
107. Culig, Z. *et al.* Androgen receptor activation in prostatic tumor cell lines by insulin-like growth factor-I, keratinocyte growth factor, and epidermal growth factor. *Cancer Res.* **54**, 5474–5478 (1994).
108. Majumder, P. K. & Sellers, W. R. Akt-regulated pathways in prostate cancer. *Oncogene* **24**, 7465–7474 (2005).
109. Wu, X., Senechal, K., Neshat, M. S., Whang, Y. E. & Sawyers, C. L. The PTEN/MMAC1 tumor suppressor phosphatase functions as a negative regulator of the phosphoinositide 3-kinase/Akt pathway. *Proc. Natl. Acad. Sci. U. S. A.* **95**, 15587–15591 (1998).
110. Lin, H.-K., Hu, Y.-C., Lee, D. K. & Chang, C. Regulation of androgen receptor signaling by PTEN (phosphatase and tensin homolog deleted on chromosome 10) tumor suppressor through distinct mechanisms in prostate cancer cells. *Mol. Endocrinol. Baltim. Md* **18**, 2409–2423 (2004).
111. Aarnisalo, P., Palvimo, J. J. & Jänne, O. A. CREB-binding protein in androgen receptor-mediated signaling. *Proc. Natl. Acad. Sci. U. S. A.* **95**, 2122–2127 (1998).
112. Yang, L. *et al.* Interleukin-6 differentially regulates androgen receptor transactivation via PI3K-Akt, STAT3, and MAPK, three distinct signal pathways in prostate cancer cells. *Biochem. Biophys. Res. Commun.* **305**, 462–469 (2003).
113. Matsuda, T. *et al.* Cross-talk between signal transducer and activator of transcription 3 and androgen receptor signaling in prostate carcinoma cells. *Biochem. Biophys. Res. Commun.* **283**, 179–187 (2001).
114. Huggins, C. & Hodges, C. V. Studies on prostatic cancer. I. The effect of castration, of estrogen and androgen injection on serum phosphatases in metastatic carcinoma of the prostate. *CA. Cancer J. Clin.* **22**, 232–240 (1972).

115. Nishiyama, T. Serum testosterone levels after medical or surgical androgen deprivation: a comprehensive review of the literature. *Urol. Oncol.* **32**, 38.e17–28 (2014).
116. Vaarala, M., Kähkönen, E., Viitanen, J., Taari, K. & Tammela, T. [The effect of castration on bone in prostate cancer patients]. *Duodecim Laaketieteellinen Aikakauskirja* **127**, 1129–1136 (2011).
117. The Nobel Prize in Physiology or Medicine 1977. NobelPrize.org. Nobel Prize Outreach AB 2023. Sat. 26 Aug 2023. <https://www.nobelprize.org/prizes/medicine/1977/summary/>).
118. Schally, A. V., Comaru-Schally, A. M. & Gonzalez-Barcena, D. Present status of agonistic and antagonistic analogs of LH-RH in the treatment of advanced prostate cancer. *Biomed. Pharmacother. Biomedecine Pharmacother.* **46**, 465–471 (1992).
119. Wex, J. *et al.* Leuprolide acetate 1-, 3- and 6-monthly depot formulations in androgen deprivation therapy for prostate cancer in nine European countries: evidence review and economic evaluation. *Clin. Outcomes Res. CEOR* **5**, 257–269 (2013).
120. Thompson, I. M. Flare Associated with LHRH-Agonist Therapy. *Rev. Urol.* **3 Suppl 3**, S10-14 (2001).
121. Bubley, G. J. Is the flare phenomenon clinically significant? *Urology* **58**, 5–9 (2001).
122. Mottet, N. *et al.* EAU-EANM-ESTRO-ESUR-SIOG Guidelines on Prostate Cancer-2020 Update. Part 1: Screening, Diagnosis, and Local Treatment with Curative Intent. *Eur. Urol.* **79**, 243–262 (2021).
123. Van Poppel, H. *et al.* Degarelix: a novel gonadotropin-releasing hormone (GnRH) receptor blocker--results from a 1-yr, multicentre, randomised, phase 2 dosage-finding study in the treatment of prostate cancer. *Eur. Urol.* **54**, 805–813 (2008).
124. Crawford, E. D. *et al.* A phase III extension trial with a 1-arm crossover from leuprolide to degarelix: comparison of gonadotropin-releasing hormone agonist and antagonist effect on prostate cancer. *J. Urol.* **186**, 889–897 (2011).
125. Garnick, M. B. & Mottet, N. New treatment paradigm for prostate cancer: abarelix initiation therapy for immediate testosterone suppression followed by a luteinizing hormone-releasing hormone agonist. *BJU Int.* **110**, 499–504 (2012).
126. Ozono, S. *et al.* The efficacy and safety of degarelix, a GnRH antagonist: a 12-month, multicentre, randomized, maintenance dose-finding phase II study in Japanese patients with prostate cancer. *Jpn. J. Clin. Oncol.* **42**, 477–484 (2012).
127. Itty, S. & Getzenberg, R. H. How do we define 'castration' in men on androgen deprivation therapy? *Asian J. Androl.* **22**, 441–446 (2020).
128. Hendriksen, P. J. M. *et al.* Evolution of the androgen receptor pathway during progression of prostate cancer. *Cancer Res.* **66**, 5012–5020 (2006).
129. Penning, T. M. New frontiers in androgen biosynthesis and metabolism. *Curr. Opin. Endocrinol. Diabetes Obes.* **17**, 233–239 (2010).
130. Barnard, M., Mostaghel, E. A., Auchus, R. J. & Storbeck, K.-H. The role of adrenal derived androgens in castration resistant prostate cancer. *J. Steroid Biochem. Mol. Biol.* **197**, 105506 (2020).
131. Touchstone, H. C., Glazer, L., Cooper, D. Y. & Roberts, J. M. The isolation of delta 4-androstene-11 beta-ol-3,17-dione from human adrenal incubates. *J. Clin. Endocrinol. Metab.* **15**, 382–384 (1955).
132. Meyer, A. S., Jeanloz, R. W. & Pincus, G. Chemical transformations of steroids by adrenal perfusion. IV. Dehydroepiandrosterone. *J. Biol. Chem.* **203**, 463–468 (1953).
133. Holownia, P., Owen, E. J., Conway, G. S., Round, J. & Honour, J. W. Studies to confirm the source of 11 beta-hydroxyandrostenedione. *J. Steroid Biochem. Mol. Biol.* **41**, 875–880 (1992).
134. Dorfman, R. I. In vivo metabolism of neutral steroid hormones. *J. Clin. Endocrinol. Metab.* **14**, 318–325 (1954).
135. Holownia, P., Owen, E. J., Hampl, R., Jacobs, H. S. & Honour, J. W. The determination of 11 beta-hydroxyandrostenedione in human follicular fluid and plasma. *J. Steroid Biochem. Mol. Biol.* **38**, 389–398 (1991).

136. Rege, J. *et al.* Liquid chromatography-tandem mass spectrometry analysis of human adrenal vein 19-carbon steroids before and after ACTH stimulation. *J. Clin. Endocrinol. Metab.* **98**, 1182–1188 (2013).
137. Xing, Y. *et al.* The effects of ACTH on steroid metabolomic profiles in human adrenal cells. *J. Endocrinol.* **209**, 327–335 (2011).
138. Rege, J. *et al.* 11-Ketotestosterone Is the Dominant Circulating Bioactive Androgen During Normal and Premature Adrenarche. *J. Clin. Endocrinol. Metab.* **103**, 4589–4598 (2018).
139. Labrie, F., Bélanger, A., Simard, J., Van Luu-The, null & Labrie, C. DHEA and peripheral androgen and estrogen formation: intracinology. *Ann. N. Y. Acad. Sci.* **774**, 16–28 (1995).
140. Penning, T. M. Dehydroepiandrosterone (DHEA)-SO4 Depot and Castration-Resistant Prostate Cancer. *Vitam. Horm.* **108**, 309–331 (2018).
141. Auchus, R. J. & Rainey, W. E. Adrenarche - physiology, biochemistry and human disease. *Clin. Endocrinol. (Oxf.)* **60**, 288–296 (2004).
142. Rainey, W. E., Carr, B. R., Sasano, H., Suzuki, T. & Mason, J. I. Dissecting human adrenal androgen production. *Trends Endocrinol. Metab. TEM* **13**, 234–239 (2002).
143. Miller, W. L. & Auchus, R. J. The molecular biology, biochemistry, and physiology of human steroidogenesis and its disorders. *Endocr. Rev.* **32**, 81–151 (2011).
144. Turcu, A., Smith, J. M., Auchus, R. & Rainey, W. E. Adrenal androgens and androgen precursors-definition, synthesis, regulation and physiologic actions. *Compr. Physiol.* **4**, 1369–1381 (2014).
145. Cai, C. & Balk, S. P. Intratumoral androgen biosynthesis in prostate cancer pathogenesis and response to therapy. *Endocr. Relat. Cancer* **18**, R175-182 (2011).
146. Storbeck, K.-H. *et al.* 11β-Hydroxydihydrotestosterone and 11-ketodihydrotestosterone, novel C19 steroids with androgenic activity: a putative role in castration resistant prostate cancer? *Mol. Cell. Endocrinol.* **377**, 135–146 (2013).
147. Chang, K.-H. *et al.* Dihydrotestosterone synthesis bypasses testosterone to drive castration-resistant prostate cancer. *Proc. Natl. Acad. Sci. U. S. A.* **108**, 13728–13733 (2011).
148. Fankhauser, M. *et al.* Canonical androstenedione reduction is the predominant source of signaling androgens in hormone-refractory prostate cancer. *Clin. Cancer Res. Off. J. Am. Assoc. Cancer Res.* **20**, 5547–5557 (2014).
149. Beilin, J., Ball, E. M., Favaloro, J. M. & Zajac, J. D. Effect of the androgen receptor CAG repeat polymorphism on transcriptional activity: specificity in prostate and non-prostate cell lines. *J. Mol. Endocrinol.* **25**, 85–96 (2000).
150. Cantagrel, V. *et al.* SRD5A3 is required for converting polyprenol to dolichol and is mutated in a congenital glycosylation disorder. *Cell* **142**, 203–217 (2010).
151. Jernberg, E. *et al.* Characterization of prostate cancer bone metastases according to expression levels of steroidogenic enzymes and androgen receptor splice variants. *PloS One* **8**, e77407 (2013).
152. Auchus, R. J. The backdoor pathway to dihydrotestosterone. *Trends Endocrinol. Metab. TEM* **15**, 432–438 (2004).
153. Bauman, D. R., Steckelbroeck, S., Williams, M. V., Peehl, D. M. & Penning, T. M. Identification of the major oxidative 3alpha-hydroxysteroid dehydrogenase in human prostate that converts 5alpha-androstane-3alpha,17beta-diol to 5alpha-dihydrotestosterone: a potential therapeutic target for androgen-dependent disease. *Mol. Endocrinol. Baltim. Md* **20**, 444–458 (2006).
154. Mohler, J. L. *et al.* Activation of the androgen receptor by intratumoral bioconversion of androstanediol to dihydrotestosterone in prostate cancer. *Cancer Res.* **71**, 1486–1496 (2011).
155. Pretorius, E. *et al.* 11-Ketotestosterone and 11-Ketodihydrotestosterone in Castration Resistant Prostate Cancer: Potent Androgens Which Can No Longer Be Ignored. *PloS One* **11**, e0159867 (2016).
156. du Toit, T. *et al.* Profiling adrenal 11β-hydroxyandrostenedione metabolites in prostate cancer cells, tissue and plasma: UPC2-MS/MS quantification of 11β-hydroxytestosterone, 11keto-testosterone and 11keto-dihydrotestosterone. *J. Steroid Biochem. Mol. Biol.* **166**, 54–67 (2017).

157. Pelletier, G., Luu-The, V., Li, S., Ouellet, J. & Labrie, F. Cellular localization of mRNA expression of enzymes involved in the formation and inactivation of hormonal steroids in the mouse prostate. *J. Histochem. Cytochem. Off. J. Histochem. Soc.* **52**, 1351–1356 (2004).
158. Gent, R., du Toit, T., Bloem, L. M. & Swart, A. C. The 11β-hydroxysteroid dehydrogenase isoforms: pivotal catalytic activities yield potent C11-oxy C19 steroids with 11βHSD2 favouring 11-ketotestosterone, 11-ketoandrostenedione and 11-ketoprogesterone biosynthesis. *J. Steroid Biochem. Mol. Biol.* **189**, 116–126 (2019).
159. Sharifi, N. & Auchus, R. J. Androstenedione is the preferred androgen source in hormone refractory prostate cancer--letter. *Clin. Cancer Res. Off. J. Am. Assoc. Cancer Res.* **20**, 4971 (2014).
160. Stanbrough, M. *et al.* Increased expression of genes converting adrenal androgens to testosterone in androgen-independent prostate cancer. *Cancer Res.* **66**, 2815–2825 (2006).
161. Luo, J., Dunn, T. A., Ewing, C. M., Walsh, P. C. & Isaacs, W. B. Decreased gene expression of steroid 5 alpha-reductase 2 in human prostate cancer: implications for finasteride therapy of prostate carcinoma. *The Prostate* **57**, 134–139 (2003).
162. Barnard, M. *et al.* 11-Oxygenated androgen precursors are the preferred substrates for aldo-keto reductase 1C3 (AKR1C3): Implications for castration resistant prostate cancer. *J. Steroid Biochem. Mol. Biol.* **183**, 192–201 (2018).
163. Ishizaki, F. *et al.* Androgen deprivation promotes intratumoral synthesis of dihydrotestosterone from androgen metabolites in prostate cancer. *Sci. Rep.* **3**, 1528 (2013).
164. Locke, J. A. *et al.* Androgen levels increase by intratumoral de novo steroidogenesis during progression of castration-resistant prostate cancer. *Cancer Res.* **68**, 6407–6415 (2008).
165. Cai, C. *et al.* Intratumoral de novo steroid synthesis activates androgen receptor in castration-resistant prostate cancer and is upregulated by treatment with CYP17A1 inhibitors. *Cancer Res.* **71**, 6503–6513 (2011).
166. Kumagai, J. *et al.* Intratumoral conversion of adrenal androgen precursors drives androgen receptor-activated cell growth in prostate cancer more potently than de novo steroidogenesis. *The Prostate* **73**, 1636–1650 (2013).
167. Hofland, J. *et al.* Evidence of limited contributions for intratumoral steroidogenesis in prostate cancer. *Cancer Res.* **70**, 1256–1264 (2010).
168. Knuuttila, M. *et al.* Castration induces up-regulation of intratumoral androgen biosynthesis and androgen receptor expression in an orthotopic VCaP human prostate cancer xenograft model. *Am. J. Pathol.* **184**, 2163–2173 (2014).
169. Hamid, A. R. A. H. *et al.* Aldo-keto reductase family 1 member C3 (AKR1C3) is a biomarker and therapeutic target for castration-resistant prostate cancer. *Mol. Med. Camb. Mass* **18**, 1449–1455 (2013).
170. Penning, T. M., Asangani, I. A., Sprenger, C. & Plymate, S. Intracrine androgen biosynthesis and drug resistance. *Cancer Drug Resist. Alhambra Calif* **3**, 912–929 (2020).
171. Hearn, J. W. D. *et al.* HSD3B1 and resistance to androgen-deprivation therapy in prostate cancer: a retrospective, multicohort study. *Lancet Oncol.* **17**, 1435–1444 (2016).
172. Chang, K.-H. *et al.* A gain-of-function mutation in DHT synthesis in castration-resistant prostate cancer. *Cell* **154**, 1074–1084 (2013).
173. Shiota, M. *et al.* Independent validation of missense polymorphism in HSD3B1 in Japanese men treated with primary androgen-deprivation therapy for metastatic prostate cancer. *J. Clin. Oncol.* **36**, 179–179 (2018).
174. Hearn, J. W. D. *et al.* Association of HSD3B1 Genotype With Response to Androgen-Deprivation Therapy for Biochemical Recurrence After Radiotherapy for Localized Prostate Cancer. *JAMA Oncol.* **4**, 558–562 (2018).
175. Wu, G. *et al.* Variant allele of HSD3B1 increases progression to castration-resistant prostate cancer. *The Prostate* **75**, 777–782 (2015).
176. Ko, H.-K. *et al.* Loss of an Androgen-Inactivating and Isoform-Specific HSD17B4 Splice Form Enables Emergence of Castration-Resistant Prostate Cancer. *Cell Rep.* **22**, 809–819 (2018).

177. Gao, X. *et al.* Functional Silencing of HSD17B2 in Prostate Cancer Promotes Disease Progression. *Clin. Cancer Res. Off. J. Am. Assoc. Cancer Res.* **25**, 1291–1301 (2019).
178. Pfeiffer, M. J., Smit, F. P., Sedelaar, J. P. M. & Schalken, J. A. Steroidogenic enzymes and stem cell markers are upregulated during androgen deprivation in prostate cancer. *Mol. Med. Camb. Mass* **17**, 657–664 (2011).
179. Montgomery, R. B. *et al.* Maintenance of intratumoral androgens in metastatic prostate cancer: a mechanism for castration-resistant tumor growth. *Cancer Res.* **68**, 4447–4454 (2008).
180. Pernigoni, N. *et al.* Commensal bacteria promote endocrine resistance in prostate cancer through androgen biosynthesis. *Science* **374**, 216–224 (2021).
181. Cui, D. *et al.* Cancer-associated fibroblast-secreted glucosamine alters the androgen biosynthesis program in prostate cancer via HSD3B1 upregulation. *J. Clin. Invest.* **133**, e161913 (2023).
182. Moon, H. H. *et al.* Osteoblasts Generate Testosterone From DHEA and Activate Androgen Signaling in Prostate Cancer Cells. *J. Bone Miner. Res. Off. J. Am. Soc. Bone Miner. Res.* **36**, 1566–1579 (2021).
183. Liu, X.-H. *et al.* Androgen-induced Wnt signaling in preosteoblasts promotes the growth of MDA-PCa-2b human prostate cancer cells. *Cancer Res.* **67**, 5747–5753 (2007).
184. Hagberg Thulin, M. *et al.* Osteoblasts promote castration-resistant prostate cancer by altering intratumoral steroidogenesis. *Mol. Cell. Endocrinol.* **422**, 182–191 (2016).
185. Potter, G. A., Barrie, S. E., Jarman, M. & Rowlands, M. G. Novel steroidal inhibitors of human cytochrome P45017 alpha (17 alpha-hydroxylase-C17,20-lyase): potential agents for the treatment of prostatic cancer. *J. Med. Chem.* **38**, 2463–2471 (1995).
186. Attard, G., Reid, A. H. M., Olmos, D. & de Bono, J. S. Antitumor activity with CYP17 blockade indicates that castration-resistant prostate cancer frequently remains hormone driven. *Cancer Res.* **69**, 4937–4940 (2009).
187. de Bono, J. S. *et al.* Abiraterone and increased survival in metastatic prostate cancer. *N. Engl. J. Med.* **364**, 1995–2005 (2011).
188. Ryan, C. J. *et al.* Abiraterone in metastatic prostate cancer without previous chemotherapy. *N. Engl. J. Med.* **368**, 138–148 (2013).
189. Richards, J. *et al.* Interactions of abiraterone, eplerenone, and prednisolone with wild-type and mutant androgen receptor: a rationale for increasing abiraterone exposure or combining with MDV3100. *Cancer Res.* **72**, 2176–2182 (2012).
190. Vasaitis, T. *et al.* Androgen receptor inactivation contributes to antitumor efficacy of 17{alpha}-hydroxylase/17,20-lyase inhibitor 3beta-hydroxy-17-(1H-benzimidazole-1-yl)androsta-5,16-diene in prostate cancer. *Mol. Cancer Ther.* **7**, 2348–2357 (2008).
191. Bruno, R. D. *et al.* Synthesis and biological evaluations of putative metabolically stable analogs of VN/124-1 (TOK-001): head to head anti-tumor efficacy evaluation of VN/124-1 (TOK-001) and abiraterone in LAPC-4 human prostate cancer xenograft model. *Steroids* **76**, 1268–1279 (2011).
192. Alyamani, M. *et al.* Steroidogenic Metabolism of Galeterone Reveals a Diversity of Biochemical Activities. *Cell Chem. Biol.* **24**, 825-832.e6 (2017).
193. McKay, R. R. *et al.* Efficacy of Therapies After Galeterone in Patients With Castration-resistant Prostate Cancer. *Clin. Genitourin. Cancer* **15**, 463–471 (2017).
194. Taplin, M.-E. *et al.* Androgen Receptor Modulation Optimized for Response-Splice Variant: A Phase 3, Randomized Trial of Galeterone Versus Enzalutamide in Androgen Receptor Splice Variant-7-expressing Metastatic Castration-resistant Prostate Cancer. *Eur. Urol.* **76**, 843–851 (2019).
195. Rafferty, S. W., Eisner, J. R., Moore, W. R., Schotzinger, R. J. & Hoekstra, W. J. Highly-selective 4-(1,2,3-triazole)-based P450c17a 17,20-lyase inhibitors. *Bioorg. Med. Chem. Lett.* **24**, 2444–2447 (2014).
196. Norris, J. D. *et al.* Androgen receptor antagonism drives cytochrome P450 17A1 inhibitor efficacy in prostate cancer. *J. Clin. Invest.* **127**, 2326–2338 (2017).

197. Gupta, S. *et al.* Phase I Study of Seviteronel, a Selective CYP17 Lyase and Androgen Receptor Inhibitor, in Men with Castration-Resistant Prostate Cancer. *Clin. Cancer Res. Off. J. Am. Assoc. Cancer Res.* **24**, 5225–5232 (2018).
198. Jacobi, G. H., Altwein, J. E., Kurth, K. H., Basting, R. & Hohenfellner, R. Treatment of advanced prostatic cancer with parenteral cyproterone acetate: a phase III randomised trial. *Br. J. Urol.* **52**, 208–215 (1980).
199. Pavone-Macaluso, M. *et al.* Comparison of diethylstilbestrol, cyproterone acetate and medroxyprogesterone acetate in the treatment of advanced prostatic cancer: final analysis of a randomized phase III trial of the European Organization for Research on Treatment of Cancer Urological Group. *J. Urol.* **136**, 624–631 (1986).
200. Dawson, N. A. *et al.* A randomized study comparing standard versus moderately high dose megestrol acetate for patients with advanced prostate carcinoma: cancer and leukemia group B study 9181. *Cancer* **88**, 825–834 (2000).
201. Schröder, F. H. *et al.* Metastatic prostate cancer treated by flutamide versus cyproterone acetate. Final analysis of the 'European Organization for Research and Treatment of Cancer' (EORTC) Protocol 30892. *Eur. Urol.* **45**, 457–464 (2004).
202. Schröder, F. H. Cyproterone acetate--mechanism of action and clinical effectiveness in prostate cancer treatment. *Cancer* **72**, 3810–3815 (1993).
203. Pridjian, G., Schmit, V. & Schreiber, J. Medroxyprogesterone acetate: receptor binding and correlated effects on steroidogenesis in rat granulosa cells. *J. Steroid Biochem.* **26**, 313–319 (1987).
204. McLeod, D. G. Tolerability of Nonsteroidal Antiandrogens in the Treatment of Advanced Prostate Cancer. *The Oncologist* **2**, 18–27 (1997).
205. Sarosdy, M. F. Which is the optimal antiandrogen for use in combined androgen blockade of advanced prostate cancer? The transition from a first- to second-generation antiandrogen. *Anticancer. Drugs* **10**, 791–796 (1999).
206. Helsen, C. *et al.* Androgen receptor antagonists for prostate cancer therapy. *Endocr. Relat. Cancer* **21**, T105-118 (2014).
207. Tran, C. *et al.* Development of a second-generation antiandrogen for treatment of advanced prostate cancer. *Science* **324**, 787–790 (2009).
208. Penson, D. F. *et al.* Enzalutamide Versus Bicalutamide in Castration-Resistant Prostate Cancer: The STRIVE Trial. *J. Clin. Oncol. Off. J. Am. Soc. Clin. Oncol.* **34**, 2098–2106 (2016).
209. Ning, Y. M. *et al.* Enzalutamide for treatment of patients with metastatic castration-resistant prostate cancer who have previously received docetaxel: U.S. Food and Drug Administration drug approval summary. *Clin. Cancer Res. Off. J. Am. Assoc. Cancer Res.* **19**, 6067–6073 (2013).
210. Scher, H. I. *et al.* Increased survival with enzalutamide in prostate cancer after chemotherapy. *N. Engl. J. Med.* **367**, 1187–1197 (2012).
211. Dai, C., Dehm, S. M. & Sharifi, N. Targeting the Androgen Signaling Axis in Prostate Cancer. *J. Clin. Oncol. Off. J. Am. Soc. Clin. Oncol.* JCO2300433 (2023) doi:10.1200/JCO.23.00433.
212. Liu, C. *et al.* Intracrine Androgens and AKR1C3 Activation Confer Resistance to Enzalutamide in Prostate Cancer. *Cancer Res.* **75**, 1413–1422 (2015).
213. Hettel, D. & Sharifi, N. HSD3B1 status as a biomarker of androgen deprivation resistance and implications for prostate cancer. *Nat. Rev. Urol.* **15**, 191–196 (2018).
214. Quigley, D. A. *et al.* Genomic Hallmarks and Structural Variation in Metastatic Prostate Cancer. *Cell* **174**, 758-769.e9 (2018).
215. Koivisto, P., Kolmer, M., Visakorpi, T. & Kallioniemi, O. P. Androgen receptor gene and hormonal therapy failure of prostate cancer. *Am. J. Pathol.* **152**, 1–9 (1998).
216. Azad, A. A. *et al.* Androgen Receptor Gene Aberrations in Circulating Cell-Free DNA: Biomarkers of Therapeutic Resistance in Castration-Resistant Prostate Cancer. *Clin. Cancer Res. Off. J. Am. Assoc. Cancer Res.* **21**, 2315–2324 (2015).
217. Romanel, A. *et al.* Plasma AR and abiraterone-resistant prostate cancer. *Sci. Transl. Med.* **7**, 312re10 (2015).

218. Annala, M. *et al.* Evolution of Castration-Resistant Prostate Cancer in ctDNA during Sequential Androgen Receptor Pathway Inhibition. *Clin. Cancer Res. Off. J. Am. Assoc. Cancer Res.* **27**, 4610–4623 (2021).
219. Suzuki, H. *et al.* Androgen receptor gene mutations in human prostate cancer. *J. Steroid Biochem. Mol. Biol.* **46**, 759–765 (1993).
220. Veldscholte, J. *et al.* A mutation in the ligand binding domain of the androgen receptor of human LNCaP cells affects steroid binding characteristics and response to anti-androgens. *Biochem. Biophys. Res. Commun.* **173**, 534–540 (1990).
221. Wilding, G., Chen, M. & Gelmann, E. P. Aberrant response in vitro of hormone-responsive prostate cancer cells to antiandrogens. *The Prostate* **14**, 103–115 (1989).
222. Taylor, B. S. *et al.* Integrative genomic profiling of human prostate cancer. *Cancer Cell* **18**, 11–22 (2010).
223. Grasso, C. S. *et al.* The mutational landscape of lethal castration-resistant prostate cancer. *Nature* **487**, 239–243 (2012).
224. Robinson, D. *et al.* Integrative clinical genomics of advanced prostate cancer. *Cell* **161**, 1215–1228 (2015).
225. Abida, W. *et al.* Genomic correlates of clinical outcome in advanced prostate cancer. *Proc. Natl. Acad. Sci. U. S. A.* **116**, 11428–11436 (2019).
226. Ledet, E. M. *et al.* Comprehensive Analysis of AR Alterations in Circulating Tumor DNA from Patients with Advanced Prostate Cancer. *The Oncologist* **25**, 327–333 (2020).
227. Steketee, K. *et al.* Broadened ligand responsiveness of androgen receptor mutants obtained by random amino acid substitution of H874 and mutation hot spot T877 in prostate cancer. *Int. J. Cancer* **100**, 309–317 (2002).
228. Veldscholte, J. *et al.* The androgen receptor in LNCaP cells contains a mutation in the ligand binding domain which affects steroid binding characteristics and response to antiandrogens. *J. Steroid Biochem. Mol. Biol.* **41**, 665–669 (1992).
229. Taplin, M. E. *et al.* Mutation of the androgen-receptor gene in metastatic androgen-independent prostate cancer. *N. Engl. J. Med.* **332**, 1393–1398 (1995).
230. Tan, J. *et al.* Dehydroepiandrosterone activates mutant androgen receptors expressed in the androgen-dependent human prostate cancer xenograft CWR22 and LNCaP cells. *Mol. Endocrinol. Baltim. Md* **11**, 450–459 (1997).
231. Taplin, M. E. *et al.* Selection for androgen receptor mutations in prostate cancers treated with androgen antagonist. *Cancer Res.* **59**, 2511–2515 (1999).
232. Yoshida, T. *et al.* Antiandrogen bicalutamide promotes tumor growth in a novel androgen-dependent prostate cancer xenograft model derived from a bicalutamide-treated patient. *Cancer Res.* **65**, 9611–9616 (2005).
233. Hara, T. *et al.* Novel mutations of androgen receptor: a possible mechanism of bicalutamide withdrawal syndrome. *Cancer Res.* **63**, 149–153 (2003).
234. Rathkopf, D. E. *et al.* Androgen receptor mutations in patients with castration-resistant prostate cancer treated with apalutamide. *Ann. Oncol. Off. J. Eur. Soc. Med. Oncol.* **28**, 2264–2271 (2017).
235. Chen, E. J. *et al.* Abiraterone treatment in castration-resistant prostate cancer selects for progesterone responsive mutant androgen receptors. *Clin. Cancer Res. Off. J. Am. Assoc. Cancer Res.* **21**, 1273–1280 (2015).
236. Gottlieb, B., Beitel, L. K., Nadarajah, A., Paliouras, M. & Trifiro, M. The androgen receptor gene mutations database: 2012 update. *Hum. Mutat.* **33**, 887–894 (2012).
237. Sun, S. *et al.* Castration resistance in human prostate cancer is conferred by a frequently occurring androgen receptor splice variant. *J. Clin. Invest.* **120**, 2715–2730 (2010).
238. Dehm, S. M., Schmidt, L. J., Heemers, H. V., Vessella, R. L. & Tindall, D. J. Splicing of a novel androgen receptor exon generates a constitutively active androgen receptor that mediates prostate cancer therapy resistance. *Cancer Res.* **68**, 5469–5477 (2008).

239. Guo, Z. *et al.* A novel androgen receptor splice variant is up-regulated during prostate cancer progression and promotes androgen depletion-resistant growth. *Cancer Res.* **69**, 2305–2313 (2009).
240. Hirayama, Y., Tam, T., Jian, K., Andersen, R. J. & Sadar, M. D. Combination therapy with androgen receptor N-terminal domain antagonist EPI-7170 and enzalutamide yields synergistic activity in AR-V7-positive prostate cancer. *Mol. Oncol.* **14**, 2455–2470 (2020).
241. Sharp, A. *et al.* Androgen receptor splice variant-7 expression emerges with castration resistance in prostate cancer. *J. Clin. Invest.* **129**, 192–208 (2019).
242. Antonarakis, E. S. *et al.* Clinical Significance of Androgen Receptor Splice Variant-7 mRNA Detection in Circulating Tumor Cells of Men With Metastatic Castration-Resistant Prostate Cancer Treated With First- and Second-Line Abiraterone and Enzalutamide. *J. Clin. Oncol. Off. J. Am. Soc. Clin. Oncol.* **35**, 2149–2156 (2017).
243. Kohli, M. *et al.* Androgen Receptor Variant AR-V9 Is Coexpressed with AR-V7 in Prostate Cancer Metastases and Predicts Abiraterone Resistance. *Clin. Cancer Res. Off. J. Am. Assoc. Cancer Res.* **23**, 4704–4715 (2017).
244. Cao, B. *et al.* Androgen receptor splice variants activating the full-length receptor in mediating resistance to androgen-directed therapy. *Oncotarget* **5**, 1646–1656 (2014).
245. Xu, D. *et al.* Androgen Receptor Splice Variants Dimerize to Transactivate Target Genes. *Cancer Res.* **75**, 3663–3671 (2015).
246. Watson, P. A. *et al.* Constitutively active androgen receptor splice variants expressed in castration-resistant prostate cancer require full-length androgen receptor. *Proc. Natl. Acad. Sci. U. S. A.* **107**, 16759–16765 (2010).
247. Sperger, J. M. *et al.* Prospective Evaluation of Clinical Outcomes Using a Multiplex Liquid Biopsy Targeting Diverse Resistance Mechanisms in Metastatic Prostate Cancer. *J. Clin. Oncol. Off. J. Am. Soc. Clin. Oncol.* **39**, 2926–2937 (2021).
248. Chmelar, R., Buchanan, G., Need, E. F., Tilley, W. & Greenberg, N. M. Androgen receptor coregulators and their involvement in the development and progression of prostate cancer. *Int. J. Cancer* **120**, 719–733 (2007).
249. Dotzlaw, H., Papaioannou, M., Moehren, U., Claessens, F. & Baniahmad, A. Agonist-antagonist induced coactivator and corepressor interplay on the human androgen receptor. *Mol. Cell. Endocrinol.* **213**, 79–85 (2003).
250. Chen, C. D. *et al.* Molecular determinants of resistance to antiandrogen therapy. *Nat. Med.* **10**, 33–39 (2004).
251. Senapati, D., Kumari, S. & Heemers, H. V. Androgen receptor co-regulation in prostate cancer. *Asian J. Urol.* **7**, 219–232 (2020).
252. Zhang, Z. *et al.* Loss of CHD1 Promotes Heterogeneous Mechanisms of Resistance to AR-Targeted Therapy via Chromatin Dysregulation. *Cancer Cell* **37**, 584-598.e11 (2020).
253. Yao, J. *et al.* The Homeobox gene, HOXB13, Regulates a Mitotic Protein-Kinase Interaction Network in Metastatic Prostate Cancers. *Sci. Rep.* **9**, 9715 (2019).
254. Faisal*, F. *et al.* MP68-10 HOXB13 EXPRESSION AND ITS ROLE IN PROSTATE CANCER PROGRESSION AND NEUROENDOCRINE DIFFERENTIATION. *J. Urol.* **201**, (2019).
255. Cheng, S. *et al.* Neuroendocrine prostate cancer has distinctive, non-prostatic HOX code that is represented by the loss of HOXB13 expression. *Sci. Rep.* **11**, 2778 (2021).
256. Büscheck, F. *et al.* The independent prognostic impact of the GATA2 pioneering factor is restricted to ERG-negative prostate cancer. *Tumour Biol. J. Int. Soc. Oncodevelopmental Biol. Med.* **41**, 1010428318824815 (2019).
257. Teng, M., Zhou, S., Cai, C., Lupien, M. & He, H. H. Pioneer of prostate cancer: past, present and the future of FOXA1. *Protein Cell* **12**, 29–38 (2021).
258. Gupta, S. *et al.* Whole Genomic Copy Number Alterations in Circulating Tumor Cells from Men with Abiraterone or Enzalutamide-Resistant Metastatic Castration-Resistant Prostate Cancer. *Clin. Cancer Res. Off. J. Am. Assoc. Cancer Res.* **23**, 1346–1357 (2017).

259. Kim, E. H., Cao, D., Mahajan, N. P., Andriole, G. L. & Mahajan, K. ACK1-AR and AR-HOXB13 signaling axes: epigenetic regulation of lethal prostate cancers. *NAR Cancer* **2**, zcaa018 (2020).
260. Hwang, J. H. *et al.* CREB5 Promotes Resistance to Androgen-Receptor Antagonists and Androgen Deprivation in Prostate Cancer. *Cell Rep.* **29**, 2355-2370.e6 (2019).
261. Ehsani, M., David, F. O. & Baniahmad, A. Androgen Receptor-Dependent Mechanisms Mediating Drug Resistance in Prostate Cancer. *Cancers* **13**, 1534 (2021).
262. Tucci, M. *et al.* Enzalutamide-resistant castration-resistant prostate cancer: challenges and solutions. *OncoTargets Ther.* **11**, 7353–7368 (2018).
263. Toren, P. & Zoubeidi, A. Targeting the PI3K/Akt pathway in prostate cancer: challenges and opportunities (review). *Int. J. Oncol.* **45**, 1793–1801 (2014).
264. Carver, B. S. *et al.* Reciprocal feedback regulation of PI3K and androgen receptor signaling in PTEN-deficient prostate cancer. *Cancer Cell* **19**, 575–586 (2011).
265. Pourmand, G. *et al.* Role of PTEN gene in progression of prostate cancer. *Urol. J.* **4**, 95–100 (2007).
266. de Bono, J. S. *et al.* Randomized Phase II Study Evaluating Akt Blockade with Ipatasertib, in Combination with Abiraterone, in Patients with Metastatic Prostate Cancer with and without PTEN Loss. *Clin. Cancer Res. Off. J. Am. Assoc. Cancer Res.* **25**, 928–936 (2019).
267. Xia, Y., Shen, S. & Verma, I. M. NF-κB, an active player in human cancers. *Cancer Immunol. Res.* **2**, 823–830 (2014).
268. Ghosh, S. & Karin, M. Missing pieces in the NF-kappaB puzzle. *Cell* **109 Suppl**, S81-96 (2002).
269. Cui, Y. *et al.* Upregulation of glucose metabolism by NF-κB2/p52 mediates enzalutamide resistance in castration-resistant prostate cancer cells. *Endocr. Relat. Cancer* **21**, 435–442 (2014).
270. Jin, R. *et al.* Inhibition of NF-kappa B signaling restores responsiveness of castrate-resistant prostate cancer cells to anti-androgen treatment by decreasing androgen receptor-variant expression. *Oncogene* **34**, 3700–3710 (2015).
271. Johnson, D. E., O'Keefe, R. A. & Grandis, J. R. Targeting the IL-6/JAK/STAT3 signalling axis in cancer. *Nat. Rev. Clin. Oncol.* **15**, 234–248 (2018).
272. Liu, C. *et al.* Inhibition of constitutively active Stat3 reverses enzalutamide resistance in LNCaP derivative prostate cancer cells. *The Prostate* **74**, 201–209 (2014).
273. Luo, M., Zhao, X., Song, Y., Cheng, H. & Zhou, R. Nuclear autophagy: An evolutionarily conserved mechanism of nuclear degradation in the cytoplasm. *Autophagy* **12**, 1973–1983 (2016).
274. Glick, D., Barth, S. & Macleod, K. F. Autophagy: cellular and molecular mechanisms. *J. Pathol.* **221**, 3–12 (2010).
275. Gump, J. M. & Thorburn, A. Autophagy and apoptosis: what is the connection? *Trends Cell Biol.* **21**, 387–392 (2011).
276. Farrow, J. M., Yang, J. C. & Evans, C. P. Autophagy as a modulator and target in prostate cancer. *Nat. Rev. Urol.* **11**, 508–516 (2014).
277. Nguyen, H. G. *et al.* Targeting autophagy overcomes Enzalutamide resistance in castration-resistant prostate cancer cells and improves therapeutic response in a xenograft model. *Oncogene* **33**, 4521–4530 (2014).
278. Scheschowitsch, K., Leite, J. A. & Assreuy, J. New Insights in Glucocorticoid Receptor Signaling-More Than Just a Ligand-Binding Receptor. *Front. Endocrinol.* **8**, 16 (2017).
279. Claessens, F., Joniau, S. & Helsen, C. Comparing the rules of engagement of androgen and glucocorticoid receptors. *Cell. Mol. Life Sci. CMLS* **74**, 2217–2228 (2017).
280. Kulik, M. *et al.* Androgen and glucocorticoid receptor direct distinct transcriptional programs by receptor-specific and shared DNA binding sites. *Nucleic Acids Res.* **49**, 3856–3875 (2021).
281. Arora, V. K. *et al.* Glucocorticoid receptor confers resistance to antiandrogens by bypassing androgen receptor blockade. *Cell* **155**, 1309–1322 (2013).
282. Puhr, M. *et al.* The Glucocorticoid Receptor Is a Key Player for Prostate Cancer Cell Survival and a Target for Improved Antiandrogen Therapy. *Clin. Cancer Res. Off. J. Am. Assoc. Cancer Res.* **24**, 927–938 (2018).

283. Isikbay, M. *et al.* Glucocorticoid receptor activity contributes to resistance to androgen-targeted therapy in prostate cancer. *Horm. Cancer* **5**, 72–89 (2014).
284. Rickman, D. S. *et al.* ERG cooperates with androgen receptor in regulating trefoil factor 3 in prostate cancer disease progression. *Neoplasia N. Y. N* **12**, 1031–1040 (2010).
285. Gerke, J. S. *et al.* Integrative clinical transcriptome analysis reveals TMPRSS2-ERG dependency of prognostic biomarkers in prostate adenocarcinoma. *Int. J. Cancer* **146**, 2036–2046 (2020).
286. Tomlins, S. A. *et al.* Recurrent fusion of TMPRSS2 and ETS transcription factor genes in prostate cancer. *Science* **310**, 644–648 (2005).
287. Powell, K. *et al.* ERG/AKR1C3/AR Constitutes a Feed-Forward Loop for AR Signaling in Prostate Cancer Cells. *Clin. Cancer Res. Off. J. Am. Assoc. Cancer Res.* **21**, 2569–2579 (2015).
288. Montanari, M. *et al.* Epithelial-mesenchymal transition in prostate cancer: an overview. *Oncotarget* **8**, 35376–35389 (2017).
289. Ware, K. E. *et al.* Snail promotes resistance to enzalutamide through regulation of androgen receptor activity in prostate cancer. *Oncotarget* **7**, 50507–50521 (2016).
290. Conteduca, V. *et al.* Clinical features of neuroendocrine prostate cancer. *Eur. J. Cancer Oxf. Engl. 1990* **121**, 7–18 (2019).
291. Lee, G. T. *et al.* TCF4 induces enzalutamide resistance via neuroendocrine differentiation in prostate cancer. *PloS One* **14**, e0213488 (2019).
292. Bishop, J. L. *et al.* PD-L1 is highly expressed in Enzalutamide resistant prostate cancer. *Oncotarget* **6**, 234–242 (2015).
293. Ponnusamy, S. *et al.* Orally Bioavailable Androgen Receptor Degrader, Potential Next-Generation Therapeutic for Enzalutamide-Resistant Prostate Cancer. *Clin. Cancer Res. Off. J. Am. Assoc. Cancer Res.* **25**, 6764–6780 (2019).
294. Mohler, M. L. *et al.* An Overview of Next-Generation Androgen Receptor-Targeted Therapeutics in Development for the Treatment of Prostate Cancer. *Int. J. Mol. Sci.* **22**, 2124 (2021).
295. Thompson, I. M. *et al.* The influence of finasteride on the development of prostate cancer. *N. Engl. J. Med.* **349**, 215–224 (2003).
296. Andriole, G. L. *et al.* Effect of dutasteride on the risk of prostate cancer. *N. Engl. J. Med.* **362**, 1192–1202 (2010).
297. Liedtke, A. J. *et al.* Development of potent and selective indomethacin analogues for the inhibition of AKR1C3 (Type 5 17β-hydroxysteroid dehydrogenase/prostaglandin F synthase) in castrate-resistant prostate cancer. *J. Med. Chem.* **56**, 2429–2446 (2013).
298. Wangtrakuldee, P. *et al.* A 3-(4-nitronaphthen-1-yl) amino-benzoate analog as a bifunctional AKR1C3 inhibitor and AR antagonist: Head to head comparison with other advanced AKR1C3 targeted therapeutics. *J. Steroid Biochem. Mol. Biol.* **192**, 105283 (2019).
299. Penning, T. M. Mechanisms of drug resistance that target the androgen axis in castration resistant prostate cancer (CRPC). *J. Steroid Biochem. Mol. Biol.* **153**, 105–113 (2015).
300. Berthold, D. R. *et al.* Docetaxel plus prednisone or mitoxantrone plus prednisone for advanced prostate cancer: updated survival in the TAX 327 study. *J. Clin. Oncol. Off. J. Am. Soc. Clin. Oncol.* **26**, 242–245 (2008).
301. Beer, T. M. *et al.* Enzalutamide in metastatic prostate cancer before chemotherapy. *N. Engl. J. Med.* **371**, 424–433 (2014).
302. Ryan, C. J. *et al.* Abiraterone in metastatic prostate cancer without previous chemotherapy. *N. Engl. J. Med.* **368**, 138–148 (2013).
303. de Bono, J. *et al.* Olaparib for Metastatic Castration-Resistant Prostate Cancer. *N. Engl. J. Med.* **382**, 2091–2102 (2020).
304. Antonarakis, E. S. *et al.* Pembrolizumab for Treatment-Refractory Metastatic Castration-Resistant Prostate Cancer: Multicohort, Open-Label Phase II KEYNOTE-199 Study. *J. Clin. Oncol. Off. J. Am. Soc. Clin. Oncol.* **38**, 395–405 (2020).

305. Fizazi, K. *et al.* Abiraterone acetate plus prednisone in patients with newly diagnosed high-risk metastatic castration-sensitive prostate cancer (LATITUDE): final overall survival analysis of a randomised, double-blind, phase 3 trial. *Lancet Oncol.* **20**, 686–700 (2019).
306. Kyriakopoulos, C. E. *et al.* Chemohormonal Therapy in Metastatic Hormone-Sensitive Prostate Cancer: Long-Term Survival Analysis of the Randomized Phase III E3805 CHAARTED Trial. *J. Clin. Oncol. Off. J. Am. Soc. Clin. Oncol.* **36**, 1080–1087 (2018).
307. Kershaw, E. E. & Flier, J. S. Adipose tissue as an endocrine organ. *J. Clin. Endocrinol. Metab.* **89**, 2548–2556 (2004).
308. Sohlström, A., Wahlund, L. O. & Forsum, E. Adipose tissue distribution as assessed by magnetic resonance imaging and total body fat by magnetic resonance imaging, underwater weighing, and body-water dilution in healthy women. *Am. J. Clin. Nutr.* **58**, 830–838 (1993).
309. Yang Loureiro, Z., Solivan-Rivera, J. & Corvera, S. Adipocyte Heterogeneity Underlying Adipose Tissue Functions. *Endocrinology* **163**, bqab138 (2022).
310. Ibrahim, M. M. Subcutaneous and visceral adipose tissue: structural and functional differences. *Obes. Rev. Off. J. Int. Assoc. Study Obes.* **11**, 11–18 (2010).
311. Fox, C. S. *et al.* Abdominal visceral and subcutaneous adipose tissue compartments: association with metabolic risk factors in the Framingham Heart Study. *Circulation* **116**, 39–48 (2007).
312. Tchoukalova, Y. D. *et al.* Subcutaneous adipocyte size and body fat distribution. *Am. J. Clin. Nutr.* **87**, 56–63 (2008).
313. Zhang, H.-M. *et al.* Macrophage infiltrates with high levels of Toll-like receptor 4 expression in white adipose tissues of male Chinese. *Nutr. Metab. Cardiovasc. Dis. NMCD* **19**, 736–743 (2009).
314. Bruun, J. M., Lihn, A. S., Pedersen, S. B. & Richelsen, B. Monocyte chemoattractant protein-1 release is higher in visceral than subcutaneous human adipose tissue (AT): implication of macrophages resident in the AT. *J. Clin. Endocrinol. Metab.* **90**, 2282–2289 (2005).
315. Laurent, V., Nieto, L., Valet, P. & Muller, C. [Adipose tissue and cancer: a high risk tandem]. *Med. Sci. MS* **30**, 398–404 (2014).
316. Bjørndal, B., Burri, L., Staalesen, V., Skorve, J. & Berge, R. K. Different adipose depots: their role in the development of metabolic syndrome and mitochondrial response to hypolipidemic agents. *J. Obes.* **2011**, 490650 (2011).
317. Frayn, K. N., Karpe, F., Fielding, B. A., Macdonald, I. A. & Coppack, S. W. Integrative physiology of human adipose tissue. *Int. J. Obes. Relat. Metab. Disord. J. Int. Assoc. Study Obes.* **27**, 875–888 (2003).
318. Cinti, S. The adipose organ at a glance. *Dis. Model. Mech.* **5**, 588–594 (2012).
319. Alligier M SK, Disse E, Laville M. Le tissu adipeux : couleur, localisation, fonctions et autres données nouvelles. Mises au point cliniques d'Endocrinologie. 2013.
320. Schipper, H. S., Prakken, B., Kalkhoven, E. & Boes, M. Adipose tissue-resident immune cells: key players in immunometabolism. *Trends Endocrinol. Metab. TEM* **23**, 407–415 (2012).
321. Chawla, A., Nguyen, K. D. & Goh, Y. P. S. Macrophage-mediated inflammation in metabolic disease. *Nat. Rev. Immunol.* **11**, 738–749 (2011).
322. Lumeng, C. N., Bodzin, J. L. & Saltiel, A. R. Obesity induces a phenotypic switch in adipose tissue macrophage polarization. *J. Clin. Invest.* **117**, 175–184 (2007).
323. Dalmas, E., Clément, K. & Guerre-Millo, M. Defining macrophage phenotype and function in adipose tissue. *Trends Immunol.* **32**, 307–314 (2011).
324. Nance, S. A., Muir, L. & Lumeng, C. Adipose tissue macrophages: Regulators of adipose tissue immunometabolism during obesity. *Mol. Metab.* **66**, 101642 (2022).
325. Feuerer, M. *et al.* Lean, but not obese, fat is enriched for a unique population of regulatory T cells that affect metabolic parameters. *Nat. Med.* **15**, 930–939 (2009).
326. Cipolletta, D. *et al.* PPAR-γ is a major driver of the accumulation and phenotype of adipose tissue Treg cells. *Nature* **486**, 549–553 (2012).
327. Spalding, K. L. *et al.* Dynamics of fat cell turnover in humans. *Nature* **453**, 783–787 (2008).

328. Tandon, P., Wafer, R. & Minchin, J. E. N. Adipose morphology and metabolic disease. *J. Exp. Biol.* **221**, jeb164970 (2018).
329. Mariman, E. C. M. & Wang, P. Adipocyte extracellular matrix composition, dynamics and role in obesity. *Cell. Mol. Life Sci. CMLS* **67**, 1277–1292 (2010).
330. Ricard-Blum, S. & Ruggiero, F. The collagen superfamily: from the extracellular matrix to the cell membrane. *Pathol. Biol. (Paris)* **53**, 430–442 (2005).
331. Mouw, J. K., Ou, G. & Weaver, V. M. Extracellular matrix assembly: a multiscale deconstruction. *Nat. Rev. Mol. Cell Biol.* **15**, 771–785 (2014).
332. Khan, T. *et al.* Metabolic dysregulation and adipose tissue fibrosis: role of collagen VI. *Mol. Cell. Biol.* **29**, 1575–1591 (2009).
333. Mori, S., Kiuchi, S., Ouchi, A., Hase, T. & Murase, T. Characteristic expression of extracellular matrix in subcutaneous adipose tissue development and adipogenesis; comparison with visceral adipose tissue. *Int. J. Biol. Sci.* **10**, 825–833 (2014).
334. Park, J. & Scherer, P. E. Adipocyte-derived endotrophin promotes malignant tumor progression. *J. Clin. Invest.* **122**, 4243–4256 (2012).
335. Sun, K. *et al.* Endotrophin triggers adipose tissue fibrosis and metabolic dysfunction. *Nat. Commun.* **5**, 3485 (2014).
336. Schultz, G. S. & Wysocki, A. Interactions between extracellular matrix and growth factors in wound healing. *Wound Repair Regen. Off. Publ. Wound Heal. Soc. Eur. Tissue Repair Soc.* **17**, 153–162 (2009).
337. Schlessinger, J. *et al.* Crystal structure of a ternary FGF-FGFR-heparin complex reveals a dual role for heparin in FGFR binding and dimerization. *Mol. Cell* **6**, 743–750 (2000).
338. Ortéga, N., L'Faqihi, F. E. & Plouët, J. Control of vascular endothelial growth factor angiogenic activity by the extracellular matrix. *Biol. Cell* **90**, 381–390 (1998).
339. Bradshaw, A. D., Graves, D. C., Motamed, K. & Sage, E. H. SPARC-null mice exhibit increased adiposity without significant differences in overall body weight. *Proc. Natl. Acad. Sci. U. S. A.* **100**, 6045–6050 (2003).
340. Pierleoni, C., Verdenelli, F., Castellucci, M. & Cinti, S. Fibronectins and basal lamina molecules expression in human subcutaneous white adipose tissue. *Eur. J. Histochem. EJH* **42**, 183–188 (1998).
341. Chun, T.-H. Peri-adipocyte ECM remodeling in obesity and adipose tissue fibrosis. *Adipocyte* **1**, 89–95 (2012).
342. Cawston, T. E. & Young, D. A. Proteinases involved in matrix turnover during cartilage and bone breakdown. *Cell Tissue Res.* **339**, 221–235 (2010).
343. Lin, D., Chun, T.-H. & Kang, L. Adipose extracellular matrix remodelling in obesity and insulin resistance. *Biochem. Pharmacol.* **119**, 8–16 (2016).
344. Gabison, E. E., Hoang-Xuan, T., Mauviel, A. & Menashi, S. [Metalloproteinases and angiogenesis]. *Pathol. Biol. (Paris)* **51**, 161–166 (2003).
345. Bergers, G. *et al.* Matrix metalloproteinase-9 triggers the angiogenic switch during carcinogenesis. *Nat. Cell Biol.* **2**, 737–744 (2000).
346. Cawston, T. E. & Young, D. A. Proteinases involved in matrix turnover during cartilage and bone breakdown. *Cell Tissue Res.* **339**, 221–235 (2010).
347. Ojima, K., Oe, M., Nakajima, I., Muroya, S. & Nishimura, T. Dynamics of protein secretion during adipocyte differentiation. *FEBS Open Bio* **6**, 816–826 (2016).
348. Nakajima, I., Muroya, S., Tanabe, R.-I. & Chikuni, K. Positive effect of collagen V and VI on triglyceride accumulation during differentiation in cultures of bovine intramuscular adipocytes. *Differ. Res. Biol. Divers.* **70**, 84–91 (2002).
349. Bouloumié, A., Sengenès, C., Portolan, G., Galitzky, J. & Lafontan, M. Adipocyte produces matrix metalloproteinases 2 and 9: involvement in adipose differentiation. *Diabetes* **50**, 2080–2086 (2001).
350. Chavey, C. *et al.* Matrix metalloproteinases are differentially expressed in adipose tissue during obesity and modulate adipocyte differentiation. *J. Biol. Chem.* **278**, 11888–11896 (2003).

351. Chun, T.-H. *et al.* A pericellular collagenase directs the 3-dimensional development of white adipose tissue. *Cell* **125**, 577–591 (2006).
352. Bouwman, F., Renes, J. & Mariman, E. A combination of protein profiling and isotopomer analysis using matrix-assisted laser desorption/ionization-time of flight mass spectrometry reveals an active metabolism of the extracellular matrix of 3T3-L1 adipocytes. *Proteomics* **4**, 3855–3863 (2004).
353. Maquart, F. X., Siméon, A., Pasco, S. & Monboisse, J. C. [Regulation of cell activity by the extracellular matrix: the concept of matrikines]. *J. Soc. Biol.* **193**, 423–428 (1999).
354. Tran, K. T., Lamb, P. & Deng, J.-S. Matrikines and matricryptins: Implications for cutaneous cancers and skin repair. *J. Dermatol. Sci.* **40**, 11–20 (2005).
355. Blaise, S. *et al.* Elastin-derived peptides are new regulators of insulin resistance development in mice. *Diabetes* **62**, 3807–3816 (2013).
356. O'Reilly, M. S. *et al.* Endostatin: an endogenous inhibitor of angiogenesis and tumor growth. *Cell* **88**, 277–285 (1997).
357. Park, J., Morley, T. S. & Scherer, P. E. Inhibition of endotrophin, a cleavage product of collagen VI, confers cisplatin sensitivity to tumours. *EMBO Mol. Med.* **5**, 935–948 (2013).
358. Hausman, G. J. & Richardson, R. L. Adipose tissue angiogenesis. *J. Anim. Sci.* **82**, 925–934 (2004).
359. Christiaens, V. & Lijnen, H. R. Angiogenesis and development of adipose tissue. *Mol. Cell. Endocrinol.* **318**, 2–9 (2010).
360. Ramakrishnan, V. M. & Boyd, N. L. The Adipose Stromal Vascular Fraction as a Complex Cellular Source for Tissue Engineering Applications. *Tissue Eng. Part B Rev.* **24**, 289–299 (2018).
361. Cao, Y. Angiogenesis modulates adipogenesis and obesity. *J. Clin. Invest.* **117**, 2362–2368 (2007).
362. Madri, J. A. & Williams, S. K. Capillary endothelial cell cultures: phenotypic modulation by matrix components. *J. Cell Biol.* **97**, 153–165 (1983).
363. Panina, Y. A. *et al.* Plasticity of Adipose Tissue-Derived Stem Cells and Regulation of Angiogenesis. *Front. Physiol.* **9**, 1656 (2018).
364. Gupta, R. K. *et al.* Zfp423 expression identifies committed preadipocytes and localizes to adipose endothelial and perivascular cells. *Cell Metab.* **15**, 230–239 (2012).
365. Tang, W. *et al.* White fat progenitor cells reside in the adipose vasculature. *Science* **322**, 583–586 (2008).
366. Lee, T.-J. *et al.* Enhancement of long-term angiogenic efficacy of adipose stem cells by delivery of FGF2. *Microvasc. Res.* **84**, 1–8 (2012).
367. McGown, C., Birerdinc, A. & Younossi, Z. M. Adipose tissue as an endocrine organ. *Clin. Liver Dis.* **18**, 41–58 (2014).
368. Coleman, R. A., Lewin, T. M. & Muoio, D. M. Physiological and nutritional regulation of enzymes of triacylglycerol synthesis. *Annu. Rev. Nutr.* **20**, 77–103 (2000).
369. Eckel, R. H. Lipoprotein lipase. A multifunctional enzyme relevant to common metabolic diseases. *N. Engl. J. Med.* **320**, 1060–1068 (1989).
370. Zimmermann, R. *et al.* Fat mobilization in adipose tissue is promoted by adipose triglyceride lipase. *Science* **306**, 1383–1386 (2004).
371. Furuhashi, M. & Hotamisligil, G. S. Fatty acid-binding proteins: role in metabolic diseases and potential as drug targets. *Nat. Rev. Drug Discov.* **7**, 489–503 (2008).
372. Lafontan, M. & Langin, D. Lipolysis and lipid mobilization in human adipose tissue. *Prog. Lipid Res.* **48**, 275–297 (2009).
373. Zimmermann, R. *et al.* Decreased fatty acid esterification compensates for the reduced lipolytic activity in hormone-sensitive lipase-deficient white adipose tissue. *J. Lipid Res.* **44**, 2089–2099 (2003).
374. Gaidhu, M. P. *et al.* Prolonged AICAR-induced AMP-kinase activation promotes energy dissipation in white adipocytes: novel mechanisms integrating HSL and ATGL. *J. Lipid Res.* **50**, 704–715 (2009).

375. Langin, D. Adipose tissue lipolysis as a metabolic pathway to define pharmacological strategies against obesity and the metabolic syndrome. *Pharmacol. Res.* **53**, 482–491 (2006).
376. Lass, A., Zimmermann, R., Oberer, M. & Zechner, R. Lipolysis - a highly regulated multi-enzyme complex mediates the catabolism of cellular fat stores. *Prog. Lipid Res.* **50**, 14–27 (2011).
377. Zhang, Y. *et al.* Positional cloning of the mouse obese gene and its human homologue. *Nature* **372**, 425–432 (1994).
378. Hoggard, N. *et al.* Localization of leptin receptor mRNA splice variants in murine peripheral tissues by RT-PCR and in situ hybridization. *Biochem. Biophys. Res. Commun.* **232**, 383–387 (1997).
379. Andreoli, M. F., Donato, J., Cakir, I. & Perello, M. Leptin resensitisation: a reversion of leptin-resistant states. *J. Endocrinol.* **241**, R81–R96 (2019).
380. 全文.
381. Kumada, M. *et al.* Adiponectin specifically increased tissue inhibitor of metalloproteinase-1 through interleukin-10 expression in human macrophages. *Circulation* **109**, 2046–2049 (2004).
382. Galic, S., Oakhill, J. S. & Steinberg, G. R. Adipose tissue as an endocrine organ. *Mol. Cell. Endocrinol.* **316**, 129–139 (2010).
383. Hotamisligil, G. S., Shargill, N. S. & Spiegelman, B. M. Adipose expression of tumor necrosis factor-alpha: direct role in obesity-linked insulin resistance. *Science* **259**, 87–91 (1993).
384. Hotamisligil, G. S. *et al.* IRS-1-mediated inhibition of insulin receptor tyrosine kinase activity in TNF-alpha- and obesity-induced insulin resistance. *Science* **271**, 665–668 (1996).
385. Tsigos, C. *et al.* Dose-dependent effects of recombinant human interleukin-6 on glucose regulation. *J. Clin. Endocrinol. Metab.* **82**, 4167–4170 (1997).
386. Patel, L. *et al.* Resistin is expressed in human macrophages and directly regulated by PPAR gamma activators. *Biochem. Biophys. Res. Commun.* **300**, 472–476 (2003).
387. Adeghate, E. Visfatin: structure, function and relation to diabetes mellitus and other dysfunctions. *Curr. Med. Chem.* **15**, 1851–1862 (2008).
388. Ronti, T., Lupattelli, G. & Mannarino, E. The endocrine function of adipose tissue: an update. *Clin. Endocrinol. (Oxf.)* **64**, 355–365 (2006).
389. Jo, J. *et al.* Hypertrophy and/or Hyperplasia: Dynamics of Adipose Tissue Growth. *PLoS Comput. Biol.* **5**, e1000324 (2009).
390. Macotela, Y. *et al.* Intrinsic differences in adipocyte precursor cells from different white fat depots. *Diabetes* **61**, 1691–1699 (2012).
391. Joe, A. W. B., Yi, L., Even, Y., Vogl, A. W. & Rossi, F. M. V. Depot-specific differences in adipogenic progenitor abundance and proliferative response to high-fat diet. *Stem Cells Dayt. Ohio* **27**, 2563–2570 (2009).
392. Tchkonia, T. *et al.* Fat depot-specific characteristics are retained in strains derived from single human preadipocytes. *Diabetes* **55**, 2571–2578 (2006).
393. Emerging Risk Factors Collaboration *et al.* Separate and combined associations of body-mass index and abdominal adiposity with cardiovascular disease: collaborative analysis of 58 prospective studies. *Lancet Lond. Engl.* **377**, 1085–1095 (2011).
394. Berrington de Gonzalez, A. *et al.* Body-mass index and mortality among 1.46 million white adults. *N. Engl. J. Med.* **363**, 2211–2219 (2010).
395. Roberto, C. A. *et al.* Patchy progress on obesity prevention: emerging examples, entrenched barriers, and new thinking. *Lancet Lond. Engl.* **385**, 2400–2409 (2015).
396. Kanda, H. *et al.* MCP-1 contributes to macrophage infiltration into adipose tissue, insulin resistance, and hepatic steatosis in obesity. *J. Clin. Invest.* **116**, 1494–1505 (2006).
397. Weisberg, S. P. *et al.* CCR2 modulates inflammatory and metabolic effects of high-fat feeding. *J. Clin. Invest.* **116**, 115–124 (2006).
398. Strissel, K. J. *et al.* Adipocyte death, adipose tissue remodeling, and obesity complications. *Diabetes* **56**, 2910–2918 (2007).
399. Cinti, S. *et al.* Adipocyte death defines macrophage localization and function in adipose tissue of obese mice and humans. *J. Lipid Res.* **46**, 2347–2355 (2005).

400. Nishimura, S. *et al.* CD8+ effector T cells contribute to macrophage recruitment and adipose tissue inflammation in obesity. *Nat. Med.* **15**, 914–920 (2009).
401. Duffaut, C., Galitzky, J., Lafontan, M. & Bouloumié, A. Unexpected trafficking of immune cells within the adipose tissue during the onset of obesity. *Biochem. Biophys. Res. Commun.* **384**, 482–485 (2009).
402. Pasarica, M. *et al.* Reduced adipose tissue oxygenation in human obesity: evidence for rarefaction, macrophage chemotaxis, and inflammation without an angiogenic response. *Diabetes* **58**, 718–725 (2009).
403. Cao, Y. Angiogenesis and vascular functions in modulation of obesity, adipose metabolism, and insulin sensitivity. *Cell Metab.* **18**, 478–489 (2013).
404. Jang, J. E. *et al.* Nitric Oxide Produced by Macrophages Inhibits Adipocyte Differentiation and Promotes Profibrogenic Responses in Preadipocytes to Induce Adipose Tissue Fibrosis. *Diabetes* **65**, 2516–2528 (2016).
405. Fernando, R. *et al.* Low steady-state oxidative stress inhibits adipogenesis by altering mitochondrial dynamics and decreasing cellular respiration. *Redox Biol.* **32**, 101507 (2020).
406. Bell, L. N. *et al.* Adipose tissue production of hepatocyte growth factor contributes to elevated serum HGF in obesity. *Am. J. Physiol. Endocrinol. Metab.* **291**, E843-848 (2006).
407. Trayhurn, P. Hypoxia and adipose tissue function and dysfunction in obesity. *Physiol. Rev.* **93**, 1–21 (2013).
408. Halberg, N. *et al.* Hypoxia-inducible factor 1alpha induces fibrosis and insulin resistance in white adipose tissue. *Mol. Cell. Biol.* **29**, 4467–4483 (2009).
409. Wynn, T. A. Cellular and molecular mechanisms of fibrosis. *J. Pathol.* **214**, 199–210 (2008).
410. Vila, I. K. *et al.* Immune cell Toll-like receptor 4 mediates the development of obesity- and endotoxemia-associated adipose tissue fibrosis. *Cell Rep.* **7**, 1116–1129 (2014).
411. Lancaster, G. I. *et al.* Evidence that TLR4 Is Not a Receptor for Saturated Fatty Acids but Mediates Lipid-Induced Inflammation by Reprogramming Macrophage Metabolism. *Cell Metab.* **27**, 1096-1110.e5 (2018).
412. Ishidoya, S., Endoh, M., Nakagawa, H., Saito, S. & Arai, Y. Novel anatomical findings of the prostatic gland and the surrounding capsular structures in the normal prostate. *Tohoku J. Exp. Med.* **212**, 55–62 (2007).
413. Kapoor, J. *et al.* Extraprostatic extension into periprostatic fat is a more important determinant of prostate cancer recurrence than an invasive phenotype. *J. Urol.* **190**, 2061–2066 (2013).
414. Oliveira, D. S. M. *et al.* The mouse prostate: a basic anatomical and histological guideline. *Bosn. J. Basic Med. Sci.* **16**, 8–13 (2016).
415. Miladinovic, D. *et al.* Assessment of Periprostatic and Subcutaneous Adipose Tissue Lipolysis and Adipocyte Size from Men with Localized Prostate Cancer. *Cancers* **12**, 1385 (2020).
416. Ribeiro, R. *et al.* Human periprostatic white adipose tissue is rich in stromal progenitor cells and a potential source of prostate tumor stroma. *Exp. Biol. Med. Maywood NJ* **237**, 1155–1162 (2012).
417. Passos, G. R., Ghezzi, A. C., Antunes, E., de Oliveira, M. G. & Mónica, F. Z. The Role of Periprostatic Adipose Tissue on Prostate Function in Vascular-Related Disorders. *Front. Pharmacol.* **12**, 626155 (2021).
418. Passos, G. R. *et al.* Periprostatic adipose tissue (PPAT) supernatant from obese mice releases anticontractile substances and increases human prostate epithelial cell proliferation: the role of nitric oxide and adenosine. *Front. Pharmacol.* **14**, 1145860 (2023).
419. David Estève, Mathieu Roumiguié, Cécile Manceau, Delphine Milhas, Catherine Muller, Periprostatic adipose tissue: A heavy player in prostate cancer progression, Current Opinion in Endocrine and Metabolic Research, Volume 10, 2020, Pages 29-35.
420. Zhang, Q., Sun, L.-J., Yang, Z.-G., Zhang, G.-M. & Huo, R.-C. Influence of adipocytokines in periprostatic adipose tissue on prostate cancer aggressiveness. *Cytokine* **85**, 148–156 (2016).

421. Finley, D. S. *et al.* Periprostatic adipose tissue as a modulator of prostate cancer aggressiveness. *J. Urol.* **182**, 1621–1627 (2009).
422. Dahran, N., Szewczyk-Bieda, M., Vinnicombe, S., Fleming, S. & Nabi, G. Periprostatic fat adipokine expression is correlated with prostate cancer aggressiveness in men undergoing radical prostatectomy for clinically localized disease. *BJU Int.* **123**, 985–994 (2019).
423. Gucalp, A. *et al.* Periprostatic adipose inflammation is associated with high-grade prostate cancer. *Prostate Cancer Prostatic Dis.* **20**, 418–423 (2017).
424. Ribeiro, R. *et al.* Obesity and prostate cancer: gene expression signature of human periprostatic adipose tissue. *BMC Med.* **10**, 108 (2012).
425. Mangiola, S. *et al.* Periprostatic fat tissue transcriptome reveals a signature diagnostic for high-risk prostate cancer. *Endocr. Relat. Cancer* **25**, 569–581 (2018).
426. Altuna-Coy, A. *et al.* The lipidomic profile of the tumoral periprostatic adipose tissue reveals alterations in tumor cell's metabolic crosstalk. *BMC Med.* **20**, 255 (2022).
427. Laurent, V. *et al.* Periprostatic adipocytes act as a driving force for prostate cancer progression in obesity. *Nat. Commun.* **7**, 10230 (2016).
428. Ito, Y. *et al.* Adipocyte-derived monocyte chemotactic protein-1 (MCP-1) promotes prostate cancer progression through the induction of MMP-2 activity. *The Prostate* **75**, 1009–1019 (2015).
429. Saha, A. *et al.* Proinflammatory CXCL12-CXCR4/CXCR7 Signaling Axis Drives Myc-Induced Prostate Cancer in Obese Mice. *Cancer Res.* **77**, 5158–5168 (2017).
430. Zhang, T. *et al.* CXCL1 mediates obesity-associated adipose stromal cell trafficking and function in the tumour microenvironment. *Nat. Commun.* **7**, 11674 (2016).
431. Nieman, K. M. *et al.* Adipocytes promote ovarian cancer metastasis and provide energy for rapid tumor growth. *Nat. Med.* **17**, 1498–1503 (2011).
432. Wang, Y. Y. *et al.* Mammary adipocytes stimulate breast cancer invasion through metabolic remodeling of tumor cells. *JCI Insight* **2**, e87489 (2017).
433. Salminen, E., Hogg, A., Binns, D., Frydenberg, M. & Hicks, R. Investigations with FDG-PET scanning in prostate cancer show limited value for clinical practice. *Acta Oncol. Stockh. Swed.* **41**, 425–429 (2002).
434. Ribeiro, R. J. T. *et al.* Tumor cell-educated periprostatic adipose tissue acquires an aggressive cancer-promoting secretory profile. *Cell. Physiol. Biochem. Int. J. Exp. Cell. Physiol. Biochem. Pharmacol.* **29**, 233–240 (2012).
435. Wang, X. *et al.* Cholesterol and saturated fatty acids synergistically promote the malignant progression of prostate cancer. *Neoplasia N. Y. N* **24**, 86–97 (2022).
436. Figiel, S. *et al.* Fatty acid profile in peri-prostatic adipose tissue and prostate cancer aggressiveness in African-Caribbean and Caucasian patients. *Eur. J. Cancer Oxf. Engl. 1990* **91**, 107–115 (2018).
437. Balaban, S. *et al.* Extracellular Fatty Acids Are the Major Contributor to Lipid Synthesis in Prostate Cancer. *Mol. Cancer Res. MCR* **17**, 949–962 (2019).
438. Fontaine, A. *et al.* Lipophagy and prostate cancer: association with disease aggressiveness and proximity to periprostatic adipose tissue. *J. Pathol.* **255**, 166–176 (2021).
439. Yue, S. *et al.* Cholesteryl ester accumulation induced by PTEN loss and PI3K/AKT activation underlies human prostate cancer aggressiveness. *Cell Metab.* **19**, 393–406 (2014).
440. Altuna-Coy, A. *et al.* The lipidomic profile of the tumoral periprostatic adipose tissue reveals alterations in tumor cell's metabolic crosstalk. *BMC Med.* **20**, 255 (2022).
441. Huang, J. *et al.* Adipocyte p62/SQSTM1 Suppresses Tumorigenesis through Opposite Regulations of Metabolism in Adipose Tissue and Tumor. *Cancer Cell* **33**, 770-784.e6 (2018).
442. Lethongsavarn, V. *et al.* Tissue cholesterol metabolism and prostate cancer aggressiveness: Ethno-geographic variations. *The Prostate* **81**, 1365–1373 (2021).
443. Habib, C. N. *et al.* Leptin influences estrogen metabolism and accelerates prostate cell proliferation. *Life Sci.* **121**, 10–15 (2015).
444. Dirat, B. *et al.* Cancer-associated adipocytes exhibit an activated phenotype and contribute to breast cancer invasion. *Cancer Res.* **71**, 2455–2465 (2011).

445. Laurent, V. *et al.* Periprostatic Adipose Tissue Favors Prostate Cancer Cell Invasion in an Obesity-Dependent Manner: Role of Oxidative Stress. *Mol. Cancer Res. MCR* **17**, 821–835 (2019).
446. Roumiguié, M. *et al.* Periprostatic Adipose Tissue Displays a Chronic Hypoxic State that Limits Its Expandability. *Am. J. Pathol.* **192**, 926–942 (2022).
447. Woo, S., Cho, J. Y., Kim, S. Y. & Kim, S. H. Periprostatic fat thickness on MRI: correlation with Gleason score in prostate cancer. *AJR Am. J. Roentgenol.* **204**, W43-47 (2015).
448. Tan, W. P., Lin, C., Chen, M. & Deane, L. A. Periprostatic Fat: A Risk Factor for Prostate Cancer? *Urology* **98**, 107–112 (2016).
449. van Roermund, J. G. H. *et al.* Periprostatic fat correlates with tumour aggressiveness in prostate cancer patients. *BJU Int.* **107**, 1775–1779 (2011).
450. Zhang, Q. *et al.* Periprostatic adiposity measured on magnetic resonance imaging correlates with prostate cancer aggressiveness. *Urol. J.* **11**, 1793–1799 (2014).
451. Dahran, N., Szewczyk-Bieda, M., Wei, C., Vinnicombe, S. & Nabi, G. Normalized periprostatic fat MRI measurements can predict prostate cancer aggressiveness in men undergoing radical prostatectomy for clinically localised disease. *Sci. Rep.* **7**, 4630 (2017).
452. Gregg, J. R. *et al.* The Association of Periprostatic Fat and Grade Group Progression in Men with Localized Prostate Cancer on Active Surveillance. *J. Urol.* **205**, 122–128 (2021).
453. Salji, M. *et al.* Peri-prostatic Fat Volume Measurement as a Predictive Tool for Castration Resistance in Advanced Prostate Cancer. *Eur. Urol. Focus* **4**, 858–866 (2018).
454. Huang, H. *et al.* Periprostatic Fat Thickness on MRI is an Independent Predictor of Time to Castration-resistant Prostate Cancer in Chinese Patients With Newly Diagnosed Prostate Cancer Treated With Androgen Deprivation Therapy. *Clin. Genitourin. Cancer* **17**, e1036–e1047 (2019).
455. Nassar, Z. D. *et al.* Peri-prostatic adipose tissue: the metabolic microenvironment of prostate cancer. *BJU Int.* **121 Suppl 3**, 9–21 (2018).
456. Taussky, D. *et al.* Changes in periprostatic adipose tissue induced by 5α-reductase inhibitors. *Andrology* **5**, 511–515 (2017).
457. Longcope, C., Kato, T. & Horton, R. Conversion of blood androgens to estrogens in normal adult men and women. *J. Clin. Invest.* **48**, 2191–2201 (1969).
458. Sadeghi, H. M. *et al.* Polycystic Ovary Syndrome: A Comprehensive Review of Pathogenesis, Management, and Drug Repurposing. *Int. J. Mol. Sci.* **23**, 583 (2022).
459. Szymczak, J., Milewicz, A., Thijssen, J. H., Blankenstein, M. A. & Daroszewski, J. Concentration of sex steroids in adipose tissue after menopause. *Steroids* **63**, 319–321 (1998).
460. Hennig, K. *et al.* Steroid hormone profiling in human breast adipose tissue using semi-automated purification and highly sensitive determination of estrogens by GC-APCI-MS/MS. *Anal. Bioanal. Chem.* **410**, 259–275 (2018).
461. Fehér, T. & Bodrogi, L. A comparative study of steroid concentrations in human adipose tissue and the peripheral circulation. *Clin. Chim. Acta Int. J. Clin. Chem.* **126**, 135–141 (1982).
462. Deslypere, J. P., Verdonck, L. & Vermeulen, A. Fat tissue: a steroid reservoir and site of steroid metabolism. *J. Clin. Endocrinol. Metab.* **61**, 564–570 (1985).
463. Falk, R. T. *et al.* Measurement of sex steroid hormones in breast adipocytes: methods and implications. *Cancer Epidemiol. Biomark. Prev. Publ. Am. Assoc. Cancer Res. Cosponsored Am. Soc. Prev. Oncol.* **17**, 1891–1895 (2008).
464. Falk, R. T. *et al.* Sex steroid hormone levels in breast adipose tissue and serum in postmenopausal women. *Breast Cancer Res. Treat.* **131**, 287–294 (2012).
465. Bélanger, C. *et al.* Omental and subcutaneous adipose tissue steroid levels in obese men. *Steroids* **71**, 674–682 (2006).
466. O'Reilly, M. W. *et al.* AKR1C3-Mediated Adipose Androgen Generation Drives Lipotoxicity in Women With Polycystic Ovary Syndrome. *J. Clin. Endocrinol. Metab.* **102**, 3327–3339 (2017).
467. Wagner, I. V. *et al.* De Novo and Depot-Specific Androgen Production in Human Adipose Tissue: A Source of Hyperandrogenism in Women with Obesity. *Obes. Facts* **15**, 281–291 (2022).

468. Yoo, H. S. & Napoli, J. L. Quantification of Dehydroepiandrosterone, 17β-Estradiol, Testosterone, and Their Sulfates in Mouse Tissues by LC-MS/MS. *Anal. Chem.* **91**, 14624–14630 (2019).
469. Ohlsson, C. *et al.* Increased adipose tissue aromatase activity improves insulin sensitivity and reduces adipose tissue inflammation in male mice. *Am. J. Physiol. Endocrinol. Metab.* **313**, E450–E462 (2017).
470. Rodriguez-Cuenca, S., Monjo, M., Proenza, A. M. & Roca, P. Depot differences in steroid receptor expression in adipose tissue: possible role of the local steroid milieu. *Am. J. Physiol. Endocrinol. Metab.* **288**, E200-207 (2005).
471. Wagner, I. V. *et al.* Adipose Tissue is a Potential Source of Hyperandrogenism in Obese Female Rats. *Obes. Silver Spring Md* **26**, 1161–1167 (2018).
472. Jung, S. M., Sanchez-Gurmaches, J. & Guertin, D. A. Brown Adipose Tissue Development and Metabolism. *Handb. Exp. Pharmacol.* **251**, 3–36 (2019).
473. Townsend, K. & Tseng, Y.-H. Brown adipose tissue: Recent insights into development, metabolic function and therapeutic potential. *Adipocyte* **1**, 13–24 (2012).
474. Ouellet, V. *et al.* Outdoor temperature, age, sex, body mass index, and diabetic status determine the prevalence, mass, and glucose-uptake activity of 18F-FDG-detected BAT in humans. *J. Clin. Endocrinol. Metab.* **96**, 192–199 (2011).
475. Fletcher, L. A. *et al.* Sexual Dimorphisms in Adult Human Brown Adipose Tissue. *Obes. Silver Spring Md* **28**, 241–246 (2020).
476. Wagner, H., Nusser, D. & Sachs, M. Steroid profiles of brown adipose tissue. *J. Steroid Biochem. Mol. Biol.* **39**, 405–407 (1991).
477. Ptak, W. THE STEROID HORMONE SYNTHESIS IN THE BROWN ADIPOSE TISSUE OF MICE. *Experientia* **21**, 26–27 (1965).
478. Kaikaew, K. *et al.* Sex difference in the mouse BAT transcriptome reveals a role of progesterone. *J. Mol. Endocrinol.* **66**, 97–113 (2021).
479. MacKenzie, S. M. *et al.* Depot-specific steroidogenic gene transcription in human adipose tissue. *Clin. Endocrinol. (Oxf.)* **69**, 848–854 (2008).
480. Emami, N. *et al.* Differences in expression of genes related to steroidgenesis in abdominal subcutaneous adipose tissue of pregnant women with and without PCOS; a case control study. *BMC Pregnancy Childbirth* **21**, 490 (2021).
481. Li, J., Daly, E., Campioli, E., Wabitsch, M. & Papadopoulos, V. De novo synthesis of steroids and oxysterols in adipocytes. *J. Biol. Chem.* **289**, 747–764 (2014).
482. Wang, L. *et al.* The expression of sex steroid synthesis and inactivation enzymes in subcutaneous adipose tissue of PCOS patients. *J. Steroid Biochem. Mol. Biol.* **132**, 120–126 (2012).
483. Kinoshita, T. *et al.* An innovative LC-MS/MS-based method for determining CYP 17 and CYP 19 activity in the adipose tissue of pre- and postmenopausal and ovariectomized women using 13C-labeled steroid substrates. *J. Clin. Endocrinol. Metab.* **99**, 1339–1347 (2014).
484. Puche, C., José, M., Cabero, A. & Meseguer, A. Expression and enzymatic activity of the P450c17 gene in human adipose tissue. *Eur. J. Endocrinol.* **146**, 223–229 (2002).
485. Molaie, S. *et al.* Dietary trans and saturated fatty acids effects on semen quality, hormonal levels and expression of genes related to steroid metabolism in mouse adipose tissue. *Andrologia* **51**, e13259 (2019).
486. Labrie, F. All sex steroids are made intracellularly in peripheral tissues by the mechanisms of intracrinology after menopause. *J. Steroid Biochem. Mol. Biol.* **145**, 133–138 (2015).
487. Luu-The, V. Assessment of steroidogenesis and steroidogenic enzyme functions. *J. Steroid Biochem. Mol. Biol.* **137**, 176–182 (2013).
488. Blouin, K. *et al.* Expression and activity of steroid aldoketoreductases 1C in omental adipose tissue are positive correlates of adiposity in women. *Am. J. Physiol. Endocrinol. Metab.* **288**, E398-404 (2005).
489. Blouin, K. *et al.* Local androgen inactivation in abdominal visceral adipose tissue. *J. Clin. Endocrinol. Metab.* **88**, 5944–5950 (2003).

490. Rhéaume, E. *et al.* Structure and expression of a new complementary DNA encoding the almost exclusive 3 beta-hydroxysteroid dehydrogenase/delta 5-delta 4-isomerase in human adrenals and gonads. *Mol. Endocrinol. Baltim. Md* **5**, 1147–1157 (1991).
491. Lorence, M. C., Murry, B. A., Trant, J. M. & Mason, J. I. Human 3 beta-hydroxysteroid dehydrogenase/delta 5----4isomerase from placenta: expression in nonsteroidogenic cells of a protein that catalyzes the dehydrogenation/isomerization of C21 and C19 steroids. *Endocrinology* **126**, 2493–2498 (1990).
492. Clarke, T. R., Bain, P. A., Sha, L. & Payne, A. H. Enzyme characteristics of two distinct forms of mouse 3 beta-hydroxysteroid dehydrogenase/delta 5-delta 4-isomerase complementary deoxyribonucleic acids expressed in COS-1 cells. *Endocrinology* **132**, 1971–1976 (1993).
493. Blouin, K. *et al.* Pathways of adipose tissue androgen metabolism in women: depot differences and modulation by adipogenesis. *Am. J. Physiol. Endocrinol. Metab.* **296**, E244-255 (2009).
494. Killinger, D. W., Strutt, B. J., Roncari, D. A. & Khalil, M. W. Estrone formation from dehydroepiandrosterone in cultured human breast adipose stromal cells. *J. Steroid Biochem. Mol. Biol.* **52**, 195–201 (1995).
495. Van Schothorst, E. M. *et al.* Adipose gene expression patterns of weight gain suggest counteracting steroid hormone synthesis. *Obes. Res.* **13**, 1031–1041 (2005).
496. Martel, C. *et al.* Distribution of 17 beta-hydroxysteroid dehydrogenase gene expression and activity in rat and human tissues. *J. Steroid Biochem. Mol. Biol.* **41**, 597–603 (1992).
497. Corbould, A. M., Judd, S. J. & Rodgers, R. J. Expression of types 1, 2, and 3 17 beta-hydroxysteroid dehydrogenase in subcutaneous abdominal and intra-abdominal adipose tissue of women. *J. Clin. Endocrinol. Metab.* **83**, 187–194 (1998).
498. Quinkler, M. *et al.* Androgen generation in adipose tissue in women with simple obesity--a site-specific role for 17beta-hydroxysteroid dehydrogenase type 5. *J. Endocrinol.* **183**, 331–342 (2004).
499. Wang, F. *et al.* 17β-Estradiol and estradiol fatty acyl esters and estrogen-converting enzyme expression in adipose tissue in obese men and women. *J. Clin. Endocrinol. Metab.* **98**, 4923–4931 (2013).
500. Blouin, K. *et al.* Androgen inactivation and steroid-converting enzyme expression in abdominal adipose tissue in men. *J. Endocrinol.* **191**, 637–649 (2006).
501. Fouad Mansour, M. *et al.* Oxidative activity of 17β-hydroxysteroid dehydrogenase on testosterone in male abdominal adipose tissues and cellular localization of 17β-HSD type 2. *Mol. Cell. Endocrinol.* **414**, 168–176 (2015).
502. Fouad Mansour, M., Blanchette, S., Pelletier, M., Poirier, D. & Tchernof, A. 17β-hydroxysteroid dehydrogenase type 2 activity, expression and cellular localization in abdominal adipose tissues from women. *Clin. Endocrinol. (Oxf.)* **98**, 229–237 (2023).
503. Corbould, A. M., Bawden, M. J., Lavranos, T. C., Rodgers, R. J. & Judd, S. J. The effect of obesity on the ratio of type 3 17beta-hydroxysteroid dehydrogenase mRNA to cytochrome P450 aromatase mRNA in subcutaneous abdominal and intra-abdominal adipose tissue of women. *Int. J. Obes. Relat. Metab. Disord. J. Int. Assoc. Study Obes.* **26**, 165–175 (2002).
504. Labrie, F. *et al.* The key role of 17 beta-hydroxysteroid dehydrogenases in sex steroid biology. *Steroids* **62**, 148–158 (1997).
505. Dufort, I., Rheault, P., Huang, X. F., Soucy, P. & Luu-The, V. Characteristics of a highly labile human type 5 17beta-hydroxysteroid dehydrogenase. *Endocrinology* **140**, 568–574 (1999).
506. Ostinelli, G., Vijay, J., Vohl, M.-C., Grundberg, E. & Tchernof, A. AKR1C2 and AKR1C3 expression in adipose tissue: Association with body fat distribution and regulatory variants. *Mol. Cell. Endocrinol.* **527**, 111220 (2021).
507. Wake, D. J. *et al.* Intra-adipose sex steroid metabolism and body fat distribution in idiopathic human obesity. *Clin. Endocrinol. (Oxf.)* **66**, 440–446 (2007).

508. Svensson, P.-A., Gabrielsson, B. G., Jernås, M., Gummesson, A. & Sjöholm, K. Regulation of human aldoketoreductase 1C3 (AKR1C3) gene expression in the adipose tissue. *Cell. Mol. Biol. Lett.* **13**, 599–613 (2008).
509. Desmond, J. C. *et al.* The aldo-keto reductase AKR1C3 is a novel suppressor of cell differentiation that provides a plausible target for the non-cyclooxygenase-dependent antineoplastic actions of nonsteroidal anti-inflammatory drugs. *Cancer Res.* **63**, 505–512 (2003).
510. Quinkler, M., Bujalska, I. J., Tomlinson, J. W., Smith, D. M. & Stewart, P. M. Depot-specific prostaglandin synthesis in human adipose tissue: a novel possible mechanism of adipogenesis. *Gene* **380**, 137–143 (2006).
511. Bellemare, V., Laberge, P., Noël, S., Tchernof, A. & Luu-The, V. Differential estrogenic 17beta-hydroxysteroid dehydrogenase activity and type 12 17beta-hydroxysteroid dehydrogenase expression levels in preadipocytes and differentiated adipocytes. *J. Steroid Biochem. Mol. Biol.* **114**, 129–134 (2009).
512. Rizner, T. L., Smuc, T., Rupreht, R., Sinkovec, J. & Penning, T. M. AKR1C1 and AKR1C3 may determine progesterone and estrogen ratios in endometrial cancer. *Mol. Cell. Endocrinol.* **248**, 126–135 (2006).
513. Vihma, V. *et al.* Metabolism of sex steroids is influenced by acquired adiposity-A study of young adult male monozygotic twin pairs. *J. Steroid Biochem. Mol. Biol.* **172**, 98–105 (2017).
514. Vihma, V. *et al.* Increased body fat mass and androgen metabolism - A twin study in healthy young women. *Steroids* **140**, 24–31 (2018).
515. Blanchette, S. *et al.* Expression and activity of 20alpha-hydroxysteroid dehydrogenase (AKR1C1) in abdominal subcutaneous and omental adipose tissue in women. *J. Clin. Endocrinol. Metab.* **90**, 264–270 (2005).
516. Zhang, Y. *et al.* Progesterone metabolism in adipose cells. *Mol. Cell. Endocrinol.* **298**, 76–83 (2009).
517. Veilleux, A. *et al.* Glucocorticoid-induced androgen inactivation by aldo-keto reductase 1C2 promotes adipogenesis in human preadipocytes. *Am. J. Physiol. Endocrinol. Metab.* **302**, E941-949 (2012).
518. Misso, M. L. *et al.* Adipose aromatase gene expression is greater in older women and is unaffected by postmenopausal estrogen therapy. *Menopause N. Y. N* **12**, 210–215 (2005).
519. Price, T. M. & O'Brien, S. N. Determination of estrogen receptor messenger ribonucleic acid (mRNA) and cytochrome P450 aromatase mRNA levels in adipocytes and adipose stromal cells by competitive polymerase chain reaction amplification. *J. Clin. Endocrinol. Metab.* **77**, 1041–1045 (1993).
520. Price, T. *et al.* Determination of aromatase cytochrome P450 messenger ribonucleic acid in human breast tissue by competitive polymerase chain reaction amplification. *J. Clin. Endocrinol. Metab.* **74**, 1247–1252 (1992).
521. McTernan, P. G. *et al.* Glucocorticoid regulation of p450 aromatase activity in human adipose tissue: gender and site differences. *J. Clin. Endocrinol. Metab.* **87**, 1327–1336 (2002).
522. Simpson, E. R. *et al.* Aromatase cytochrome P450, the enzyme responsible for estrogen biosynthesis. *Endocr. Rev.* **15**, 342–355 (1994).
523. Bulun, S. E., Chen, D., Moy, I., Brooks, D. C. & Zhao, H. Aromatase, breast cancer and obesity: a complex interaction. *Trends Endocrinol. Metab. TEM* **23**, 83–89 (2012).
524. Zhao, H. *et al.* A novel promoter controls Cyp19a1 gene expression in mouse adipose tissue. *Reprod. Biol. Endocrinol. RBE* **7**, 37 (2009).
525. Kim, N. R. *et al.* Testosterone Reduces Body Fat in Male Mice by Stimulation of Physical Activity Via Extrahypothalamic ERα Signaling. *Endocrinology* **162**, bqab045 (2021).
526. Andersson, S. & Russell, D. W. Structural and biochemical properties of cloned and expressed human and rat steroid 5 alpha-reductases. *Proc. Natl. Acad. Sci. U. S. A.* **87**, 3640–3644 (1990).
527. Samson, M., Labrie, F., Zouboulis, C. C. & Luu-The, V. Biosynthesis of dihydrotestosterone by a pathway that does not require testosterone as an intermediate in the SZ95 sebaceous gland cell line. *J. Invest. Dermatol.* **130**, 602–604 (2010).

528. Fouad Mansour, M., Pelletier, M. & Tchernof, A. Characterization of 5α-reductase activity and isoenzymes in human abdominal adipose tissues. *J. Steroid Biochem. Mol. Biol.* **161**, 45–53 (2016).
529. Mostaghel, E. A. *et al.* Contribution of Adrenal Glands to Intratumor Androgens and Growth of Castration-Resistant Prostate Cancer. *Clin. Cancer Res. Off. J. Am. Assoc. Cancer Res.* **25**, 426–439 (2019).
530. Blaak, E. Gender differences in fat metabolism. *Curr. Opin. Clin. Nutr. Metab. Care* **4**, 499–502 (2001).
531. Seyfart, T. *et al.* Association of sex hormones with physical, laboratory, and imaging markers of anthropometry in men and women from the general population. *PloS One* **13**, e0189042 (2018).
532. Gapstur, S. M. *et al.* Serum androgen concentrations in young men: a longitudinal analysis of associations with age, obesity, and race. The CARDIA male hormone study. *Cancer Epidemiol. Biomark. Prev. Publ. Am. Assoc. Cancer Res. Cosponsored Am. Soc. Prev. Oncol.* **11**, 1041–1047 (2002).
533. Tchernof, A. & Labrie, F. Dehydroepiandrosterone, obesity and cardiovascular disease risk: a review of human studies. *Eur. J. Endocrinol.* **151**, 1–14 (2004).
534. Tchernof, A. *et al.* Reduced testosterone and adrenal C19 steroid levels in obese men. *Metabolism.* **44**, 513–519 (1995).
535. Blouin, K. *et al.* Contribution of age and declining androgen levels to features of the metabolic syndrome in men. *Metabolism.* **54**, 1034–1040 (2005).
536. Blouin, K., Veilleux, A., Luu-The, V. & Tchernof, A. Androgen metabolism in adipose tissue: recent advances. *Mol. Cell. Endocrinol.* **301**, 97–103 (2009).
537. Evans, D. J., Hoffmann, R. G., Kalkhoff, R. K. & Kissebah, A. H. Relationship of androgenic activity to body fat topography, fat cell morphology, and metabolic aberrations in premenopausal women. *J. Clin. Endocrinol. Metab.* **57**, 304–310 (1983).
538. van Londen, G. J., Levy, M. E., Perera, S., Nelson, J. B. & Greenspan, S. L. Body composition changes during androgen deprivation therapy for prostate cancer: a 2-year prospective study. *Crit. Rev. Oncol. Hematol.* **68**, 172–177 (2008).
539. Sheikhbahaei, S., Reyes, D. K., Rowe, S. P. & Pienta, K. J. CT-based assessment of body composition following neoadjuvant chemohormonal therapy in patients with castration-naïve oligometastatic prostate cancer. *The Prostate* **81**, 127–134 (2021).
540. Mangiola, S. *et al.* Androgen deprivation therapy promotes an obesity-like microenvironment in periprostatic fat. *Endocr. Connect.* **8**, 547–558 (2019).
541. Antoun, S. *et al.* High subcutaneous adipose tissue predicts the prognosis in metastatic castration-resistant prostate cancer patients in post chemotherapy setting. *Eur. J. Cancer Oxf. Engl. 1990* **51**, 2570–2577 (2015).
542. Newell-Fugate, A. E. The role of sex steroids in white adipose tissue adipocyte function. *Reprod. Camb. Engl.* **153**, R133–R149 (2017).
543. Dieudonne, M. N., Pecquery, R., Boumediene, A., Leneveu, M. C. & Giudicelli, Y. Androgen receptors in human preadipocytes and adipocytes: regional specificities and regulation by sex steroids. *Am. J. Physiol.* **274**, C1645-1652 (1998).
544. Joyner, J., Hutley, L. & Cameron, D. Intrinsic regional differences in androgen receptors and dihydrotestosterone metabolism in human preadipocytes. *Horm. Metab. Res. Horm. Stoffwechselforschung Horm. Metab.* **34**, 223–228 (2002).
545. Carson-Jurica, M. A., Schrader, W. T. & O'Malley, B. W. Steroid receptor family: structure and functions. *Endocr. Rev.* **11**, 201–220 (1990).
546. Anderson, L. A., McTernan, P. G., Harte, A. L., Barnett, A. H. & Kumar, S. The regulation of HSL and LPL expression by DHT and flutamide in human subcutaneous adipose tissue. *Diabetes Obes. Metab.* **4**, 209–213 (2002).
547. Sjögren, J., Li, M. & Björntorp, P. Androgen hormone binding to adipose tissue in rats. *Biochim. Biophys. Acta* **1244**, 117–120 (1995).

548. De Pergola, G., Xu, X. F., Yang, S. M., Giorgino, R. & Bjorntorp, P. Up-regulation of androgen receptor binding in male rat fat pad adipose precursor cells exposed to testosterone: study in a whole cell assay system. *J. Steroid Biochem. Mol. Biol.* **37**, 553–558 (1990).
549. Rodriguez-Cuenca, S. *et al.* Sex steroid receptor expression profile in brown adipose tissue. Effects of hormonal status. *Cell. Physiol. Biochem. Int. J. Exp. Cell. Physiol. Biochem. Pharmacol.* **20**, 877–886 (2007).
550. Rosen, E. D. & MacDougald, O. A. Adipocyte differentiation from the inside out. *Nat. Rev. Mol. Cell Biol.* **7**, 885–896 (2006).
551. Blouin, K. *et al.* Effects of androgens on adipocyte differentiation and adipose tissue explant metabolism in men and women. *Clin. Endocrinol. (Oxf.)* **72**, 176–188 (2010).
552. Gupta, V. *et al.* Effects of dihydrotestosterone on differentiation and proliferation of human mesenchymal stem cells and preadipocytes. *Mol. Cell. Endocrinol.* **296**, 32–40 (2008).
553. Chazenbalk, G. *et al.* Androgens inhibit adipogenesis during human adipose stem cell commitment to preadipocyte formation. *Steroids* **78**, 920–926 (2013).
554. Zhang, Y. *et al.* Response of the adipose tissue transcriptome to dihydrotestosterone in mice. *Physiol. Genomics* **35**, 254–261 (2008).
555. Singh, R. *et al.* Testosterone inhibits adipogenic differentiation in 3T3-L1 cells: nuclear translocation of androgen receptor complex with beta-catenin and T-cell factor 4 may bypass canonical Wnt signaling to down-regulate adipogenic transcription factors. *Endocrinology* **147**, 141–154 (2006).
556. Rice, S. P. L. *et al.* Dehydroepiandrosterone (DHEA) treatment in vitro inhibits adipogenesis in human omental but not subcutaneous adipose tissue. *Mol. Cell. Endocrinol.* **320**, 51–57 (2010).
557. McNelis, J. C. *et al.* Dehydroepiandrosterone exerts antiglucocorticoid action on human preadipocyte proliferation, differentiation, and glucose uptake. *Am. J. Physiol. Endocrinol. Metab.* **305**, E1134-1144 (2013).
558. Zerradi, M., Dereumetz, J., Boulet, M.-M. & Tchernof, A. Androgens, body fat Distribution and Adipogenesis. *Curr. Obes. Rep.* **3**, 396–403 (2014).
559. Gordon, G. B., Newitt, J. A., Shantz, L. M., Weng, D. E. & Talalay, P. Inhibition of the conversion of 3T3 fibroblast clones to adipocytes by dehydroepiandrosterone and related anticarcinogenic steroids. *Cancer Res.* **46**, 3389–3395 (1986).
560. Lea-Currie, Y. R., Wen, P. & McIntosh, M. K. Dehydroepiandrosterone reduces proliferation and differentiation of 3T3-L1 preadipocytes. *Biochem. Biophys. Res. Commun.* **248**, 497–504 (1998).
561. Li, Q. & Spalding, K. L. The regulation of adipocyte growth in white adipose tissue. *Front. Cell Dev. Biol.* **10**, 1003219 (2022).
562. Saponaro, C., Gaggini, M., Carli, F. & Gastaldelli, A. The Subtle Balance between Lipolysis and Lipogenesis: A Critical Point in Metabolic Homeostasis. *Nutrients* **7**, 9453–9474 (2015).
563. Tchernof, A. *et al.* Androgens and the Regulation of Adiposity and Body Fat Distribution in Humans. *Compr. Physiol.* **8**, 1253–1290 (2018).
564. Li, M. & Björntorp, P. Effects of testosterone on triglyceride uptake and mobilization in different adipose tissues in male rats in vivo. *Obes. Res.* **3**, 113–119 (1995).
565. Mårin, P. *et al.* Assimilation of triglycerides in subcutaneous and intraabdominal adipose tissues in vivo in men: effects of testosterone. *J. Clin. Endocrinol. Metab.* **81**, 1018–1022 (1996).
566. Boyanov, M. A., Boneva, Z. & Christov, V. G. Testosterone supplementation in men with type 2 diabetes, visceral obesity and partial androgen deficiency. *Aging Male Off. J. Int. Soc. Study Aging Male* **6**, 1–7 (2003).
567. Varlamov, O. *et al.* Androgen effects on adipose tissue architecture and function in nonhuman primates. *Endocrinology* **153**, 3100–3110 (2012).
568. Varlamov, O. *et al.* Ovarian cycle-specific regulation of adipose tissue lipid storage by testosterone in female nonhuman primates. *Endocrinology* **154**, 4126–4135 (2013).
569. Rebuffé-Scrive, M., Mårin, P. & Björntorp, P. Effect of testosterone on abdominal adipose tissue in men. *Int. J. Obes.* **15**, 791–795 (1991).

570. Xu, X., De Pergola, G. & Björntorp, P. The effects of androgens on the regulation of lipolysis in adipose precursor cells. *Endocrinology* **126**, 1229–1234 (1990).
571. Xu, X. F., De Pergola, G. & Björntorp, P. Testosterone increases lipolysis and the number of beta-adrenoceptors in male rat adipocytes. *Endocrinology* **128**, 379–382 (1991).
572. Hernández-Morante, J. J., Pérez-de-Heredia, F., Luján, J. A., Zamora, S. & Garaulet, M. Role of DHEA-S on body fat distribution: gender- and depot-specific stimulation of adipose tissue lipolysis. *Steroids* **73**, 209–215 (2008).
573. Tagliaferro, A. R., Ronan, A. M., Payne, J., Meeker, L. D. & Tse, S. Increased lipolysis to beta-adrenergic stimulation after dehydroepiandrosterone treatment in rats. *Am. J. Physiol.* **268**, R1374-1380 (1995).
574. Di Nisio, A. *et al.* Testosterone is sequestered in dysfunctional adipose tissue, modifying androgen-responsive genes. *Int. J. Obes. 2005* **44**, 1617–1625 (2020).
575. Fan, W. *et al.* Androgen receptor null male mice develop late-onset obesity caused by decreased energy expenditure and lipolytic activity but show normal insulin sensitivity with high adiponectin secretion. *Diabetes* **54**, 1000–1008 (2005).
576. Ek, I. *et al.* A unique defect in the regulation of visceral fat cell lipolysis in the polycystic ovary syndrome as an early link to insulin resistance. *Diabetes* **51**, 484–492 (2002).
577. Mannerås-Holm, L. *et al.* Adipose tissue has aberrant morphology and function in PCOS: enlarged adipocytes and low serum adiponectin, but not circulating sex steroids, are strongly associated with insulin resistance. *J. Clin. Endocrinol. Metab.* **96**, E304-311 (2011).
578. Dicker, A. *et al.* Effect of testosterone on lipolysis in human pre-adipocytes from different fat depots. *Diabetologia* **47**, 420–428 (2004).
579. Douchi, T. *et al.* Body fat distribution in women with polycystic ovary syndrome. *Obstet. Gynecol.* **86**, 516–519 (1995).
580. Seow, K.-M. *et al.* Omental adipose tissue overexpression of fatty acid transporter CD36 and decreased expression of hormone-sensitive lipase in insulin-resistant women with polycystic ovary syndrome. *Hum. Reprod. Oxf. Engl.* **24**, 1982–1988 (2009).
581. Moreira-Pais, A. *et al.* Sex differences on adipose tissue remodeling: from molecular mechanisms to therapeutic interventions. *J. Mol. Med. Berl. Ger.* **98**, 483–493 (2020).
582. Nishizawa, H. *et al.* Androgens decrease plasma adiponectin, an insulin-sensitizing adipocyte-derived protein. *Diabetes* **51**, 2734–2741 (2002).
583. Xu, A. *et al.* Testosterone selectively reduces the high molecular weight form of adiponectin by inhibiting its secretion from adipocytes. *J. Biol. Chem.* **280**, 18073–18080 (2005).
584. Horenburg, S., Fischer-Posovszky, P., Debatin, K.-M. & Wabitsch, M. Influence of sex hormones on adiponectin expression in human adipocytes. *Horm. Metab. Res. Horm. Stoffwechselforschung Horm. Metab.* **40**, 779–786 (2008).
585. Yarrow, J. F. *et al.* Influence of androgens on circulating adiponectin in male and female rodents. *PloS One* **7**, e47315 (2012).
586. Böttner, A. *et al.* Gender differences of adiponectin levels develop during the progression of puberty and are related to serum androgen levels. *J. Clin. Endocrinol. Metab.* **89**, 4053–4061 (2004).
587. Lanfranco, F., Zitzmann, M., Simoni, M. & Nieschlag, E. Serum adiponectin levels in hypogonadal males: influence of testosterone replacement therapy. *Clin. Endocrinol. (Oxf.)* **60**, 500–507 (2004).
588. Jenks, M. Z., Fairfield, H. E., Johnson, E. C., Morrison, R. F. & Muday, G. K. Sex Steroid Hormones Regulate Leptin Transcript Accumulation and Protein Secretion in 3T3-L1 Cells. *Sci. Rep.* **7**, 8232 (2017).
589. Wabitsch, M. *et al.* Contribution of androgens to the gender difference in leptin production in obese children and adolescents. *J. Clin. Invest.* **100**, 808–813 (1997).
590. Piñeiro, V. *et al.* Dihydrotestosterone, stanozolol, androstenedione and dehydroepiandrosterone sulphate inhibit leptin secretion in female but not in male samples of omental adipose tissue in vitro: lack of effect of testosterone. *J. Endocrinol.* **160**, 425–432 (1999).

591. Yao, Y.-C. *et al.* Influence of castration-induced sex hormone deficiency on serum lipid levels and the genes expression in male pigs. *Horm. Metab. Res. Horm. Stoffwechselforschung Horm. Metab.* **43**, 674–680 (2011).
592. Lerner, A. *et al.* Androgen Reduces Mitochondrial Respiration in Mouse Brown Adipocytes: A Model for Disordered Energy Balance in Polycystic Ovary Syndrome. *Int. J. Mol. Sci.* **22**, 243 (2020).
593. Monjo, M., Rodríguez, A. M., Palou, A. & Roca, P. Direct effects of testosterone, 17 beta-estradiol, and progesterone on adrenergic regulation in cultured brown adipocytes: potential mechanism for gender-dependent thermogenesis. *Endocrinology* **144**, 4923–4930 (2003).
594. Rodríguez-Cuenca, S., Monjo, M., Gianotti, M., Proenza, A. M. & Roca, P. Expression of mitochondrial biogenesis-signaling factors in brown adipocytes is influenced specifically by 17beta-estradiol, testosterone, and progesterone. *Am. J. Physiol. Endocrinol. Metab.* **292**, E340-346 (2007).
595. Rodriguez, A. M., Monjo, M., Roca, P. & Palou, A. Opposite actions of testosterone and progesterone on UCP1 mRNA expression in cultured brown adipocytes. *Cell. Mol. Life Sci. CMLS* **59**, 1714–1723 (2002).
596. Shorakae, S. *et al.* Brown adipose tissue thermogenesis in polycystic ovary syndrome. *Clin. Endocrinol. (Oxf.)* **90**, 425–432 (2019).
597. Gasparini, S. J. *et al.* Androgens sensitise mice to glucocorticoid-induced insulin resistance and fat accumulation. *Diabetologia* **62**, 1463–1477 (2019).
598. Movérare-Skrtic, S. *et al.* Dihydrotestosterone treatment results in obesity and altered lipid metabolism in orchidectomized mice. *Obes. Silver Spring Md* **14**, 662–672 (2006).
599. Ryu, J.-W. *et al.* DHEA administration increases brown fat uncoupling protein 1 levels in obese OLETF rats. *Biochem. Biophys. Res. Commun.* **303**, 726–731 (2003).
600. Nohara, K., Laque, A., Allard, C., Münzberg, H. & Mauvais-Jarvis, F. Central mechanisms of adiposity in adult female mice with androgen excess. *Obes. Silver Spring Md* **22**, 1477–1484 (2014).
601. Kaikaew, K., Grefhorst, A. & Visser, J. A. Sex Differences in Brown Adipose Tissue Function: Sex Hormones, Glucocorticoids, and Their Crosstalk. *Front. Endocrinol.* **12**, 652444 (2021).
602. Cai, C. & Balk, S. P. Intratumoral androgen biosynthesis in prostate cancer pathogenesis and response to therapy. *Endocr. Relat. Cancer* **18**, R175-182 (2011).
603. Harris, W. P., Mostaghel, E. A., Nelson, P. S. & Montgomery, B. Androgen deprivation therapy: progress in understanding mechanisms of resistance and optimizing androgen depletion. *Nat. Clin. Pract. Urol.* **6**, 76–85 (2009).
604. Zwick, R. K., Guerrero-Juarez, C. F., Horsley, V. & Plikus, M. V. Anatomical, Physiological, and Functional Diversity of Adipose Tissue. *Cell Metab.* **27**, 68–83 (2018).
605. Sharifi, N. Clinical implications of the 5α-androstanedione pathway for castration-resistant prostate cancer. *Future Oncol. Lond. Engl.* **7**, 1239–1241 (2011).
606. Ando, T. *et al.* Dihydrotestosterone synthesis pathways from inactive androgen 5α-androstane-3β,17β-diol in prostate cancer cells: Inhibition of intratumoural 3β-hydroxysteroid dehydrogenase activities by abiraterone. *Sci. Rep.* **6**, 32198 (2016).
607. McAdam, K. P., Elin, R. J., Sipe, J. D. & Wolff, S. M. Changes in human serum amyloid A and C-reactive protein after etiocholanolone-induced inflammation. *J. Clin. Invest.* **61**, 390–394 (1978).
608. Kaminski, R. M., Marini, H., Kim, W.-J. & Rogawski, M. A. Anticonvulsant activity of androsterone and etiocholanolone. *Epilepsia* **46**, 819–827 (2005).
609. Yoshida, S. *et al.* Anti-proliferative action of endogenous dehydroepiandrosterone metabolites on human cancer cell lines. *Steroids* **68**, 73–83 (2003).
610. Zhu, B. T., Han, G.-Z., Shim, J.-Y., Wen, Y. & Jiang, X.-R. Quantitative structure-activity relationship of various endogenous estrogen metabolites for human estrogen receptor alpha and beta subtypes: Insights into the structural determinants favoring a differential subtype binding. *Endocrinology* **147**, 4132–4150 (2006).

611. Liang, Z. *et al.* Aromatase-induced endogenous estrogen promotes tumour metastasis through estrogen receptor-α/matrix metalloproteinase 12 axis activation in castration-resistant prostate cancer. *Cancer Lett.* **467**, 72–84 (2019).
612. Grindstad, T. *et al.* Estrogen receptors α and β and aromatase as independent predictors for prostate cancer outcome. *Sci. Rep.* **6**, 33114 (2016).
613. Zhang, C.-Y., Wang, W.-Q., Chen, J. & Lin, S.-X. Reductive 17beta-hydroxysteroid dehydrogenases which synthesize estradiol and inactivate dihydrotestosterone constitute major and concerted players in ER+ breast cancer cells. *J. Steroid Biochem. Mol. Biol.* **150**, 24–34 (2015).
614. Lynes, M. D. & Tseng, Y.-H. Deciphering adipose tissue heterogeneity. *Ann. N. Y. Acad. Sci.* **1411**, 5–20 (2018).
615. Blouin, K. *et al.* Pathways of adipose tissue androgen metabolism in women: depot differences and modulation by adipogenesis. *Am. J. Physiol. Endocrinol. Metab.* **296**, E244-255 (2009).
616. Ackerman, G. E., Smith, M. E., Mendelson, C. R., MacDonald, P. C. & Simpson, E. R. Aromatization of androstenedione by human adipose tissue stromal cells in monolayer culture. *J. Clin. Endocrinol. Metab.* **53**, 412–417 (1981).
617. Alvarez-García, V., González, A., Martínez-Campa, C., Alonso-González, C. & Cos, S. Melatonin modulates aromatase activity and expression in endothelial cells. *Oncol. Rep.* **29**, 2058–2064 (2013).
618. Thomas, L. N. *et al.* Differential alterations in 5alpha-reductase type 1 and type 2 levels during development and progression of prostate cancer. *The Prostate* **63**, 231–239 (2005).
619. Deb, S. *et al.* Characterization of Precursor-Dependent Steroidogenesis in Human Prostate Cancer Models. *Cancers* **10**, 343 (2018).
620. Sakai, M., Martinez-Arguelles, D. B., Aprikian, A. G., Magliocco, A. M. & Papadopoulos, V. De novo steroid biosynthesis in human prostate cell lines and biopsies. *The Prostate* **76**, 575–587 (2016).
621. Ko, H.-K. *et al.* Loss of an Androgen-Inactivating and Isoform-Specific HSD17B4 Splice Form Enables Emergence of Castration-Resistant Prostate Cancer. *Cell Rep.* **22**, 809–819 (2018).
622. Song, W. & Khera, M. Physiological normal levels of androgen inhibit proliferation of prostate cancer cells in vitro. *Asian J. Androl.* **16**, 864–868 (2014).
623. Byrns, M. C., Mindnich, R., Duan, L. & Penning, T. M. Overexpression of aldo-keto reductase 1C3 (AKR1C3) in LNCaP cells diverts androgen metabolism towards testosterone resulting in resistance to the 5α-reductase inhibitor finasteride. *J. Steroid Biochem. Mol. Biol.* **130**, 7–15 (2012).
624. Ribeiro, R. *et al.* Human periprostatic adipose tissue promotes prostate cancer aggressiveness in vitro. *J. Exp. Clin. Cancer Res. CR* **31**, 32 (2012).
625. Liotti, A. *et al.* Periprostatic adipose tissue promotes prostate cancer resistance to docetaxel by paracrine IGF-1 upregulation of TUBB2B beta-tubulin isoform. *The Prostate* **81**, 407–417 (2021).
626. Fatima, L. A. *et al.* Estrogen receptor 1 (ESR1) regulates VEGFA in adipose tissue. *Sci. Rep.* **7**, 16716 (2017).
627. Arnold, J. T., Le, H., McFann, K. K. & Blackman, M. R. Comparative effects of DHEA vs. testosterone, dihydrotestosterone, and estradiol on proliferation and gene expression in human LNCaP prostate cancer cells. *Am. J. Physiol. Endocrinol. Metab.* **288**, E573-584 (2005).
628. Arnold, J. T. *et al.* Androgen receptor or estrogen receptor-beta blockade alters DHEA-, DHT-, and E(2)-induced proliferation and PSA production in human prostate cancer cells. *The Prostate* **67**, 1152–1162 (2007).
629. Li, Q. *et al.* Linking prostate cancer cell AR heterogeneity to distinct castration and enzalutamide responses. *Nat. Commun.* **9**, 3600 (2018).
630. Rebeaud, M. *et al.* A novel 3D culture model for human primary mammary adipocytes to study their metabolic crosstalk with breast cancer in lean and obese conditions. *Sci. Rep.* **13**, 4707 (2023).

631. Harms, M. J. *et al.* Mature Human White Adipocytes Cultured under Membranes Maintain Identity, Function, and Can Transdifferentiate into Brown-like Adipocytes. *Cell Rep.* **27**, 213-225.e5 (2019).
632. Estève, D. *et al.* Lobular architecture of human adipose tissue defines the niche and fate of progenitor cells. *Nat. Commun.* **10**, 2549 (2019).
633. Folch, J., Lees, M. & Sloane Stanley, G. H. A simple method for the isolation and purification of total lipides from animal tissues. *J. Biol. Chem.* **226**, 497–509 (1957).